FABRICATED HELICOPTER TRANSMISSION HOUSING ANALYSIS

Alexander Korzun, et al

United Aircraft Corporation

Prepared for:

Army Air Mobility Research and Development Laboratory

January 1975

EUSTIS DIRECTORATE POSITION STATEMENT

The information contained in this report is a result of research conducted to investigate advanced structural concepts for a helicopter main transmission housing.

The objective of the fabricated helicopter transmission housing study was to provide a housing design that was structurally superior to the conventional magnesium cast housing, with additional attributes of reliability, maintainability, and cost.

The report has been reviewed by the Eustis Directorate, U.S. Army Air Mobility Research and Development Laboratory and is considered to be technically sound.

This program was conducted for the Military Operations Technology Division under the technical management of Mr. L. Thomas Mazza, Technology Applications Division.

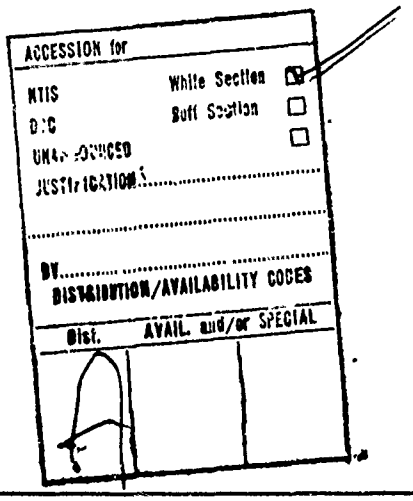

DISCLAIMERS

The findings in this report are not to be construed as an official Department of the Army position unless so designated by other authorized documents.

When Government drawings, specifications, or other data are used for any purpose other than in connection with a definitely related Government procurement operation, the United States Government thereby incurs no responsibility nor any obligation whatsoever; and the fact that the Government may have formulated, furnished, or in any way supplied the said drawings, specifications, or other data is not to be regarded by implication or otherwise as in any manner licensing the holder or any other person or corporation, or conveying any rights or permission, to manufacture, use, or sell any patented invention that may in any way be related thereto.

Trade names cited in this report do not constitute an official endorsement or approval of the use of such commercial hardware or software.

DISPOSITION INSTRUCTIONS

Destroy this report when no longer needed. Do not return it to the originator.

Unclassified

SECURITY CLASSIFICATION OF THIS PAGE (When Data Entered)

REPORT DOCUMENTATION PAGE

READ INSTRUCTIONS BEFORE COMPLETING FORM

1. REPORT NUMBER: USAAMRDL-TR-74-14	2. GOVT ACCESSION NO.
3. RECIPIENT'S CATALOG NUMBER: AD-A008 995	
4. TITLE (and Subtitle): FABRICATED HELICOPTER TRANSMISSION HOUSING ANALYSIS	5. TYPE OF REPORT & PERIOD COVERED: Final Report - December 18, 1972 to October 18, 1973
	6. PERFORMING ORG. REPORT NUMBER
7. AUTHOR(s): Alexander Korzun, Stephen Schuman	8. CONTRACT OR GRANT NUMBER(s): DAAJ02-73-C-0022
9. PERFORMING ORGANIZATION NAME AND ADDRESS: Sikorsky Aircraft Division of United Aircraft Corporation, Stratford, Connecticut 06602	10. PROGRAM ELEMENT, PROJECT, TASK AREA & WORK UNIT NUMBERS: TASK 1F162203A11902
11. CONTROLLING OFFICE NAME AND ADDRESS: Eustis Directorate, U.S. Army Air Mobility Research and Development Laboratory, Fort Eustis, Virginia 23604	12. REPORT DATE: January 1975
	13. NUMBER OF PAGES: 300
14. MONITORING AGENCY NAME & ADDRESS (if different from Controlling Office)	15. SECURITY CLASS. (of this report): Unclassified
	15a. DECLASSIFICATION/DOWNGRADING SCHEDULE

16. DISTRIBUTION STATEMENT (of this Report)

Approved for public release; distribution unlimited.

17. DISTRIBUTION STATEMENT (of the abstract entered in Block 20, if different from Report)

18. SUPPLEMENTARY NOTES

19. KEY WORDS (Continue on reverse side if necessary and identify by block number)

Fabricated Helicopter Transmission Housing, Magnesium Casting, Corrosion resistance, Custom 455 Stainless Steel, Ti-6Al-4V Titanium, CRT, NASTRAN, Welded steel truss, Titanium truss

20. ABSTRACT (Continue on reverse side if necessary and identify by block number)

The objective of the fabricated helicopter transmission housing study was to provide a transmission housing design superior to the conventional magnesium cast housing. The new design is a welded steel fabricated truss-like structure, approximately 15 percent lighter than the magnesium casting, and in small quantities offers a 30-percent reduction in cost. The truss structure is superior to the casting in reliability and maintainability. It is corrosion resistant and not susceptible to creep. The fabricated housing is feasible using today's

DD FORM 1 JAN 73 1473 EDITION OF 1 NOV 65 IS OBSOLETE S/N 0102-014-6601

Unclassified

SECURITY CLASSIFICATION OF THIS PAGE (When Data Entered)

materials, analytical methods, and fabrication tecniques.

The aircraft selected as the vehicle for this study was the U.S. Army CH-54B helicopter. The new fabricated truss-like housing was designed to be interchangeable with the present CH-54B magnesium main transmission housing. It meets all the interface and functional requirements of the cast housing design. Loads for flight and crash conditions, as well as stiffness criteria, were developed to permit structural analysis and comparison with the existing casting design.

During preliminary design, seven candidate truss arrangements were considered in conjunction with material and joining trade-off studies. Of the sixteen materials considered, only titanium Ti-6Al-4V and stainless stell Custom 455 had an adequate combination of ultimate strength, fatigue joint strength, and high-temperature creep properties. Of the five joining methods investigated, only welding had the static and fatigue joint efficiencies essential for a fabricated truss-like housing made of titanium or steel.

The structural analysis of the seven candidate truss arrangements with titanium and steel was simplified by grouping the arrangements into three fundamentally distinct configurations. The geometry of each arrangement was coded and then corrected through use of a cathode-ray tube (CRT) display program. The analysis was then performed by a redundant NASA structures analysis program (NASTRAN). During the analysis, the results were iterated and compared with a conventional casting to satisfy stiffness and support conditions.

From an anlysis of the preliminary results, a single detail configuration evolved: a truncated conical structure with rings at each bearing or interface connected by many structural members forming a truss. Further analysis yielded the final detail design configuration: a welded steel truss arrangement weighing 305 lbs. An alternate titanium truss arrangement weighs 313 pounds. The present magnesium transmission housing weighs 362 pounds.

To determine the effects on the housing design of a ±25 percent change in input torque, the CH-54B aircraft was scaled parametrically, and new applied housing loads were developed. Included in the load development were crash loads and flight loads as well as servo, scissor, accessory, and internal gear and bearing loads. For a 25-percent increase in input torque, the scaled-up welded steel truss fabricated housing weighs 362 pounds. For a 25 percent decrease, the housing weighs 254 pounds. The alternate welded titanium truss fabricated housing weighs 386 pounds, for a 25-percent increase, and 262 pounds, for a 25-percent decrease in input torque.

Areas requiring additional development effort before the fabricated housing concept can become operational include a welding development program and improved analytical methods. The welding development program is necessary to improve joint integrity through better quality control of welded joints. Improved analytical methods should include determination of skin covering strength effects, a method for plastic and thermal stress analysis, development of a preprocessor to reduce coding of input data, and development of a specific program to handle the required structural analysis.

A fabricated housing should be built and tested as outlined in the proposed follow-on program to verify cost, analysis, fabrication techniques, and weight savings.

PREFACE

The program reported herein was conducted during a nine-month period from December 18, 1972, to October 18, 1973, for the Eustis Directorate, U. S. Army Air Mobility Research and Development Laboratory (USAAMRDL), Fort Eustis, Virginia, under Contract DAAJ02-73-C-0022, Task 1F162203A11902.

USAAMRDL technical direction was provided by Mr. L. Thomas Mazza, of the Eustis Directorate, Technology Applications Division.

The program was conducted at Sikorsky Aircraft, Stratford, Connecticut, under the technical supervision of Mr. Harold K. Frint, Sikorsky Aircraft Transmission Design and Development Section. Principal investigators for the program were Mr. A. Korzun and Mr. S. Schuman of the Transmission Design and Development Section, and Mr. W. Degnan of the Material and Processes Section.

TABLE OF CONTENTS

	Page
PREFACE	1
LIST OF ILLUSTRATIONS	6
LIST OF TABLES	16
INTRODUCTION	19
DESIGN APPROACH	26
Aircraft Selection	29
Description of Aircraft	29
Description of Drive Train	30
Description of Main Gearbox	33
Description of Main Transmission Casting	43
Design Criteria for Main Transmission	47
Design Criteria for the Fabricated Housing	48
Interface Requirements for Fabricated Housing	49
PRELIMINARY DESIGN	50
Load Development	50
Stiffness Criteria	74
Selection of Materials and Joining Methods	78
Candidate Materials	79
Rationale for Joining Method Selection	90
Candidate Materials for Skin Covering	98
Candidate Truss Geometries	100

Page

Modeling of the Truss Geometry 114

Method of Analysis 119

Discussion of Results of Analysis 125

DETAIL DESIGN OF THE TRUSS FABRICATED HOUSING . . . 130

Design Criteria 130

Description of Truss Geometry 130

Analysis 139

COMPARISON OF THE FABRICATED TRUSS-LIKE HOUSING WITH THE CH-54B CASTING 141

Cost Comparison 141

Reliability and Maintainability Comparison . . 142

Corrosion Properties Comparison 145

Crashworthiness 145

Heat Dissipation 146

Survivability and Vulnerability 146

Manufacturing 147

Summary 148

EFFECT OF SCALING A FABRICATED HOUSING DESIGN . . . 149

Parametric Scaling of Loads 149

Analysis 158

DEVELOPMENTAL AREA DEFINITION 162

Analysis 162

Experimental Verification 163

Test Plan 163

Design Guidelines 168

AREAS FOR FUTURE STUDY. 170

		Page
SUMMARY		172
CONCLUSIONS		173
LITERATURE CITED		174
APPENDIXES	I - CH-54B DIMENSIONS AND PERFORMANCE DATA	175
	II - MATERIAL CHARACTERISTICS	183
	III - DISCUSSION OF SYNERGISTIC INTERACTION BETWEEN CREEP AND FATIGUE PROPERTIES	280
LIST OF SYMBOLS		281

LIST OF ILLUSTRATIONS

Figure		Page
1	H-5 Main Housing	20
2	H-19 Main Housing	20
3	H-34 Main Housing	20
4	H-37 Main Housing	20
5	Three-View of H-3 Main Housing	21
6	H-54 Main Housing, Composite Views . . .	22
7	H-53 Main Housing, Side View	24
8	H-53 Main Housing, Front View	24
9	XH-59A Main Housing, Three-Quarter View .	24
10	Three-View, CH-53E Main Housing	25
11	Flow Chart of Approach to Fabricated Helicopter Transmission Housing Analysis	27
12	U. S. Army CH-54B Aircraft	30
13	U. S. Army CH-54B Aircraft, Three-View Drawing	31
14	Isometric of Drive Train Components of the CH-54B Aircraft	33
15	Intermediate Gearbox, CH-54B Aircraft . .	34
16	Tail Gearbox, CH-54B	35
17	Isometric of CH-54B Main Transmission Drive Train Scheme	37
18	Rear Cover and Accessory Location of the CH-54B Main Transmission	39
19	Cross Section of the CH-54B Main Transmission	41
20	Isometric of CH-54B Main Transmission Housing	44

Figure		Page
21	Cross Section of CH-54B Main Transmission Housing	45
22	Forward Crash Loads on Housing Due to Rotor Head and Accessory Inertia	51
23	Initial Loading - 20g Forward Crash Condition	54
24	Initial Loading - 18g Side Crash Condition	55
25	Initial Loading - 20g Down Crash Condition	56
26	Sign Convention for Applied Main Rotor Loads	57
27	Bearing Reaction Geometry	60
28	Outer Shaft Load Geometry	63
29	Loading for Accessory Drive Train	66
30	Summary of Bearing and Gear Loads	71
31	Applied Housing Loads for Flight Conditions (Hover)	72
32	Applied Housing Loads for Flight Conditions (Symmetrical Dive and Pullout)	73
33	Shell Model for Casting Stiffness Analysis	77
34	Specific 10^7 Cycle Fatigue Strength Versus Temperature	80
35	Specific Fracture Toughness Versus Specific Yield Strength	83
36	Specific Stiffness Versus Specific Yield Strength	84
37	Specific 10^7 Fatigue Strength Versus Specific Yield Strength	85
38	Specific Ultimate Tensile Strength Versus Temperature	86

Figure		Page
39	Specific Ultimate Shear Strength Versus Temperature	87
40	Various Joining Methods	91
41	Friction Trapped Joint Used for Composite Material	92
42	Typical Welded Joint	94
43	Typical Welded Joint	95
44	Sketch of Typical Skin Truss Connection .	99
45	Truss Geometry Constraints	101
46	Plan View of Truss Geometry	102
47	Half-Size Model of Typical Truss Housing	103
48	Sketch of "A" Frame Truss Design	104
49	Sketch of Pyramid Truss Design	105
50	Sketch of Pure Truss Design	106
51	Sketch of Pure Truss Design	107
52	Sketch of "A" Frame Truss Design With Composite Material	108
53	Sketch of Pyramid Truss Design With Composite Material	109
54	Sketch of Pure Truss Design With Composite Material	110
55	Three-View Preliminary Layout of "A" Frame Truss Housing	111
56	Three-View Preliminary Layout of Pyramid Truss Housing	115
57	Three-View Preliminary Layout of Pure Truss Housing	117
58	Typical Truss-Like Structure in Display Program	121

Figure		Page
59	NASTRAN Card Deck Setup	122
60	Truss-Like Structure with Some Initial Error	124
61	Photograph of a Designer Using CRT To Change a Structure Element	124
62	CRT Display of "A" Frame Truss Design . .	126
63	CRT Display of Pyramid Truss Design . . .	127
64	CRT Display of Pure Truss Design	128
65	Detail Design Layout of the Fabricated Transmission Housing (View Looking Aft) .	131
66	Detail Design Layout of the Fabricated Transmission Housing (View Looking Forward)	133
67	Detail Design Layout of the Fabricated Transmission Housing (Plan View)	135
68	Detail Design Layout of the Fabricated Transmission Housing (Auxiliary Plan View)	137
69	CRT Display of the Final Fabricated Housing Transmission Design	138
70	Detail of Typical Casting Mounting Arrangement	143
71	Detail of Typical Fabricated Housing Mounting Arrangement	144
72	Historical Data - Hub Moment Versus Design Gross Weight	150
73	Historical Data - Hub Moment Constant Versus Design Gross Weight	151
74	Design Gross Weight Ratio Versus Design Torque Ratio	152
75	Head Moment Constant Ratio Versus Design Torque Ratio	153

Figure		Page
76	Main Transmission Rotor Group Weight Versus Design Torque Ratio	154
77	Main Rotor Group Weight Ratio Versus Design Torque Ratio	155
78	Flight Control Group Weight Ratio Versus Design Torque Ratio	156
79	Head Moment Constant Ratio Versus Design Gross Weight Ratio	157
80	CH-54A/B Regenerative Test Stand - View of Test Stand	164
81	CH-54A/B Regenerative Test Stand Control Room	164
82	CH-54A/B Regenerative Test Stand - View of Drive	164
83	Test Rig To Simulate Main Rotor Shaft Loads	165
84	Isometric of a Tail Gearbox Housing as a Truss-Like Structure	171
85	Forward-Flight Performance, Sea Level Standard	176
86	Hover Ceiling, Two-Engine CH-54B	180
87	Productivity Versus Mission Radius, CH-54B	181
88	Forward Climb Performance, CH-54B	182
89	Effect of Temperature on the Tensile and Compressive Moduli (E and E_c) of Cast AZ91C-T6	188
90	Effect of Temperature on the Physical Properties of Cast AZ91C-T6	188
91	Dimensional Changes of AZ91C-T6 Sand Castings at 200° to 400°F	189
92	Effect of Cycles on K_T, S_M = 0, + 10 KSI, K_T = 3.3, AZ91C-T6 Magnesium Alloy	190

Figure		Page
93	Constant-Life Fatigue Diagram, AZ91C-T6 Magnesium Alloy, K_T = 1.0	191
94	Crack Growth Rate Versus Stress Intensity Factor, AZ91C-T6 With As-Cast Surface in Laboratory Environment	192
95	Constant-Life Fatigue Diagram For Welded and Heat-Treated 6061-T6	194
96	Constant-Life Fatigue Diagram For 6061-T6 Wrought Products at 200°F	195
97	Bending Modulus of Rupture For 6061-T6 Round Tubing	198
98	Constant-Life Fatigue Diagram For 6061-T6 Wrought Products, K_t = 1.0	198
99	Constant-Life Fatigue Diagram for 6061-T6 Extrusions	199
100	Crack Growth Rate Versus Stress Intensity Factor, 6061-T6 Extrusions	200
101	Constant-Life Fatigue Diagram 7175-T736 Aluminum Alloy, K_T = 1.0	204
102	Effect of Cycles on K_T, R = 0.00, 7175-T736 Aluminum Alloy	205
103	Effect of Temperature on the Ultimate Tensile Strength (F_{tu}) of 7075-T651 Aluminum Alloy	206
104	Effect of Temperature on the Tensile Yield Strength (F_{ty}) of 7075-T651 Aluminum Alloy	207
105	Constant-Life Fatigue Diagram for 7075-T736 Wrought Products at 200°F	208
106	Notch Sensitivity of Ti-6Al-4V Weld Metal (K_f Versus K_t) at Two Steady Stresses . .	214
107	K_t as a Function of Defect Geometry . . .	215

Figure		Page
108	Constant-Life Diagram for Shot-Peened Ti-6Al-4V	217
109	Fatigue Crack Propagation Rate in Ti-6Al-4V, BETA-STOA	218
110	Fracture Toughness of Beta-Processed Titanium Ti-6Al-4V	218
111	Constant-Life Diagram, Ti-6Al-4V Annealed Sheet, Room Temperature, K_t = 1.0	219
112	Crack Growth Rate Versus Stress Intensity Factor, Mill Annealed Ti-6Al-4V Titanium Sheet	220
113	Plane Strain Fracture Toughness of Ti-6Al-4V	223
114	Constant-Life Diagram of Titanium Ti-6Al-4V BETA-STOA 0.5 Inch From As-Quenched Surface, Polished Specimens . .	224
115	Effect of Temperature on the Ultimate Tensile Strength of Annealed Ti-6Al-4V Sheet and Bar	225
116	Effect of Temperature on the Tensile Yield Strength of Annealed Ti-6Al-4V Sheet and Bar	226
117	Effect of Temperature on the Compressive Yield Strength of Annealed Ti-6Al-4V Sheet and Bar	227
118	Effect of Temperature on the Ultimate Tensile Shear Strength of Annealed Ti-6Al-4V Sheet and Bar	227
119	Effect of Temperature on the Ultimate Bearing Strength and Bearing Yield Strength of Annealed Ti-6Al-4V Sheet and Bar . . .	228
120	Effect of Temperature on the Tensile and Compressive Moduli of Annealed Ti-6Al-4V Sheet and Bar	229
121	Effect of Temperature on the Thermal Conductivity of Ti-6Al-4V (Annealed or Solution Heat-Treated and Aged)	230

Figure		Page
122	Effect of Temperature on the Specific Heat of Ti-6Al-4V (Annealed or Solution Heat-Treated and Aged)	231
123	Effect of Temperature on the (Mean) Linear Coefficient of Thermal Expansion of Ti-6Al-4V	232
124	Creep Properties of Solution Heat-Treated and Aged Ti-6Al-4V Sheet	234
125	Effect of Temperature on the Physical Properties of 17-4PH Stainless Steel . .	237
126	Effect of Temperature on the Ultimate Tensile Strength (F_{tu}) of 17-4PH Stainless Steel (Bar and Forgings)	238
127	Effect of Temperature on the Tensile Yield Strength (F_{ty}) of 17-4PH Stainless Steel (Bar and Forgings)	238
128	Effect of Temperature on the Compressive Yield Strength (F_{cy}) of 17-4PH Stainless Steel (Bar and Forgings)	239
129	Effect of Temperature on the Ultimate Shear Strength (F_{su}) of 17-4PH Stainless Steel (Bar and Forgings)	239
130	Effect of Temperature on the Bearing Ultimate Strength (F_{bru}) of 17-4PH Stainless Steel (Bar and Forgings)	240
131	Effect of Temperature on the Bearing Yield Strength (F_{bry}) of 17-4PH Stainless Steel (Bar and Forgings)	240
132	Effect of Temperature on the Tensile and Compressive Modulus (E and E_c) of 17-4PH Stainless Steel (Bar and Forgings) . . .	241
133	Constant-Life Diagram, 17-4PH Bar and Wire	242
134	Plane Strain Fracture Toughness of Ten Heats of Annealed and Aged Plate as a Function of Yield Strength	244

Figure		Page
135	Effect of Temperature on Compressive Yield Strength of 280-KSI Bar	244
136	Effect of Test Temperature on Tensile Properties of Annealed and Aged Bar . . .	245
137	Effect of Test Temperature on Shear Ultimate Strength of 250- and 280-KSI Bar	245
138	Effect of Test Temperature on Bearing Strength of 280-KSI Bar	246
139	Effect of Test Temperature on the Tensile Properties of Two Heats of 250-KSI CVM Sheet	246
140	Constant-Life Fatigue Diagram for 18 Ni (250 Grade) Maraging Steel; Room Temperature, K_t = 1.0, Smooth, Polished .	247
141	K_f Versus Cycles, Welded 250 Grade Maraging Steel, R = 0.1	248
142	Effect of Temperature on the Physical Properties of AISI 4130	251
143	Effect of Temperature on the Ultimate Strength (F_{tu}) of AISI Alloy Steels . . .	252
144	Effect of Temperature on the Tensile Yield Strength (F_{ty}) of AISI Alloy Steels	253
145	Effect of Temperature on the Compressive Yield Strength (F_{cy}) of Heat-Treated AISI Alloy Steels	254
146	Effect of Temperature on the Shear Ultimate Strength (F_{su}) of Heat-Treated AISI Alloy Steel	254
147	Effect of Temperature on Ultimate Bearing Strength (F_{bru}) of Heat-Treated AISI Alloy Steels	255
148	Effect of Temperature on the Bearing Yield Strength (F_{bry}) of Heat-Treated AISI Alloy Steels	255

Figure		Page
149	Effect of Temperature on Tensile and Compressive Modulus (E and E_c) of AISI Alloy Steels .	256
150	Typical Tensile Tangent-Modulus Curves at Room Temperature for Heat-Treated AISI 4340 Alloy Steel	257
151	Constant-Life Fatigue Diagram for 4130/4340 Steel Weldments, Heat-Treated to 150-KSI Ultimate Tensile Strength	258
152	Constant-Life Fatigue Diagram for 4340 Steel Weldments, Heat-Treated to 180-KSI.	259
153	Constant-Life Fatigue Diagram for Carpenter Custom 455 at Room Temperature and 200°F . .	262
154	Baron Epoxy Characterization - Goodman Diagram	264
155	Goodman Strain Diagram at 10^7 Cycles for E and S Glass Epoxy Unidirectional Laminates .	268
156	Goodman Strain Diagram at 10^7 Cycles for E and S Glass Epoxy $\pm$ 45° Laminates	275
157	Goodman Strain Diagram at 10^7 Cycles for E and S Glass Epoxy 50%-0°/50%-90° Laminates .	276

LIST OF TABLES

Table		Page
I	Gear Mesh Speed and Reduction Ratios - Main Transmission	33
II	CH-54B Acessories, Design Powers, Speeds and Unit Weights	38
III	CH-54B Component Weight and Center of Gravity Locations	53
IV	Summary Crash Load Design Criteria	57
V	CH-54B Planetary Gear Data	70
VI	Strength Criteria for Final Selection of Materials for Fabricated Housing Analysis . .	78
VII	Material Cost Criteria for Final Selection of Materials for Fabricated Housing Analysis.	79
VIII	Material Trade-Off Selection Chart	81
IX	Thermal Conductivities of Material Candidates	88
X	Static Joint Efficiencies of Weldments for Material Candidates	97
XI	Summary of Weight and Housing Stiffness for Various Candidate Materials	129
XII	Cost Comparison, Conventional Casting Versus Fabricated Housing Design	141
XIII	Summary Table of a Cast Magnesium Housing with the Fabricated Truss Housing Design	148
XIV	Changes in Applied Housing Loads for a $\pm$ 25 Percent Change in Input Torque	159
XV	10-Hour Dual-Engine Endurance Test Cycle . .	166
XVI	R/H Input Accessory Pad Loading	167
XVII	Dual-Engine Overtorque Test Cycle	169
XVIII	General Dimensions, CH-54B	175
XIX	Rotor Dimensions, CH-54B	177

Table		Page
XX	Fuselage/Landing Gear Data, CH-54B	178
XXI	Mechanical Properties of AZ91C-T6	185
XXII	Mechanical Properties of ZE41A-T5	187
XXIII	Mechanical Properties of 6061-T6	197
XXIV	Mechanical Properties of 7075-T736	203
XXV	Fracture Toughness Properties of 7175-T736 Aluminum Alloy Forging	209
XXVI	Typical Room Temperature Fracture Toughness Properties for Several High-Strength Aluminum Alloys	210
XXVII	Mechanical Properties of Titanium Beta Forging ST0A MIL-T-9097 Type III, Composition A . .	216
XXVIII	Mechanical Properties of Titanium 6Al-4V Extrusions, BETA extruded MIL-T-81556, Type III, Composition A	221
XXIX	Typical Elevated Temperature Deformation and Rupture Properties of Mill Annealed Ti-6Al-4V Sheet	233
XXX	Mechanical Properties of 17-4PH Stainless Steel H1025	236
XXXI	Mechanical Properties of 4130/4340 Steel . .	250
XXXII	Mechanical Properties of Carpenter Custom 455	261
XXXIII	Physical Properties of Boron Epoxy, Boron Filament and Resin Matrices	265
XXXIV	Elastic Constants of Boron Epoxy Composites	267
XXXV	Strength and Proportional Limit of Boron Epoxy Composites	269
XXXVI	Physical Properties of Glass Epoxy Composites, Glass Filament and Epoxy Resin Matrices . .	271
XXXVII	Ultimate Strength, Proportional Limit and Elastic Constants for Glass Epoxy	273

Table		Page
XXXVIII	Elastic Constants for Graphite Epoxy Composites	277
XXXIX	Physical Properties of Graphite Epoxy Graphite Filaments and Resin Matrices	278
XXXX	Strength and Elastic Constants for Graphite Epoxy Composites	279

INTRODUCTION

Since 1946, helicopter transmission housings have been made of cast magnesium alloys, generally AZ91C and ZE41A. Such housings are extremely light in weight and can be cast in complex shapes for gear and bearing supports. Their disadvantage is that the alloys possess relatively low strength and are subject to problems of porosity, segregation, and other defects as a result of the casting process. AZ91C magnesium casting alloy has an allowable fatigue strength of only 3,000 psi, compared with high-strength steel, which has fatigue strengths approximately ten times this value. In addition, magnesium alone lacks corrosion resistance. The corrosion resistance of magnesium housings is achieved through use of protective coatings, such as baked resins and acrylic lacquers. Low fracture toughness and low fatigue propagation resistance also make cast magnesium housings susceptible to ballistic damage. Another disadvantage of magnesium castings is that they require excessive wall thickness to compensate for core shift during pouring and to assure adequate fill in large sections. Weld repair of castings was developed to solve this lack-of-fill problem and is widely used in the aircraft industry. The problems with present-day castings have increased as cast housings have become increasingly large and complex, and there is an increasing need for stronger and lighter-weight designs.

One of the first uses of cast magnesium for a helicopter transmission housing was on the H-5 aircraft. This casting was used primarily for oil retention and for gear and bearing support structure. A tube-truss arrangement was designed, in conjunction with the casting, to transfer the large main rotor loads to the airframe. Figures 1 through 4 show the cast housing designs with tube truss structures for the H-5 in 1946, H-19 in 1949, H-34 in 1953, and H-37 in 1954. In 1958, with the development of the H-3 transmission, knowledge of magnesium alloy properties and casting technology had improved sufficiently so that a three-piece cast main housing could be designed to react main rotor loads in addition to internal gear and bearing loads. The H-3 housing, shown in Figure 5, is shaped as a box and is an assembly of three separate castings. In this arrangement, the main rotor loads are reacted in the center casting and then transferred through flexibly connected end housings to the mounting feet.

Housing deflections associated with this design caused problems in developing proper bevel gear meshing. In addition, low-stress/high-time creep problems occurred in service, requiring corrective overhaul procedures. With the H-54 transmission, designed in 1961, the problems of lack of stiffness and creep were eliminated by a design in which main rotor load path to the airframe was minimized. Figure 6 shows the two-piece conical H-54 main housing, which consists of an upper cast

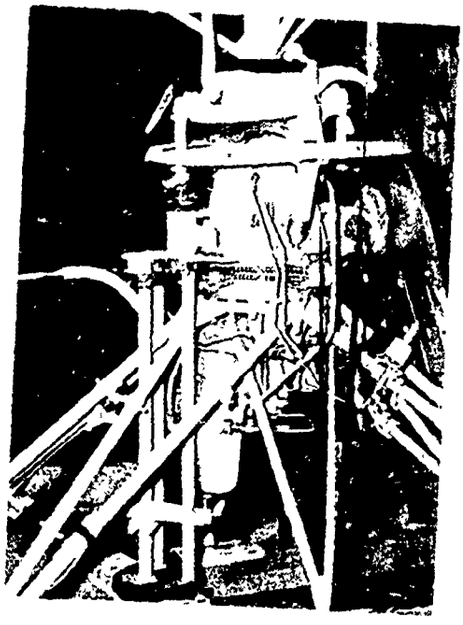

Figure 1. H-5 Main Housing.

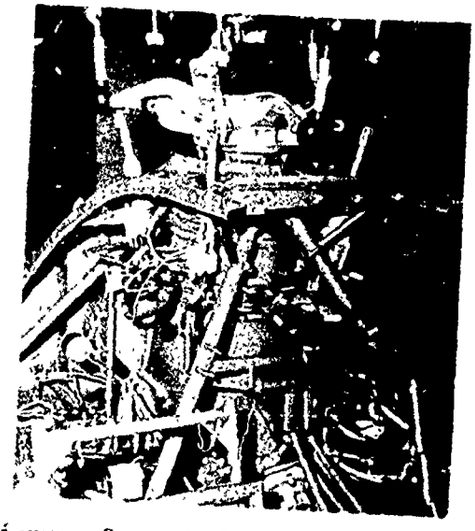

Figure 2. H-19 Main Housing.

Figure 3. H-34 Main Housing.

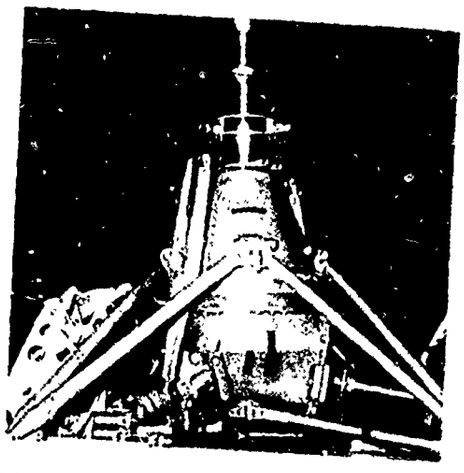

Figure 4. H-37 Main Housing.

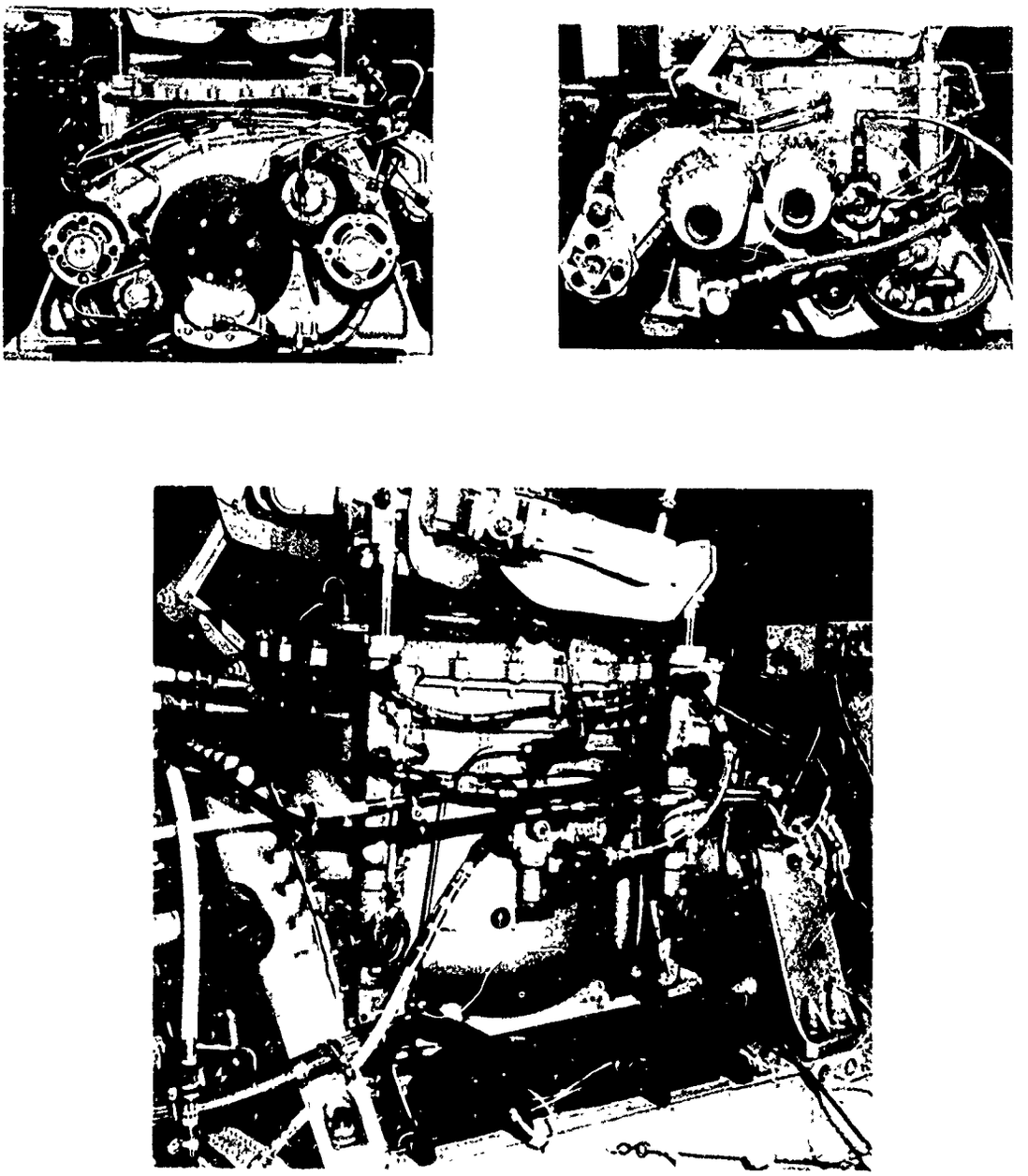

Figure 5. Three-View of H-3 Main Housing.

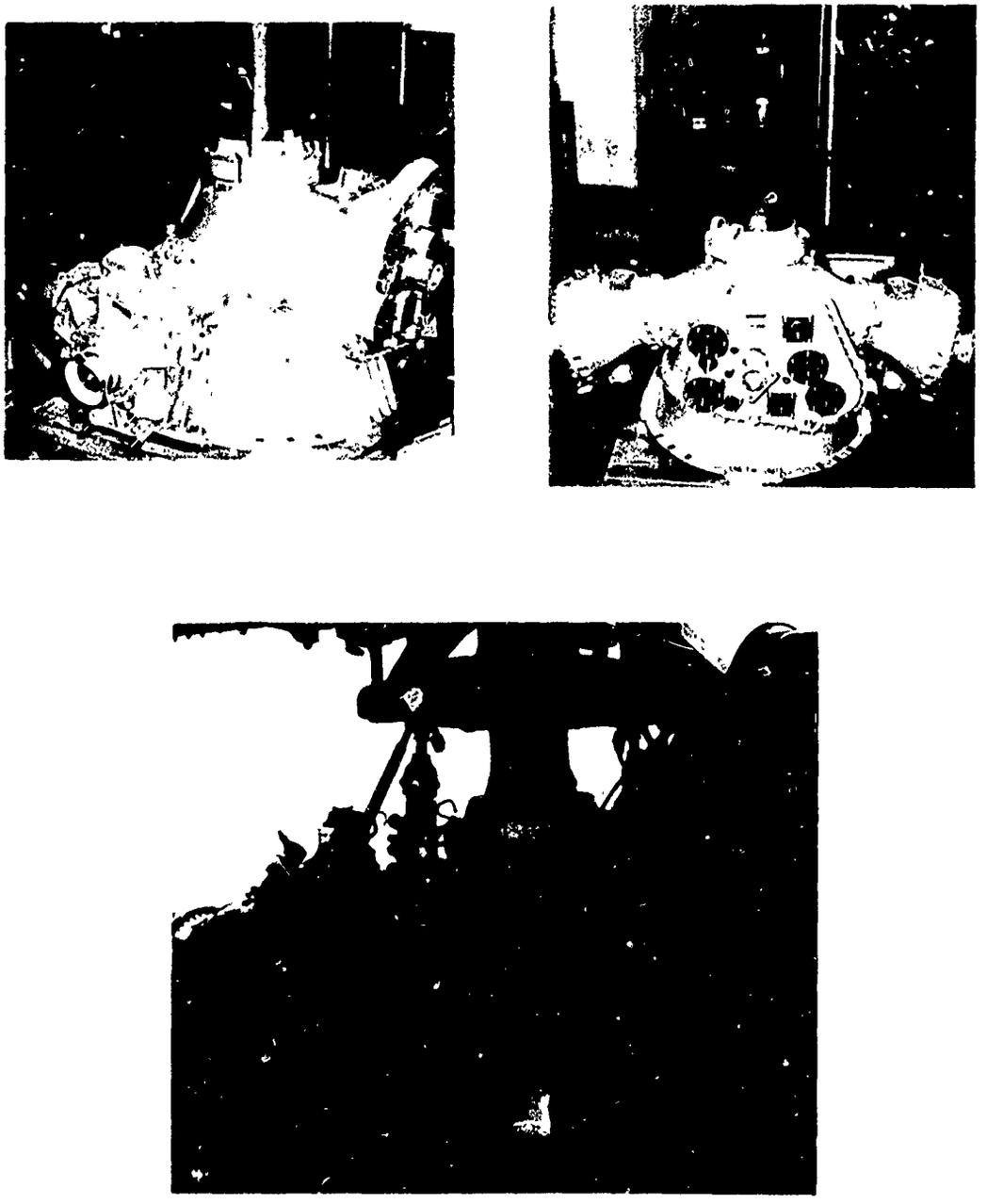

Figure 6. H-54 Main Housing, Composite Views.

magnesium housing and a lower forged magnesium support housing with four mounting feet. At the time, the H-54 upper cast housing represented one of the world's largest magnesium castings. Casting technology continued to improve, however, and the H-53 main housing was designed in 1963 as a one-piece conical housing have cast mounting feet as shown in Figures 7 and 8. The XH-59A main housing, shown in Figure 9, designed in 1972, is very similar to the H-53 but less complex. The CH-53E cast housing designed in 1973, is similar to the H-53, but is more complex because of the third engine input. This housing, shown in Figure 10, makes extensive use of the weld repair procedure to obtain a structurally adequate casting.

Due to the size and complexity of a cast housing, it is difficult, if not impossible, to analyze it to the degree necessary to minimize its weight. The result is often an over-designed and overweight housing.

Little improvement is seen in the future of magnesium casting technology, and changing design requirements will demand increased size and complexity for transmission castings. Static and fatigue strength of cast magnesium housings remains relatively low. At transmission overhaul, the rework frequency is high as a result of corrosion and creep. These problems are still unresolved.

As a result, a new design is being sought that would eliminate casting and material problems, enable accurate structural analysis, and provide a structure with improved stiffness and support characteristics. Improvements are also sought in weight, reliability, crashworthiness, corrosion resistance, inspectability, and maintainability.

One approach that is being considered is a skin-covered truss-like fabricated structure that performs the functions of a cast magnesium transmission housing. By exploiting the latest advances in material technology, joining methods, and structural analysis techniques, such a structure promises low weight, high reliability, improved crashworthiness, increased corrosion resistance, increased access for inspection, and elimination of creep.

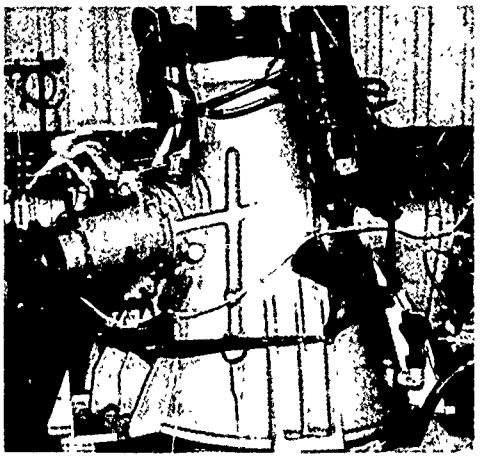

Figure 7. H-53 Main Housing, Side View.

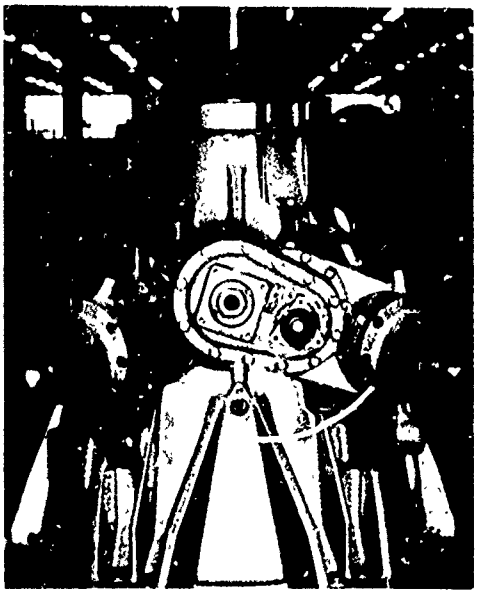

Figure 8. H-53 Main Housing, Front View.

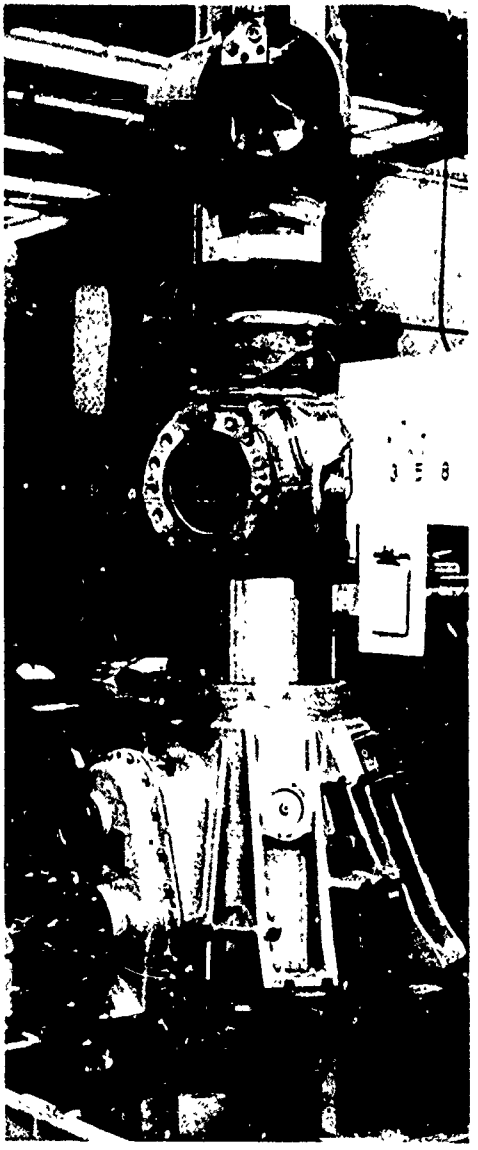

Figure 9. XH-59A Main Housing, Three-Quarter View.

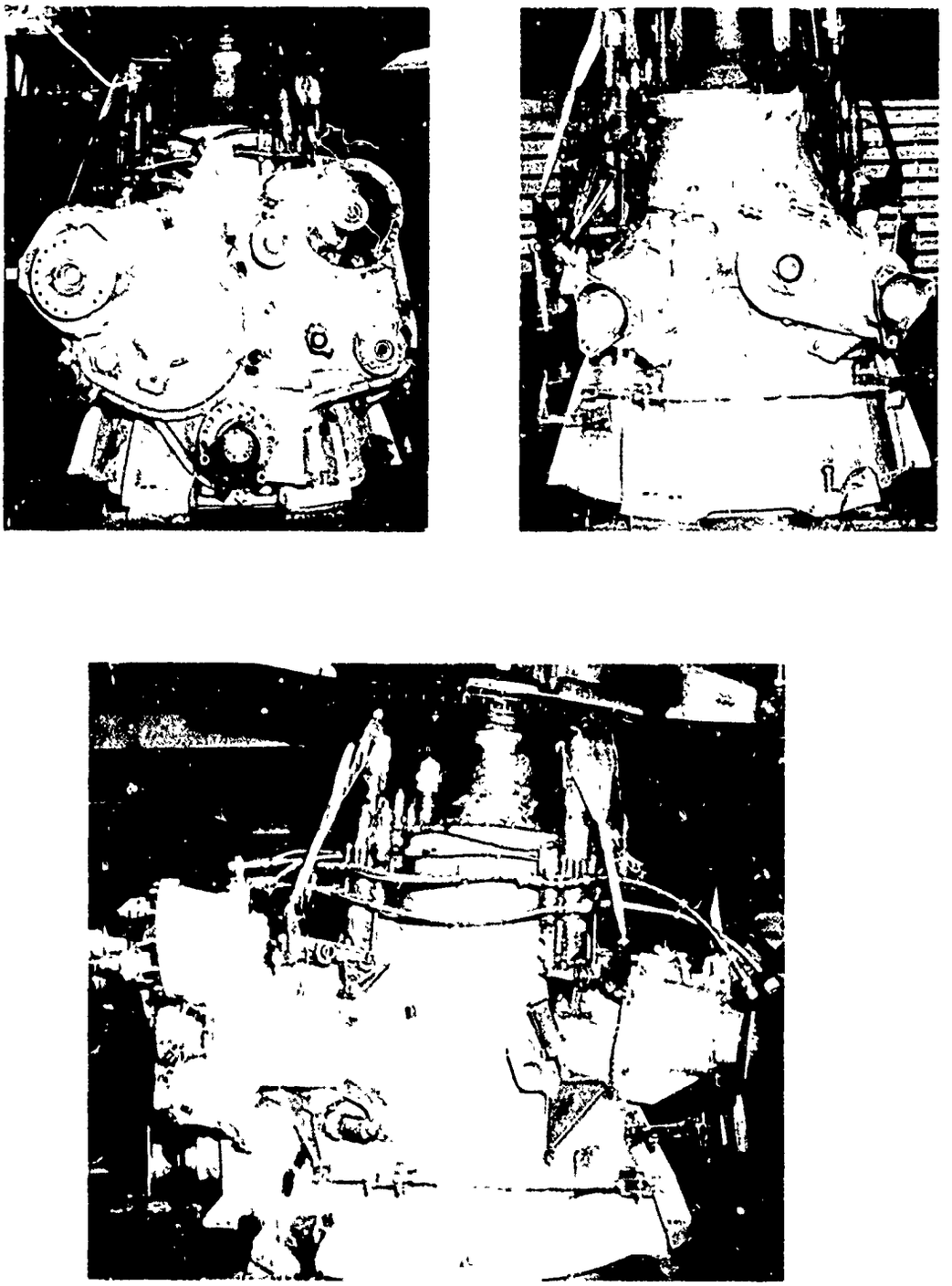

Figure 10. Three-View, CH-53E Main Housing.

DESIGN APPROACH

Figure 11 is a flow chart of the approach taken in designing the truss-like fabricated transmission housing.

The cast housing was examined to ascertain interface requirements between the fabricated housing and its mating housings and accessories. The fabricated truss-like housing will replace the upper main casting and the lower support forging and meet all the functional and structural requirements of the CH-54B housing.

The design criteria were then established. These included applied loads for flight and crash conditions, and housing stiffness requirements. To determine crash loads for 18g side, 20g forward, and 20g vertical given in Reference 13, weights were determined for all accessories and modules suspended from the main housing, and for all dynamic components. Items included in the component weights were the main rotor head, rotor blades, swashplate assembly, main rotor controls, and internal gearing. Flight loads on the fabricated housing were determined for the most severe loading condition, i.e., the symmetric dive and pullout maneuver. Stiffness and deflection criteria were derived from a simplified membrane analysis of the cast housing.

Truss geometries, materials and joining methods were then investigated. Design layouts of possible truss configurations were produced for preliminary analysis. Concurrently, materials and joining methods studies were conducted. The materials investigated included steel, aluminum, titanium, magnesium and composites. The joining methods reviewed for possible use with these materials included bonding, brazing, bolting, riveting and welding. This investigation resulted in the selection of three possible truss configurations and the decision to use welded steel, welded titanium or brazed Borsical®. Design plan views of the three configurations chosen are shown in Figure 11.

Through an analysis in a redundant structures program (NASTRAN), and a comparison with the cast housing design, the fabricated structures were modified to satisfy the design criteria. For the analysis, the structure geometry and the applied loads for various maneuver conditions were coded for NASTRAN. This redundant structures program was used in conjunction with Sikorsky's Data Editor Program, which has a cathode-ray tube display capability.

At the conclusion of these analyses, a final design configuration was selected. A plan view of the final design configuration is shown in the flow chart. The final design was subjected to structural analysis and to assessment of reliability, maintainability, inspectability, cost, weight, crash-

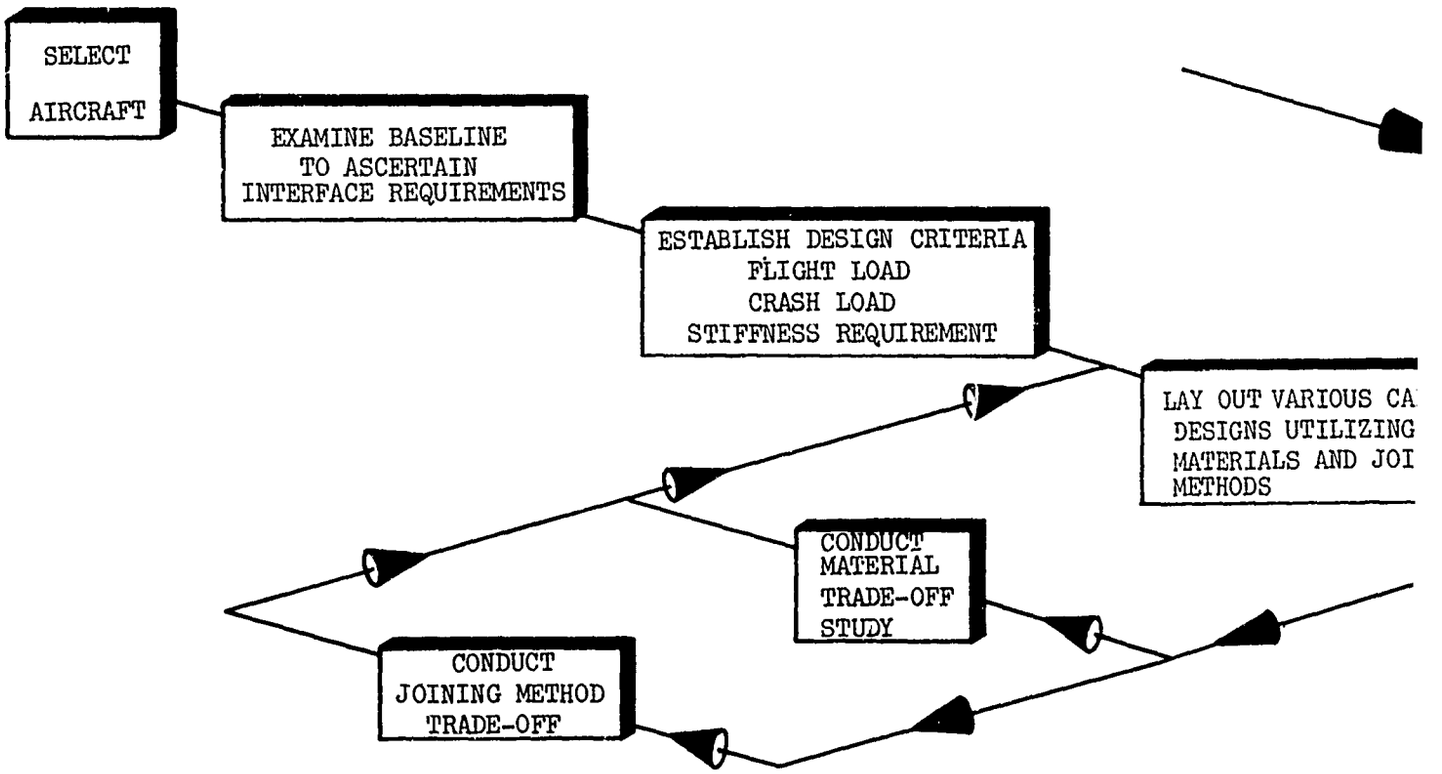

Figure 11. Flow Chart of Approach to Fabricated Helicopter Transmission Housing Analysis.

LAY OUT VARIOUS CANDIDATE DESIGNS UTILIZING VARIOUS MATERIALS AND JOINING METHODS

COMBINE VARIOUS CONFIGURATIONS FOR 3 FUNDAMENTALLY DIFFERENT DESIGNS WITH VARIOUS MATERIALS

ANALYZE REDUNDANT STRUCTURE USING -NASTRAN

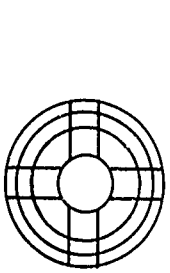

"A" FRAME

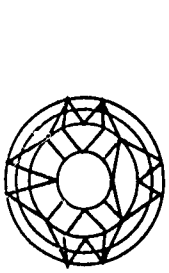

TRUSS

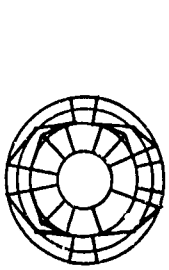

PYRAMID

COMPARE FABRICATED HOUSING WITH CASTING DESIGN

EDUNDANT STRUCTURE
STRAN

ANALYZE DETAIL DESIGN CONFIGURATION

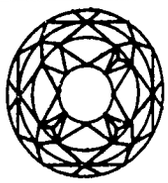

FINAL DESIGN

CONDUCT SENSITIVITY STUDY ± 25% IN LOAD

ESTABLISH DEVELOPMENTAL AREA DEFINITION

DERIVE CONCLUSION

worthiness, corrosion resistance, and heat dissipation characteristics.

To acquire trending data, a sensitivity study was conducted for a +25% change in input torque. Payload to gross weight fraction and rotor tip speed were held constant. Rotor size, head moment constant, and group weight fractions were determined. The fabricated housings were then resized, with the newly developed flight and crash applied loads and the scaled internal gear and bearing loads.

During the course of the study, problem areas were uncovered that would require additional development before a fabricated housing design could be incorporated in flight hardware. As a result, development areas were defined, and a test plan was written to demonstrate functional and structural aspects of the design.

On the basis of the analysis, the characteristics of the final design were assessed, and overall conclusions drawn.

Aircraft Selection

The U. S. Army CH-54B is the largest operational helicopter in the free world. It also has the best payload/gross weight ratio. With expanding heavy lift helicopter uses, weight and cost might be reduced significantly through application of the fabricated truss-like housing to the CH-54B aircraft.

The CH-54B aircraft was selected for this study because of the large size of its components, the large number of aircraft in the field, and the existence of extensive reliability and maintainability data.

Appendix I presents the dimensional and performance characteristics of the CH-54B aircraft.

Description of Aircraft

The U. S. Army CH-54B helicopter (Figure 12) chosen for this study is a heavy-duty vertical lift aircraft. It has the ability to pick up, transport, and place heavy external loads with precision.

The CH-54B has twin engines rated at 4,800 horsepower each and transmits 7,800 horsepower to the main rotor. The six main rotor blades form a diameter of 72.2 feet. The CH-54B helicopter has a lifting ability exceeding 12 tons and an overall length of 88 feet 6 inches. Figure 13 is a three-view drawing of the CH-54B aircraft.

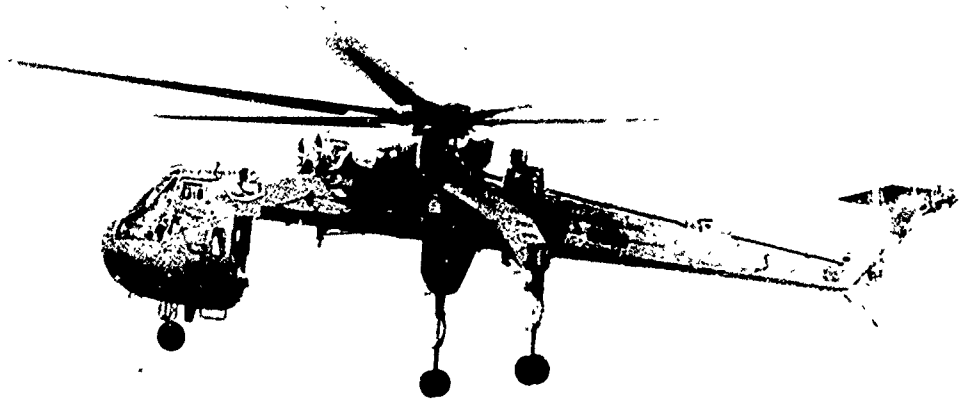

Figure 12. U. S. Army CH-54B Aircraft.

Description of Drive Train

The drive train for the CH-54B helicopter (Figure 14) consists of two JFTD12A-5A engines rated at 4,800 horsepower each, a main transmission, intermediate gearbox, a tail gearbox and interconnecting shafting. Power is transmissted by each engine directly to a four-stage reduction main transmission, which reduces the engine speed of 9,000 rpm to 185 rpm at the main rotor, an overall reduction ratio of 48.54 to 1. Power is also transmitted from the tail/accessory drive section of the main transmission through the tail drive shaft at 3016 rpm to the intermediate gearbox. The intermediate gearbox in turn drives through the tail gearbox to the tail rotor, which turns at 850 rpm.

The intermediate gearbox (Figure 15) consists of an input bevel gear, idler bevel gear, and output bevel gear. The design incorporates a self-contained lubrication system. The sump-located oil pump is driven from the back of the idler bevel gear.

The tail gearbox assembly (Figure 16) consists of a right-angle bevel mesh, with the output bevel attached through a series of bolts to the tail rotor shaft. The tail rotor servo, which is fixed to the back of the cast magnesium gearbox housing, is attached through thrust bearings to the pitch control shaft. The pitch control shaft is concentric and supported in a bushing by the tail rotor output shaft. The pitch control shaft, which is capable of linear motion within the tail rotor

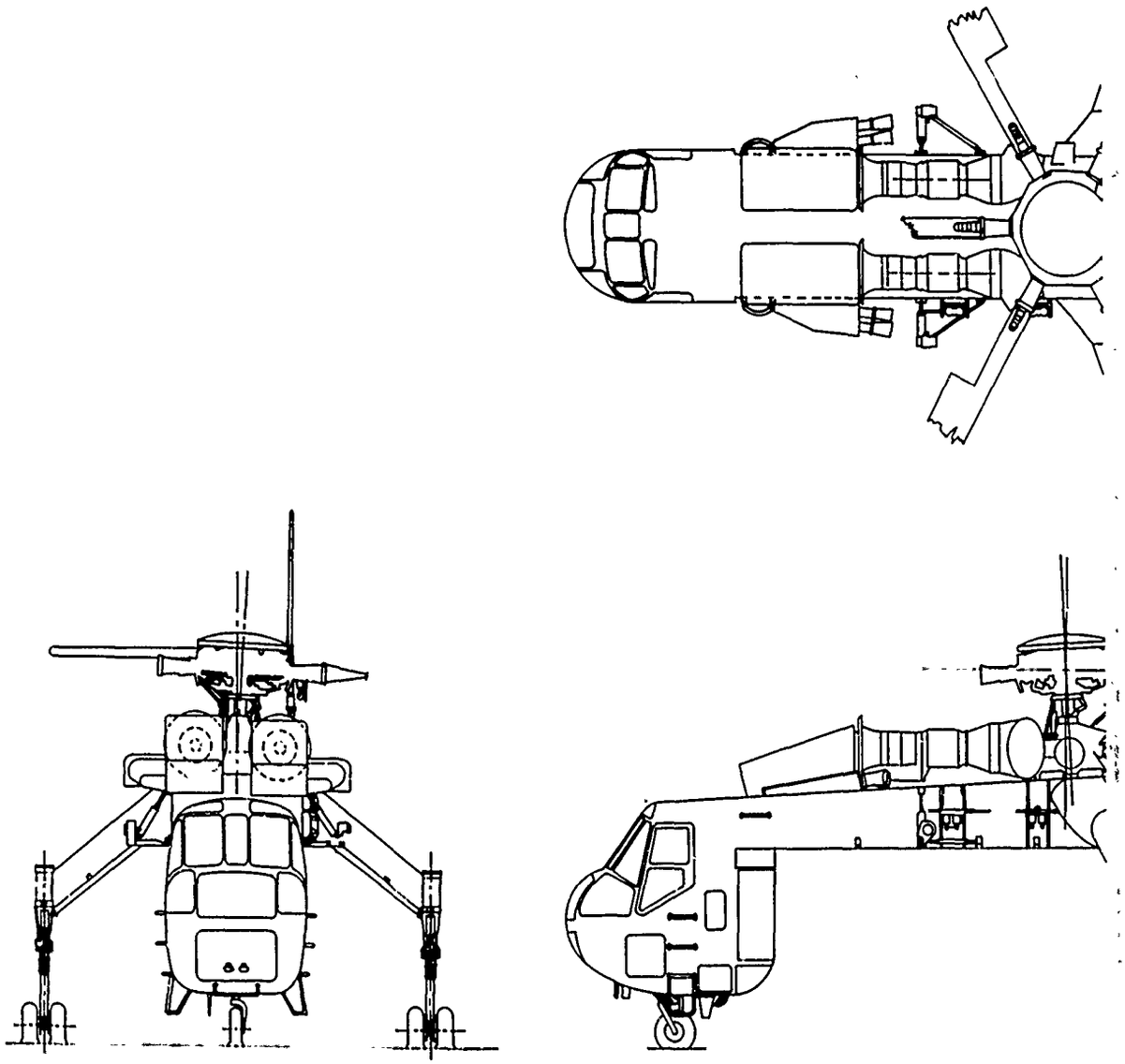

Figure 13. U. S. Army CH-54B Aircraft, Three-View Drawing.

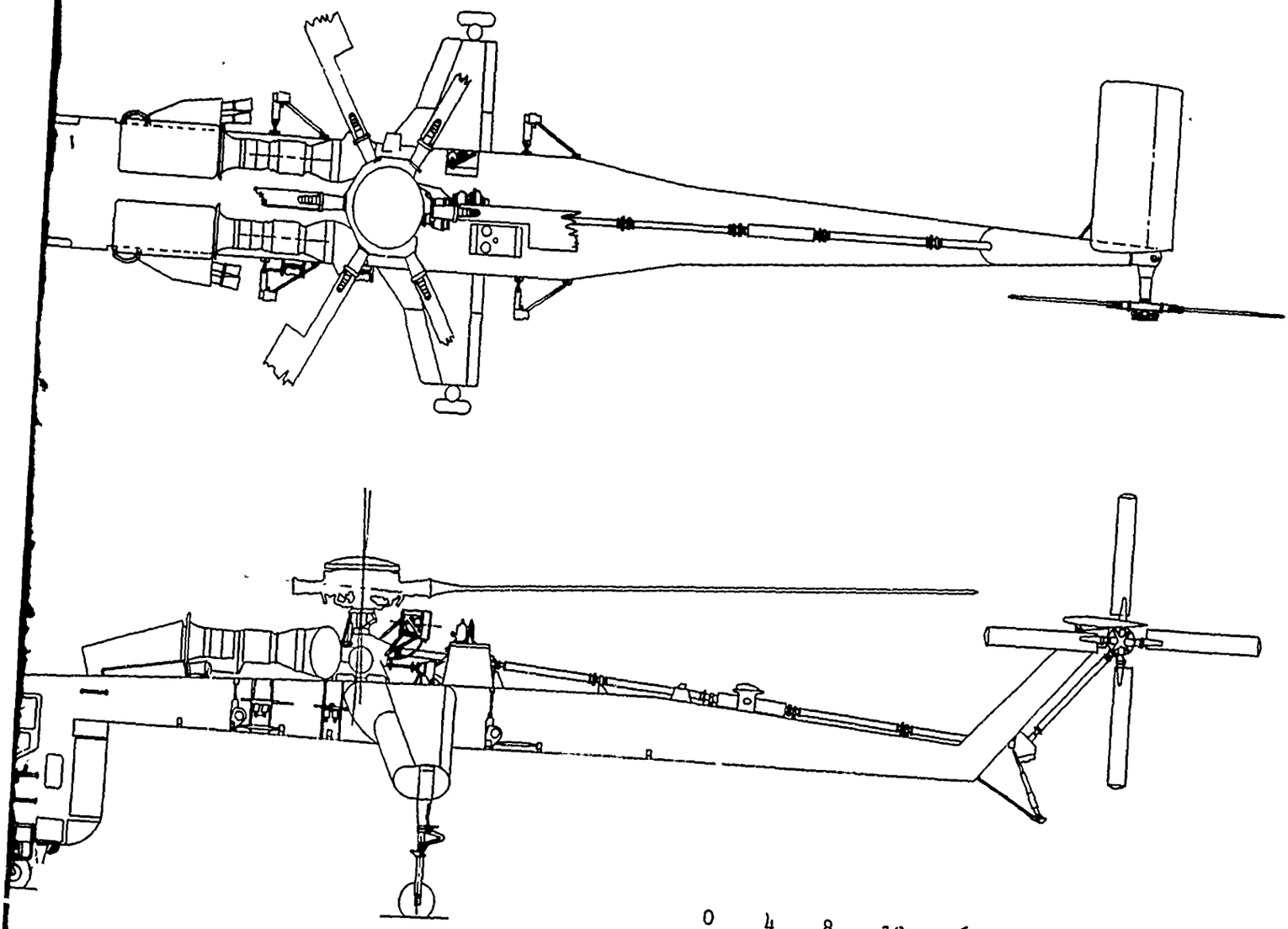

ft, Three-View

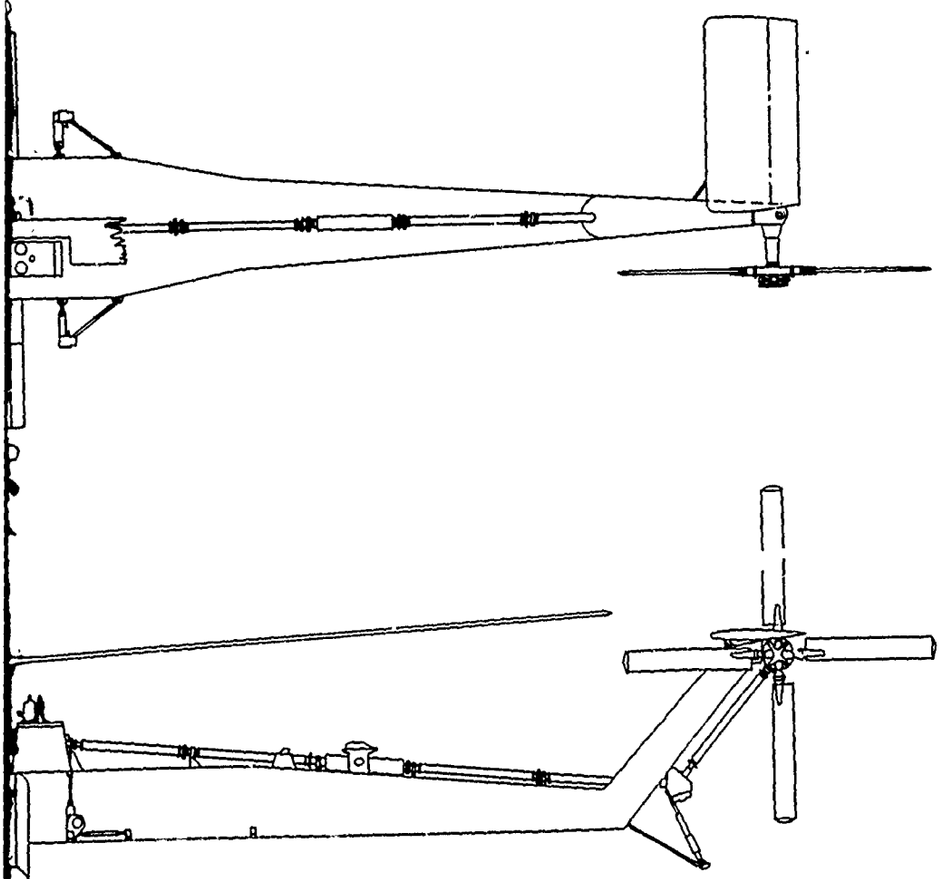

0 4 8 12 16

SCALE (feet)

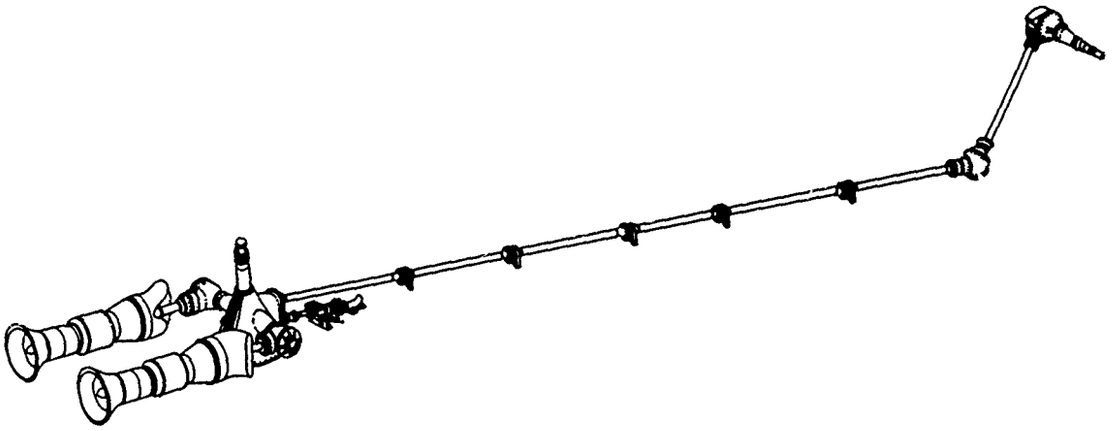

Figure 14. Isometric of Drive Train Components of the CH-54B Aircraft.

output shaft, supports the pitch beam. Tail rotor blade pitch is controlled through a series of pitch links. The lubrication system of the tail rotor gearbox is of simple splash design.

Description of Main Gearbox

An isometric of the CH-54B main transmission drive train scheme is presented in Figure 17. Table I contains a list of reduction ratios and speeds for each gear mesh.

TABLE I. GEAR MESH SPEED AND REDUCTION RATIOS - MAIN TRANSMISSION

Gear Mesh	Reduction	Input (rpm)	Output (rpm)
Input Bevel Set	27/53	9000	4585.9
Main Bevel Set	25/76	4585.9	1508.2
First-Stage Planetary	78/55/188	1508.2	442.3
Second-Stage Planetary	166/32/230	442.3	185.4
Tail-Takeoff Bevel Set	76/38	1508.2	3016.4

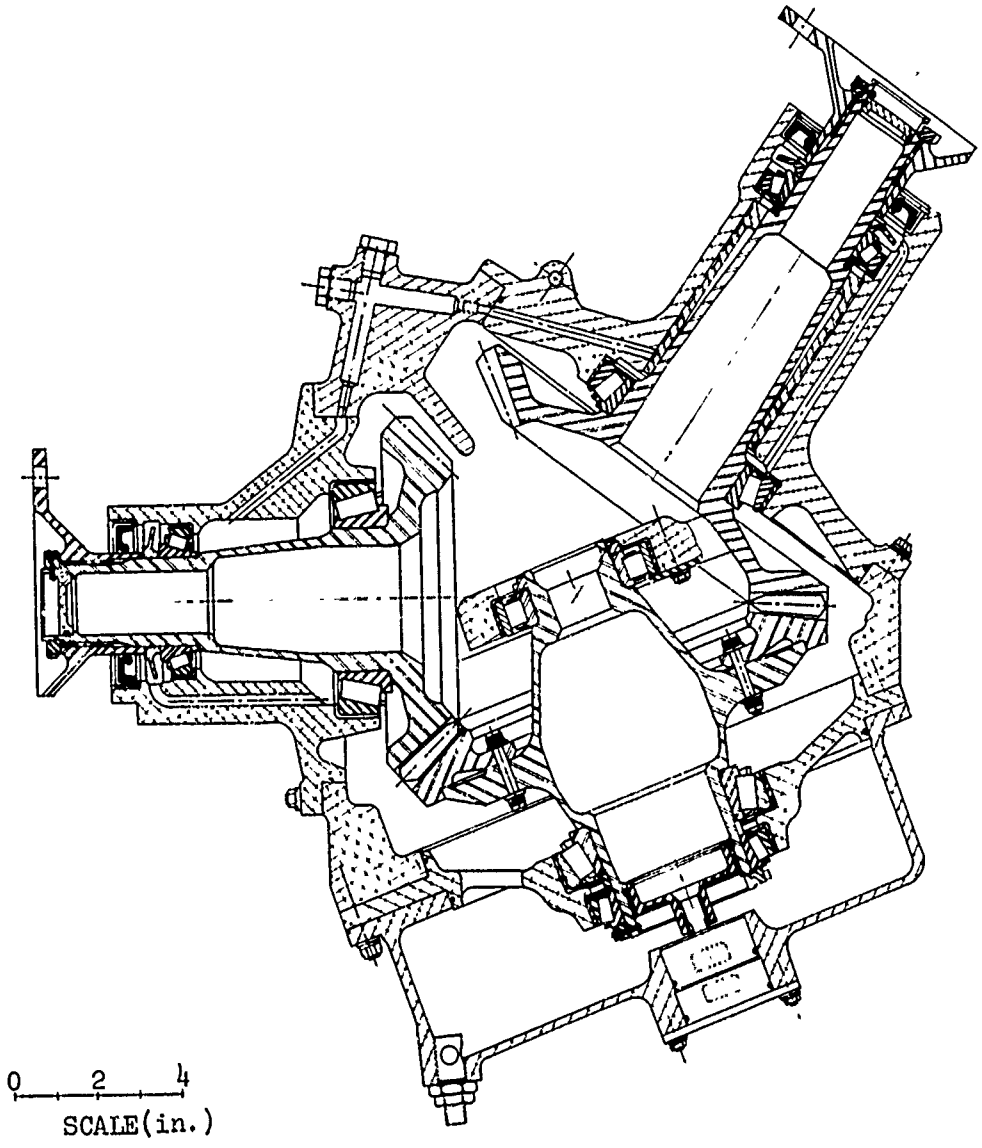

Figure 15. Intermediate Gearbox, CH-54B Aircraft.

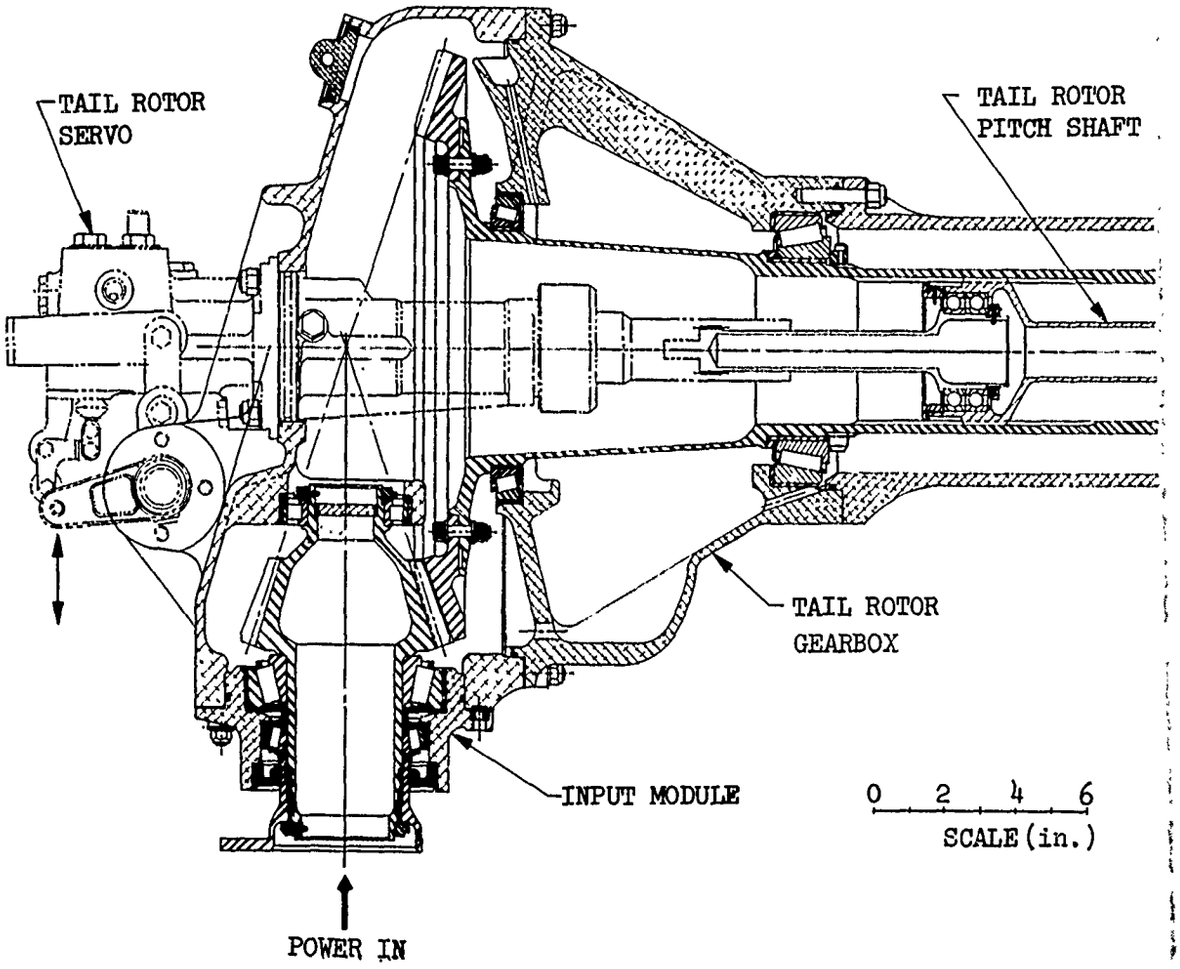

Figure 16. Tail Gearbox, CH-54B.

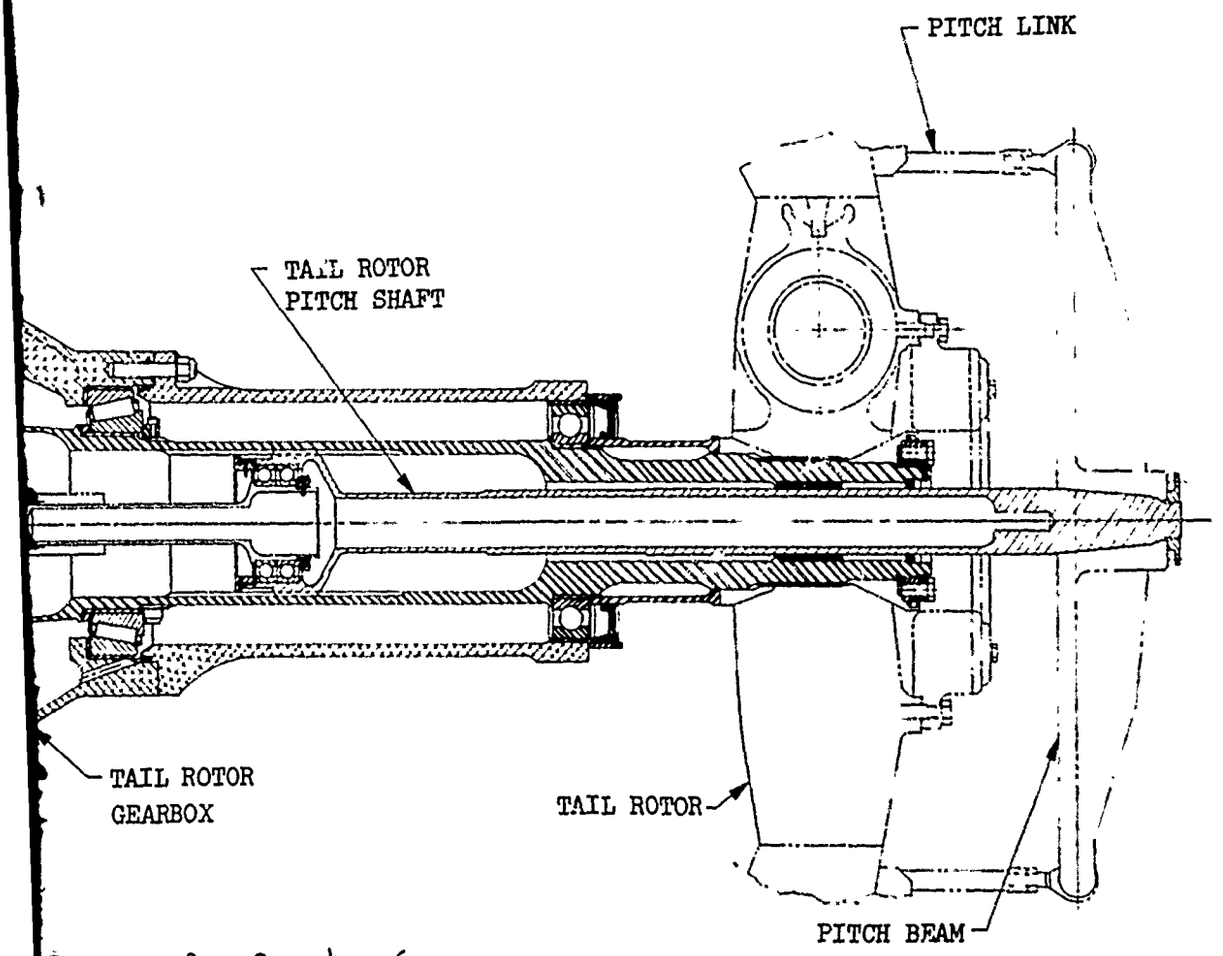
PITCH LINK
TAIL ROTOR
PITCH SHAFT
TAIL ROTOR
GEARBOX
TAIL ROTOR
PITCH BEAM
0 2 4 6
SCALE (in.)

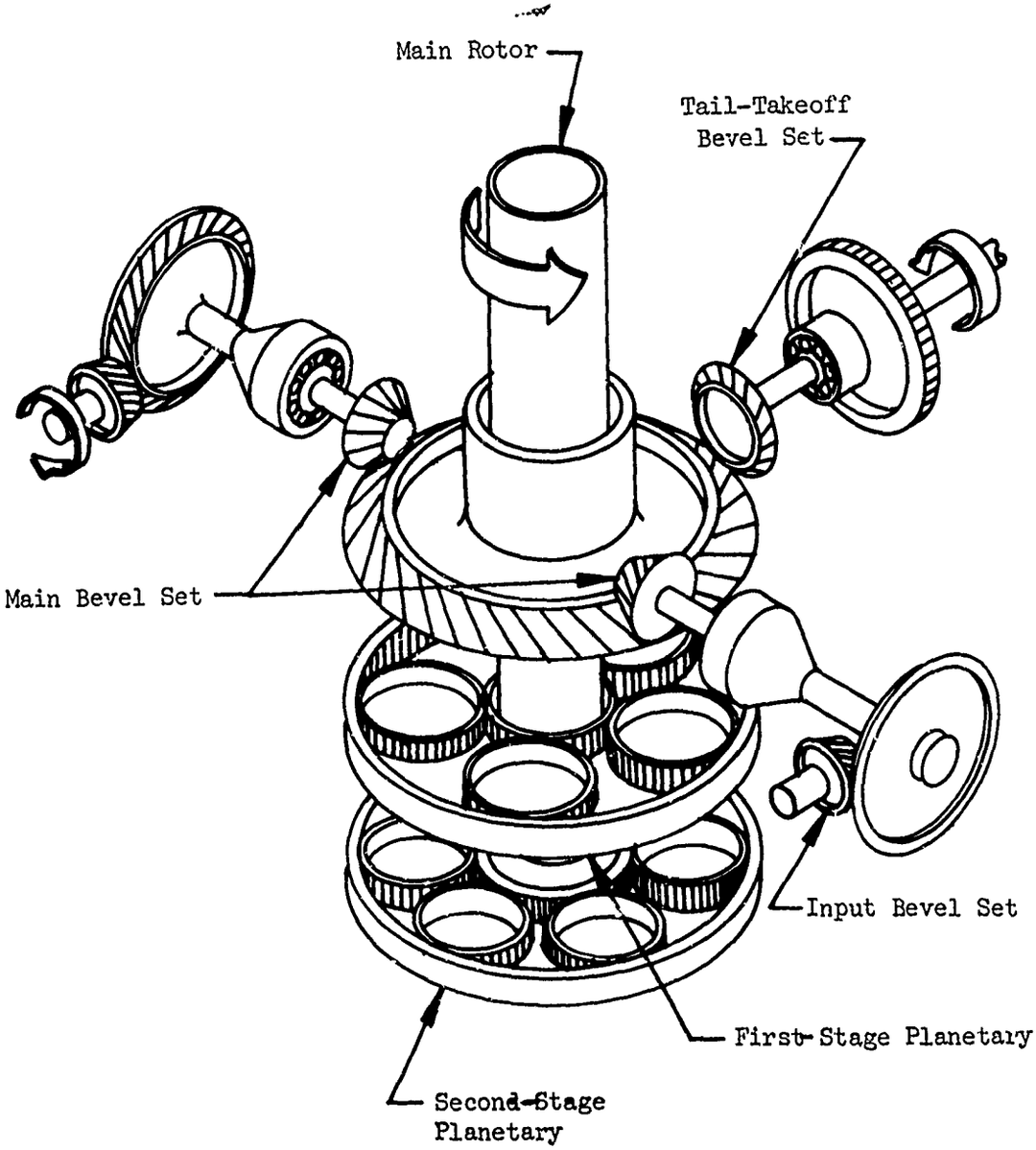

Figure 17. Isometric of CH-54B Main Transmission Drive Train Scheme.

The accessories driven by the main transmission are located on the right-hand input bevel housing and on the main transmission rear cover. Figure 18 shows the location of the various rear cover mounted accessories. Table II lists the CH-54B accessories, design powers, speeds, and accessory weights.

TABLE II. CH-54B ACCESSORIES, DESIGN POWERS, SPEEDS, AND UNIT WEIGHTS

Accessory Name	Design Horsepower	Speed (rpm)	Weight (lb)
#1 Generator	49.2	8025.7	64
#2 Generator	49.2	8025.7	64
Tachometer Generator	1.0	4200.	.2
Utility Pump	53.0	4321	22.16
Winch Pump	100.0	3797.	20.
Second-Stage Servo Pump	24.0	4585.	14.1
First-Stage Servo Pump	19.0	4321.	14.7
Tail-Takeoff Drive	1220.0	3016	-

Figure 19 is a cross section of the CH-54B main transmission assembly. Power is transmitted from the engines through a drive shaft, with a torquemeter mounted concentric to the shaft, to a first-stage spiral bevel gear mesh. This mesh has a 27-to-53 ratio. It is designed to transmit 4,800 horsepower continuously at an engine input speed of 9,000 rpm. The spiral bevel gears used in the first stage have a 3.313-diametral pitch, a 2.875-inch face width, a 20-degree pressure angle, and a 25-degree spiral angle. The first-stage spiral bevel gear mesh is identical on right and left inputs to the main housing. This permits both inputs and housings to be interchangeable.

Located between the first-stage bevel mesh and second-stage bevel mesh on both the right and left sides are ramp roller overrunning clutches. These clutches enable disengagement of the engine power turbine and first-stage spiral bevel mesh from the rest of the drive train during autorotation and under

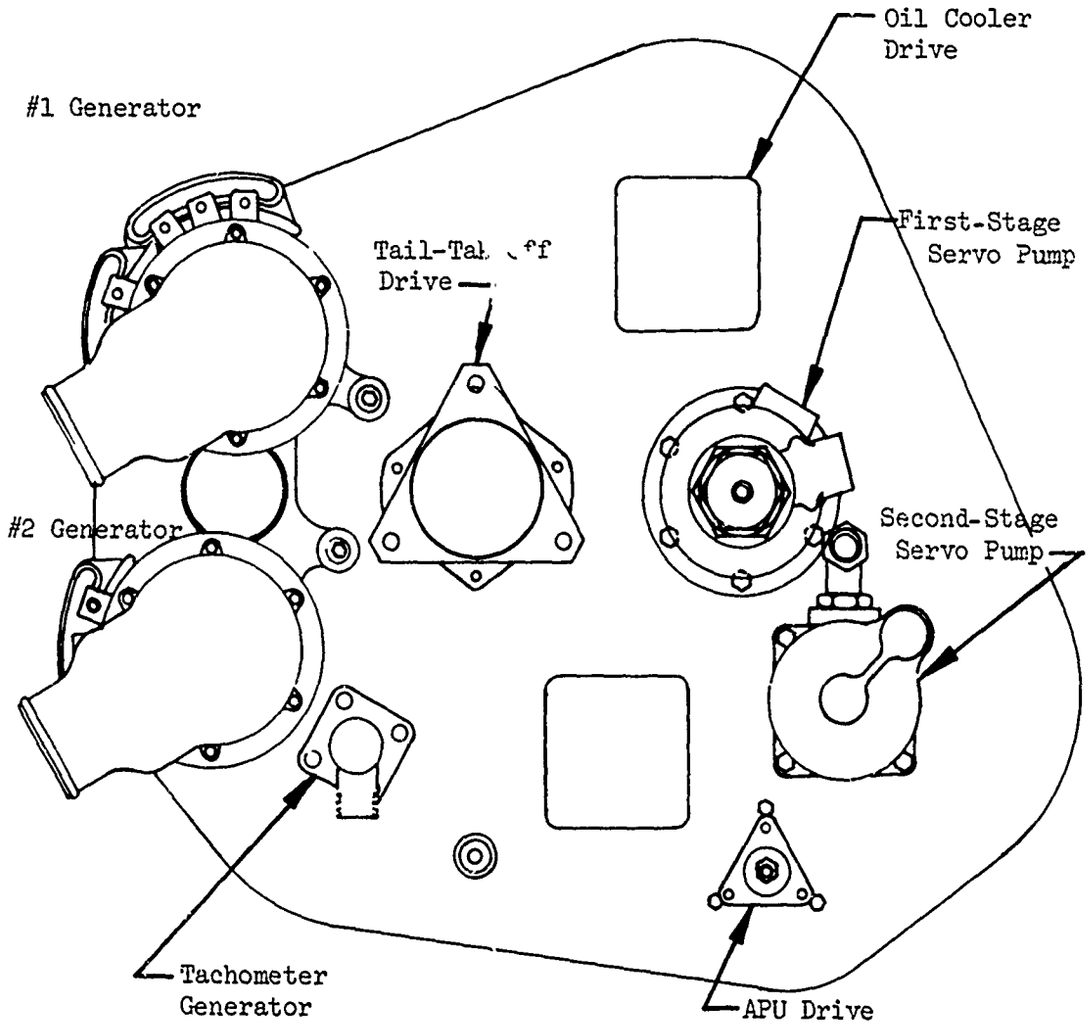

Figure 18. Rear Cover and Accessory Location of the CH-54B Main Transmission.

single-engine operation. The clutch is arranged with the outer housing driven by the first-stage bevel gear and the cam driving through to the second-stage bevel gear.

The cam output of the ramp roller overrunning clutch drives the second-stage bevel pinion of the second-stage bevel mesh. This 25-to-76 ratio bevel mesh has an output bevel gear common to both inputs. This common bevel gear combines power from both the right and left engines. The spiral bevel gears used in this second-stage bevel mesh have a 3.125-diametral pitch, a 4.0-inch face width, a 20-degree pressure angle, and a 25-degree spiral angle. Lubrication and cooling oil is fed centrifugally from an oil distribution tube inside the second-stage pinion to the free-wheel unit and the support bearings of the pinion.

Mating with the 76-tooth common bevel gear is a 38-tooth bevel pinion that provides the drive for the accessories and tail rotor. Included in the accessory packages are an oil cooler, APU, generator, hydraulic pumps, and tachometer generator. A ramp-roller overrunning clutch mounted on the tail-takeoff bevel gear shaft permits the APU drive to be operated without driving both the main and tail rotors. This feature permits ground operation of the accessories through the auxiliary power unit with the main engines off.

The common bevel gear of the second-stage bevel set, which is concentric to the main rotor shaft, drives the input sun gear of a two-stage 8.14-to-1 reduction ratio simple planetary gear set. A simple planetary is defined as a driving sun gear, planetary carrier output and a fixed ring gear. The first-stage planetary set has a 3.41 reduction ratio and contains seven pinions. The first-stage planetary pinion is mounted on a two-row roller bearing whose inner race is supported by two planetary plates. The ring gear is rigidly bolted to the main transmission lower housing. This ring gear contains both first- and second-stage planetary internal gear members.

The carrier of the first-stage planetary is connected through dowel pins to the sun gear of the second-stage planetary. The second-stage planetary contains eighteen pinions, has a reduction ratio of 2.385-to-1, and is similar in construction to the first-stage planetary. The lower plate of the second-stage planetary is splined to and drives the main rotor shaft.

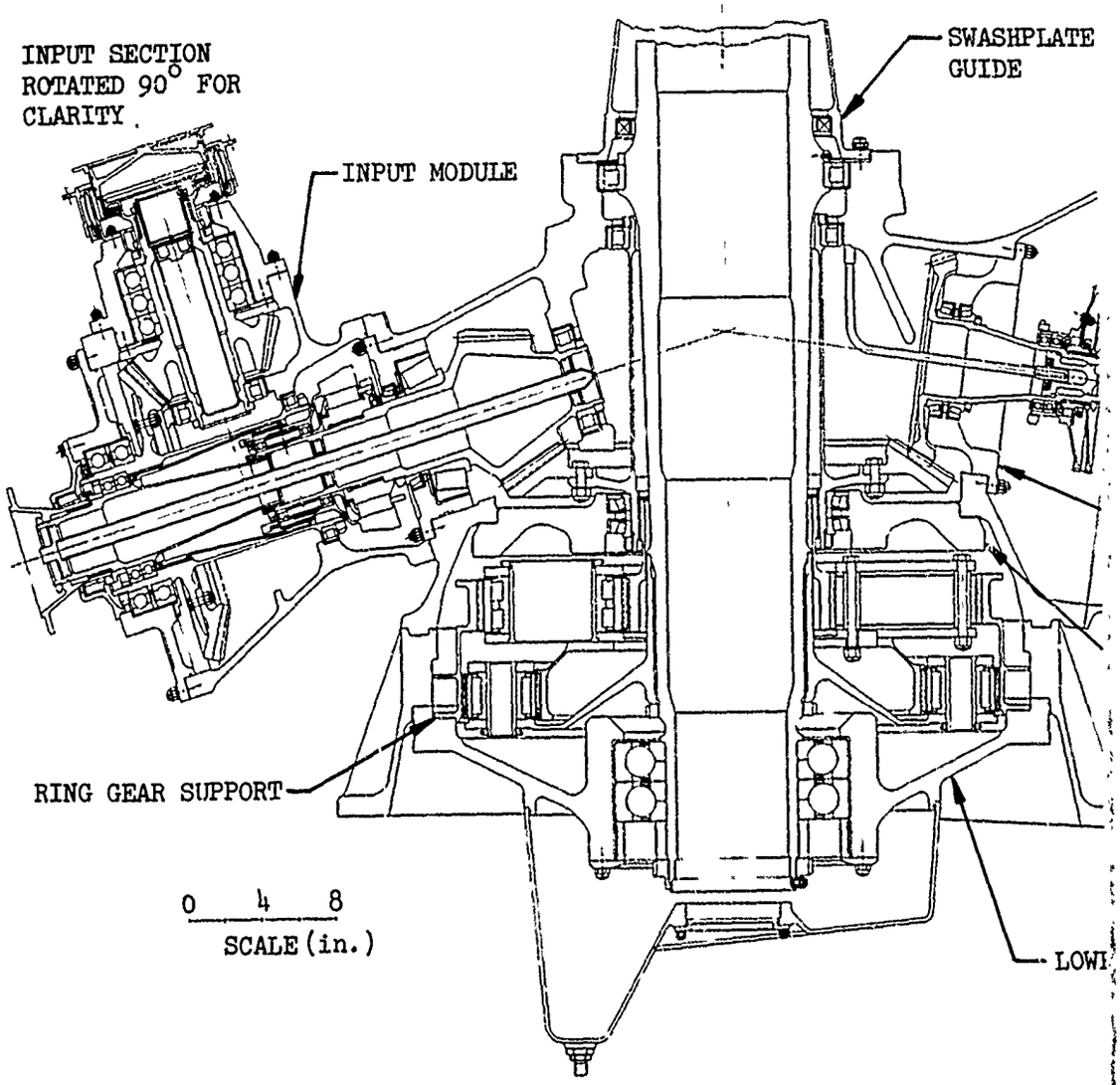

Figure 19. Cross Section of the CH-54B Main Transmission.

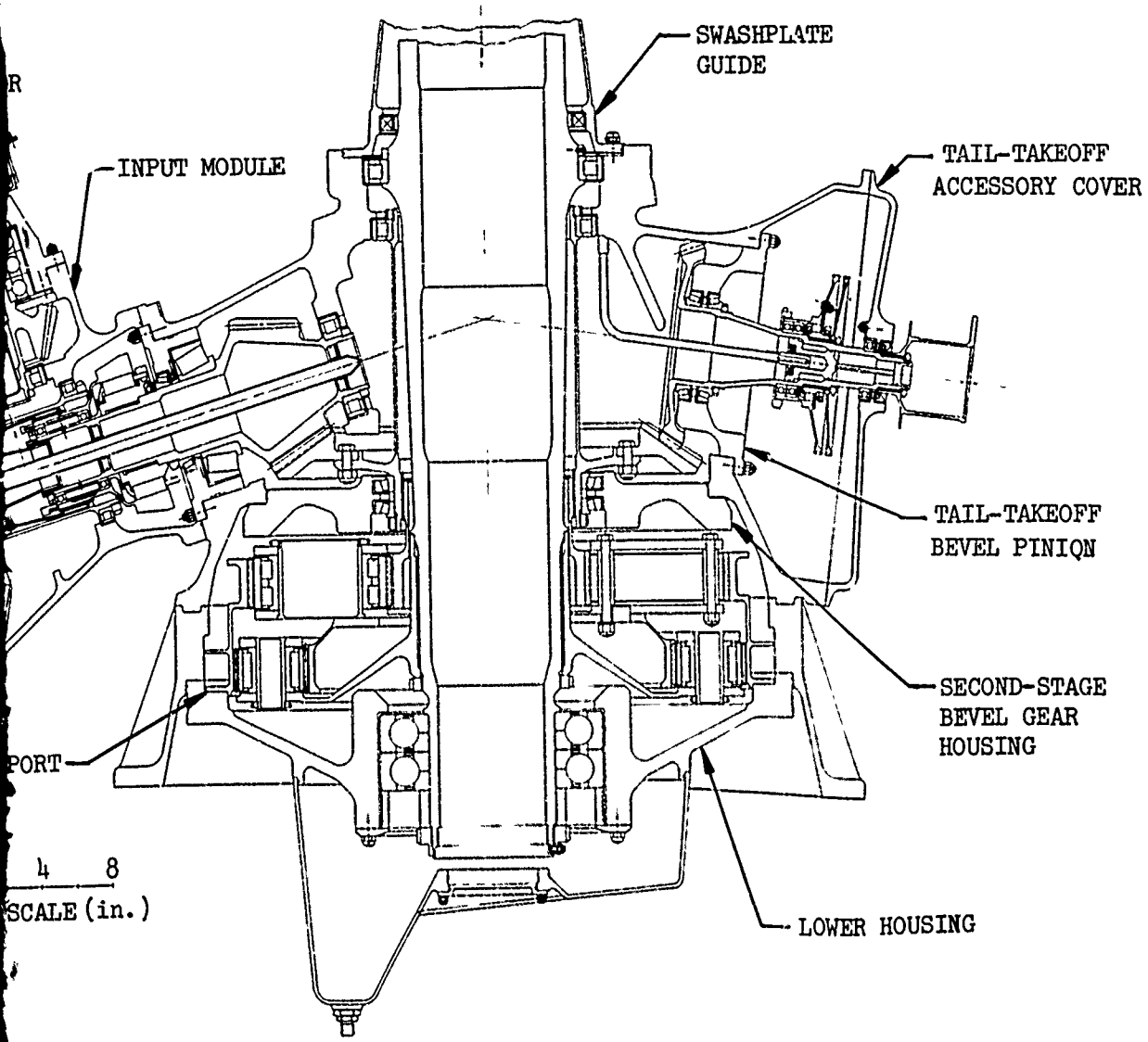

Cross Section of the CH-54B Main Transmission.

Description of Main Transmission Casting

The main transmission housing consists of an upper cast housing of AZ91C magnesium, a lower housing forged from ZK60A; and lower cover, accessory cover, left and right input housings, and sump, all cast in AZ91C. Figure 20 is an isometric of the CH-54B main transmission housing, showing upper transmission housing. All seven housings, in addition to providing reaction and support for main transmission components, provide a containment for transmission lubricant. They serve as a support for servos, oil cooler, scissor bracket, rotor brake, and accessories. They also contain interface pilot diameters and attachments, and serve as a conduit for distributing oil to various components.

Three servo support brackets are mounted on the main transmission casting at increments of 45°, 225°, and 315°. The servo support brackets react induced loads from the swashplate on the servos. A swashplate guide is mounted to the top of the upper housing and serves to locate the swashplate and react any induced side loads. The scissor bracket connects the upper main housing and the stationary swashplate. This bracket permits the swashplate assembly to translate up and down as well as be tipped out of a horizontal plane, but it prevents rotation of the stationary swashplate assembly.

Mounted on the main transmission casting are brackets that permit connection of a series of structural tubes used to support the main transmission oil cooler and blower assembly.

The main transmission housing reacts first-stage input bevel assembly loads, second-stage bevel gear and pinion loads, first- and second-stage planetary reaction loads, and main rotor shaft loads. The tail-takeoff and accessory drive bevel pinion, driven by the second-stage input bevel gear, is also supported in the main transmission housing.

The main transmission housing is attached to the main transmission support housing through a series of studs. The support housing has four mounting feet with three bolts in each mounting foot. All net rotor and transmission loads are reacted by the mounting feet and distributed to the airframe.

The main rotor shaft is supported by a roller bearing at the top of the upper main housing and by a set of tandem-mounted split inner race thrust bearings in the bottom of the lower cover. The lower support housing, which transfers loads to the airframe, is located between the lower cover and the upper main housing. The lower cover transfers the side and thrust loads to the lower support housing. The upper housing transfers side loads from the upper roller bearing to the lower support housing.

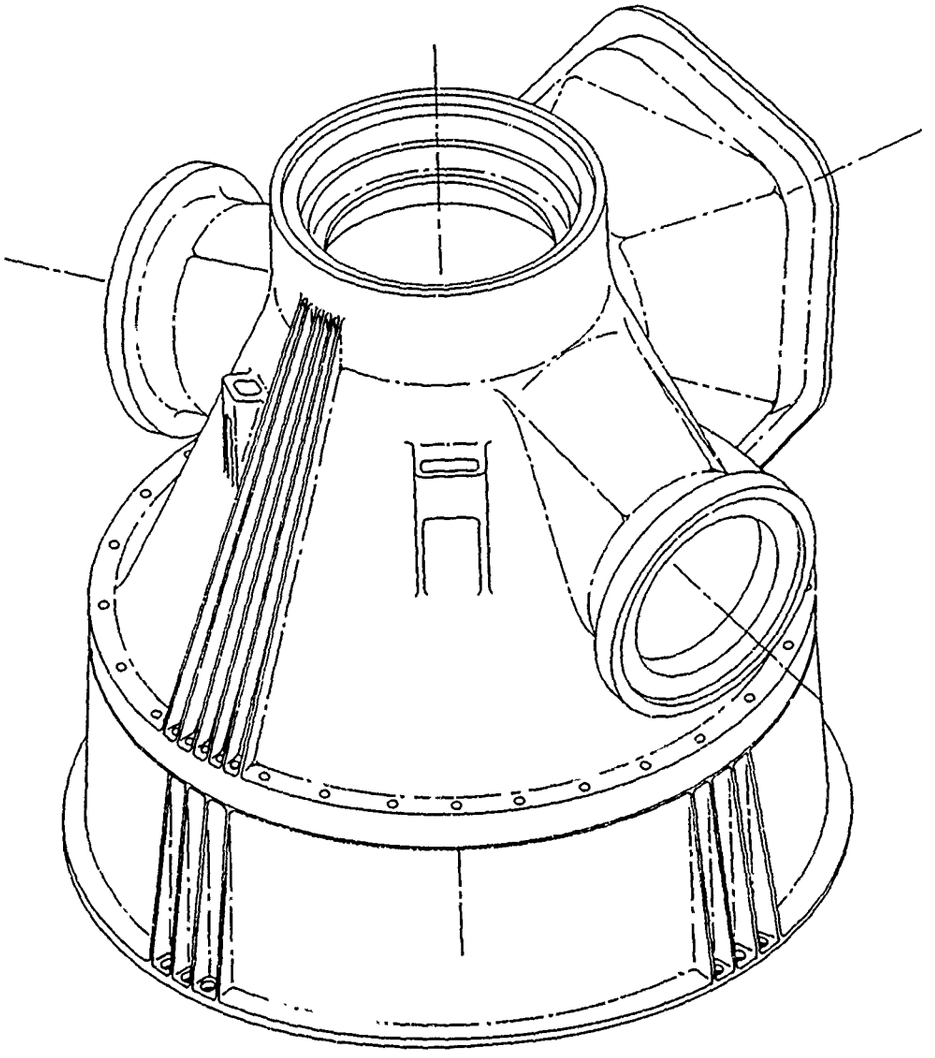

Figure 20. Isometric of CH-54B Main Transmission Housing.

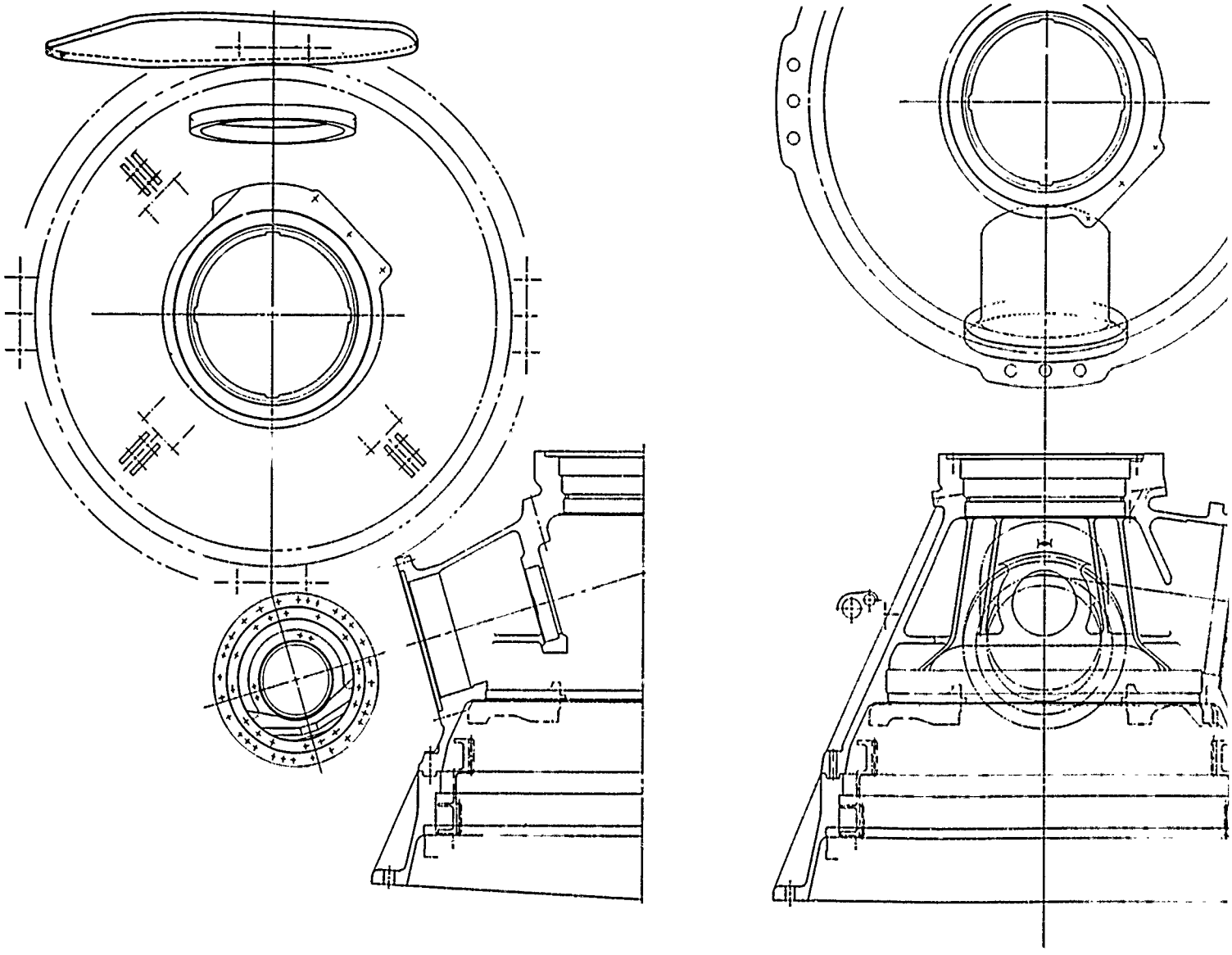

Figure 21. Cross Section of CH-54B Main Transmission Housing.

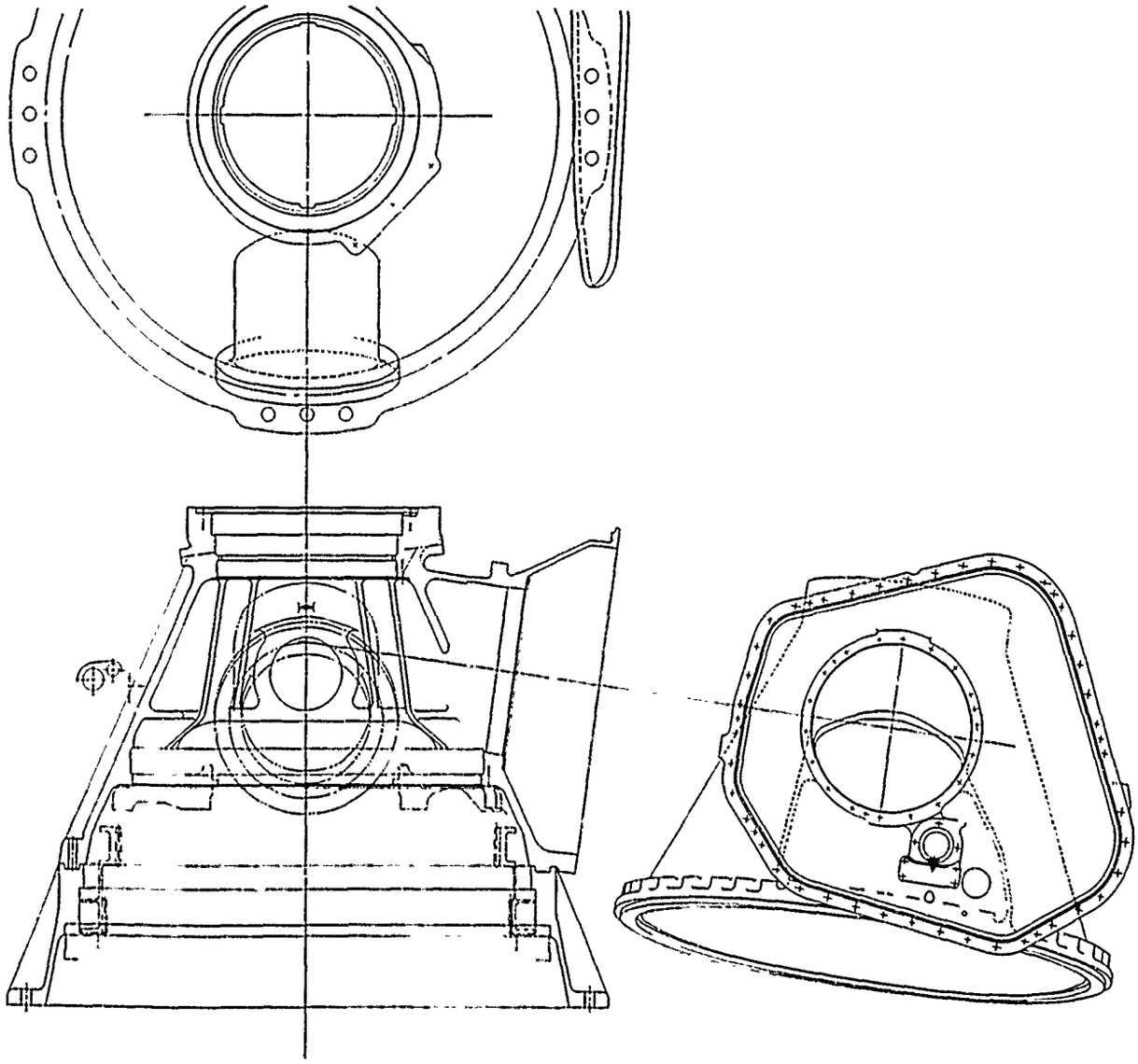

ransmission Housing.

Attached to the lower cover is the oil sump casting, which has cored lubrication lines and a pad for an oil pump drive. The accessory cover is attached to the rear cover flanges of the main transmission assembly. All of the accessories, with the exception of the hoist and utility pumps, are attached to, and supported by, the rear cover.

Attached to the upper main housing are the left and right side input housings. The input housings support and contain the first-stage bevel gears as well as the aft engine support. A rotor brake disc is attached to the left side input bevel gear shaft, and a brake caliper assembly is mounted to the left-hand input housing. The brake reaction torque is carried through the left-hand input housing to the main housing. Drives for the hydraulic hoist pump and the utility system hydraulic pump have been provided on the right side input housing.

Design Criteria for Main Transmission

The CH-54B main transmission design is typical of modern helicopter transmission practice.

Castings and housings of the main transmission are designed for crash conditions of 20g vertical, 20g forward, and 18g lateral. The worst loading condition for the structural design of the main transmission is the 20g forward crash.

Gears and shafting are designed for unlimited fatigue life at maximum torque conditions. For example, since the CH-54B can continue flight with one engine inoperative, the first- and second-stage bevel meshes are designed for maximum single-engine power of 4,800 horsepower, whereas the first- and second-stage planetaries are designed for 6,800 horsepower.

Bearings are designed for a minimum B10 life of 3,000 hours at a prorated load. The prorated loads are determined from the expected operating spectrum and represent a weighted average load. The shafting is also designed for maximum slope under the bearing of .0007 in./in. at maximum operating torque.

Steel liners are provided at the interface of bearing outer races and the magnesium castings. These liners serve both as stress buffer and wear member. The bearing liners are designed to have a positive interference fit with the magnesium housing at 250°F, while maintaining a low enough interference fit at -65°F to keep the magnesium from yielding.

All threaded fasteners on the main transmission are provided with locking features to prevent loosening of nuts. Nuts and bolts, cotter pins, clevis pins, or Shurlocks are used to provide positive retention of larger nuts. On smaller threads, using standard nuts, a deformed thread type locking device is used.

The lubrication system for the CH-54B main transmission is typical of current modern aircraft pressure oil systems. Oil from the gearbox sump is pumped through an oil filter to an air/oil heat exchanger. The blower fan of the heat exchanger is driven from the accessory case of the main transmission. The oil is then forced from the heat exchanger into the main transmission manifold. Oil from this manifold is distributed through a series of jets to bearings, gear meshes, and oil distribution tubes within the transmission.

Design Criteria for the Fabricated Housing

The truss-like fabricated housing, in order to be an acceptable alternative to the conventional magnesium casting, must meet the CH-54B functional requirements and in addition possess the following attributes:

- The fabricated housing must be at least as strong as a magnesium casting.
- Stiffness of the fabricated housing should be similar to that of a casting. As a minimum, the stiffness should be sufficient for proper operation of the dynamic components.
- The fabricated housing should weigh less than a conventional casting.
- Maintainability and reliability should be at least equal to those of a casting design.
- Inspectability of a fabricated housing should be superior to that of a cast housing.
- The fabricated housing should be easier and simpler to manufacture than a magnesium casting.
- Total cost of a fabricated housing should be lower than that of a casting.
- Overall heat transfer should be greater than that of a magnesium cast housing.
- The fabricated housing should exhibit characteristics of improved survivability and reduced vulnerability.

In assessing these desired attributes, a quantitative approach was used where possible. In certain areas, such as thermal characteristics, a true assessment will be possible only after experimental data are developed.

Interface Requirements for Fabricated Housing

The fabricated housing must be interchangeable with the present CH-54B casting. A cross section of the CH-54B transmission is shown in Figure 19. The items and modules that must be interchangeable are labeled. Included in the interchangeability list are input section assembly (first-stage bevel mesh and housing), tail-takeoff/accessory cover, lower cover assembly, swashplate guide, ring gear support, second-stage bevel gear housing, tail-takeoff bevel pinion housing, and the scissor bracket. The upper housing and lower support housing for which the truss structure is modeled have been joined together, as shown in the isometric of Figure 20. This permits a lighter truss structure and eliminates the need for a mounting flange and row of studs. The servo bracket fittings have also been eliminated, since it is possible to have a ligher truss structure through use of a more direct load path. All oil transfer tubes between the housings and all fittings, manifolds, and jets have been kept in the same location. In brief, the fabricated housing is directly interchangeable with the upper housing casting and the lower housing support considered as a single unit.

All internal transmission gears, bearings, and seals are identical with those used in the current CH-54B transmission. Bearing fits and backup are adjusted for thermal expansion, so bearing clearances are the same under operating load as in the current CH-54B casting. Seal fits are maintained as in the current CH-54B transmission at normal operating temperature. The fabricated housing is designed to maintain the location of the jets and oil flows that are used in the present CH-54B transmission design. Bearing supports, in particular bevel pinion bearing supports, are located in the plane of the present casting walls. Truss members are so oriented that loads can be distributed easily. The transmission mounting arrangement is the same as for the present CH-54B, with four mounting pads and three mounting bolts in each pad.

PRELIMINARY DESIGN

In the preliminary design phase, the objective was to select a material, fabrication methods, and structural arrangement suited for a detail design analysis. The approach was to conduct a NASTRAN analysis of various combinations of materials, joining methods, and structural geometry under crash loading conditions and to use the results of those analyses as a basis for determination of the most promising housing configurations.

Load Development

Table III is a list of component weights and center of gravity locations taken from Reference 1, CH-54B Weight Control Status Report. This data was used in developing crash loads for the analysis. The loading conditions were 20g forward, 18g side, and 20g down. Figure 22 shows the load orientation for forward crash conditions due to rotor head and accessory inertia. The applied loads for these conditions are shown in Figures 23, 24, and 25, respectively.

The applied loads on the upper and lower main rotor bearing support rings result from the masses of the main rotor head, rotor blade, control rods, scissor, and swashplate assembly. These loads are determined by multiplying the masses by a load factor and then calculating the reactions at the main rotor shaft bearings.

Loads transmitted to the main housing through the servos are due only to the weight of the servos themselves for both forward and side crash conditions. For the vertical crash condition, additional loads due to the rotating and stationary swashplates are also transmitted to the main housing. Loads on both the right and left side input housing consist of the mass effect of the aft end of each engine plus the weight of the first-stage bevel input housing assembly. The loads on the rear cover flange consist of the mass effect of the oil cooler and supports, rear cover assembly, first-stage servo pump, utility pump, generator, and tachometer generator. The total applied load on the rear cover was distributed on the rear cover flange by a series of point loads. The internal gear driving loads were not added to the crash load conditions, since they are small in magnitude. The applied crash loads are summarized in Table IV. Figure 26 is a sketch of the sign convention used with the applied main rotor loads.

To develop the applied transmission loads for flight conditions, the critical maneuver condition was used. The aircraft loads report (Reference 2) and the structural design criteria report (Reference 3) indicate that the critical loading condition occurs for a symmetric dive and pullout maneuver.

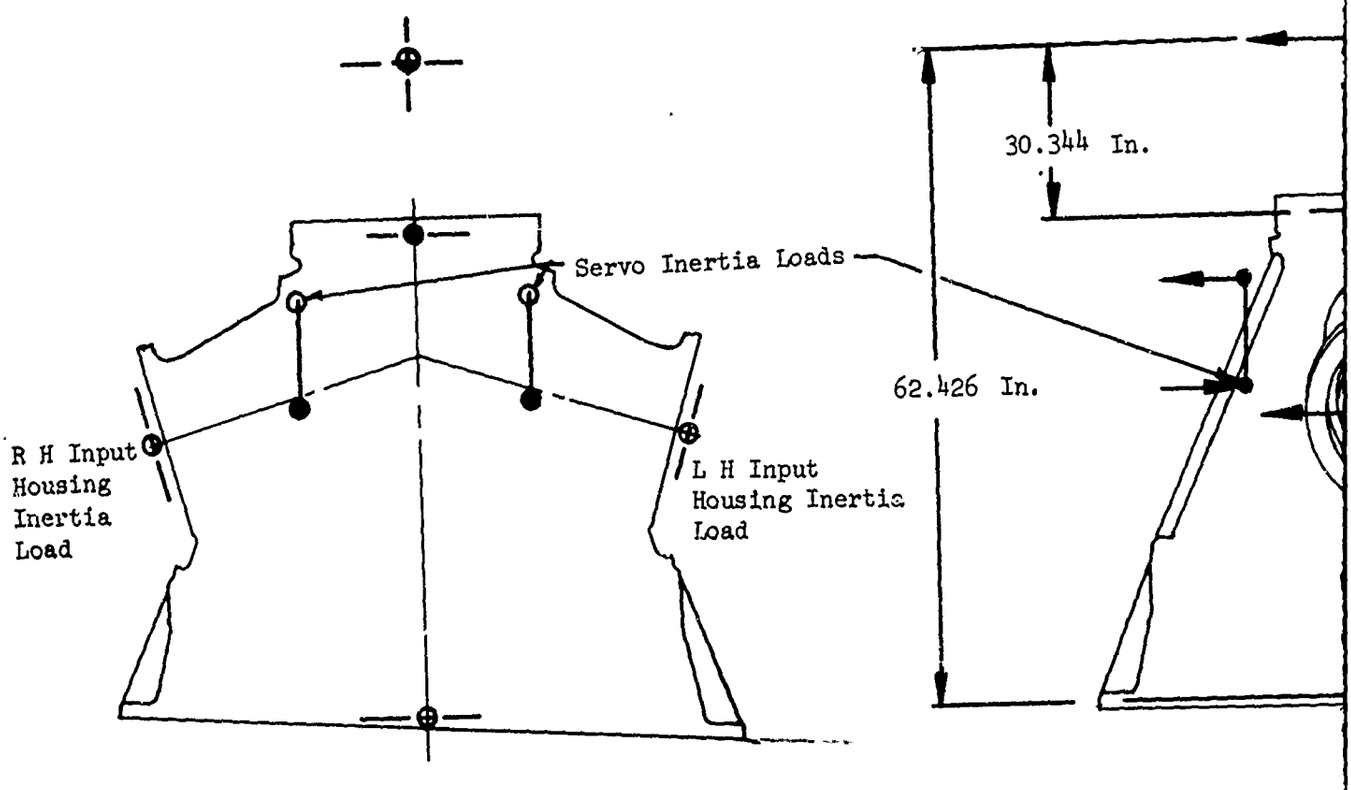

Figure 22. Forward Crash Loads on Housing Due to Rotor Head and Accessory Inertia.

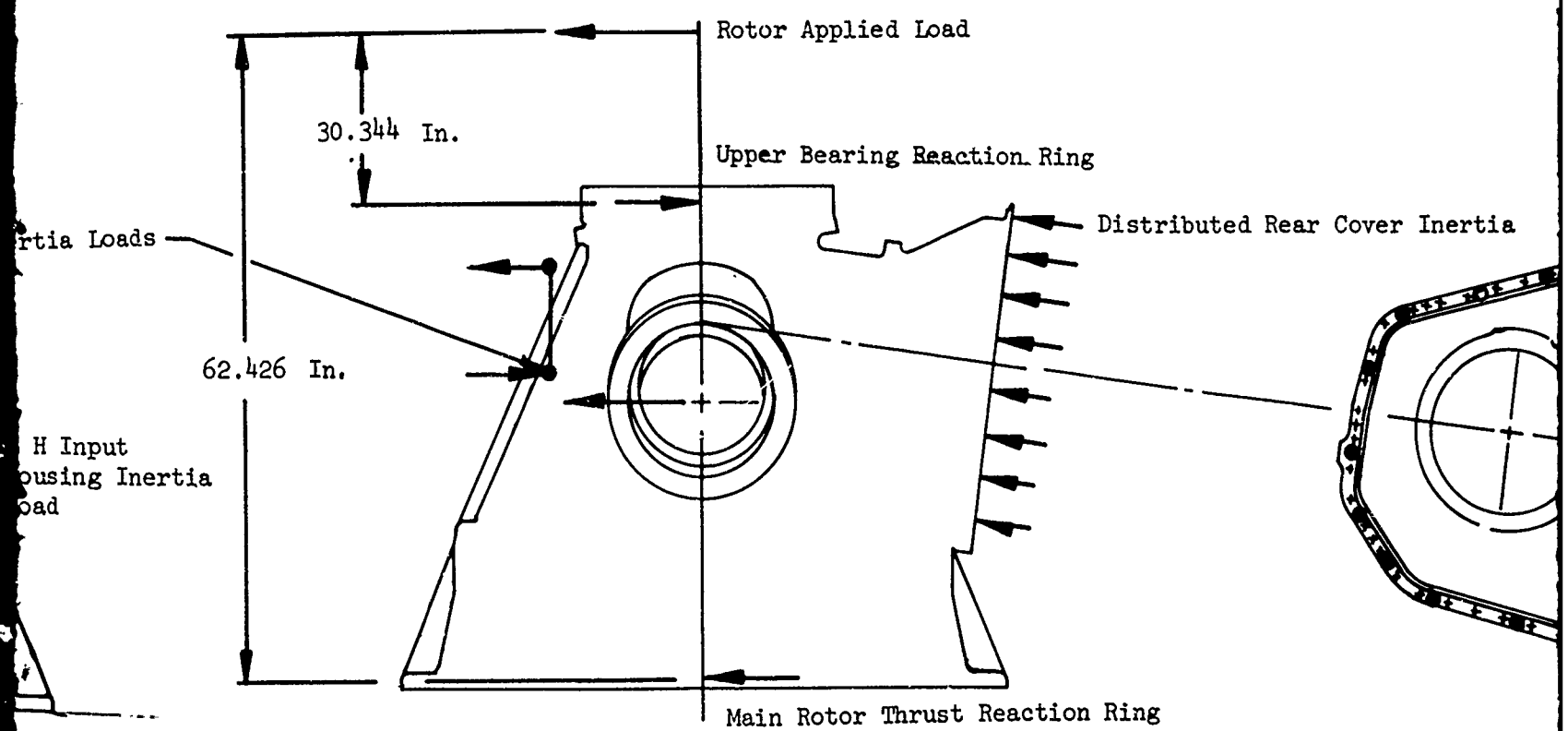

ousing Due to
Inertia.

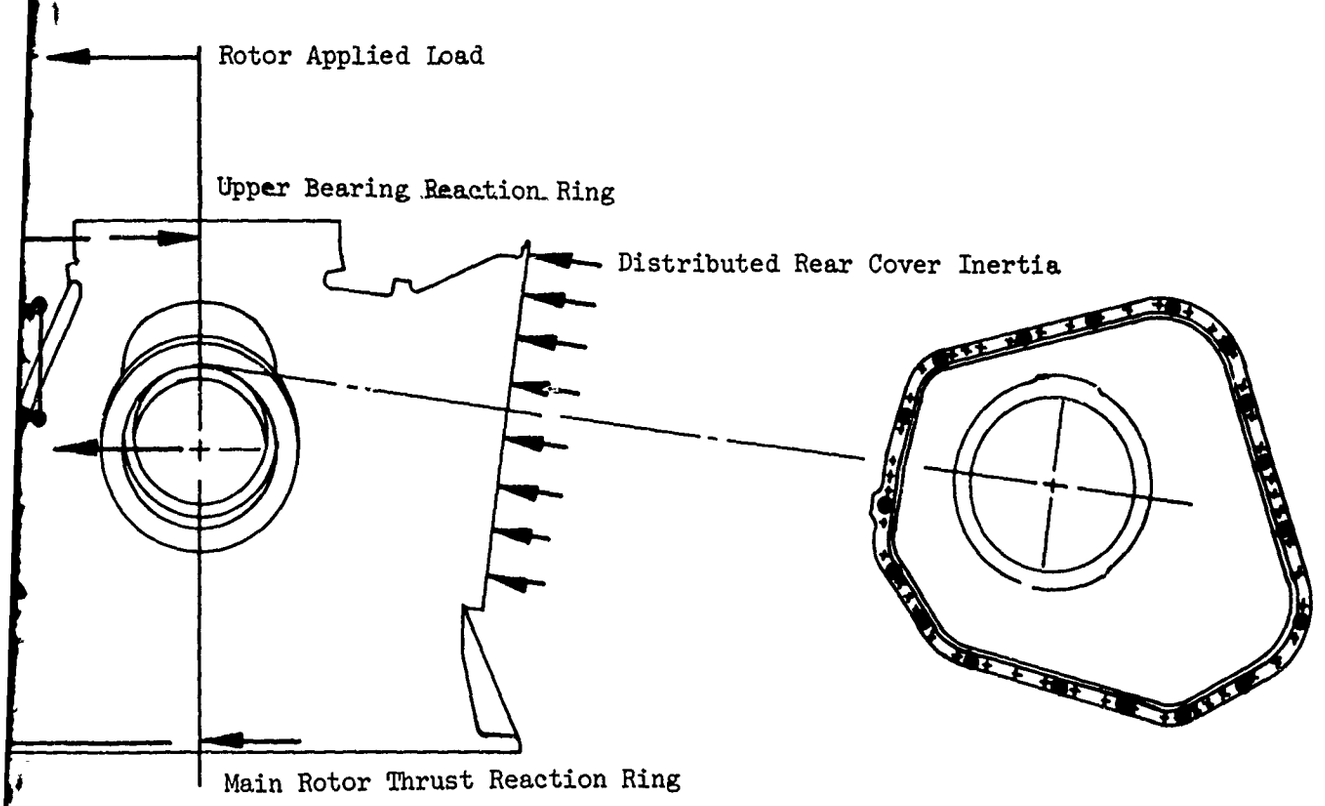
Rotor Applied Load
Upper Bearing Reaction Ring
Distributed Rear Cover Inertia
Main Rotor Thrust Reaction Ring

TABLE III. CH-54B COMPONENT WEIGHT AND CENTER OF GRAVITY LOCATIONS

Item	Weight (lb)	Station	Waterline	Buttline
Main Rotor Blades	2187.	336.0	257.9	0
Main Rotor Head	1798.6	336.0	257.7	0
Flight Controls				
Rotating Swashplate	215.3	337.4	247.7	0
Control Rods	24.3	336.7	254.1	0
Rotating Scissor	22.3	337.1	248.9	0
Fixed Swashplate	112.4	337.4	245.6	0
Stationary Scissor	15.7	337.2	237.9	0
Main Rotor Servos	147.6	335.0	225.0	0
Main Transmission				
Main Gearbox With Shaft	3165.8	338.2	212.4	0
Oil Cooler and Support	74.5	352.4	235.2	.40
Rotor Brake	46.96	322.3	223.0	30.40
First-Stage Servo Pump	14.70	364.0	214.0	8.0
Second-Stage Servo Pump	14.10	333.0	212.0	-44.0
Hoist Pump	20.0	344.0	215.0	-46.0
Utility Pump	22.16	365.0	221.0	10.0
Left Side Input Assembly (w/o brake)	270.85	337.8	213.8	23.1
Right Side Input Assembly	277.71	337.8	216.2	-18.6
Transmission Oil	100.5	339.0	214.0	0
Rear Cover Assembly	130.32	359.6	220.5	0
Generator	64.0	364.0	219.0	0

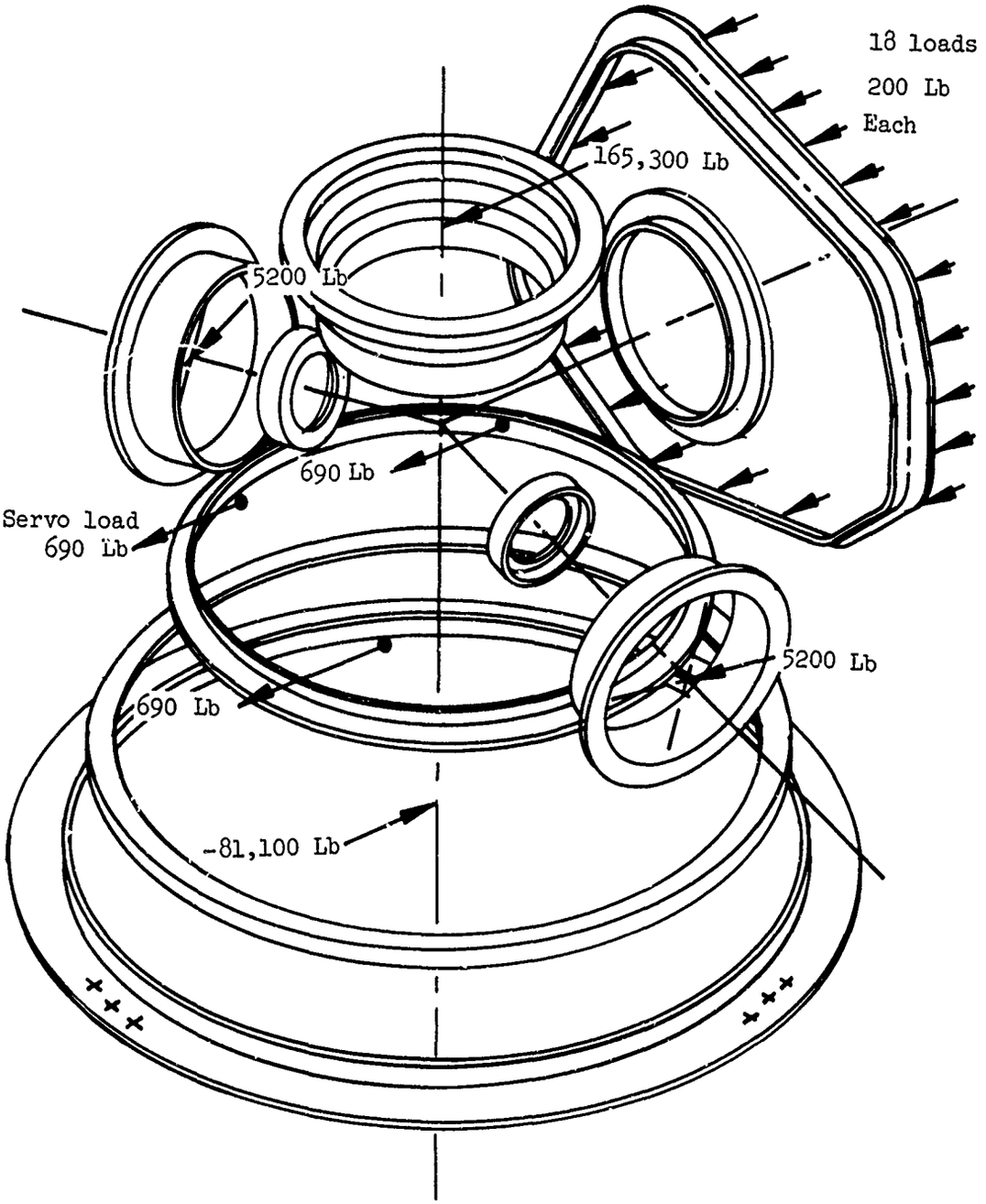

Mounting Feet Constrained in All Directions
Except for Twist About ℄ of Each Bolt

Figure 23. Initial Loading - 20g Forward Crash Condition.

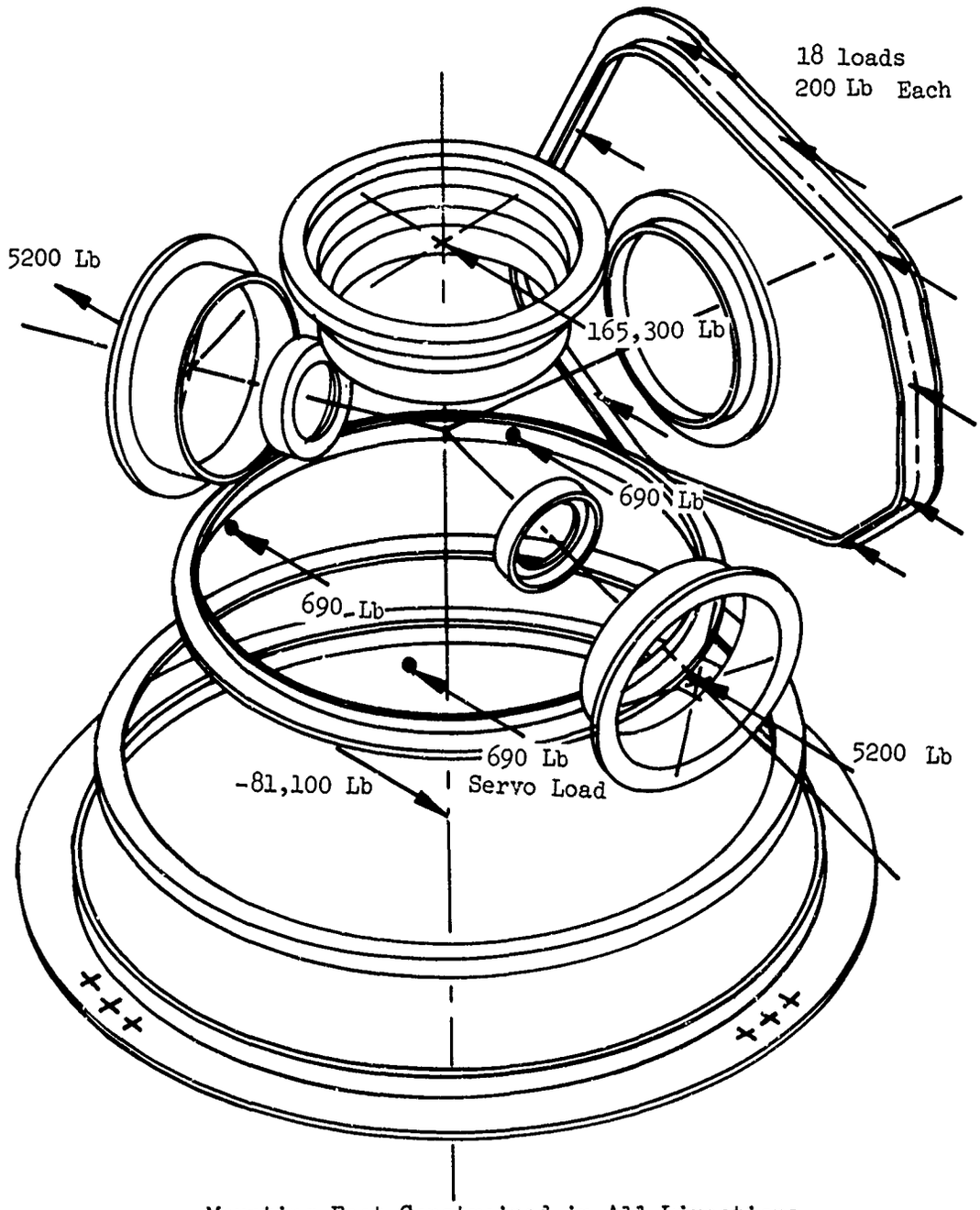

Figure 24. Initial Loading - 18g Side Crash Condition.

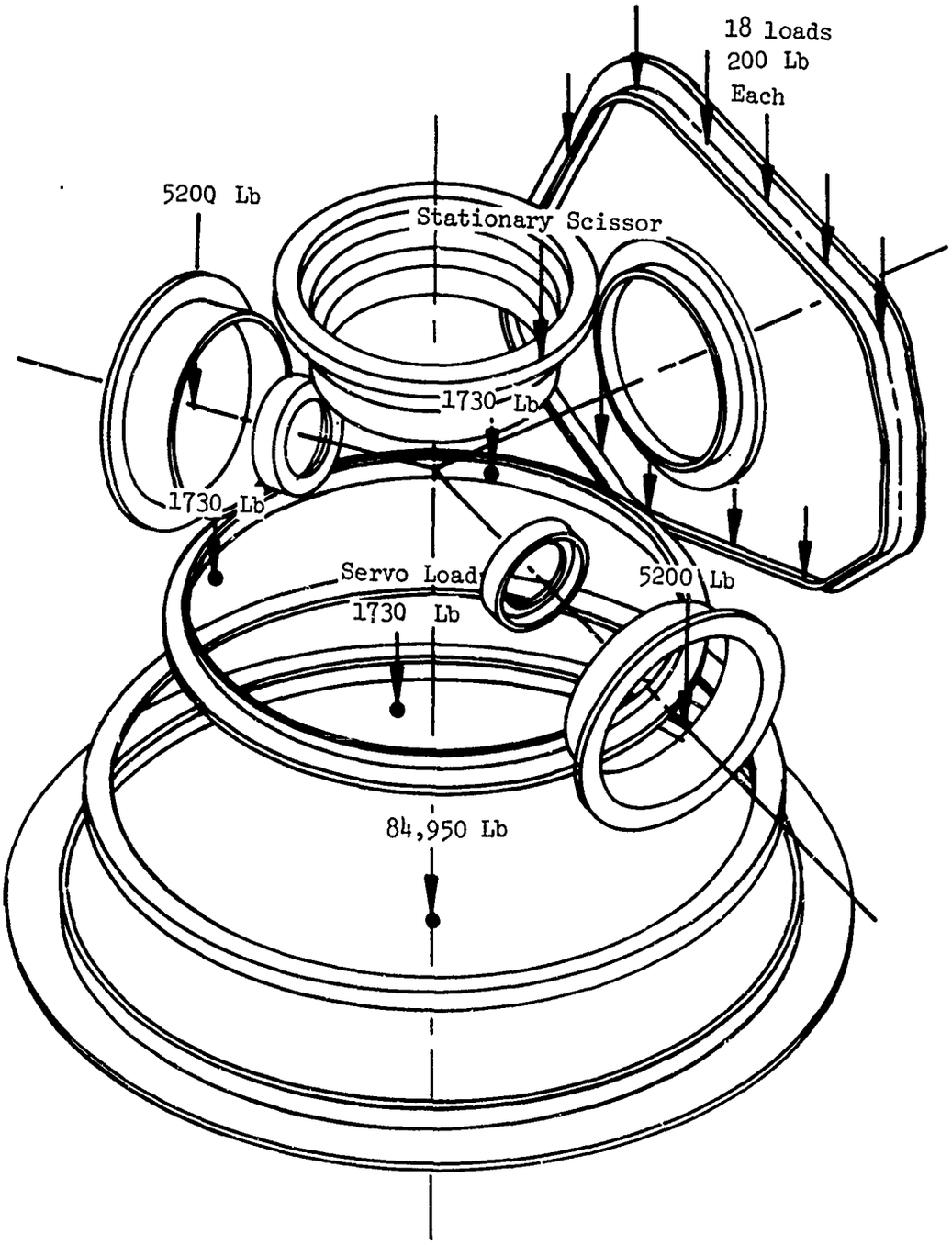

Figure 25. Initial Loading - 20g Down Crash Condition.

TABLE IV. SUMMARY CRASH LOAD DESIGN CRITERIA			
Location	Condition		
	Forward 20G	Side 18G	Down 20G
Upper Roller Bearing	165,300	165,300	0
Servo Pads	690/pad	690/pad	1730/pad
Input Section	5,200	5,200	5,200
Rear Cover	3,600	3,600	3,600
Lower Housing Support	-81,100	-81,100	-84,950

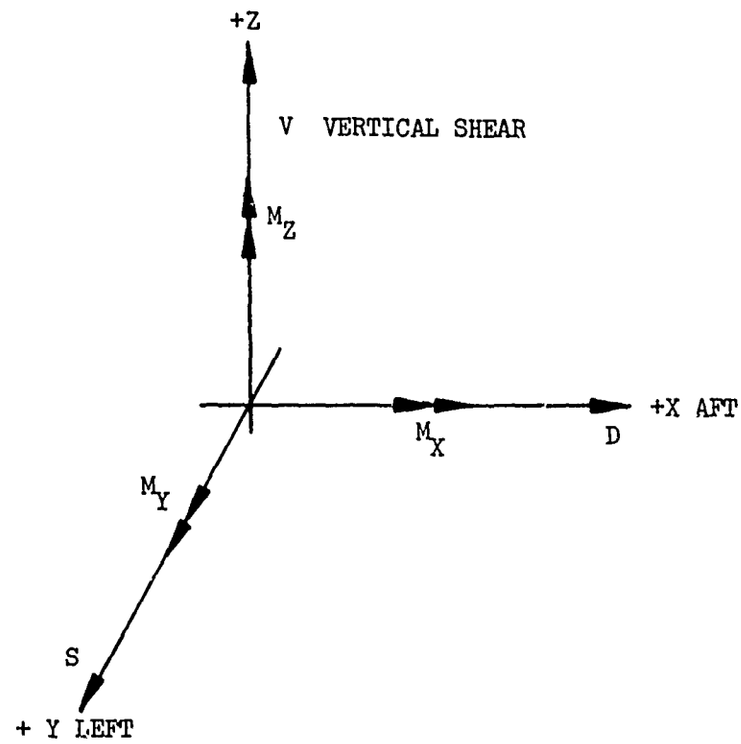

Figure 26. Sign Convention for Applied Main Rotor Loads.

For the critical flight conditions, the loads at the aerodynamic center of gravity of the main rotor are:

V_R = 94,263

S_R = 5,220

D_R = 14,685

M_{xR} = -15,426

M_{yR} = 1,322,271

M_{zR} = -70,106

These loads are resolved into reactions at the main rotor shaft upper roller bearing and the lower stack bearing set. Figure 22 shows the geometry used in determining the reactions, which are listed below:

R_{Ax} = 12,641

R_{Ay} = 9,676

R_{Bx} = 27,326

R_{By} = -9,676

The thrust associated with this condition is 94,263 pounds.

Internal gear and bearing loads were developed for each primary mesh of the CH-54B drive train.

The first-stage input housing is supported by the fabricated housing structure, which must react a moment due to the weight of the cantilevered input section. The loads due to this moment are much smaller than those due to the second-stage bevel mesh and were ignored.

The second-stage input pinion is driven by the first-stage input bevel gear and in turn drives the second-stage bevel gear. The input pinion is a right-hand spiral bevel gear rotating counter-clockwise as viewed from the shaft end. Gear data for the second-stage input pinion are as follows:

Pitch angle γ = 16° 5'

Pressure angle Φ = 20°

Spiral angle Ψ = 25°

Pinion diameter d_p = 8.0

Face width $F = 4.0$

Pinion rpm $n = 4585$

The axial component of the gear tooth load is given by

$$W_x = W_t \frac{\tan\Phi \sin\Gamma + \sin\Psi \cos\Gamma}{\cos\Psi} \quad (1)$$

$$W_x = W_t \ (.560)$$

The radial component of the gear tooth load is given by

$$W_r = W_t \frac{\tan\Phi \cos\Gamma - \sin\Psi \sin\Gamma}{\cos\Psi} \quad (2)$$

$$W_r = W_t \ (.257)$$

The bevel gear mean pitch diameter is given by

$$d_m = d_p - F \sin\Gamma \quad (3)$$

$$d_m = 6.892 \text{ inch}$$

For the maximum fatigue design power condition of 4800 horsepower,

$$T = \frac{HP\ 63025}{rpm} \quad (4)$$

$$T = 65{,}980 \text{ in.-lb}$$

The tangential tooth load is given by

$$W_t = \frac{2T}{d_m} \quad (5)$$

$$W_t = 19{,}150 \text{ lb}$$

Substituting the maximum tangential tooth load in Equations 1 and 2, the axial and radial components of the gear tooth loads are

$$W_x = (.560)\ (W_t)$$

$$W_x = 10{,}724 \text{ lb}$$

$$W_r = (.257)\ (W_t)$$

$$W_r = 4{,}920 \text{ lb}$$

The bearing reactions are calculated from the geometry shown in Figure 27.

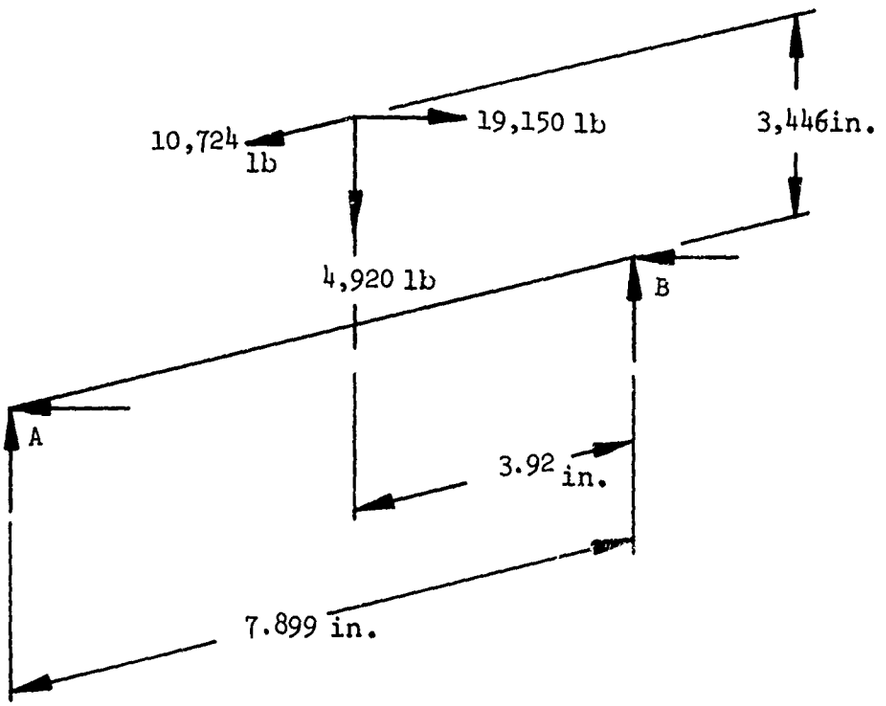

Figure 27. Bearing Reaction Geometry.

At the tapered roller bearings, or end A (Figure 27), the vertical and horizontal reactions are given by

$$R_{A_V} = \frac{(W_r)(3.92) + (W_x)(3.446)}{7.899}$$

$$R_{A_V} = 7{,}120 \text{ lb}$$

$$R_{A_T} = \frac{(W_t)(3.92)}{7.899}$$

$$R_{A_T} = 9{,}500 \text{ lb}$$

$$\text{Thrust} = 10{,}724 \text{ lb}$$

At the roller bearing, or end B (Figure 27), the vertical and horizontal reactions are given by

$$R_{B_V} = \frac{(W_x)(3.446) - (W_r)(3.979)}{7.899}$$

$$R_{B_V} = 2{,}200 \text{ lb}$$

$$R_{B_t} = \frac{(W_t)(3.979)}{7.899}$$

$$R_{B_t} = 9{,}650 \text{ lb}$$

The second-stage bevel gear is driven by the second-stage bevel pinion. In turn, the second-stage bevel pinion transmits power to the first-stage planetary sun gear and to the tail-takeoff bevel pinion. The second-stage input gear is a left-hand spiral bevel gear rotating clockwise as viewed from the shaft end. The gear data for the second-stage input spiral bevel gear are given below:

Pitch angle	γ =	57° 21'
Pressure angle	Φ =	20°
Spiral angle	Ψ =	25°
Gear diameter	d_p =	24.320
Tail-takeoff face width	F =	1.375
Pinion and gear face width	F =	4.0

Gear rpm $n = 1508$

The axial component of the gear tooth load is given by

$$W_{x_{in}} = W_{t_{in}} \frac{\tan\Phi \sin\Gamma - \sin\Psi\cos\Gamma}{\cos\Psi} \quad (6)$$

$$W_{x_{in}} = .0866\ W_{t_{in}}$$

The radial component of the gear tooth load is given by

$$W_{r_{in}} = W_{t_{in}} \frac{\tan\Phi\cos\Gamma + \sin\Psi\sin\Gamma}{\cos\Psi} \quad (7)$$

$$W_{r_{in}} = W_{t_{in}}\ (.609)$$

Using the geometry of Figure 28 and summing the moments about each reaction point yields the following results:

$\Sigma M_B = 0$ in butt line plane

$$R_{A_{bl}} = .355\ W_{t_{out}} - .0205\ W_{t_{in}} \quad (8)$$

$\Sigma M_A = 0$ in butt line plane

$$R_{B_{bl}} = .531\ W_{t_{out}} - .00152\ W_{t_{in}} \quad (9)$$

$\Sigma M_B = 0$ in station plane

$$R_{A_{sta}} = .930\ W_{t_{out}} - .0296\ W_{t_{in}} \quad (10)$$

$\Sigma M_A = 0$ in station plane

$$R_{B_{sta}} = .0700\ W_{t_{out}} + .00152\ W_{t_{in}} \quad (11)$$

The critical design condition is 5400 horsepower to both inputs, with 1220 horsepower taken off at the tail-takeoff bevel gear and the remainder delivered to the main rotor. The input and output tangential tooth loads are

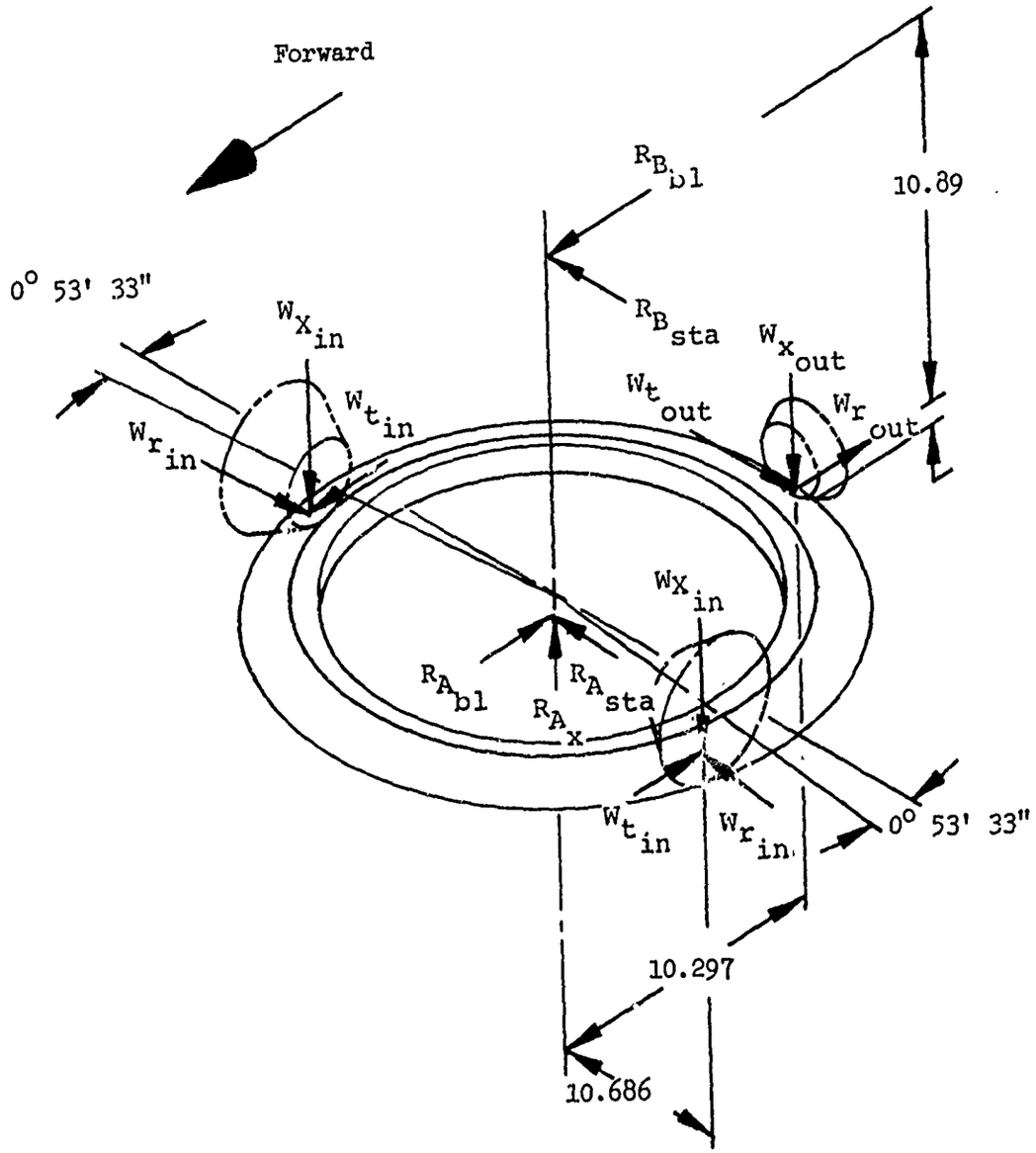

Figure 28. Outer Shaft Load Geometry.

$$W_{t_{in}} = 10{,}560 \text{ lb}$$

$$W_{t_{out}} = 4{,}960 \text{ lb}$$

Substituting the tangential tooth loads in Equations 8, 9, 10, and 11 leads to the reactions at A, the tapered roller bearing loads, and B, the roller bearing loads (Figure 28):

$$R_{A_{bl}} = 1544 \text{ lb}$$

$$R_{A_{sta}} = 4300 \text{ lb}$$

$$R_{B_{bl}} = 2617 \text{ lb}$$

$$R_{B_{sta}} = 331 \text{ lb}$$

The axial load on the thrust bearings is found from

$$R_{A_x} = (.0866)\ (W_{t_{in}})\ (2) + (.0866)\ (W_{t_t})$$

$$R_{A_x} = 2258 \text{ lb}$$

The tail-takeoff bevel pinion is a right-hand spiral bevel pinion driven counterclockwise by the main bevel gear. The gear data for the tail-takeoff bevel pinion are as follows:

Pitch angle	γ	=	24° 54"
Pressure angle	Φ	=	20°
Spiral angle	ψ	=	22° 52'
Face width	F	=	1.375
Tail-takeoff speed	n	=	3016

The axial component of the gear tooth load is given by Equation (6).

$$W_x = W_t \frac{\tan\Phi \sin\gamma - \sin\psi \cos\gamma}{\cos\psi}$$

$$W_x = W_t \ (-.2162)$$

The radial component of the gear tooth load is given by Equation (7).

$$W_r = W_t \frac{\tan\Phi \cos\Upsilon + \sin\Psi \sin\Upsilon}{\cos\Psi}$$

$$W_r = W_t \ (.5359)$$

The bevel pinion mean pitch diameter is found from Equation (3).

$$d_m = d_p - F \sin\Upsilon$$

$$d_m = 10.297$$

The tangential component of the gear tooth load is given by Equation (12).

$$W_t = \frac{126050 \ HP}{d_m \ n} \qquad (12)$$

$$W_t = 4952 \text{ lb}$$

The accessory drive loads acting on the tail-takeoff gear shaft are shown in Figure 29. The loads are based on the maximum accessory power requirements shown in Table II.

For the utility pump, the tangential component of the gear tooth load is computed from Equation (12).

$$W_t = \frac{126050 \ HP}{d_p}$$

$$W_t = 237 \text{ lb}$$

The radial component of the gear tooth load is given by

$$W_r = W_t \tan\Phi = 237 \text{ lb}$$

The horizontal and vertical gear load components are found through use of the geometry shown in Figure 29.

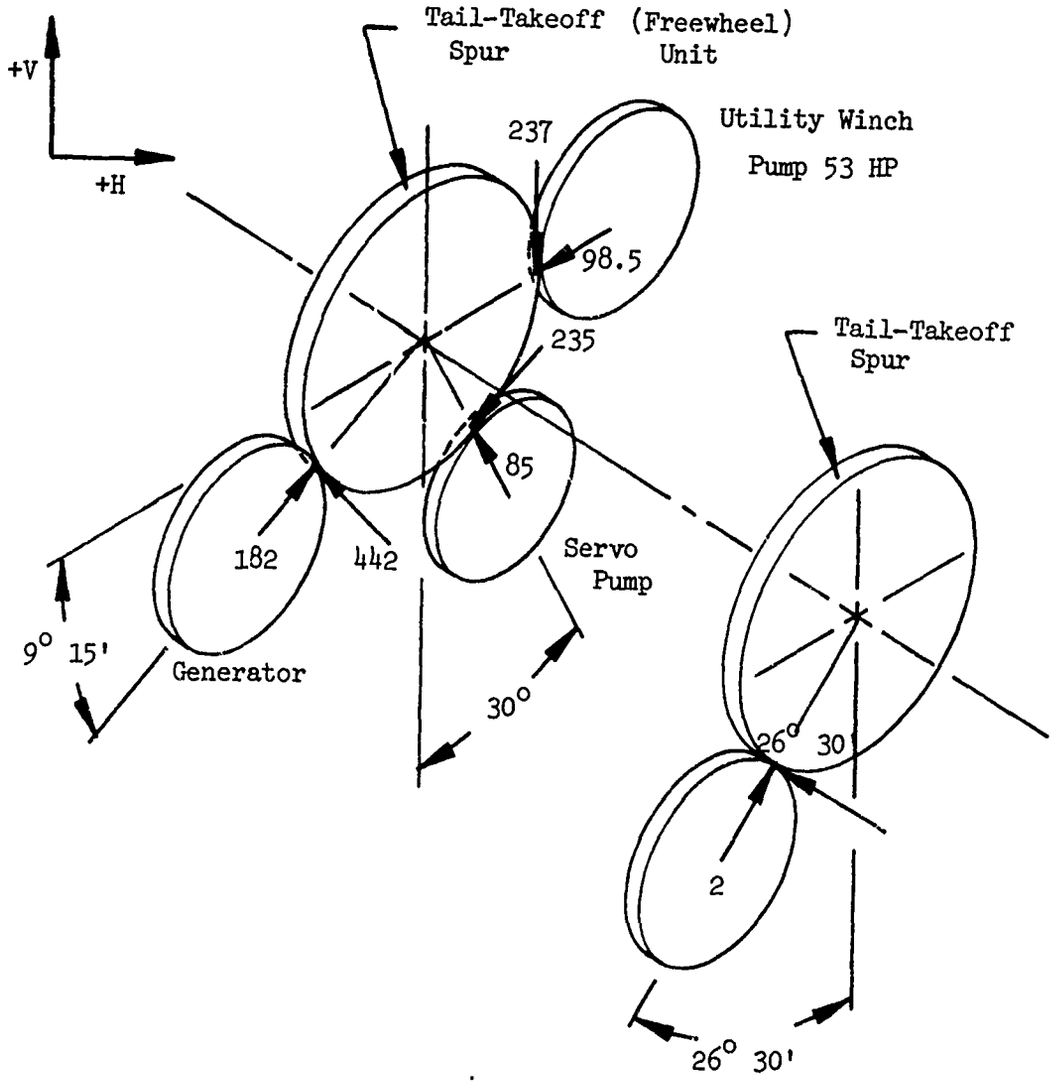

Figure 29. Loading for Accessory Drive Train.

$$W_H = W_r = -98.5 \text{ lb}$$

$$W_v = W_t = -237 \text{ lb}$$

For the first-stage servo, the tangential component of the gear tooth load is computed from Equation (12).

$$W_t = 85.37 \text{ lb}$$

The radial component of the gear tooth load is given by

$$W_r = W_t \tan 22\text{-}1/2°$$

$$W_r = 35.3 \text{ lb}$$

The horizontal and vertical components of the tangential and radial gear loads are calculated with the aid of Figure 29.

$$W_H = -W_r \sin 30° + W_t \cos 30°$$

$$W_H = -91.5$$

$$W_v = W_r \cos 30° - W_t \sin 30°$$

$$W_v = 12.1 \text{ lb}$$

For the generator, the tangential component of the gear tooth load is given by Equation 12, in which

$$W_t = 442 \text{ lb}$$

The radial component of the gear tooth load is given by

$$W_r = W_t \tan 22\text{-}1/2°$$

$$W_r = 183 \text{ lb}$$

The radial and tangential gear tooth loads are resolved into vertical and horizontal components with the aid of Figure 29.

$$W_H = W_r \cos 9° 15' - W_t \sin 9° 15'$$

$$W_H = 110 \text{ lb}$$

$$W_v = W_r \sin 9° 15' + W_t \cos 9° 15'$$

$$W_v = 466 \text{ lb}$$

For the tachometer generator, the tangential component of the gear tooth load is given by Equation 12, in which

$$W = 5 \text{ lb}$$

$$W_r = W_t \tan 22\text{-}1/2°$$

$$W_r = 2 \text{ lb}$$

The radial and tangential gear tooth loads are resolved into vertical and horizontal components with the aid of Figure 29.

$$W_H = W_r \cos 26° 30' - W_t \sin 26° 30'$$

$$W_H = 1 \text{ lb}$$

$$W_v = W_r \sin 26° 30' + W_t \cos 26° 30'$$

$$W_v = 5 \text{ lb}$$

The resulting loads on the tail-takeoff gear that drives the utility winch pump, servo pump, and generator are given by

$$W_H = - 98.5 - 91.5 + 110$$

$$W_H = - 80 \text{ lb}$$

$$W_v = - 237 + 12.1 + 466$$

$$W_v = + 241 \text{ lb}$$

The resulting loads on the aft tail-takeoff spur gear that drives the tachometer generator are

$$W_{H_2} = 1 \text{ lb}$$

$$W_{v_2} = 5 \text{ lb}$$

The bearing reactions at the tapered roller bearing, A, and the roller bearing, B, are given by

$$R_{A_v} = \frac{(.5359)(W_t)(10.91)}{9.22} + \frac{(.2162)(W_t)(5.15 - W_{v_2}(1.94) - W_v(2.37)}{9.22}$$

$$R_{A_v} = .7548\, W_t - 63$$

$$R_{A_H} = \frac{W_t(10.92) + W_{H_2}(1.94) - W_H(2.37)}{9.22}$$

$$R_{A_H} = 1.1832\ W_t + 20.77$$

$$R_{B_v} = \frac{(.5359)(W_t)(1.69}{9.22} + \frac{(.2162)(W_t)(5.5) + W_{v_2}\ (7.28) + W_v(6.85)}{9.22}$$

$$R_{B_v} = .2271\ W_t + 182.9$$

$$R_{B_H} = W_t\ (1.69) - W_{H_2}\ (7.26) + W_H\ (6.85)$$

$$R_{B_H} = .1832\ W_t - 60.19$$

For the maximum tail-takeoff bevel pinion design power condition of 1220 horsepower, the bearing reactions are found to be

$$R_{A_v} = (.7548)\ (4952) - 63 = 3674\ \text{lb}$$

$$R_{A_H} = (1.1832)\ (4952) + 20.77 = 5880\ \text{lb}$$

$$R_{B_v} = (.2271)\ (4952) + 182.9 = 1307\ \text{lb}$$

$$R_{B_H} = (.1832)\ (4952) - 60.19 = 847\ \text{lb}$$

The two-stage planetary unit, which is driven by the output bevel gear, drives the main rotor shaft. The two-stage planetary unit consists of two simple planetary units, with sun gear input, planetary plate output, and ring gears. The ring gears are attached to the upper main housing through a series of studs. This housing counteracts the reaction torque. The planetary gear data are given in Table V.

The loads on the upper main casting from the planetary units result from the planetary weight and reaction ring gear torque. The torque on the first-stage ring gear is given by

$$T_{R_1} = \frac{W_t\ DN}{2}$$

$$T_{R_1} = 753{,}217\ \text{in.-lb}$$

The reaction torque on the second-stage ring gear is given by

$$T_{R_2} = \frac{W_t\ DN}{2}$$

TABLE V. CH-54B PLANETARY GEAR DATA

	Reduction Ratio	Diametral Pitch Pd	Pitch Diameter D	Number of Teeth t	Pressure Angle 0	Number of Pinions n
First Stage	3.41025		-	-		7
Sun	-	7	11.142	78	22.5	-
Planet	-	7	7.8571	55	22.5	-
Ring	-	7	26.857	188	22.5	-
Second Stage	2.38554	-	-	-		18
Sun	-	8	20.750	166	22.5	-
Planet	-	8	4.000	32	22.5	-
Ring	-	8	28.750	230	22.5	-

$$T_{R_2} = 1,342,912$$

Figure 30 is a summary of the internal bearing and gear loads that must be reacted by the truss fabricated housing. Figures 31 and 32 show the applied loads on the fabricated housing.

The loadings are identical on the CH-54B servo bracket and the fabricated housing servo support bracket. For the fabricated housing design, the servo brackets have been eliminated, and a truss arrangement is designed to keep the servo attachment lug in the same location. The load on the attachment lug consists of a steady load plus vibratory load of 2,500 $\pm$ 6,000 pounds, from Reference 2.

The loading on the stationary scissor bracket, located on the top of the main gearbox housing, is a result of reacting the drag torque and pitching loads of the stationary swashplate. The load that will be used to design the stationary scissor consists of a steady load plus vibratory load of -250 $\pm$ 1,100 pounds, from Reference 2.

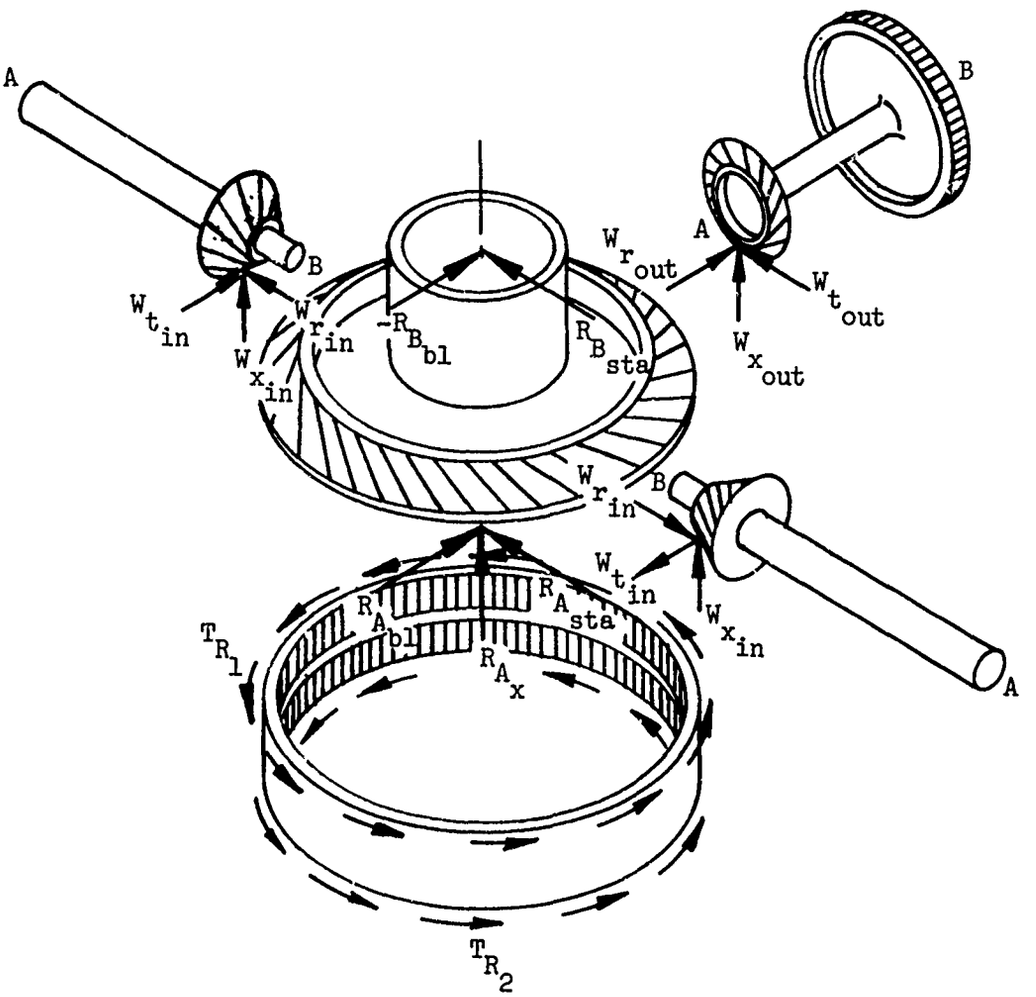

Figure 30. Summary of Bearing and Gear Loads.

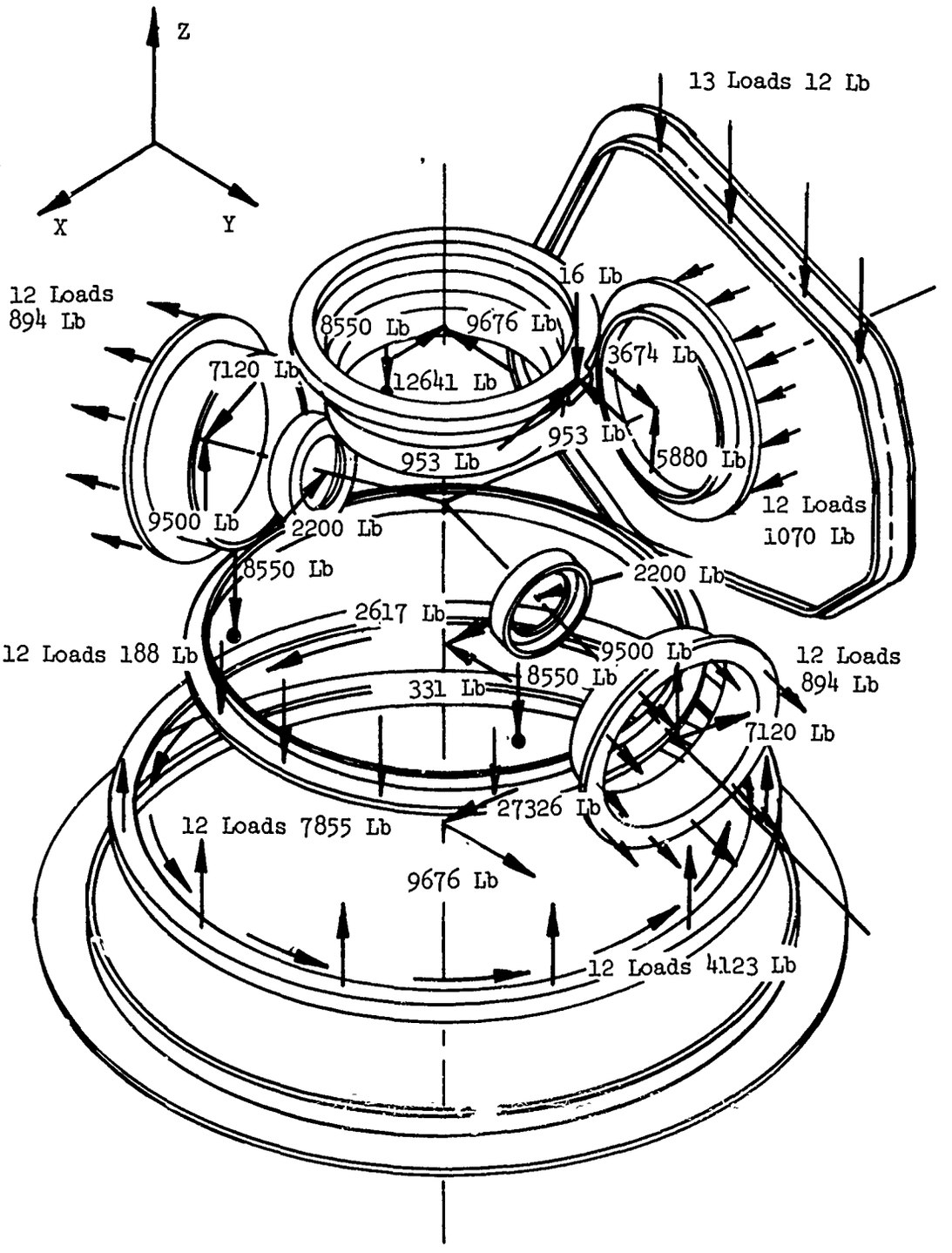

Figure 31. Applied Housing Loads for Flight Conditions (Hover).

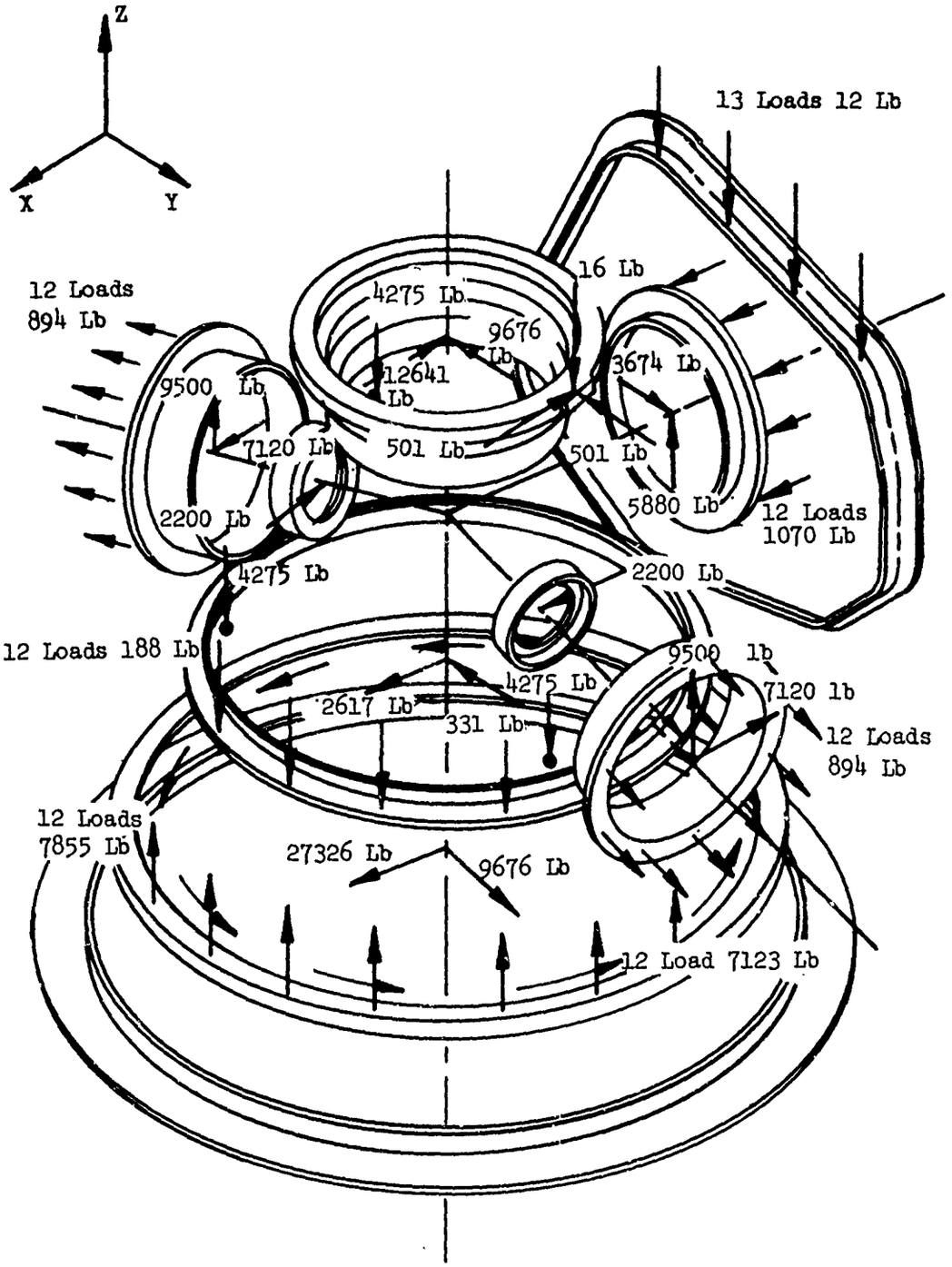

Figure 32. Applied Housing Loads for Flight Conditions (Symmetrical Dive and Pullout).

Stiffness Criteria

With the results calculated for the cast housing, only lateral and vertical spring rates can be computed at the top of the conical shell.

The stiffness requirements for the fabricated housing were determined from a simplified analysis of the conventional casting. The conventional casting was modeled as a thin-wall conical shell with boundary conditions shown in Figure 33. With the use of Reference 4, the vertical and lateral spring rates were calculated as follows

$$w = \frac{\text{ctn}^2\alpha}{E\pi r_1}\left[\frac{C_w^P}{3.3}P + \frac{C_w^V}{6.6}V\,\text{ctn}\alpha\right] \quad (13)$$

$$u = \frac{\text{ctn}\alpha}{E\pi r_1}\left[\frac{C_u^P}{3.3}P + \frac{C_u^V}{6.6}V\,\text{ctn}\alpha\right] \quad (14)$$

where:

P is the horizontal applied load

V is the vertical applied load

r_1 = 7.5 inch - upper cone radius

r_2 = 19.9 inch - lower cone radius

α = 23°14' - half cone pitch angle

h = .63 inch - shell wall thickness

μ = .35 - poisson's ratio

$\frac{r_1}{r_2} = \frac{7.5}{19.9} = .3678$

$a = \frac{\text{ctn}\,\alpha \quad h}{[12(1-\mu^2)]\ 1/2}$

$z_1 = 0$

The coefficients for use in Equations (13) and (14) are determined from the curves in Reference 4.

$$C_W^P = -10.1$$

$$C_W^V = -15.0$$

$$C_Y^P = 17.0$$

$$C_u^V = 0$$

Substituting the coefficients:

$$w = \frac{ctn^2 \alpha}{E\ r_1} \left[\frac{-10.1}{3.3} P + \frac{-15.0}{6.6} (2.3294)\ V \right]$$

$$u = \frac{ctn\, \alpha}{E\ r_1} \left[\frac{17.0}{3.3} P \right]$$

Since there is no vertical load applied to the casting V is equal to zero.

$$w = \frac{ctn^2 \alpha}{E\ r_1} \left[\frac{-10.1}{3.3} P \right]$$

$$u = \frac{ctn\, \alpha}{E\ r_1} \left[\frac{17.0}{3.3} P \right]$$

The vertical deflection is

$$w = .1084 \times 10^{-6} P$$

The vertical spring rate due to a horizontal applied load is

$$K_{Vertical} = 9.22 \times 10^6 \text{ lb/in.}$$

The lateral deflection is

$$u = .08019 \times 10^{-6} P$$

The lateral spring rate due to a hoizontal applied load is

$$K_{Lateral} = 12.47 \times 10^6 \text{ lb/in.}$$

To compare the fabricated truss-like housing with a conventional housing, the methods must be comparable. With the results calculated in the study, it was possible to determine the spring rate of any member of the truss structure. For purposes of comparison, the spring rate of the truss structure (both vertical and horizontal due to a horizontal load) at the center of the top of the truncated cone was used.

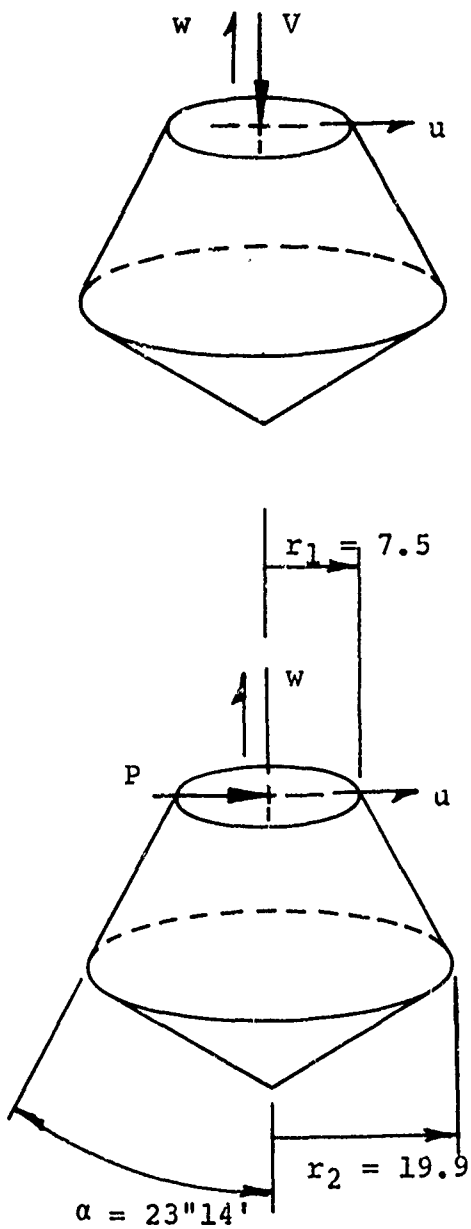

Figure 33. Shell Model for Casting Stiffness Analysis.

Selection of Materials and Joining Methods

Of the sixteen materials considered for the fabricated housing design, only three appeared to be usable in the near future: Ti-6Al-4V, Custom 455 stainless steel, and Borsical®. When compared with the titanium and Borsical®, the stainless steel alloy, Custom 455, has the highest allowable critical buckling strength, highest fracture toughness, and best combination of specific ultimate shear strength, specific ultimate tensile strength, and specific fatigue strength with temperature.

Welding was chosen as the joining method for steel and titanium. This choice was based on the fact that welding has the highest strength-to-weight ratio for steel and titanium of all the joining methods considered. Brazing-bonding was chosen as the joining method for Borsical®. Once again the decision was based on the strength-to-weight ratio as compared to other joining methods.

As discussed previously, the crash condition, 20g forward, 18g side, and 20g down, is the critical design condition. As a result, specific ultimate strength was the primary ranking item. Table VI is a list of the final material candidates and their ultimate and specific ultimate tensile strengths.

TABLE VI. STRENGTH CRITERIA FOR FINAL SELECTION OF MATERIALS FOR FABRICATED HOUSING ANALYSIS

Material	Ultimate Tensile Strength (psi)	Specific Ultimate Tensile Strength* ((psi)/(lb/in.^{3}))
Borsical®	95,000	1,000,000
Titanium, Ti-6Al-4V	140,000	875,000
Stainless Steel, Custom 455	220,000	785,000

* Specific ultimate strength is equal to ultimate strength, divided by density.

The final material candidates are ranked by cost in Table VII.

TABLE VII. MATERIAL COST CRITERIA FOR FINAL SELECTION OF MATERIALS FOR FABRICATED HOUSING ANALYSIS

Material	Rank	Approximate Cost Dollars/lb
Stainless Steel, Customer 455	1	1.40
Titanium, Ti-6Al-4V	2	9.00
Borsical®	3	20.00

Candidate Materials

The sixteen materials considered were composites and alloys of magnesium, aluminum, titanium, and steel. Important properties of each material are summarized in Table VIII. The table shows absolute and specific properties, at room temperature, 200°F, and 600°F for tensile strength, shear strength, fatigue strength, and fracture toughness. A compilation of the materials data collected during the study is included as Appendix II.

Additional data on the characteristics of the materials is included in Figures 34 through 39. Figure 34 shows the relationship between fatigue strength and temperature. Figure 35 is a graph of the specific static and fatigue properties of the materials under consideration. Figure 36 contains data on the specific tensile moduli and yield strength, while Figure 37 is a plot of specific fracture toughness versus specific yield strength. Figure 38 shows the relationship between ultimate shear strength and temperature. Figure 39 is a plot of the ultimate tensile strengths of the materials.

Whereas magnesium and aluminum alloys have relatively low strength, fatigue, and creep properties, they have excellent thermal characteristics. Table IX lists thermal conductivities of the material candidates. In the worst case, magnesium has about twelve times the thermal conductivity of steel alloys.

The thermal characteristics of a fabricated housing can be assessed realistically only through testing. The material (steel) finally selected for the fabricated housing was chosen independently of its thermal characteristics, since only 12 to 15 percent of the heat generated in the drive train is transferred through the housing. The convective heat transfer coefficient, the most significant factor in determining overall gearbox housing heat rejection rate, can be determined only through testing, and no analytical estimates were made.

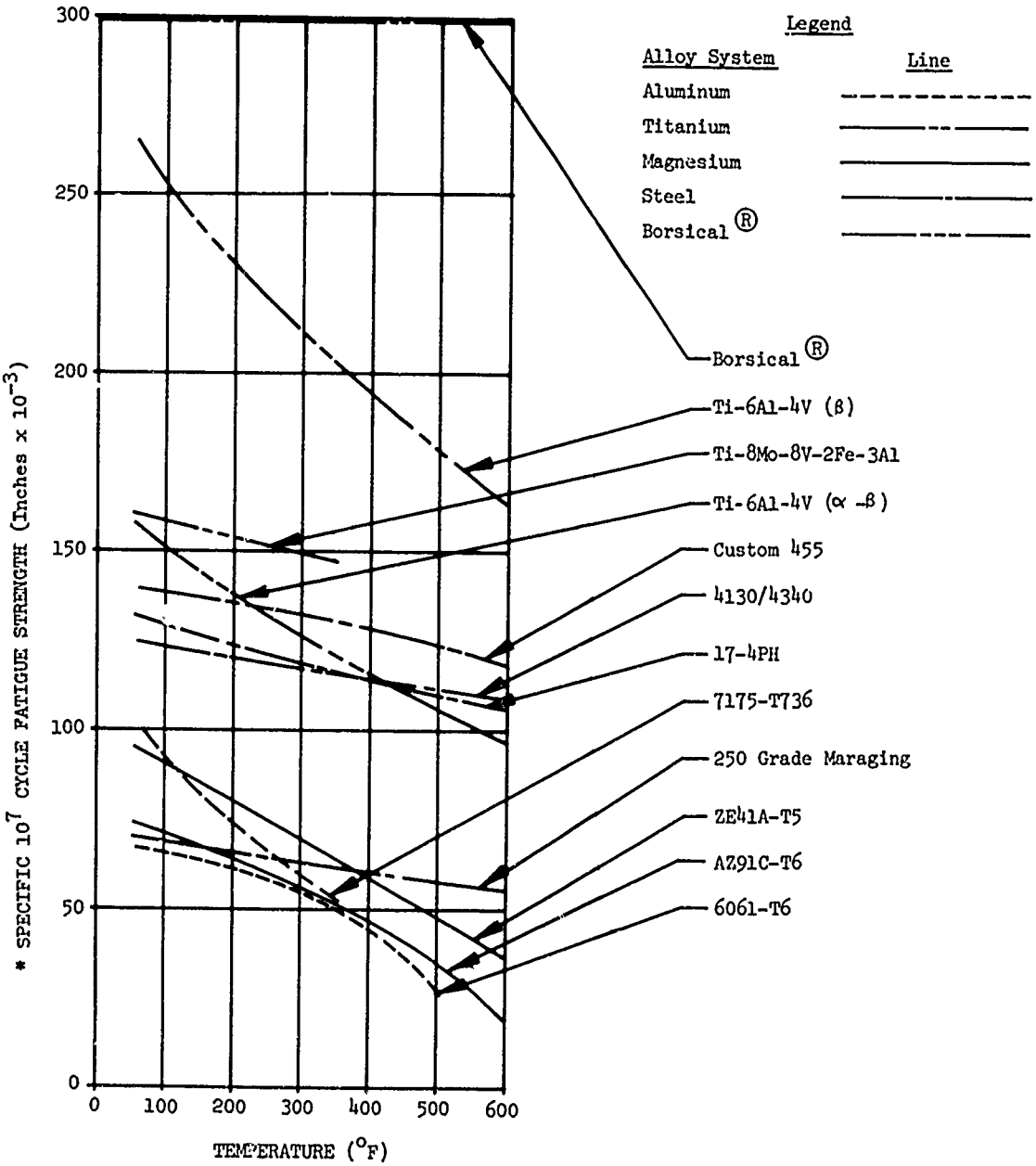

*NOTE: 600° Fatigue Strength Estimated in a Number of Cases

Figure 34. Specific 10^7 Cycle Fatigue Strength Versus Temperature.

MATERIAL/CONDITION	DENSITY ($lb/in.^3$)	ULTIMATE TENSILE STRENGTH (ksi)					
		R.T.	(Ab. R.T)	200°F	(Ab 200°F)	600°F	(Ab 600°F
AZ91C-T6 (CLASS 3)	0.0652	27	(414)	23.5	(360)	6.8	(104)
ZE41A-T5 (OVER 50 LB)	0.066	26	(395)	24	(364)	10	(150)
6061-T6(bar)	0.098	42	(429)	38	(388)	(½hr) 8.8	(86)
7175-T736	0.101	76	(750)	10,000 hr 73	(720)	(½hr) 42	(415)
Ti-6Al-4V(α-β)	0.160	130	(812)	118	(737)	97.5	(610)
Ti-6Al-4V(β)	0.160	140	(875)	127	(795)	105	(650)
Ti-8Mo-8V-2Fe-3Al	0.175	180	(1030)	160	(915)	145	(828)
17-4PH(1025)	0.282	155	(550)	149	(529)	130	(460)
250 GRADE MARAGING	0.289	295	(848)	244	(844)	240	(830)
4130/4340	0.283	180	(636)	175	(618)	160	(565)
CUSTOM 455	0.280	220	(785)	214	(765)	187	(668)
"S" GLASS/EPOXY	0.067	195	(2900)	195	(2900)	~175	(2600)
"E" GLASS/EPOXY		160	(2390)	160	(2390)	~145	(2170)
HIGH STRENGTH GRAPHITE	0.057 ($E=20\times10^6$)	134	(2350)	134	(2350)	~120	(~2100)
HIGH MODULUS GRAPHITE	0.053 ($E=26\times10^6$)	100	(1880)	100	(1880)	~90	(~1690)
BORSIC ALUMINUM	0.098	95	(930)	95	(930)	95	(930)

TABLE VIII MATERIAL TRADE-OFF SELECTION CHART

STRENGTH (ksi)			ULTIMATE SHEAR STRENGTH (ksi)						(Reduced ap FATIGUE STRE		
200°F)	600°F	(Ab 600°F)	R.T.	(Ab R.T.)	200°F	(Ab 200°F)	600°F	(Ab 600°F)	R.T.	(Ab R.T.)	2(
360)	6.8	(104)	15.0 (CLASS 3)	(230)	16	(245)	4.5	(68)	4.8	(73)	
384)	10	(150)	20.0	(300)	18.5	(280)	7.7	(115)	6.2	(94)	
388)	(½hr) 8.8	(86)	27	(275)	24.5	(250)	5.6	(57)	6.5	(66)	
720)	(½hr) 42	(415)	42	(415)	40	(395)	23	(228)	10	(99)	
937)	97.5	(610)	76	(475)	71	(444)	57	(356)	25 (Plate)	(156)	
795)	105	(650)	86	(537)	80	(500)	64	(400)	42	(262)	
915)	145	(828)	105	(600)	97	(555)	78	(445)	28	(160)	
729)	130	(460)	100	(354)	95	(337)	71	(252)	37	(131)	
844)	240	(830)	150	(518)	145	(502)	120	(415)	20	(69)	
618)	160	(565)	108	(382)	105	(371)	99	(350)	35	(124)	
765)	187	(6[illegible])	135	(482)	130	(465)	113	(403)	39	(139)	
2900)	~ 175	(2600)	5.4	(80)	5.4	(80)	~ 2.7	(~ 40)	18	(270)	
2390)	~ 145	(2170)	5.2	(77)	5.2	(77)	~ 2.6	(~ 38)	12	(180)	
350)	~ 120	(~ 2100)	16	(280)	16	(280)	~ 8	(~ 140)	30	(525)	
880)	~ 90	(~ 1690)	9	(150)	8	(150)	~ 4	(~ 750)	22	(415)	
930)	95	(930)	17.5	(180)	17.5	(180)	~ 4	(~ 40)	17.5(T)	(178)	

BLE VIII MATERIAL TRADE-OFF SELECTION CHART

RENGTH (ksi)			(Reduced approx. for Scatter & Size Effect) FATIGUE STRENGTH @ 10^7 CYCLES(20ksi Fs)						CRITICAL BUCKLIN		
00°F)	600°F	(Ab 600°F)	R.T.	(Ab R.T.)	200°F	Ab 200°F	600°F	(Ab 600°F)	R.T.	(Ab R.T.)	200
5)	4.5	(68)	4.8	(73)	4.2	(64)	~ 1.2	(18)	16ksi @ R/t=17	(245)	
0)	7.7	(115)	6.2	(94)	5.3	(80)	~ 2.4	(36)	22ksi @ R/t=17	(333)	1
50)	5.6	(57)	6.5	(66)	6.0	(61)	unkown		(tan. mod) 25	(255)	2
5)	23	(228)	10	(99)	7.5	(74)	2.5	(84)	(tan. mod) 50	(495)	
4)	57	(356)	25 (Plate)	(156)	22	(138)	15.5	(97)	107	(670)	~
0)	64	(400)	42	(262)	37	(231)	26	(163)	117	(730)	~
5)	78	(445)	28	(160)	27	(154)			~ 145	(~ 825)	~1
7)	71	(252)	37	(131)	35	(124)	30	(106)	126	(446)	
2)	120	(415)	20	(69)	19	(66)	16	(55)	200	(692)	~
1)	99	(350)	35	(124)	34	(120)	31	(109)	135	(477)	
5)	113	(403)	39	(139)	38	(135)	33	(118)	~ 156	(~ 557)	~
0)	~ 2.7	(~ 40)	18	(270)	18	(270)	~ 16	(~ 240)	~ 60	(~ 895)	~
7)	~ 2.6	(~ 38)	12	(180)	12	(180)	~10	(~ 150)	~ 70	(~ 1040)	~
0)	~ 8	(~140)	30	(525)	30	(525)	~ 25	(~ 440)	182	(3190)	
0)	~ 4	(~750)	22	(415)	22	(415)	~ 18	(~ 340)	100	(1880)	1
0)	~ 4	(~ 40)	17.5(T)	(178)	17.5(T)	(178)	~ 4(T)	~ 40	200	(3750)	2

CRITICAL BUCKLING STRENGTH (F_{cc} OR SECANT)						FRACTURE TOUGHNESS (ksi (in)½)		
R.T.	(Ab R.T.)	200°F	(Ab 200°F)	600°F	(Ab 600°F)	R.T.	200°F	600°F
16ksi @ R/t=17	(245)	13	(199)	3.2	(49)	11.7	~	~50
22ksi @ R/t=17	(333)	19.5	(295)	9.8	(148)	14.1	~35	~55
(tan. mod) 25	(255)	23.8	(243)	3.9	(40)	very high	higher	highest
(tan. mod) 50	(495)	46	(455)	4.4	(43)	23.8	34	≫ 34
107	(670)	~ 100	(625)	75	(469)	40	44	≫ 44
117	(730)	~ 110	(687)	82	(512)	74	81	≫ 81
~ 145	(~ 825)	~139	~795	~100	(~570)	52	60	≫ 60
126	(446)	114	(405)	77	(273)	~ 55	> 60	≫ 60
200	(692)	~ 190	(657)	175	(605)	67	~ 90	≫ 90
135	(477)	120	(425)	97	(343)	110	124	≫124
~ 156	(~ 557)	~ 150	(~535)	~ 120	(~429)	90	~ 100	≫100
~ 60	(~ 895)	~ 60	(~ 895)	~ 45	(~ 670)			
~ 70	(~ 1040)	~ 70	(~ 1040)	~ 55	(~ 815)	N/A		
182	(3190)	182	(3190)	~145	(2540)	N/A		
100	(1880)	100	(1880)	~ 80	(~1500)	N/A		
200	(3750)	200	(3750)	~160	(~ 3000)	N/A		

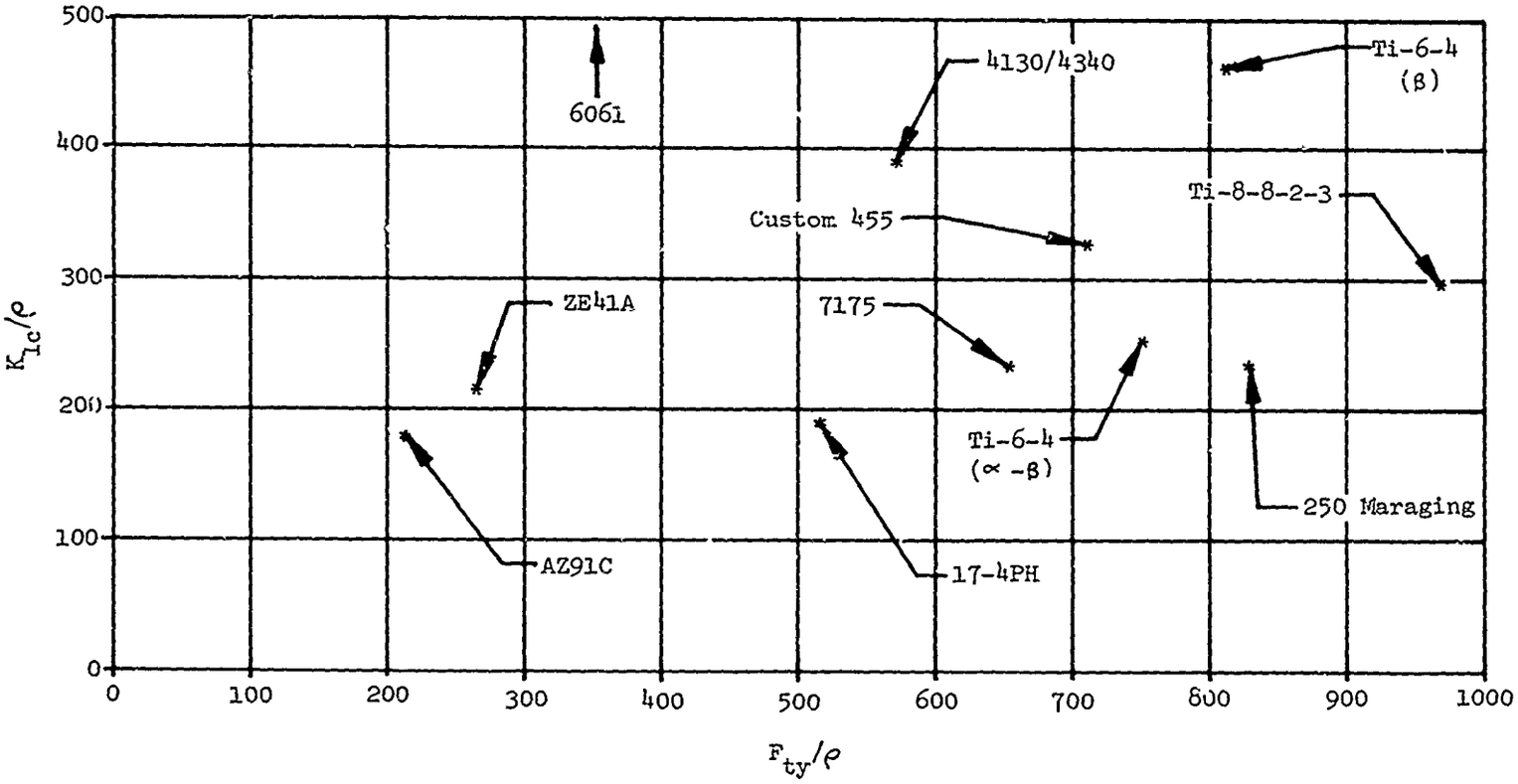

Figure 35. Specific Fracture Toughness Versus Specific Yield Strength.

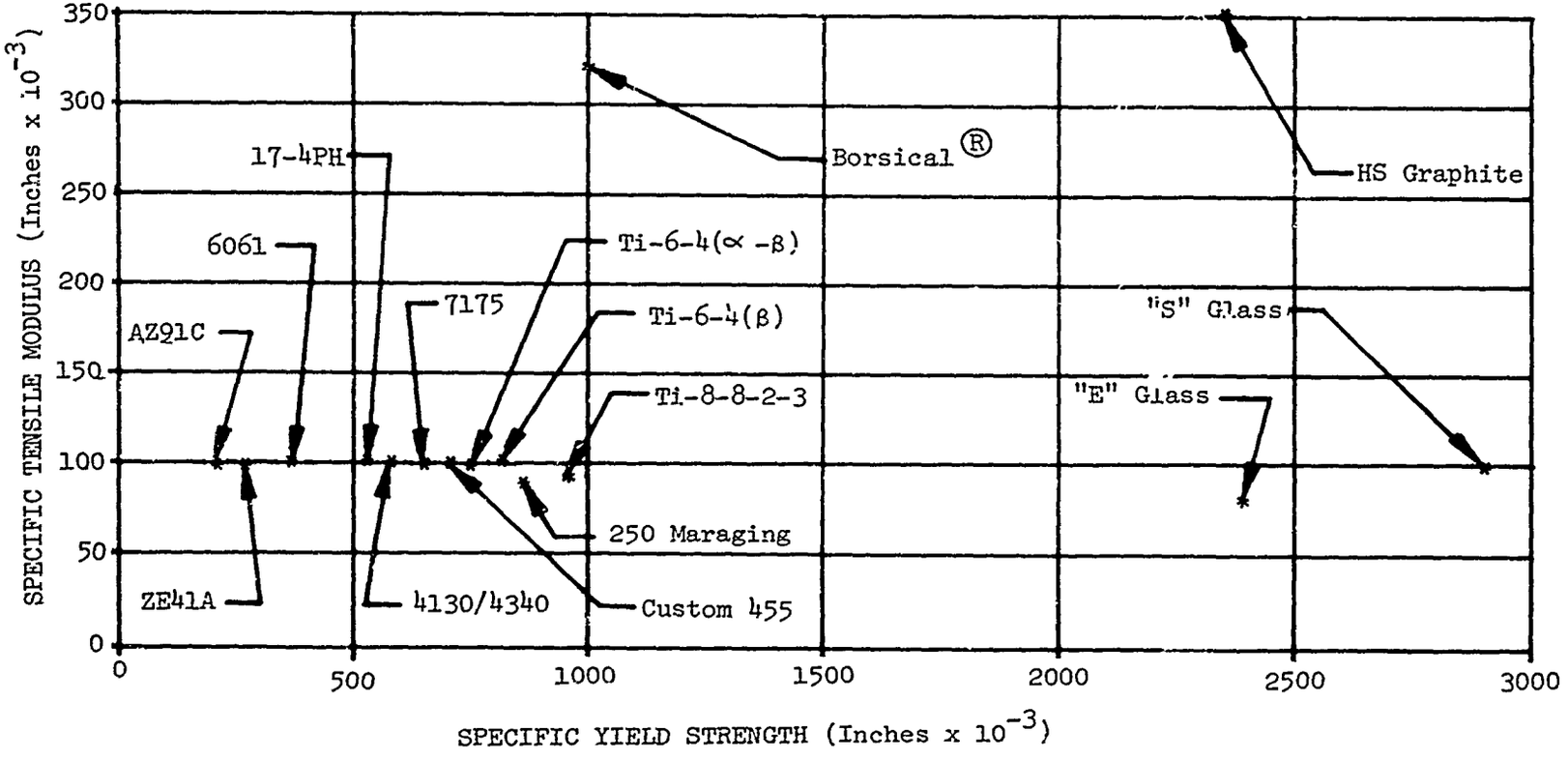

Figure 36. Specific Stiffness Versus Specific Yield Strength.

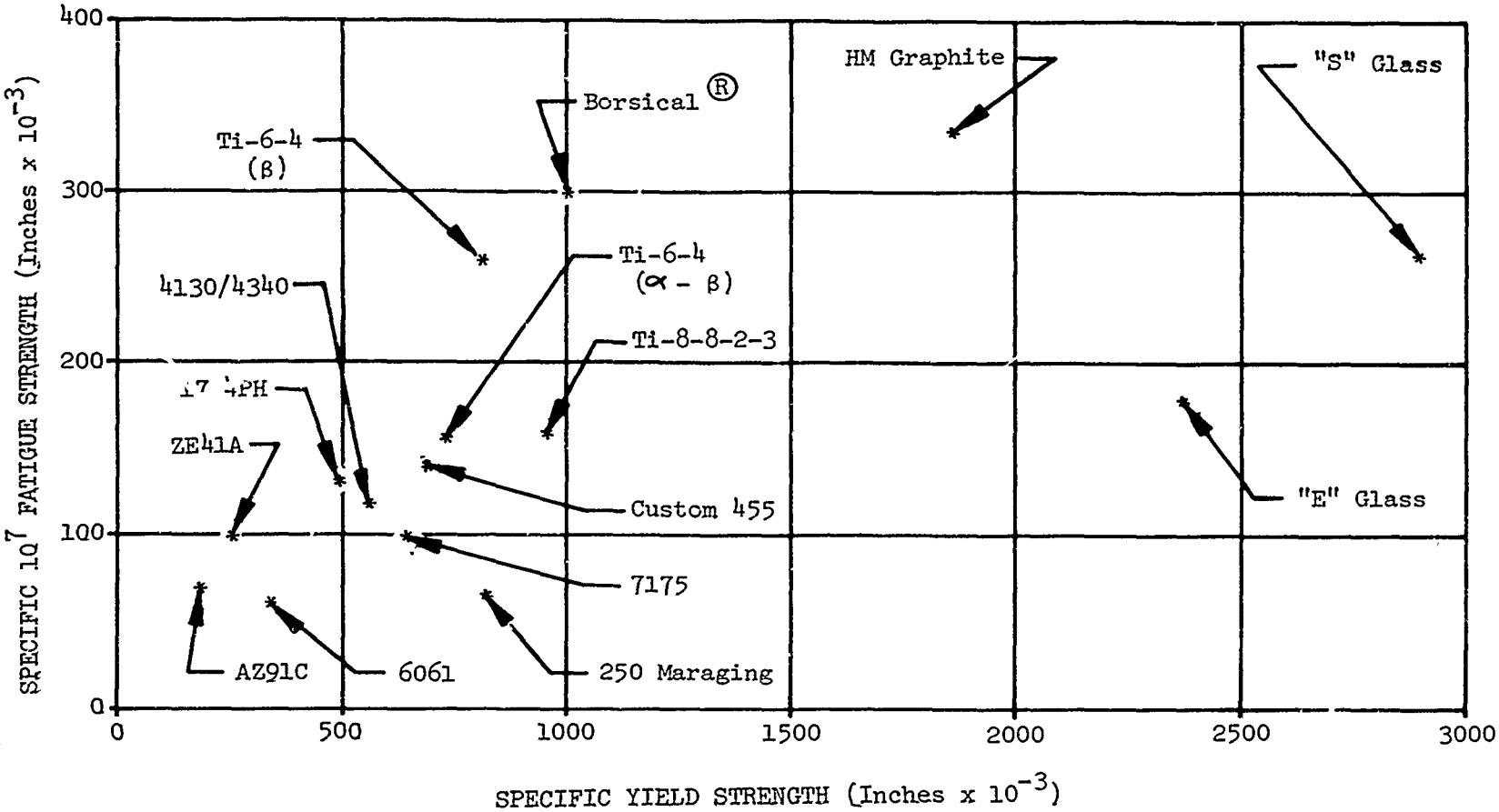

Figure 37. Specific 10^7 Fatigue Strength Versus Specific Yield Strength.

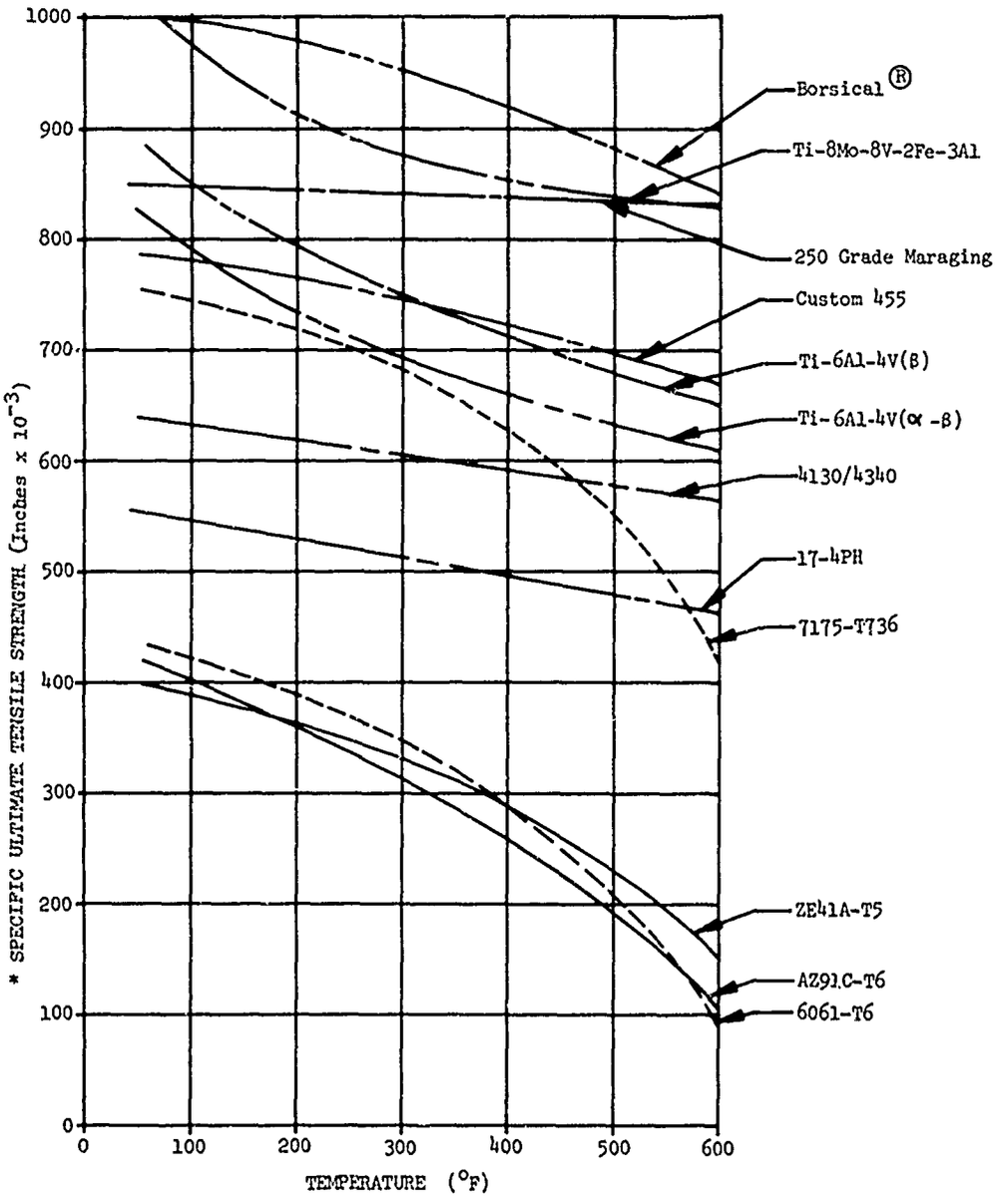

Legend

Alloy System	Line
Aluminum	– – – – –
Titanium	—·—·—
Magnesium	———
Steel	—— – ——
Borsical®	—— · · ——

* NOTE: Strength at 600°F is After 1/2 Hour Exposure

Figure 38. Specific Ultimate Tensile Strength Versus Temperature.

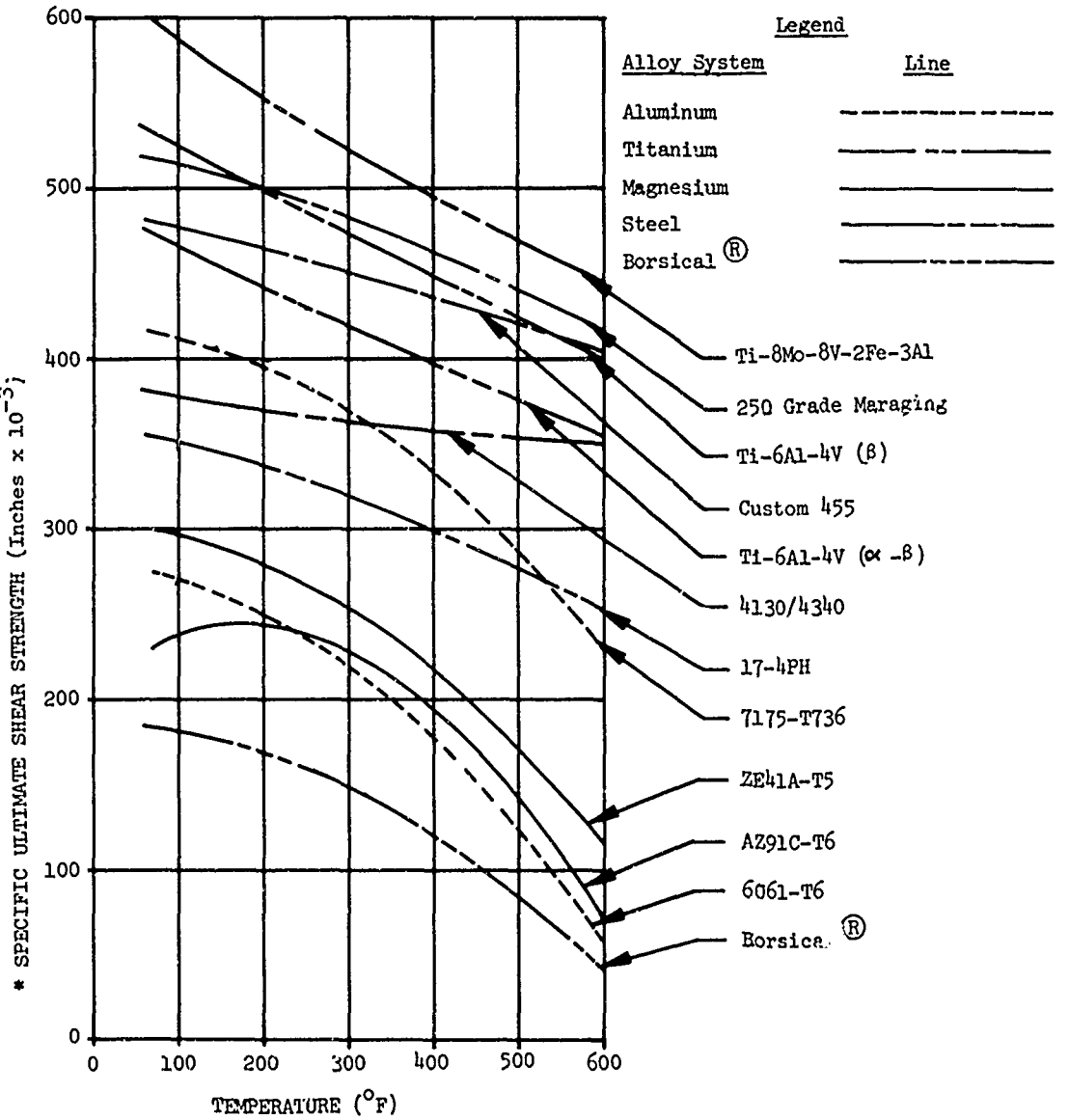

* NOTE: Strength at 600°F is After 1/2 Hour Exposure

Figure 39. Specific Ultimate Shear Strength Versus Temperature.

The magnesium alloys were eliminated from consideration on the basis of low yield, ultimate and fatigue strength at room and elevated temperatures. An additional problem is that thin wall castings are difficult to achieve. Casting technology has remained static, so magnesium casting alloys were considered to hold no future promise.

Aluminum alloys 6061-T6 and 7175-T736 in wrought form were eliminated from consideration due to poor properties at high temperatures. In the 600°F temperature range (emergency operaging condition), all aluminum alloys are significantly above their aging temperature. Interaction of fatigue and creep is not defined in this region, so the material is considered to be an unnecessarily high risk.

Titanium alloys, Ti-6Al-4V in either the alpha or alpha-beta form and Ti-8Mo-8V-2Fe-3Al, show promise for application in a truss fabricated housing design and were retained in the study.

TABLE IX. THERMAL CONDUCTIVITIES OF MATERIAL CANDIDATES

Material	Thermal Conductivity (Btu/ft/hr ft^2 °F)
AZ91C-T6	32.4
ZE41A-T5	61.8
6061-T6	96
7175-T736	70
Ti-6Al-4V	4.7
Ti-8Mo-8V-2Fe-3Al	4.8
17-4PH	8.5
250 Grade Maraging	14.5
4130/4340	21.7
Custom 455	10.4
"S" Glass	.12
"E" Glass	.12
HS Graphite	.8
HM Graphite	.8
Borsical ®	56

The data on the material selection chart shown in Table VIII and the data in Appendix II are displayed graphically in Figures 34 through 39.

Steel alloys 17-4PH, 250 Grade Maraging, 4xxx series, and Custom 455 were considered. 17-4PH was eliminated from consideration, since an improved version with higher strength is available in Custom 455. Production experience with 17-4PH is directly applicable to Custom 455. The 250 Grade Maraging steel has excellent properties, but it was eliminated because of production and processing problems. One problem with 250 Grade Maraging processing is that a stratified composition (banding) often results which is associated with austenitic segregation and alloy (chemical) segregation. Property variations in different lots and this stratified composition problem have occurred in Air Force production. As a result, 250 Grade Maraging steel was not considered for fabricated housings. The 4xxx series alloys, in particular 4130 and 4340, have the necessary specific properties, but require heat treatment to obtain these properties. The 4xxx series alloys were eliminated from consideration, since the quenching process during heat treatment will result in some warpage even with a quench fixture.

Glass, graphite, boron and PRD-49 composites were considered in the study. The high-strength, highly oriented filaments in these materials make them possible choices for use in fabricated housings. However, when joining methods are investigated, it is found that effective shear transfer methods for these materials are undeveloped. Thus, these materials were dropped from consideration.

From an investigation of all the figures and material characteristics, the most promising materials for design of a fabricated truss-like housing are Ti-6Al-4V, Custom 455 stainless steel, and Borsical®.

The material study did not include an evaluation of fatigue crack propagation. Although damage tolerance analyses, including ballistic lateral damage, fracture toughness, and fatigue crack propagation exist and are in routine use, a more conservative approach was applied in this sutdy. For the study, initiation of a crack in any member or joint was considered to result in immediate loss of load-carrying capability of the entire member. This approach simplified the analytical work in the NASTRAN analysis and added conservatism to the study approach.

Rationale for Joining Method Selection

Six methods were considered for joining members of the fabricated housing: mechanical fastening, riveting, bolting, welding, bonding, and brazing. Figure 40 shows the different types of joints applied to a fabricated housing design.

For a mechanical, friction, riveted or bolted joint, a fitting or overlap area is required between the two joined materials. This results in increased weight and a greater cost per unit volume of joined material than for any other fastening method.

Figure 41 is a typical friction trapped joint that would be used in a composite material design. Increased axial load in the fibers results in axial load in the fitting plus radial tension or compression. The mechanical joint is an unnecessarily heavy way of making a connection, so it is unsatisfactory for a fabricated housing design.

Riveting was eliminated from consideration for the following reasons:

1. For the large loads in the structural members, many rivets are required to transfer the load. The result is a heavy, bulky joint. The typical fabricated housing has more than one hundred joints.

2. The clamping force in the rivet, which permits load transfer through friction, cannot be controlled adequately.

3. Expansion of the rivet in the hole is not always uniform and can cause stress concentrations and nonuniform load distribution in the rivets.

4. Vibration in the structure can cause loss of clamping force in the rivet, which would require excessive inspection and re-riveting.

Riveting is one possible method of attaching the skin covering for retention of oil in the truss housing structure. Because the loads are not large, this is an ideal application for riveting.

Parts that are riveted can also be bolted. If a joint is designed for rivets, a bolt of the same size can be substituted for each rivet. The resulting joint is stronger by approximately fifty percent. The best loading design occurs when the fasteners are loaded in shear. When it is impossible to avoid tension loading, as would occur in at least some of the main truss joints, the bolt should be used over a rivet. An important advantage of bolts over rivets is the ability to

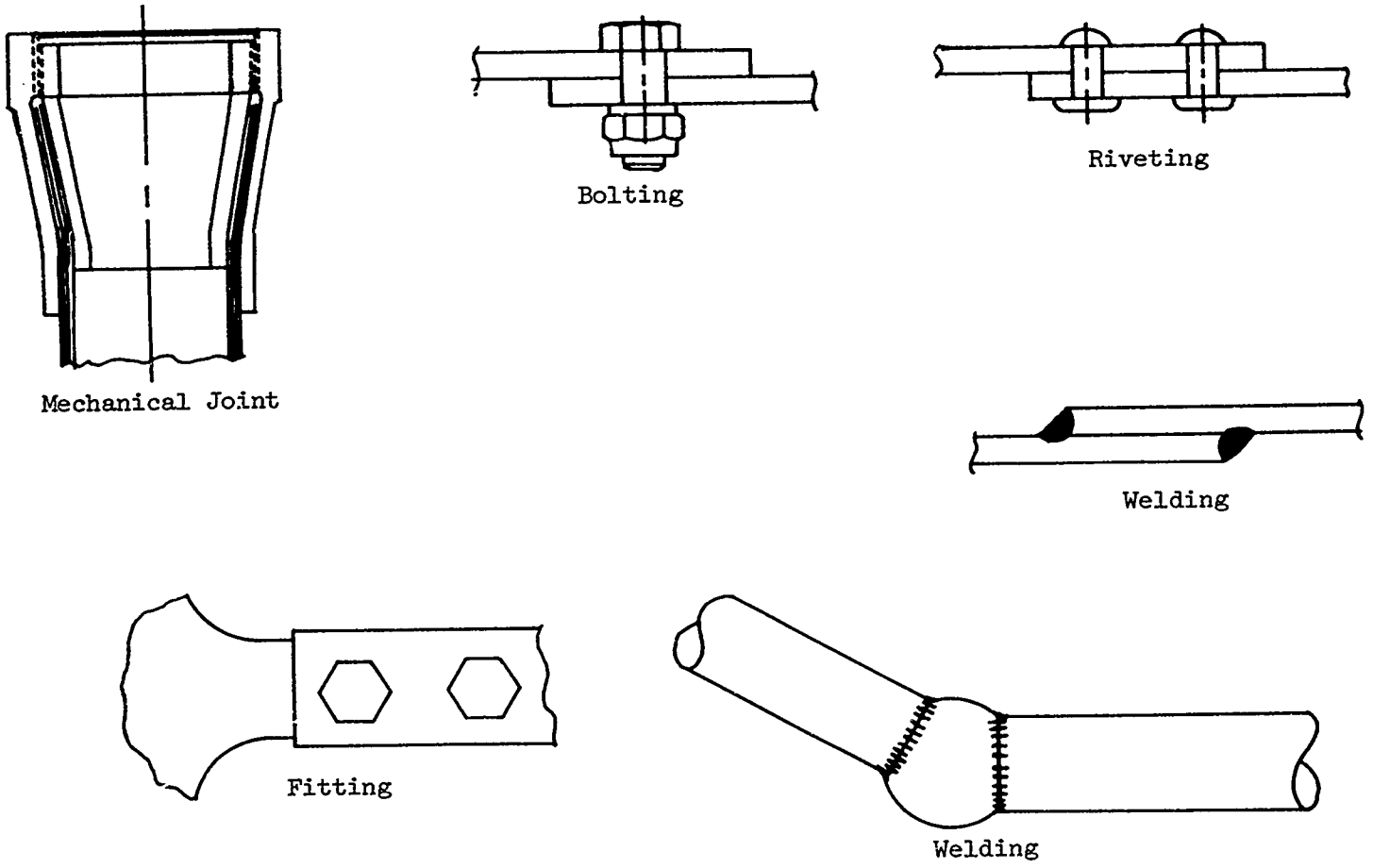

Figure 40. Various Joining Methods.

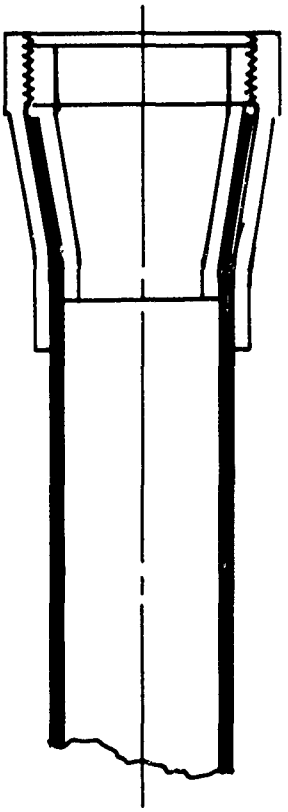

Figure 41. Friction Trapped Joint Used for Composite Material.

control the clamping force accurately. The clamping, or preload, force tends to distribute the load over a larger area and give the bolted joint greater fatigue strength than the riveted joint. The bolted joint has the added advantage of easy assembly and disassembly with standard field equipment.

With each joint, bolted or riveted, some form of fitting is required. The design of the fitting is heavy, due to the many unknowns in the analysis of fittings. Typical practice in the design of aircraft is to require a fitting factor of +.25 as the minimum margin of safety instead of a 0.0 margin of safety based on yield or ultimate criteria. The analysis of joints is quite complicated, due to the combined stresses in the joint and fastener, tolerance buildup, and the values for allowable chafing stress and stress concentration factors for fatigue applications.

The relatively high weight of the bolted or riveted joint and the relatively high cost of fabrication make the bolted or riveted connection unsatisfactory for the fabricated housing design.

Bonded joints for a fabricated housing design would require large, heavy lap joints to have a high joint fatigue strength. The bonding agent serves a multiple purpose, since it also acts as insulator to prevent galvanic corrosion between dissimilar materials.

To use bonding properly in a fabricated housing design, it is necessary to protect the adhesive from the internal gearbox environment. The joint would be exposed to approximately 240°F synthetic diester base oil. This oil has a severe degrading effect on most bonding agents. At present, only two possible adhesives, American Cyanamid HT 424 and Hysol EA 912, appear able to survive in the internal gearbox environment. These two adhesives may allow the placing of structural joints internal to the oil-holding skin covering. However, these adhesives require verification, so bonding will be considered only for joining the skin covering external to the load-carrying truss structure.

Brazing exhibits relatively low joint strength and is thus not considered for attaching structural truss members. However, brazing is the only feasible way of joining Borsical®, since it is not weldable. Borsical®, appears to have little potential in a fabricated housing application due to the high risk of brazing.

The most practical way of fabricating a truss-like housing appears to be weldment construction; welding offers a simple joint design and high static joint efficiency. Figures 42 and 43 are typical welded details considered acceptable for a fabricated housing design.

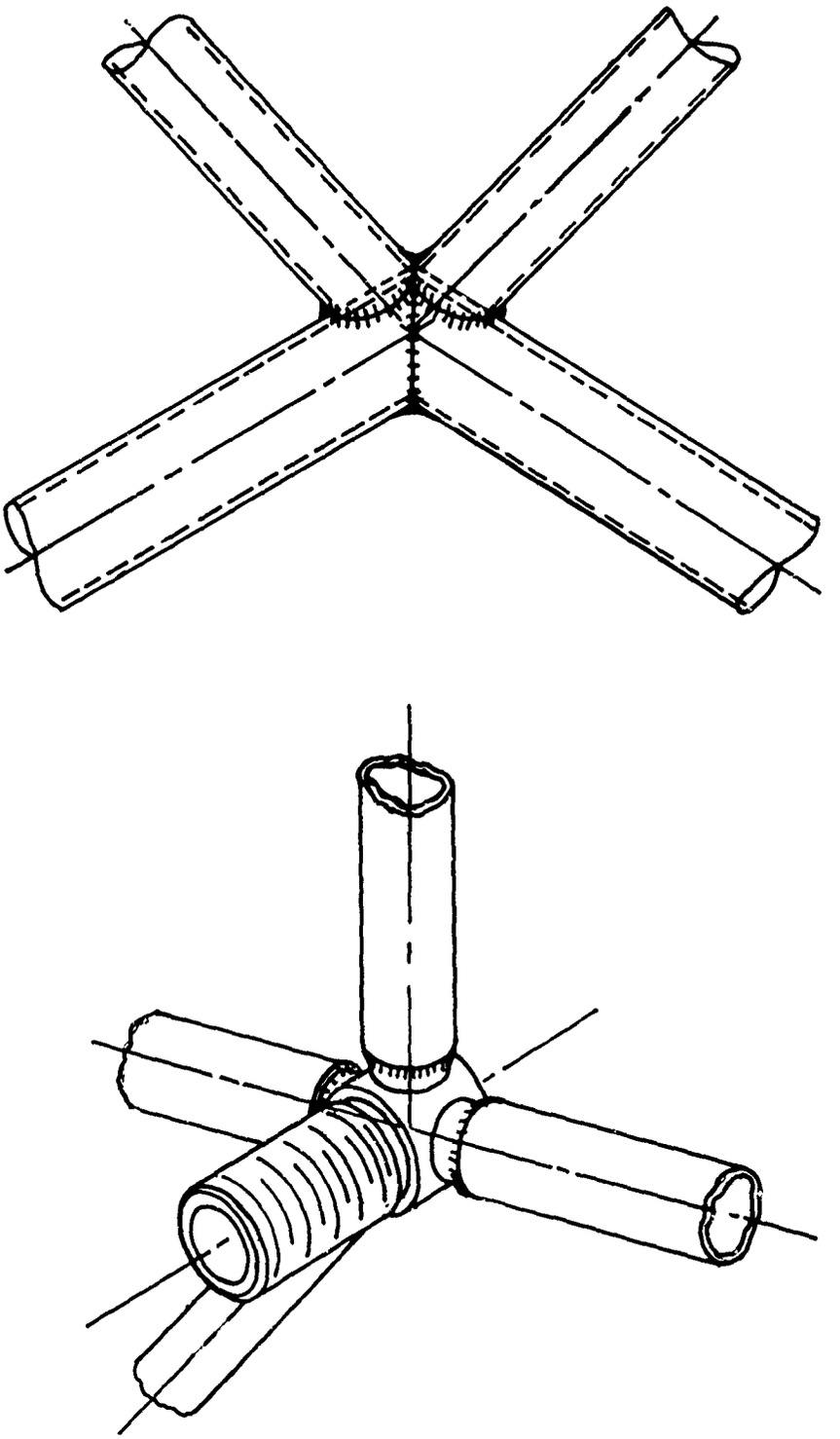

Figure 42. Typical Welded Joint.

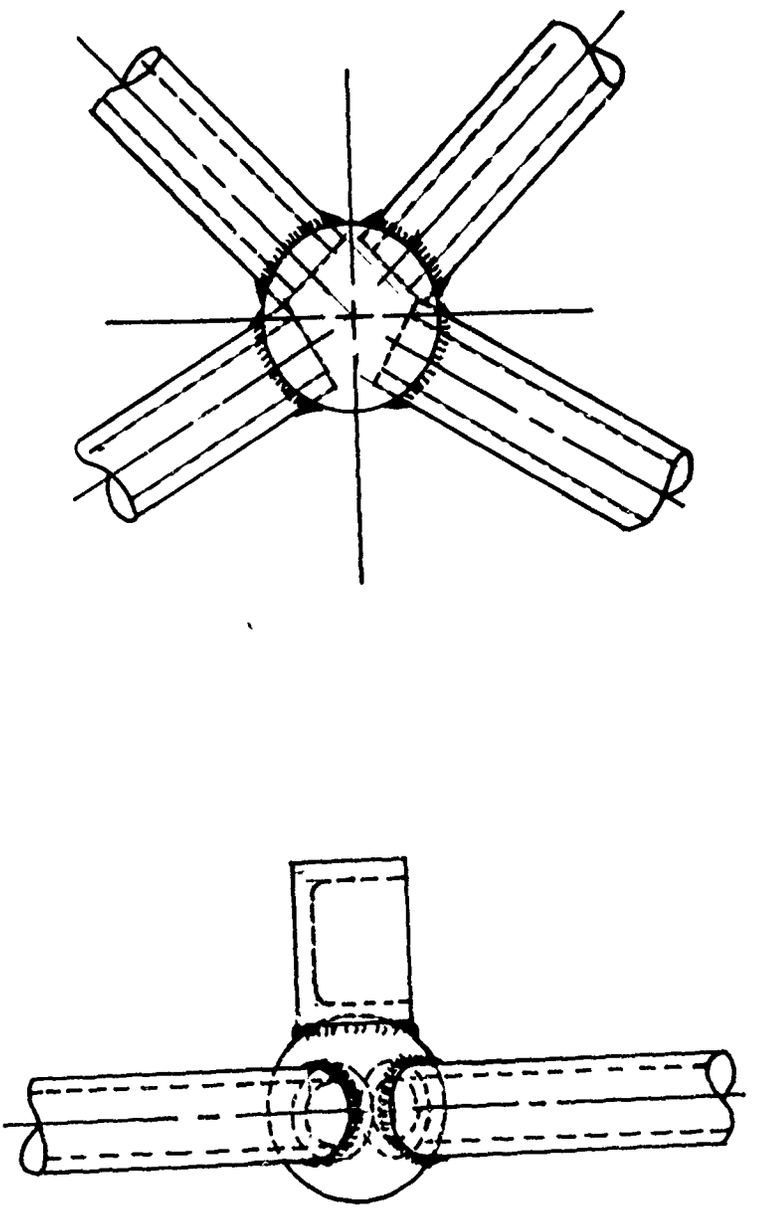

Figure 43. Typical Welded Joint.

The titanium alloys considered in this study may be joined by electron-beam welding, plasma-arc welding, inertia bonding, or diffusion bonding.

Electron-beam welding is generally considered more reliable (and more expensive) than the other methods as long as the joint can be designed to allow machining off the weld protrusion which occurs on the side of the weld away from the incoming beam. This protrusion is the region where weld voids occur.

Plasma-arc welding is less expensive than electron-beam welding but requires close quality control to limit hydrogen gas voids in the weldment due to reduction of water vapor by the molten titanium. The state of welding art has been advanced to the point where the hydrogen void is only a minimal problem in fatigue. Stress concentration factors from hydrogen-gas voids are negligible for static (crash loads) analysis, and the static joint efficiency is very close to unity.

Inertia bonding (also known as friction welding) requires a symmetrical structure since no control exists of the angular position of one portion of the structure relative to the other. Present structural designs are asymmetrical, effectively eliminating this process from consideration.

Diffusion bonding, either low-pressure long-time or forge-diffusion bonding, may be effectively applied to housing fabrication. Properties have been degraded by long times at high temperatures (press-diffusion bonding), and costs of press-diffusion bonding do not appear to hold much promise for reductions in the future. Forge diffusion bonding may be applied to attachments where maximum strength is required, applying some other fastening method to a lower-stressed area. Results of Contract Number DAAG46-73-C-0126 (USAAMMRC) indicate that static and fatigue properties across the forge-diffusion bond line are the same as the parent metal properties. Data from that contract will be available for follow-on design in a short time.

Static joint efficiencies of weldments for various material candidates are summarized in Table X. While magnesium and aluminum alloys exhibit high static joint efficiencies in the weld, they rank low in the product of ultimate tensile strength and static joint efficiencies. The only materials being considered for a welded fabricated housing design, based on material study, are Custom 455 stainless steel and Ti-6Al-4V.

TABLE X. STATIC JOINT EFFICIENCIES OF WELDMENTS FOR MATERIAL CANDIDATES.

Material	Static Joint Efficiency	Product of Specific Ultimate Tensile Strength and Static Joint Efficiency (psi x 10^3)
AZ91C-T6	.95	394
ZE41A-T5	.95	375
6061-T6	.95	408
7175-T736	N/A	Not Weldable
Ti-6Al-4V	.95	790
Ti-8Mo-8V-2Fe-3Al	1.00	1030
17-4PH	.95	522
250 Maraging	.90	762
4340	.90	572
Custom 455	.95	742

Evaluation of joint fatigue strength is extremely difficult in light of the number of variables involved. A qualitative approach requires that design requirments for fatigue strength be met through quality control.

It remains to be seen whether a rigorous fatigue analysis of welded joints is required for transmission housings. The high static crash load conditions normally size the structure, and the fatigue loads remain relatively low under 1g forward flight. However, some qualitative discussion of welding quality control and fatigue strength interactions appears required to outline the state of the art, the trends of the state of the art, and the method of analysis which can be applied to fatigue analysis of welded joints.

At this time, hydrogen voids in titanium weldments are being found in the thicknesses which would be used in a built-up transmission. These voids are of the order of 0.006 inch in diameter (maximum). With improved techniques, it is expected to find voids whose diameters are as small as 0.004 inch with 80 percent probability. Voids as small as 0.002 inch in diameter have been the origins of fatigue failures in laboratory specimens. Theoretical and experimental analyses agree that the controlling variable in determining the stress concentration of a void in a weldment is not the diameter of the void but the ratio of the void diameter to the distance of the void's center from the free (stressed) surface. With the residual stresses from shotpeening, the effective depth of any size void

may be limited to the depth of the residual compressive stresses from peening. This limits the effective stress concentration factor of the worst possible void (described above) to a theoretical stress concentration factor of 2.6, the same as a filled rivet hole.

The effects of voids in titanium weldments are negligible in static conditions. Sound welds in titanium approach unity for static joint efficiency. Joint efficiencies in fatigue may be further improved by applying a static load slightly in excess of 50 percent of the yield load of the structure. This would yield out the local areas around any voids and induce residual compressive stresses on springback of the surrounding structure. To apply this technique, the fatigue stress vector must be known, must never change direction, and must always be low enough so that cyclic-stress induced fading is not a problem. Although promising, this concept would require further research before it could be applied in practice.

Custom 455 is not prone to formation of voids in welding. It is possible, should the heat-input to the weld go out of control, to overheat the material and boil off copper from the weld. However, this is not a normal problem with plasma-arc welds and does not require serious consideration. Welds in Custom 455 have been shown to have nearly unity joint efficiency. Further improvements in welding techniques will probably improve the welded strength of Custom 455 more than titanium (i.e., heat input control, cleanliness, radiographic inspection).

Candidate Materials for Skin Covering

A skin covering material is required to contain transmission oil within the truss members of the fabricated housing. A number of materials were considered, including stainless steel sheet, titanium sheet, and a composite. Various joining methods were studied, including mechanical fastening, brazing, welding, and bonding.

The combinations of skin-truss investigated include Carpenter 455 stainless steel truss with a stainless steel sheet covering, Ti-6Al-4V truss with a titanium sheet covering, and a stainless steel or titanium truss with a composite covering. Figure 44 is a sketch of the detail of typical skin-truss member joints. The connections include brazing or welding the sheet to the tube (a), a bonded joint to tube structure (b), and a mechanical trapped fastening system (c).

Sealing provisions require that the assembled joint be oil tight for at least 5,000 hours at 200°F. The skin is nonstructural. Thickness is stainless and titanium is .020 inch. The relatively large panel size results in oil canning if any appreciable load is applied. The joining method of attaching skin to truss is,

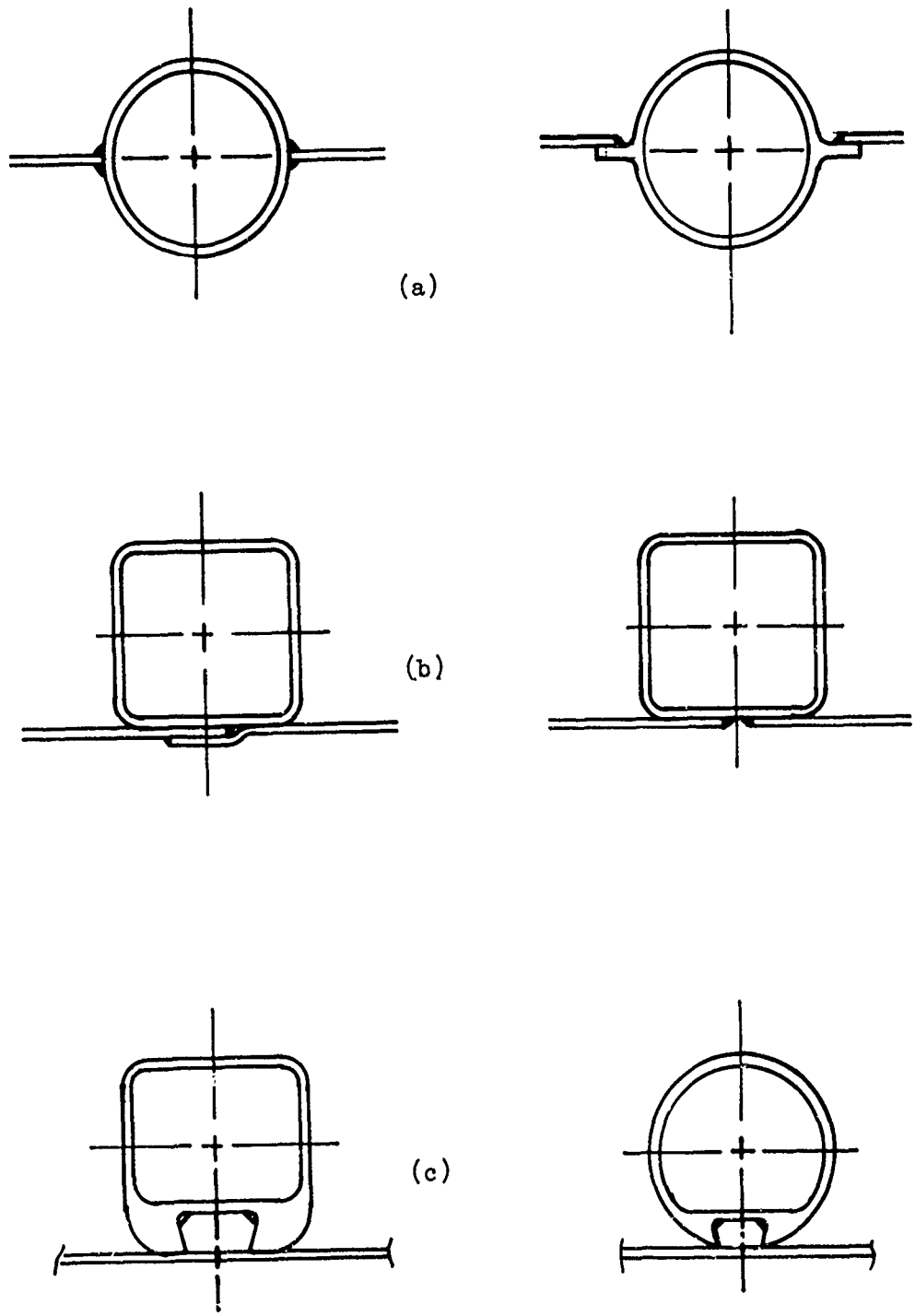

Figure 44. Sketch of Typical Skin Truss Connection.

therefore, expected to be lightly loaded. At 600°F for approximately one-half hour, skin-panel truss connection need not be oil tight, but the skin panels must not fall out of place and cause meshing problems with the gears. The skin panel truss connection is exposed to hot, synthetic, diester base oil with thermal cycling for long periods.

Access panels are provided to permit inspection of the input bevel gear mesh, tail-takeoff gear mesh, and planetary gear unit. The access panel is provided with quick-disconnect fasteners used for joining the access panel to the skin panel. A simple gasket or "O" ring is used for sealing the oil in the truss structure.

For joining the skin covering to the truss, mechanical fastening with screws and a simple gasket are practical, but the heaviest solution. A welded or brazed joint in fastening the skin to the truss is a simpler solution, but requires equal compatibility of truss member and skin material to welding or brazing. The lightest solution is bonding fiberglass/polyimide to truss members. Two products that would be acceptable are American Cyanamid HT424 adhesive film and Hysol EA 929 adhesive film.

There remains the problem of verification of the performance of the adhesive or, at worst, definition of the shear strength degradation that would allow accurate calculation of a reliable bonded skin on the built-up transmission.

The approach taken for the detail design configuration is the one with the least amount of risk: a metallic skin covering with gasket screwed to the truss structure. Even though this is slightly heavier than other covering methods, the skin covering weight is only 6 percent of the total weight.

Candidate Truss Geometries

The truss-like housing shapes considered reflect the present casting design. This is a result of interface and interchangeability requirements with the CH-54B upper and lower housing casting and forging. Figure 45 is an isometric of the geometry.

Since there are infinite possible truss geometries that could have been chosen for a fabricated housing design, the problem is how to minimize the possibilities. Analysis of the various loading conditions shows that the largest loads act on the uppermost ring. All the net housing loads must be distributed to the lower mounting ring to transfer load to the airframe. Included are the main rotor load, net bevel gear reactions, tail takeoff gear and accessory weights, ring gear reaction torque, and many minor loads. Three geometry arrangements were considered: an "A" frame design, a pyramid design, and a pure

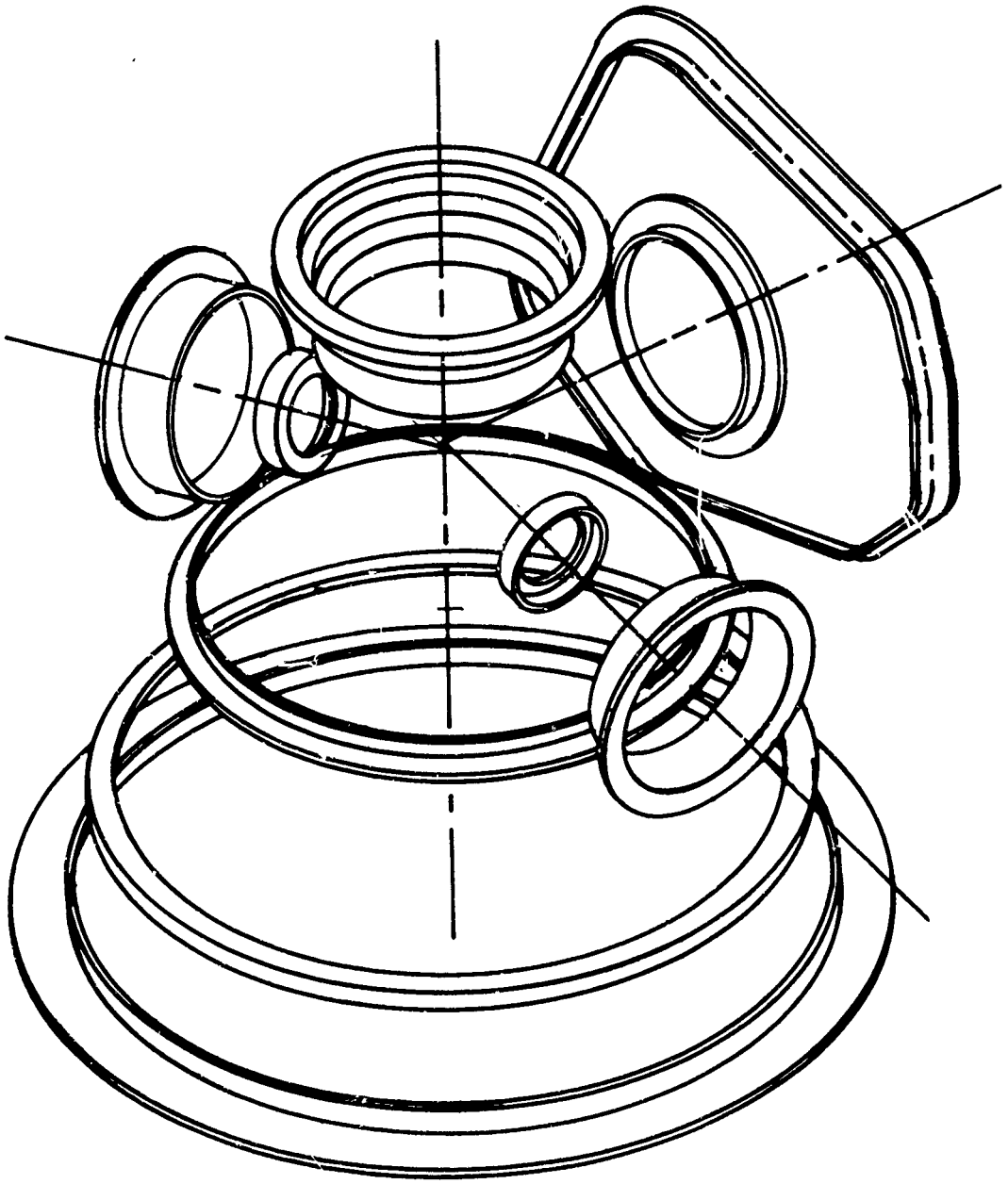

Figure 45. Truss Geometry Constraints.

truss arrangement. A plan view of each design is shown in Figure 46.

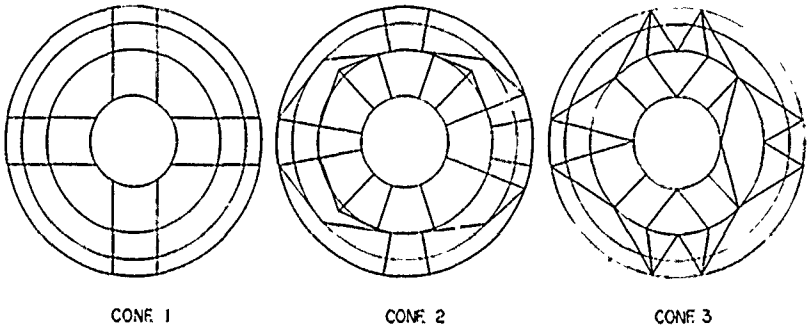

Figure 46. Plan View of Truss Geometry.

A half-size model was constructed as illustrated in Figure 47. The model has all the required interface, support, and mounting rings. With the model it was easier to determine load and path and to identify such requirements as servo pad and bevel gear roller bearing supports.

With these data a number of isometric sketches were made to show the geometry in more detail. Figures 48 through 54 are sketches that correspond to the "A" frame design, pyramid design, and pure truss arrangement of Figure 46.

Three-view preliminary layouts were made of the candidate truss arrangements.

The "A" frame truss arrangement, Figure 55, consists of a series of rings and eight main load-carrying members arranged orthogonally to each other in pairs in the plan view. They form an "A" shape when viewed from the front or side. This arrangement transfers main rotor shaft horizontal reaction loads at the uppermost ring, through the mounting ring, to the airframe. The horizontal rings which the "A" frame members support provide stability and transfer loads from side to side. The base ring is tipped five degrees in a side plane relative to the main rotor shaft and is constructed as a circle instead of the present casting ellipse. A vertical ring welded to the "A" frame member and stabilized through supports provides the reaction for the tail-takeoff bevel pinion tapered roller bearing set. Parallel to the tail-takeoff bevel support ring is the rear cover support flange. This flange, which is

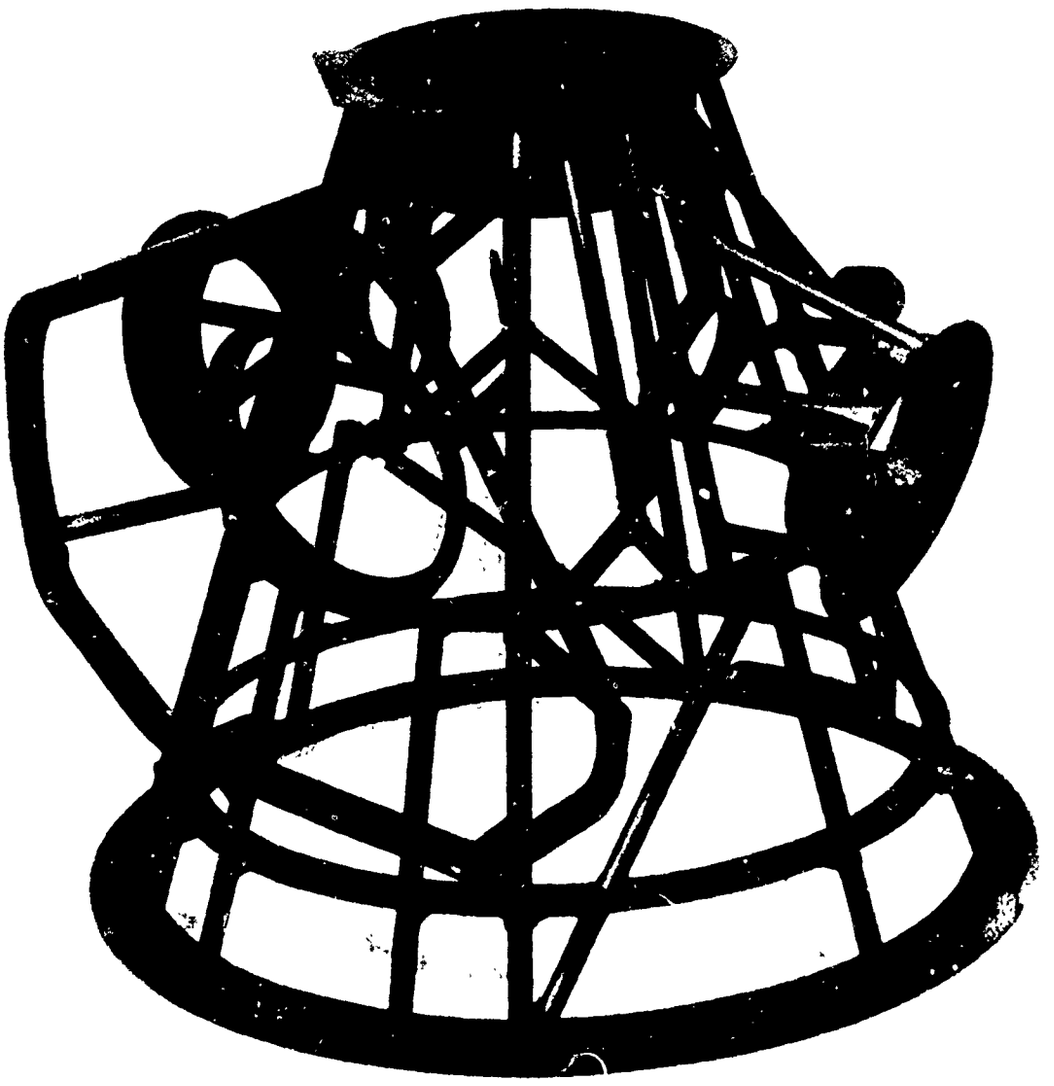

Figure 47. Half-Size Model of Typical Truss Housing.

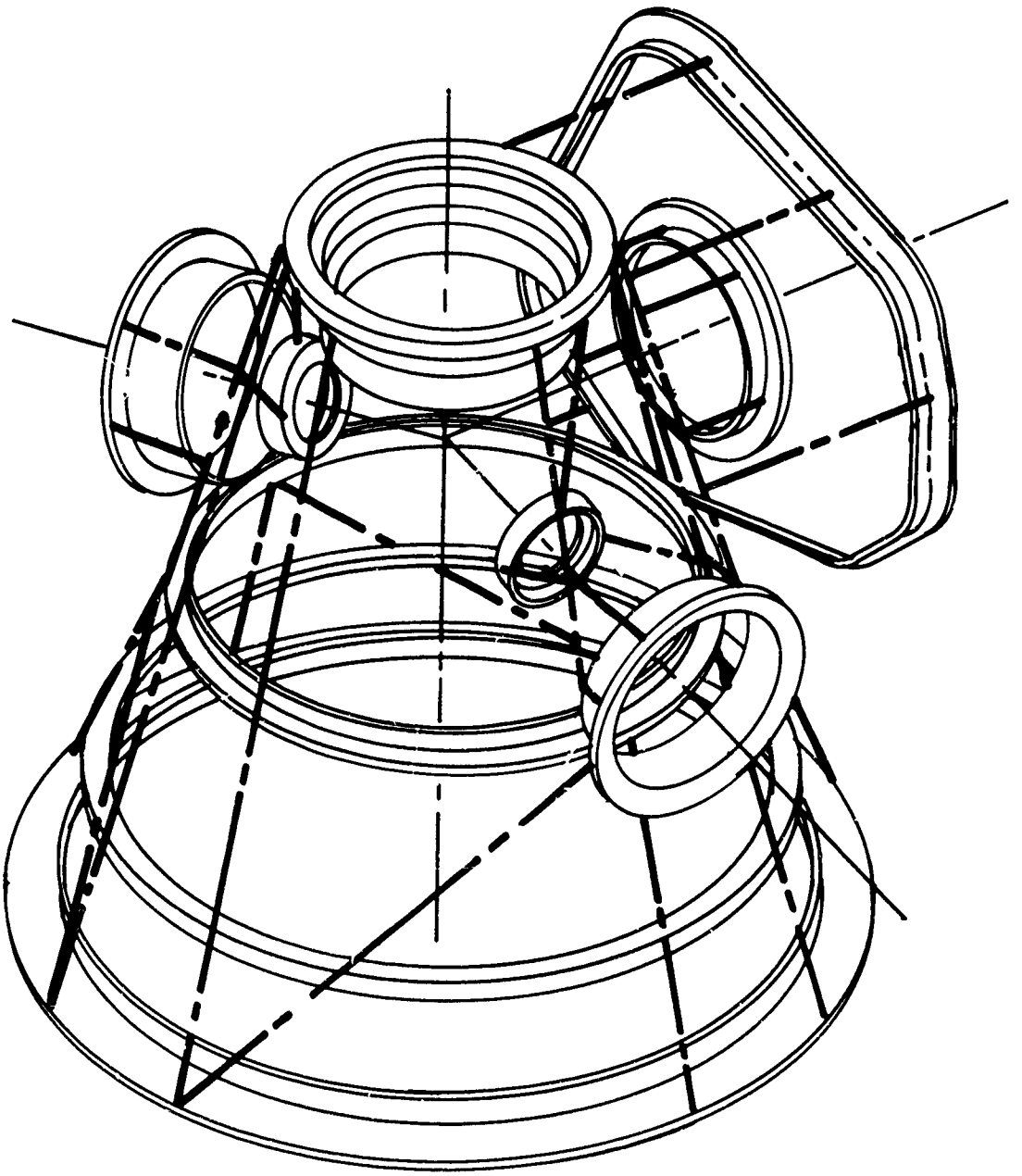

Figure 48. Sketch of "A" Frame Truss Design.

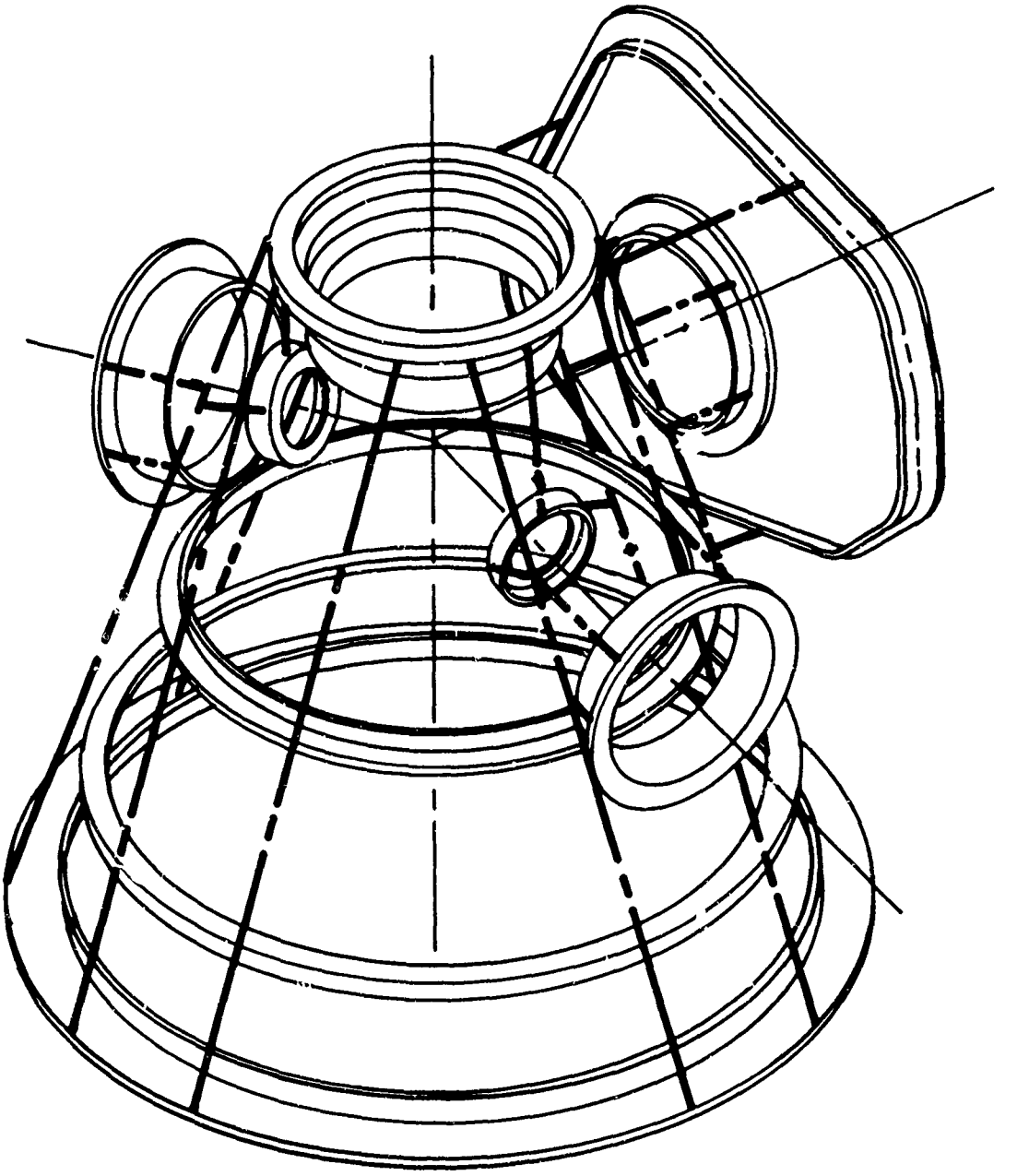

Figure 49. Sketch of Pyramid Truss Design.

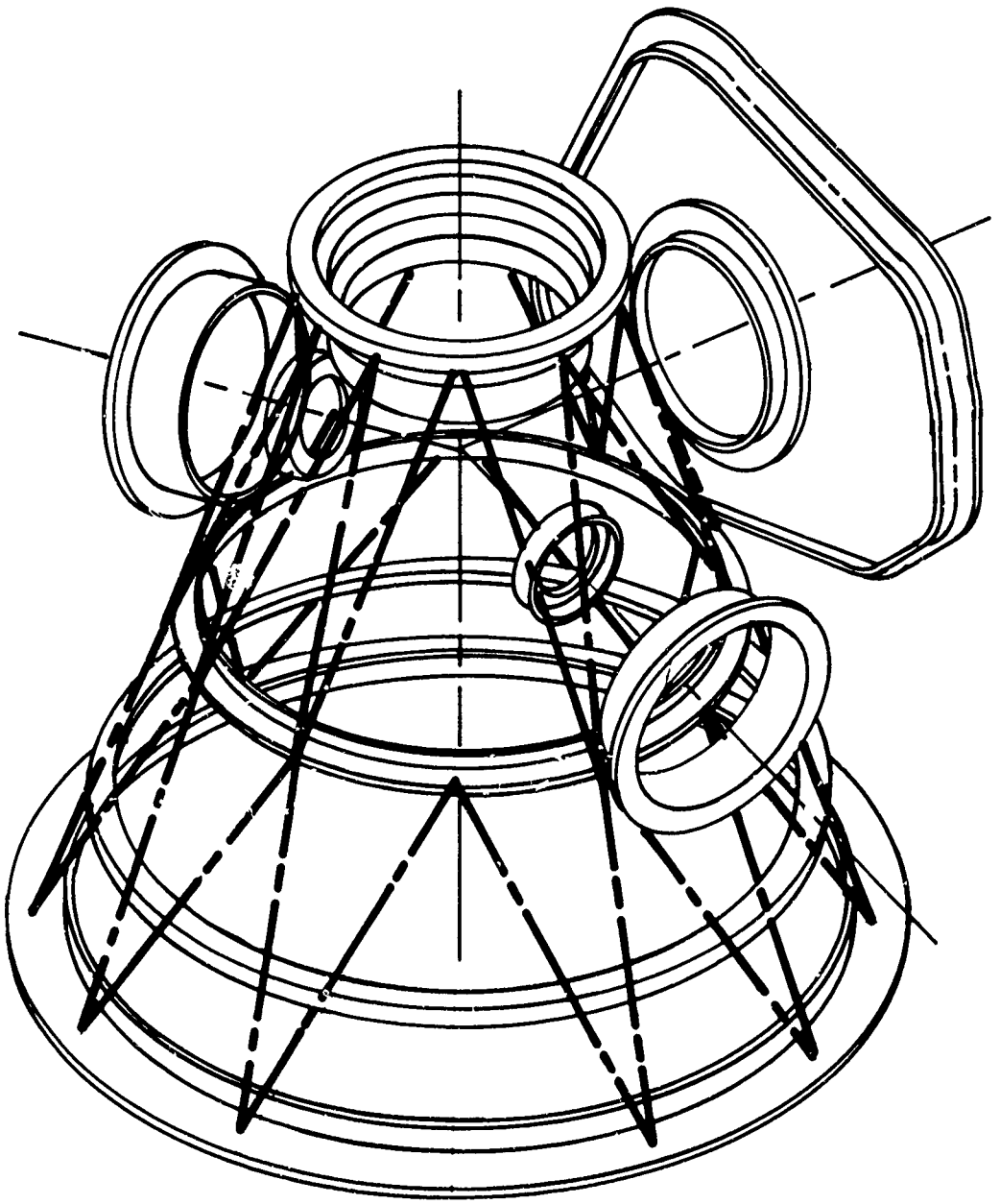

Figure 50. Sketch of Pure Truss Design.

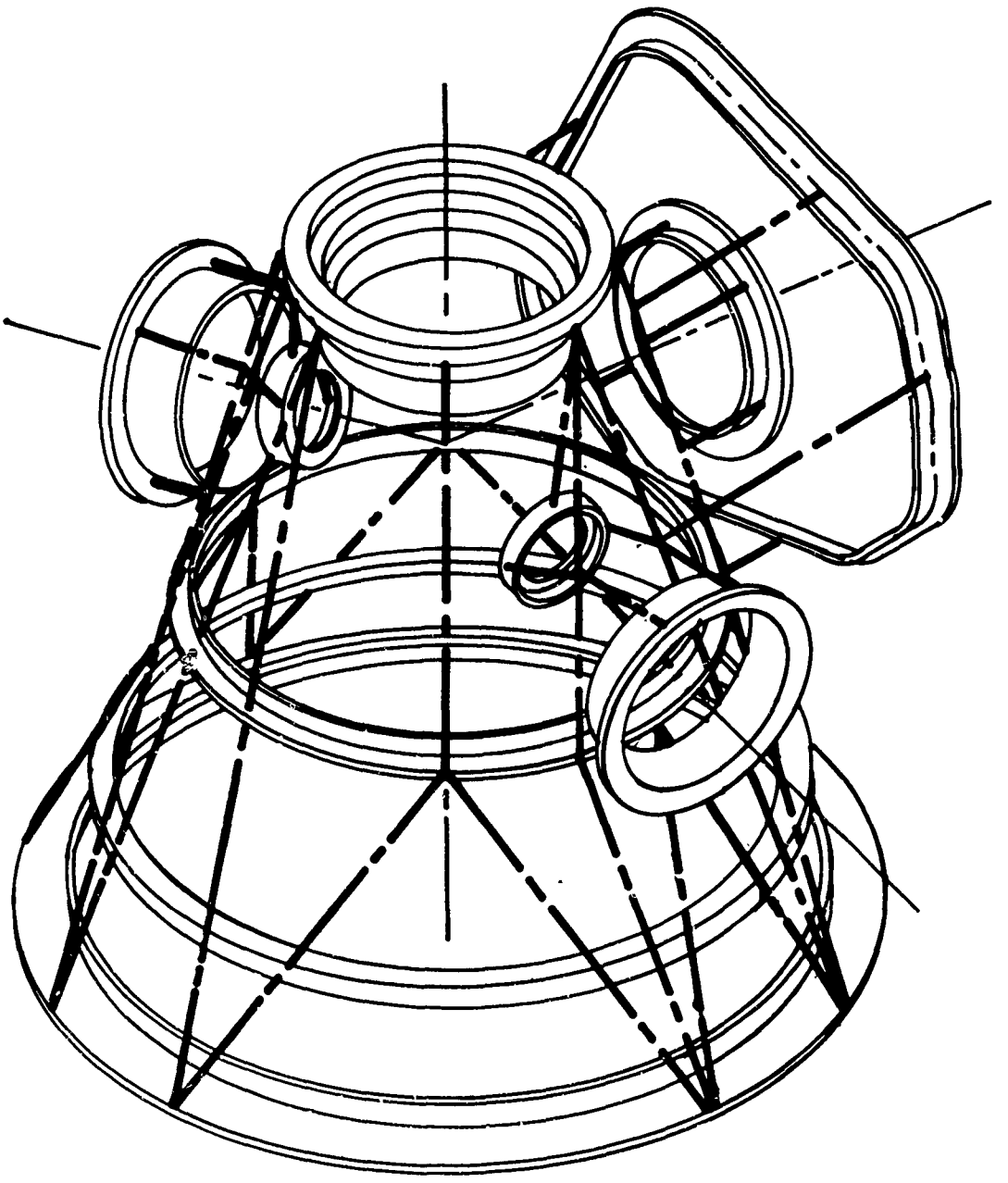

Figure 51. Sketch of Pure Truss Design.

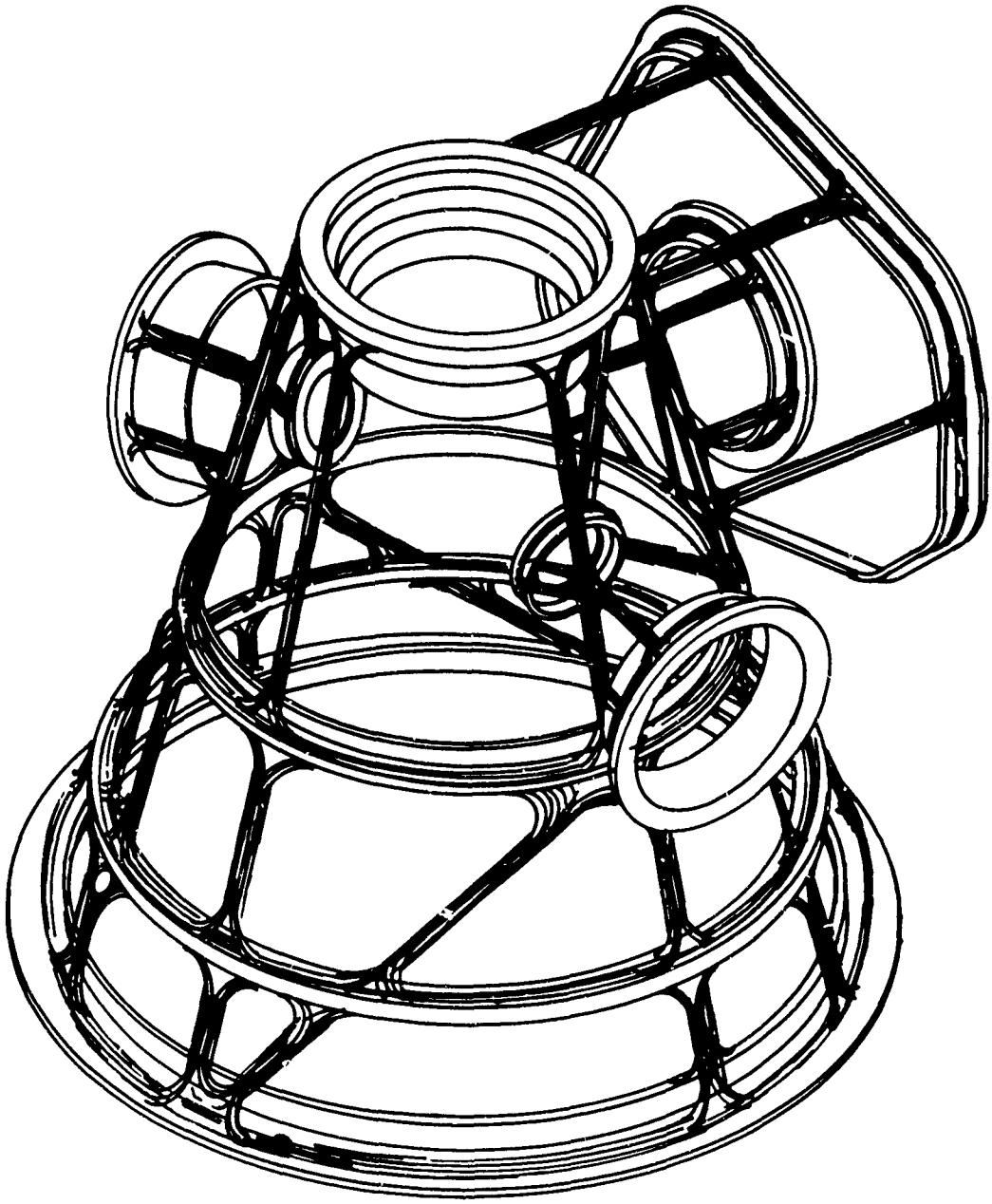

Figure 52. Sketch of "A" Frame Truss Design With Composite Material.

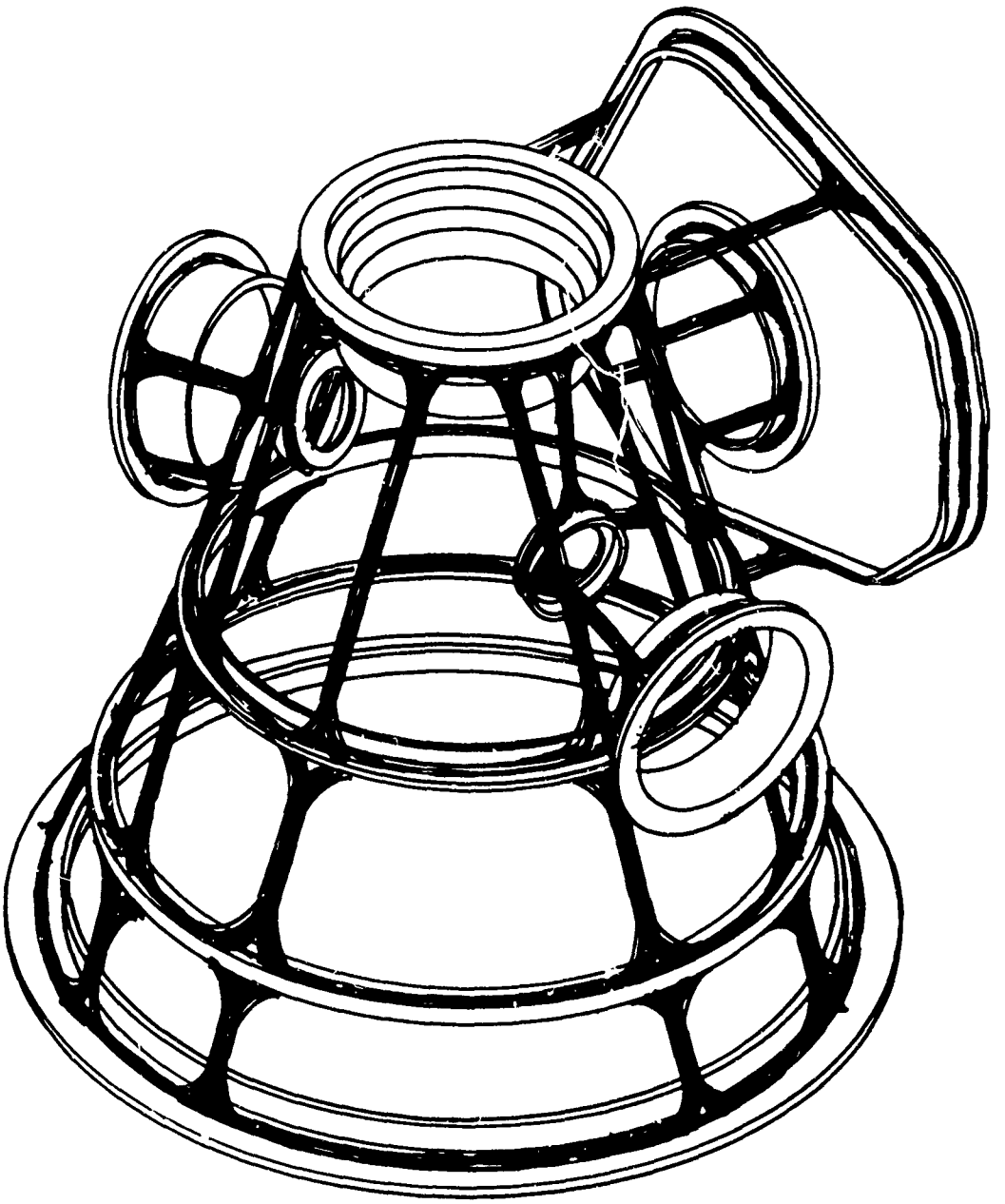

Figure 53. Sketch of Pyramid Truss Design With Composite Material.

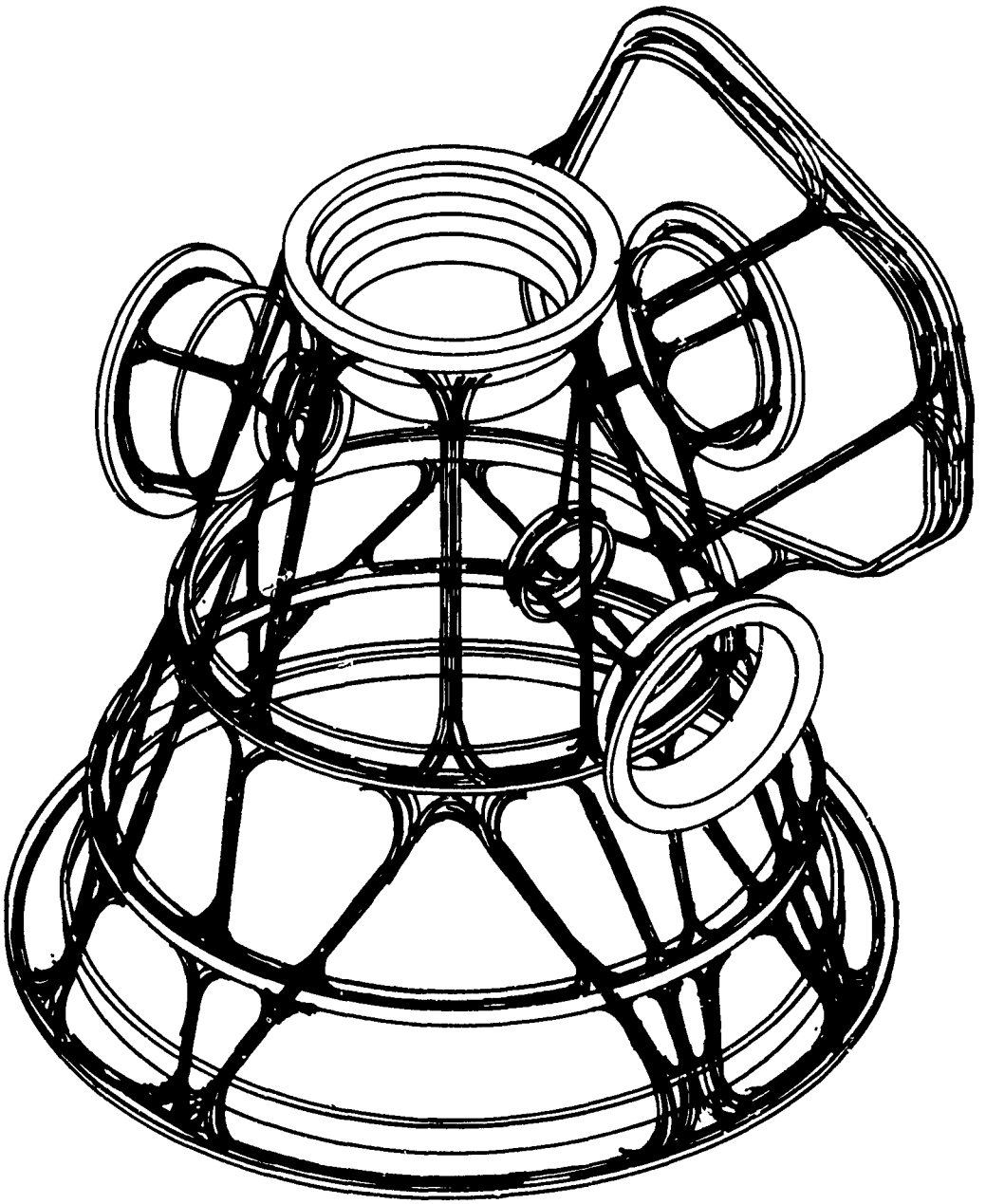

Figure 54. Sketch of Pure Truss Design With Composite Material.

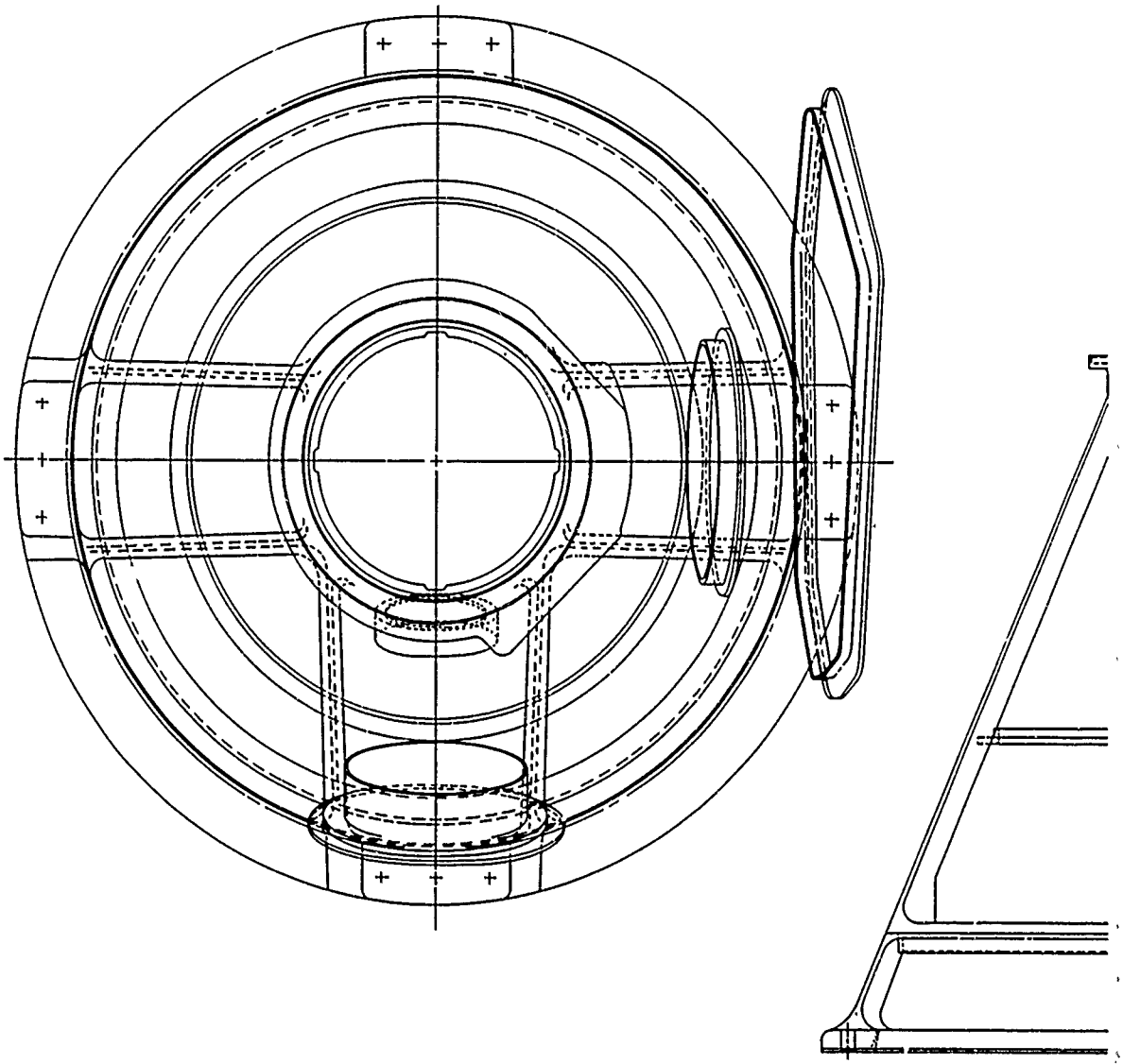

Figure 55. Three-View Preliminary Layout of "A" Frame Truss Housing.

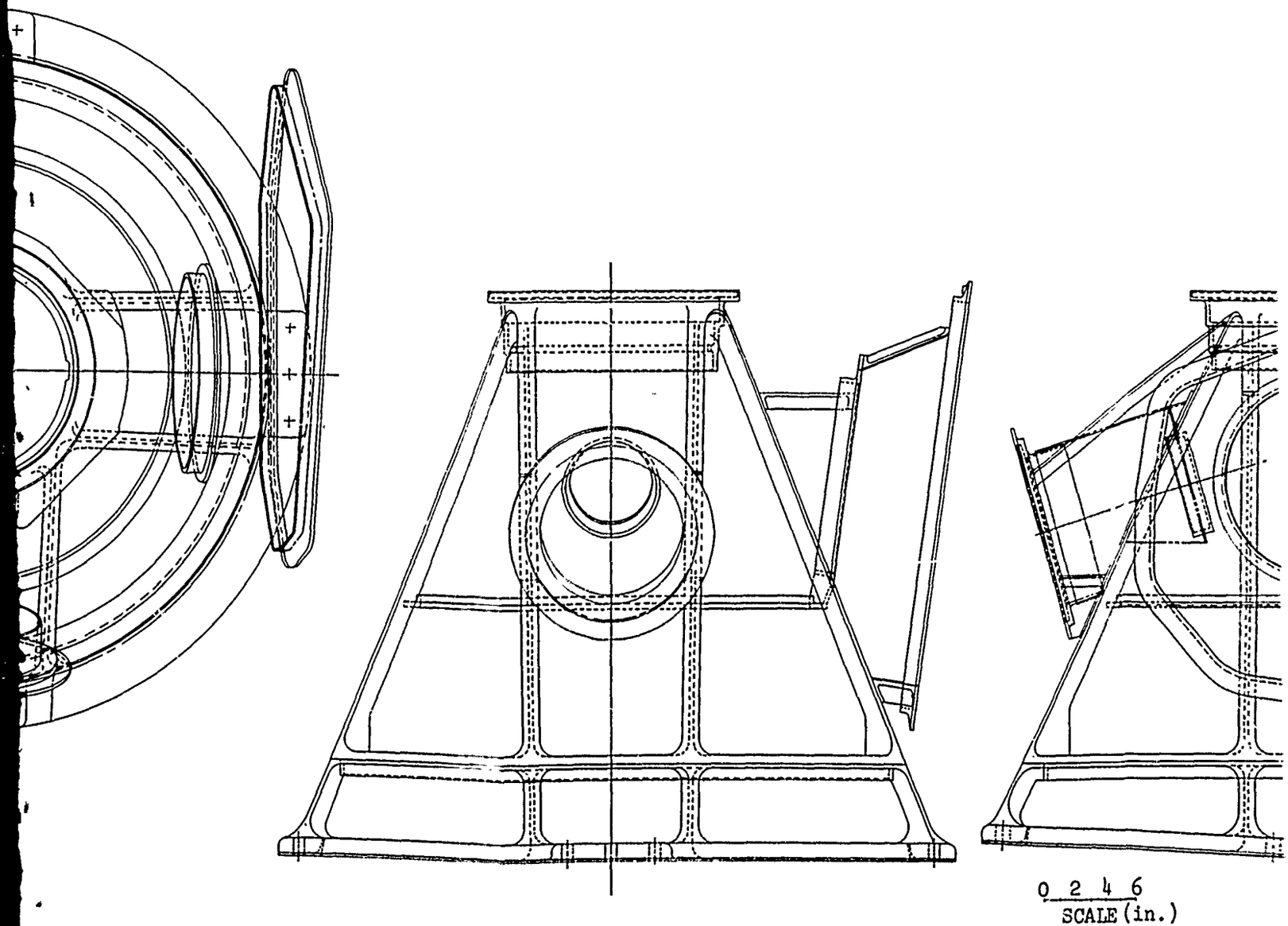

0 2 4 6
SCALE (in.)

iminary Layout of "A"
sing.

1

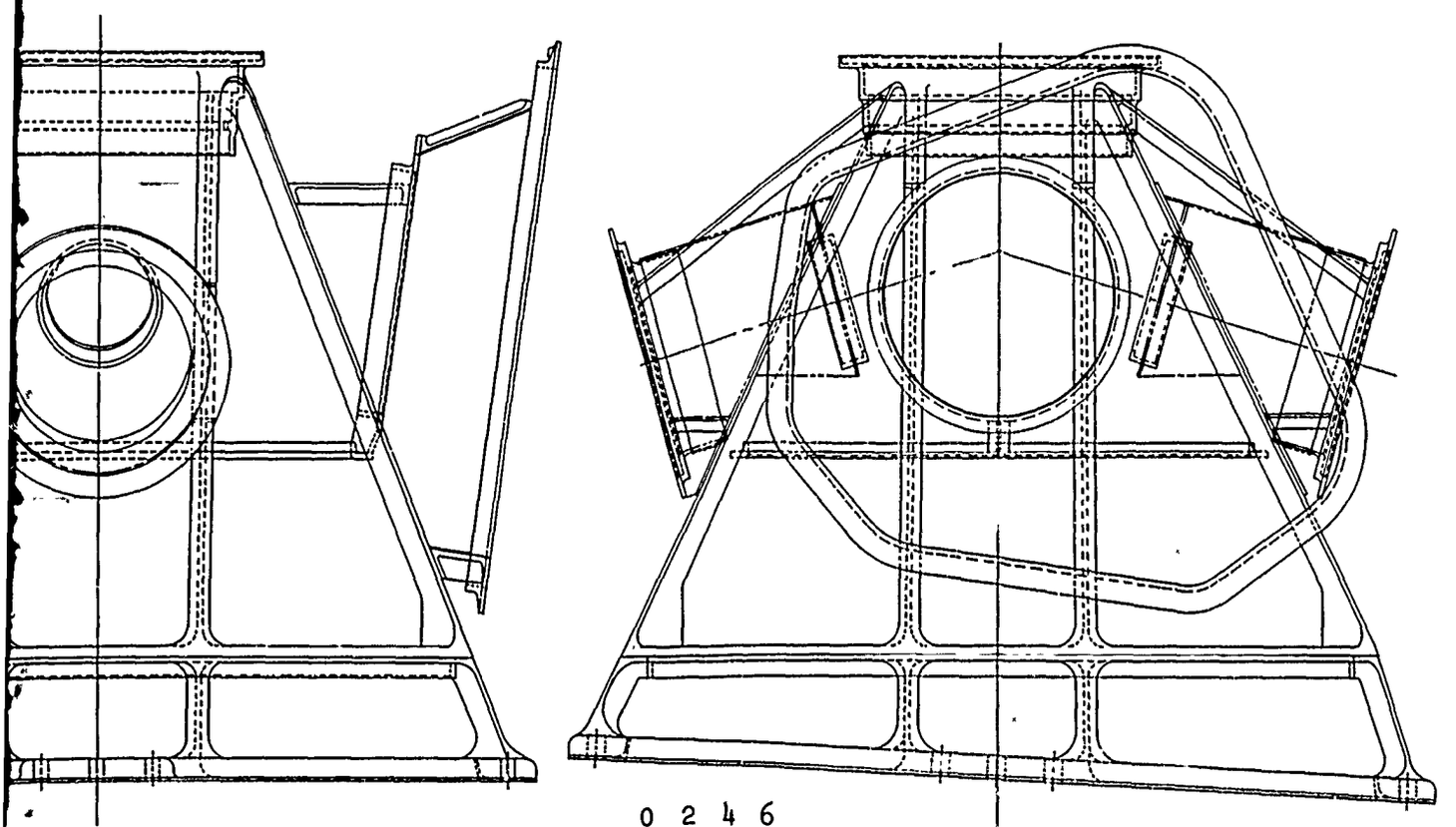
0 2 4 6
SCALE (in.)

supported from the main structure, contains an "O" ring groove and bolt holes for mounting the present rear cover assembly. The second-stage inputs located on the right and left sides are mounted in rings supported by the sheet metal structure of the main housing. The first-stage input casting bolts directly to the support ring mounted to the sheet metal structure. The second-stage input bevel pinion roller bearing is supported by the sheet metal structure.

The pyramid truss arrangement, Figure 56, consists of a series of rings and eight main load-carrying members arranged to have a theoretical intersection point to form a cone. This arrangement transfers main rotor shaft horizontal reaction loads applied in any direction at the uppermost ring through the mounting ring to the airframe. The horizontal ring, in addition to supporting bevel gear housings and providing ring gear reaction torque, provides stability to the pyramid members and transfers loads side to side. The base ring containing the mounting is tipped five degrees to the side relative to the main rotor shaft and is constructed as a circle instead of an ellipse. A vertical ring joined to the middle horizontal ring and stabilized through supports to the top horizontal ring and pyramid members provides the reaction for the tail-takeoff bevel pinion tapered roller bearings. Parallel to the tail-takeoff bevel support ring is the rear cover support flange. This flange is supported from the pyramid member by a series of tubes. It contains an "O" ring groove and bolt holes for attaching the present rear cover assembly. Each second-stage bevel pinion thrust bearing housing located on the right and left sides, is mounted in a ring supported by a series of tubes from the pyramid main members. The first-stage input casting bolts directly to this tube-supported ring. The second-stage input bevel pinion roller bearing ring is supported by a series of tubes from the pyramid structural members.

The pure truss arrangement, Figure 57, consists of a series of rings forming elements of the cone and a series of diagonal members to transfer loads between the rings. This arrangement transfers the main rotor shaft horizontal reaction loads, applied in any direction at the uppermost ring, and transfers them indirectly through the mounting ring to the airframe. The horizontal rings, in addition to supporting bevel gear housings and providing ring gear reaction torque, provide stability to the truss members and transfers loads from side to side. The base plane ring containing the mounting feet is tipped five degrees to the side relative to the main shaft and is constructed as a circle instead of an ellipse. The tail-takeoff bevel pinion tapered roller bearing set is supported by a vertical ring joined to the middle horizontal ring and is stabilized by supports attached to the other truss members. Parallel to the tail-takeoff bevel support ring is the rear cover support flange. This flange, which is supported from

the truss by a series of tubes, contains an "O" ring and bolt holes for attaching the present rear cover assembly. The second-stage input bevel pinion roller bearing ring is supported by a member from the top ring, which is an oil transfer tube, and by a series of tubes to the truss members.

Modeling of the Truss Geometry

A model of the fabricated housing truss geometry was developed.

Nine assumptions were used to simplify the analysis.

1. The skin covering does not contribute to structure stiffness and carries no load.

2. Any connection to another member has complete rigidity.

3. The bearing loads are sinusoidal and lie in the same plane.

4. Any structure element is a beam in which the shear stresses are ignored.

5. Each connection has the same properties as the structural element it is connecting.

6. The mounting ring used to transfer loads from the truss housing to the airframe is mounted rigidly. The mounting pads are constrained in five directions, but allowed to twist about the axis of each bolt. The base ring in areas other than the mounting pads is constrained in the vertical direction only.

7. The truss structure members join other members on the line of axes of their common centroid.

8. All applied loads are concentrated forces applied as discrete point loads in the structure. The aggregate of these applied loads has the correct magnitude. The sinusoidal distribution for bearing loads has the correct magnitude even though it consists of a finite number of points.

9. All cross sections use structural elements that have no holes, and bolt loads are concentrated on the bolt centerline.

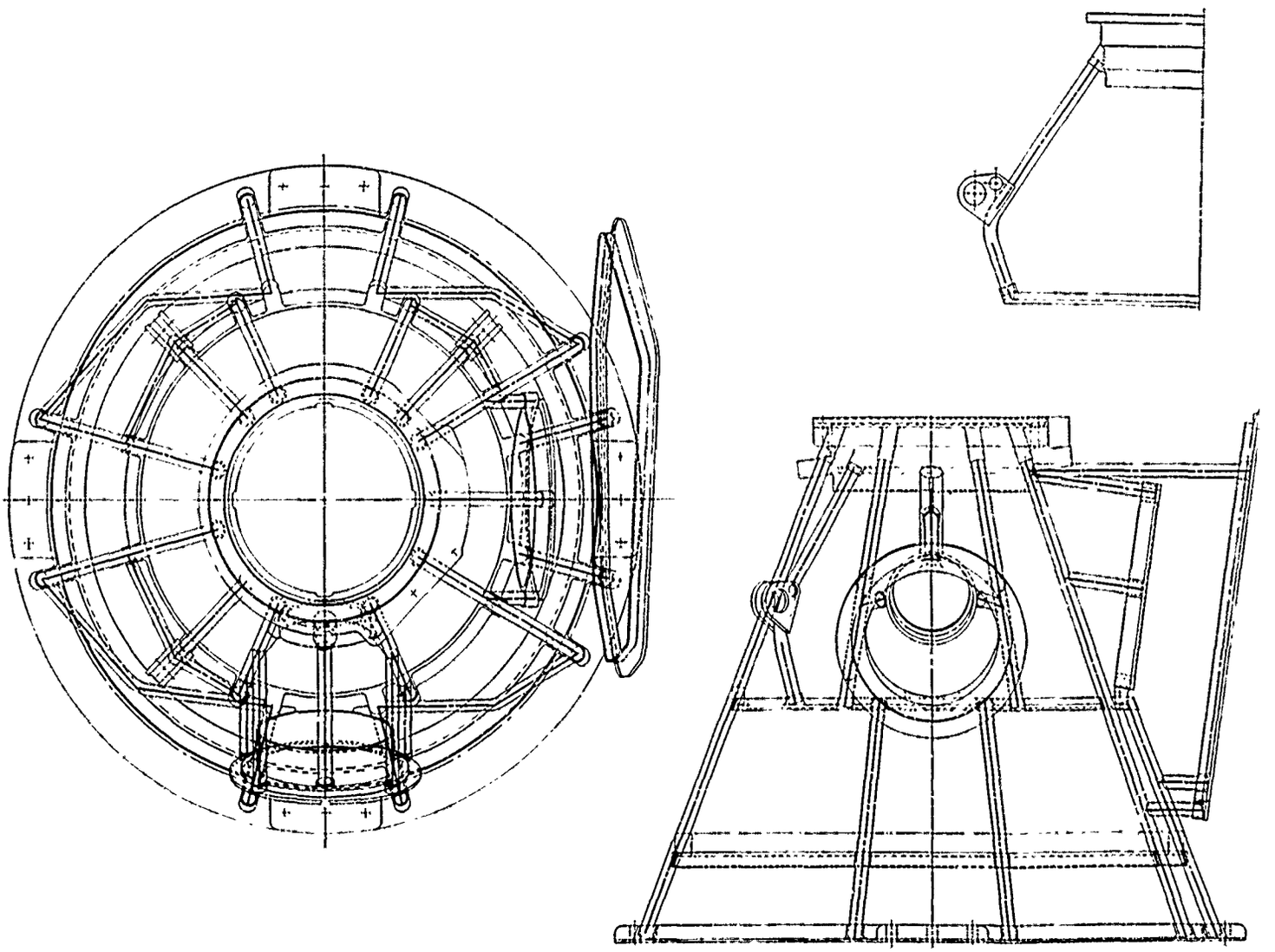

Figure 56. Three-View Preliminary Layout of Pyramid Truss Housing.

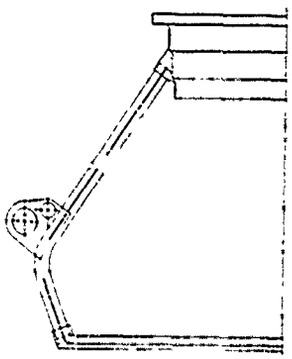

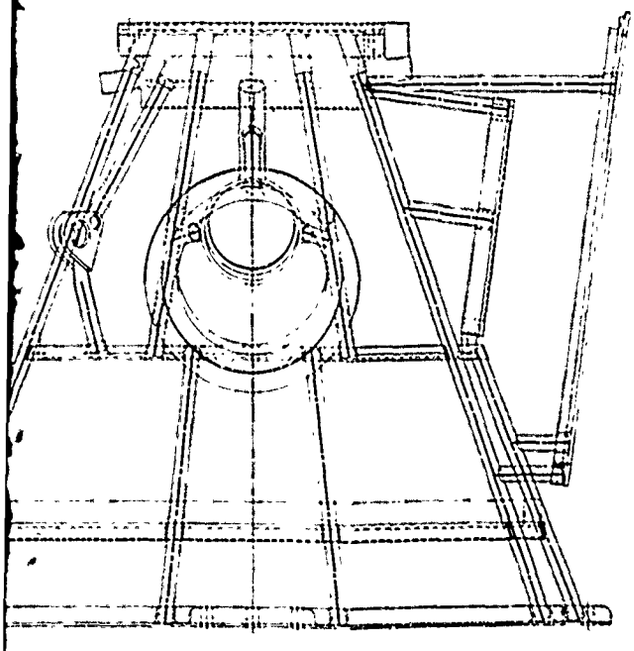

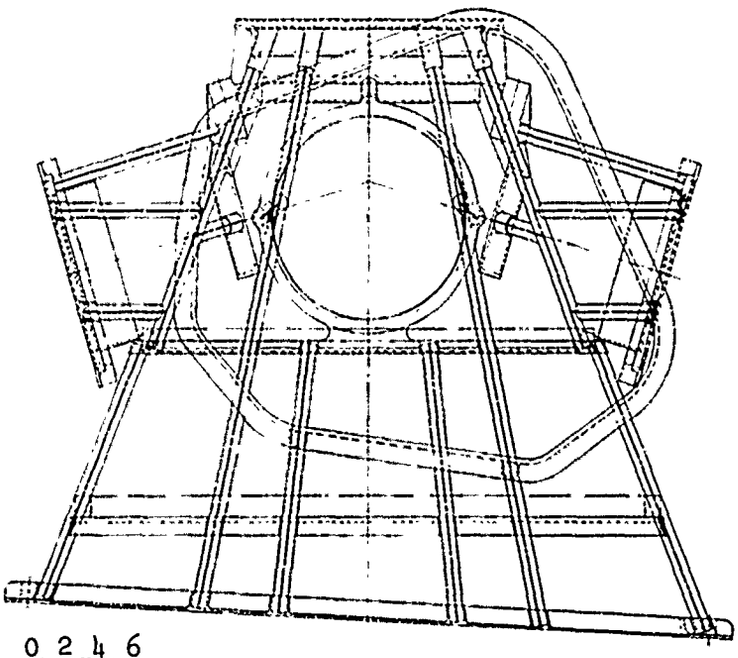

0 2 4 6
SCALE (in.)

of

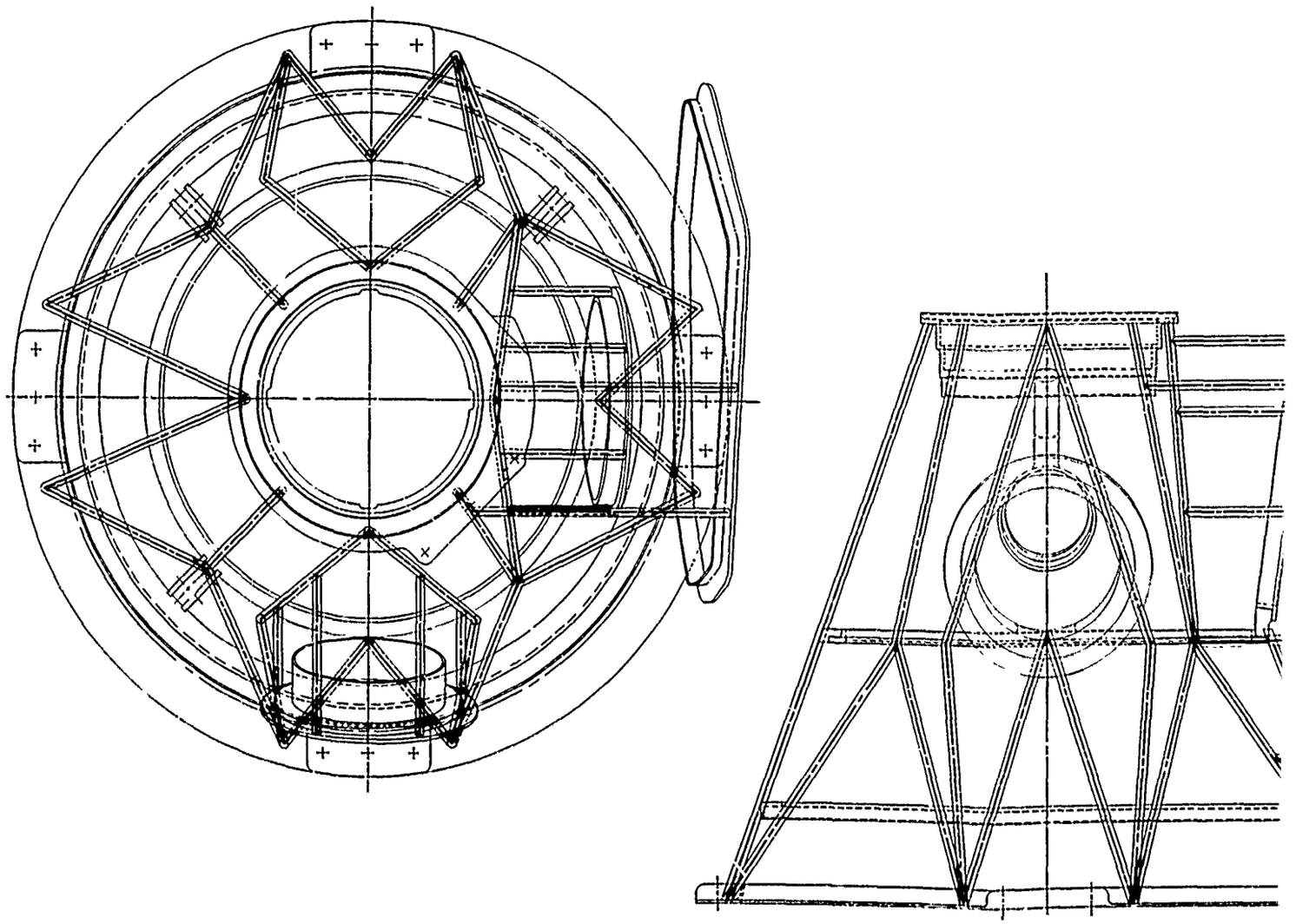

Figure 57. Three-View Preliminary Layout of Pure Truss Housing.

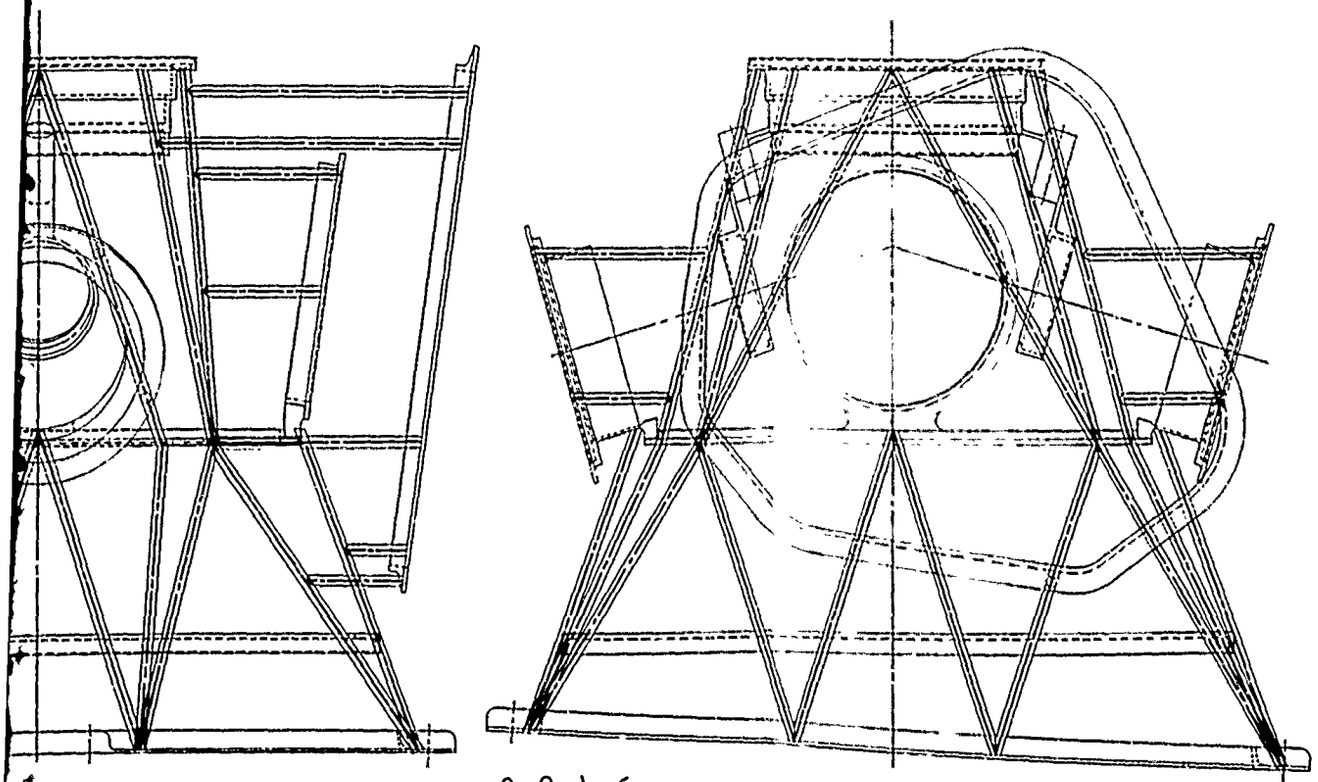

0 2 4 6

SCALE (in.)

Method of Analysis

Extensive use was made of the NASTRAN finite element computer analysis coupled with a CRT graphic display.

The finite element method was used as a part of NASTRAN. This program has a library of eighteen finite elements that can be used to perform a variety of analyses.

Although specifically designed to solve large structural problems, NASTRAN has an efficient executive subprogram that selects only those parts of the program needed to perform the required calculations. With the statics option of NASTRAN, three-dimensional frameworks can be analyzed by modeling the structure with bar elements connected at grid points. The bar element of NASTRAN is a generalized beam capable of transmitting axial load and torque as well as moments in two planes. It enables the user to model the stiffness of beams having asymmetric cross sections by defining offsets from grid points to locate the neutral axes. The program calculates displacements of the structure, and internal loads are referred to the neutral axis of the beam. By inputting fiber distances from the neutral axis and specifying the orientation of the cross section, the user can define four points of each beam element cross section, where the stresses are calculated. When the material density and allowable material stresses have been inputted, the structure weights and margins of safety are calculated.

Capability exists for constraining any of the six degrees of freedom of a point. This enables fixing rotations and displacements at a point. In addition, the capability exists for specifying the spring rate at any particular point in the structure.

Loads are applied to a structure at a grid point by specifying the magnitude and the direction of the load. The capability exists for handling uniform loads and sinusoidally distributed loads.

As part of the input data for a NASTRAN analysis, it is necessary to specify grid points relative to some arbitrary set of axes and the connection of these parts. The elements are thus defined. With a large, complicated, truss-like fabricated structure of an asymmetrical shape in two coordinate directions, the voluminous input data required make it next to impossible to check the data without display capability.

Display capability is provided by a Sikorsky Aircraft developed program employing an IBM 2250 CRT console. This device consists of a cathode-ray tube (CRT), typewriter keyboard, function box, and light pen. The CRT console is linked with Sikorsky Aircraft's system 370 Model 145 computer.

The display capability makes use of the Sikorsky developed Data Editor Program. The designer views the geometric structure created by his connectivity cards, checks previously inputted data, and interacts with the computer to create design changes.

The Data Editor Program has the following capabilities.

1. The Batch Card Processor section runs in the batch mode to read in the NASTRAN deck. It establishes the defined connectivity relations and stores the results in the permanent files storage. A printout is generated with minimal diagnostics for the NASTRAN deck.

2. The graphics Files Storage section permits the user to store and retrieve up to twenty individual NASTRAN decks and their associated display data in a permanent storage area.

3. The graphics Display program permits the user to display any selected portions of the connectivity geometry of a NASTRAN deck retrieved from permanent storage. With the display program, errors in connectivity can be detected and corrected.

4. The graphics Card Edit program permits the user to display and alter the card images of a NASTRAN deck retrieved from permanent storage.

All three graphics programs are interconnected by the NASTRAN System Monitor. This assembler language program permits the user to enter any of these programs, operate on his data, and return to the monitor repetitively. The Batch Card Processor must be scheduled as a separate batch run to be completed prior to the scheduled graphics run.

As an example of the method of analysis, consider the modeling of a typical truss-like fabricated housing structure. The fabricated housing design, Figure 58, is a simplified model of a truss-like structure to replace the present casting. Bar elements are used for the connecting members, because they are capable of having specified section properties in the plane of the neutral axis and orthogonal to it. The bar elements are so joined that there is rigidity at joints, and the weight of the bar element is considered to be uniformly distributed over its length. The structure has a conical shape, with a ring at the upper main shaft roller bearing, two intermediate rings, and a large-diameter base or mounting ring. On each side of the structure are input support rings and an input roller bearing reaction ring. In the rear of the transmission is the accessory cover support ring and a tail-takeoff support ring. The servos are modeled as a series of pyramids at the servo locations. All

support rings are connnected to the main structure by bar elements. The rings, as modeled, consist of a number of points defined on a circle with straight line segments connecting them. These straight line segments are the centerline of a bar element, each of which has specified section and material properties. Each defined point, or grid point, is located in the global coordinate system or in a coordinate system defined relative to the global system.

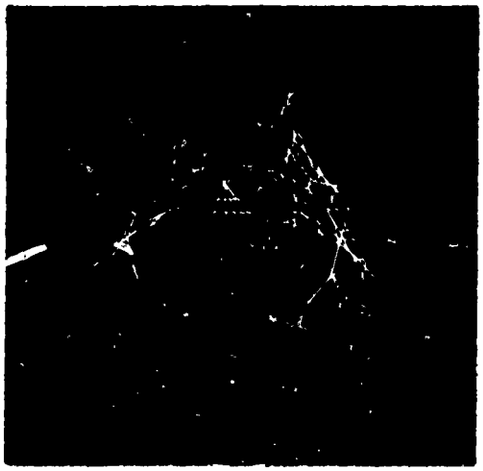

Figure 58. Typical Truss-Like Structure in Display Program.

Figure 59 illustrates the cards used in the NASTRAN deck setup. For the display capability, coordinate system definition cards (CØRD2c), mesh point description cards (GRID), and connectivity cards (CBAR) are necessary to execute the batch card processor. The results are stored in a file, and error messages are printed. If many errors are found during a run, a considerable saving in graphics time can be achieved by correcting the deck and re-submitting it for another run through the batch card processor. If there are minor errors, they can be corrected at the CRT using either the Display Program or the Card Edit program. Figure 60 shows typical errors in the NASTRAN deck setup. Figure 61 shows a designer changing an element in the Display Program with the light pen. When the structure shown on the Display Program has been corrected and modified to the satisfaction of the designer, a deck of the updated and corrected version is punched through use of the Files program.

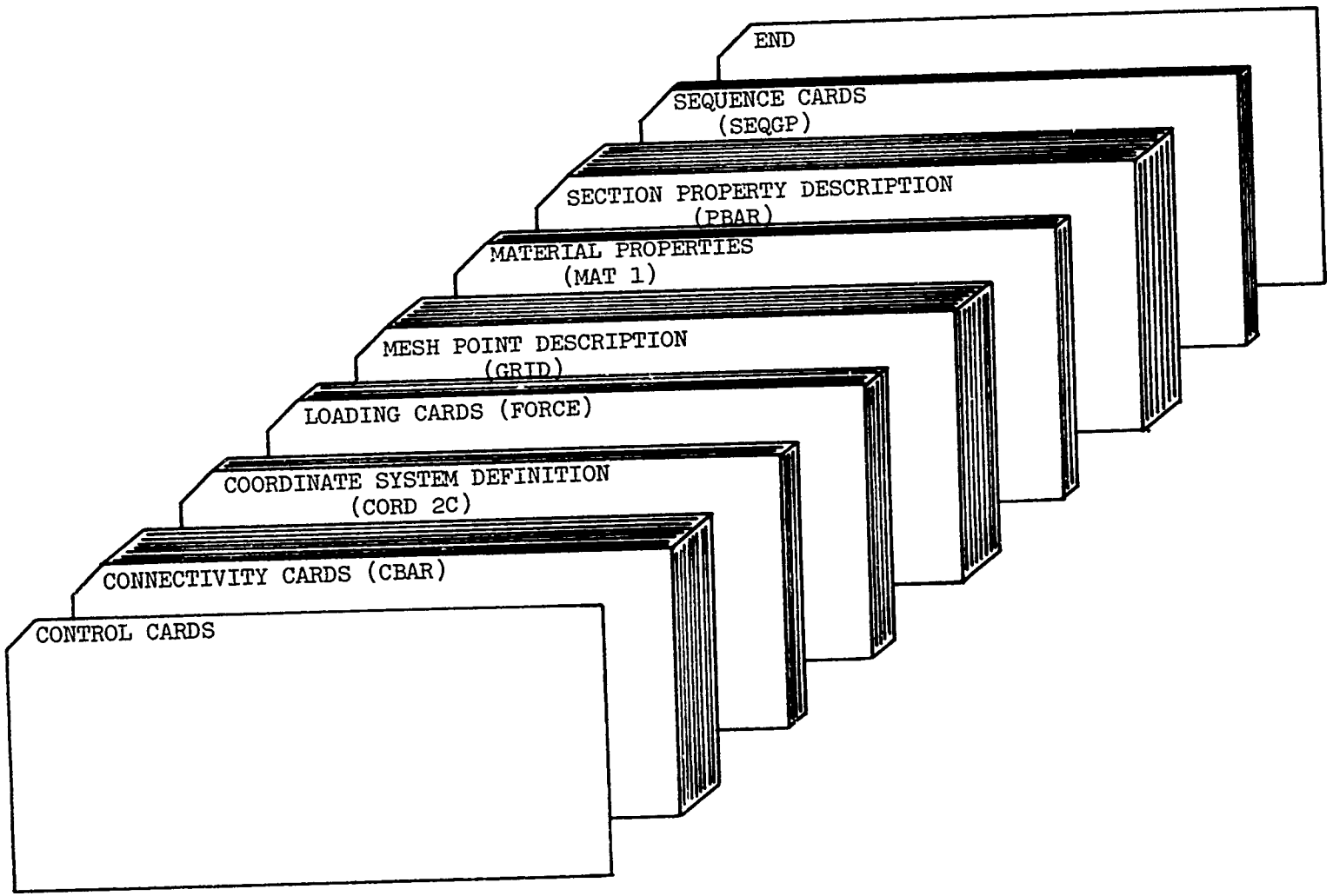

Figure 59. NASTRAN Card Deck Setup.

If they have not already been added, it is necessary to add the rest of the NASTRAN deck setup at this point, as shown in Figure 59. These cards include a series of control cards to specify the type of output required, internal moments, stresses and displacement for each end of all elements, and descriptive information for each loading condition. A series of connectivity cards (CBAR) specifies each bar element and the grid points it interconnects. Also specified on connectivity cards are the orientation of the neutral axis of the section and the applicable property card.

The next series of cards consists of coordinate system identification cards, which specify the orientation of a particular coordinate system relative to some arbitrarily defined global coordinate system. Specified for each new coordinate system relative to the global system are the location of the origin, direction of the plus "Z" axis, and direction of the azimuth plane. The capability exists for definition of coordinates in rectangular, cylindrical, and spherical coordinate systems. For the truss-like fabricated housing, coordinate systems are defined in rectangular and cylindrical systems. Various loading conditions are added through a series of force cards, which specify the loading case, grid point of the applied load, and magnitude and direction vector.

The grid cards define the coordinates in any specified axes and the degrees of freedom of point. It is possible to define reference points, interfaces, and boundaries.

Through a series of material property cards, the allowable stresses, moduli, and densities are specified.

The section property cards are referenced by the connectivity cards and determine the applicable material, as well as give areas, inertias, and torsional constraints of each bar element.

The sequence cards (SEQGP) in the deck setup are generated by a program called BANDIT. The purpose is to reduce the use of computer time for stiffness matrix inversion by minimizing matrix size. The sequence cards renumber all grid points internally within the computer for a minimum matrix size.

After deck setup, the program control cards are altered to prevent execution of the program, and the program is run through the data check. The data check helps locate errors that may remain after checkout by the display program.

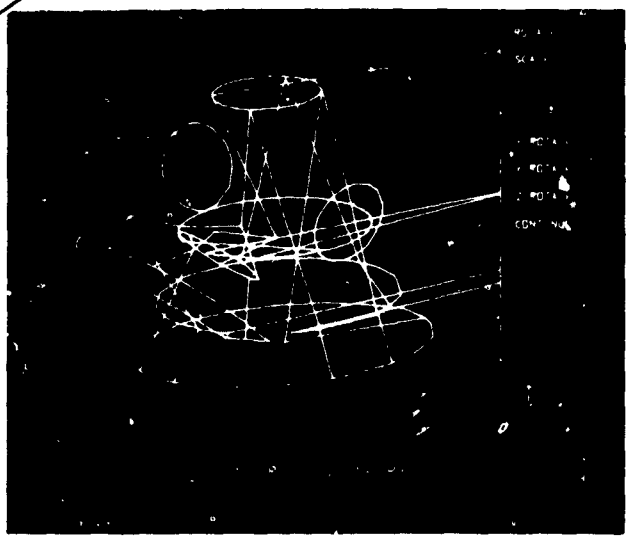

Figure 60. Truss-Like Structure with Some Initial Error.

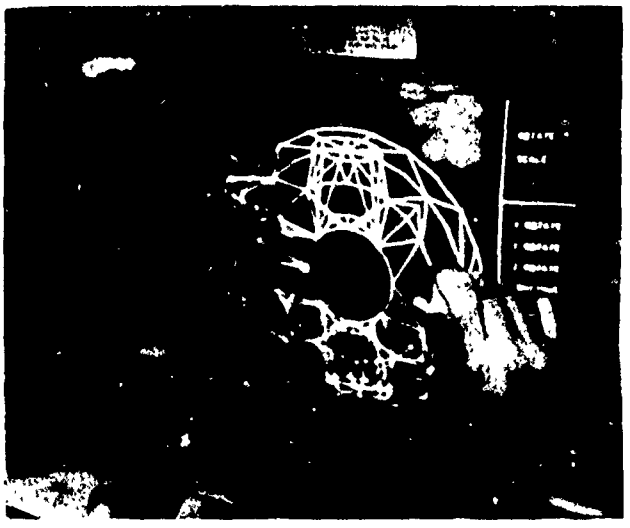

Figure 61. Photograph of a Designer Using CRT To Change a Structure Element.

When the NASTRAN deck is executed, the outputs include a data echo check, grid point weight generator table, estimates of decomposition time, and the accuracy of the solution received. In addition, a displacement vector table, load vector table, table of forces in bar elements, and table of stresses in bar elements are printed out. From analysis of the various tables, section properties, element number, and location cards are altered. The deck is then rerun to obtain a solution.

Discussion of Results of Analysis

The three housing configurations initially considered in the preliminary analysis are shown in Figures 62 through 64 as they appeared on the graphic display terminal. Views (a) and (b) include the loading spokes which were used to model sinusoidally distributed loads at the bearing reaction rings.

Of the three basic designs, the pure truss was by far the stiffest, followed by the pyramid and the "A" frame in that order. The analysis shows that the pure truss was most effective in distributing loads over the greatest number of members. During forward crash loading, for example, a substantial portion of the load is carried by the side support members for the pure truss configuration. In the case of the "A" frame and pyramid designs configuration, nearly the entire load is carried by the forward and aft support members. These load distribution characteristics of the fabricated housing designs have tremendous impact on the vulnerability of the transmission. Should a key load-carrying member be lost in either the "A" frame or pyramid designs, the housing would collapse since no other load path to the airframe would be available. The truss design, however, would simply redistribute the load over other members, thereby decreasing substantially the possibility of housing failure.

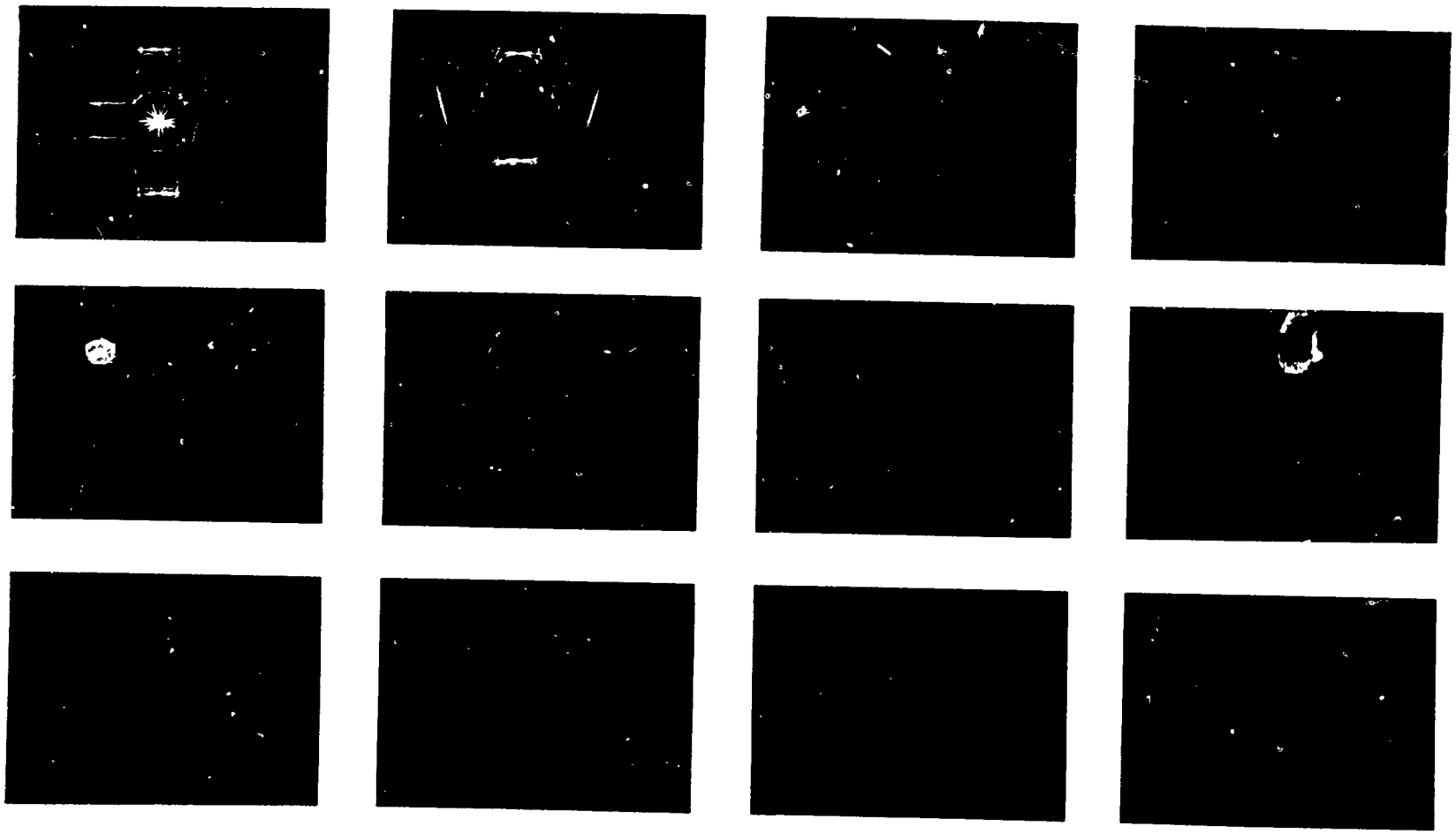

Figure 62. CRT Display of "A" Frame Truss Design.

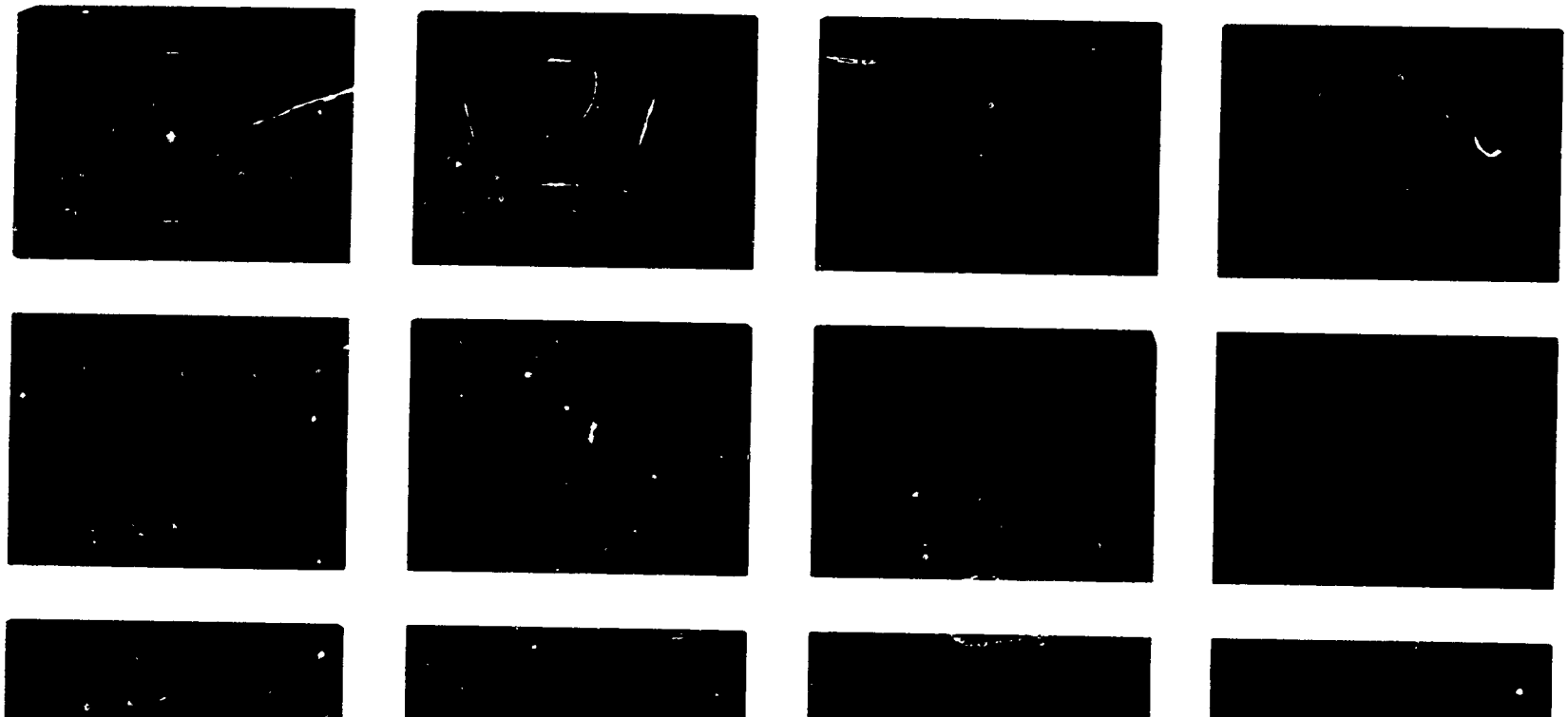

Figure 63. CRT Display of Pyramid Truss Design.

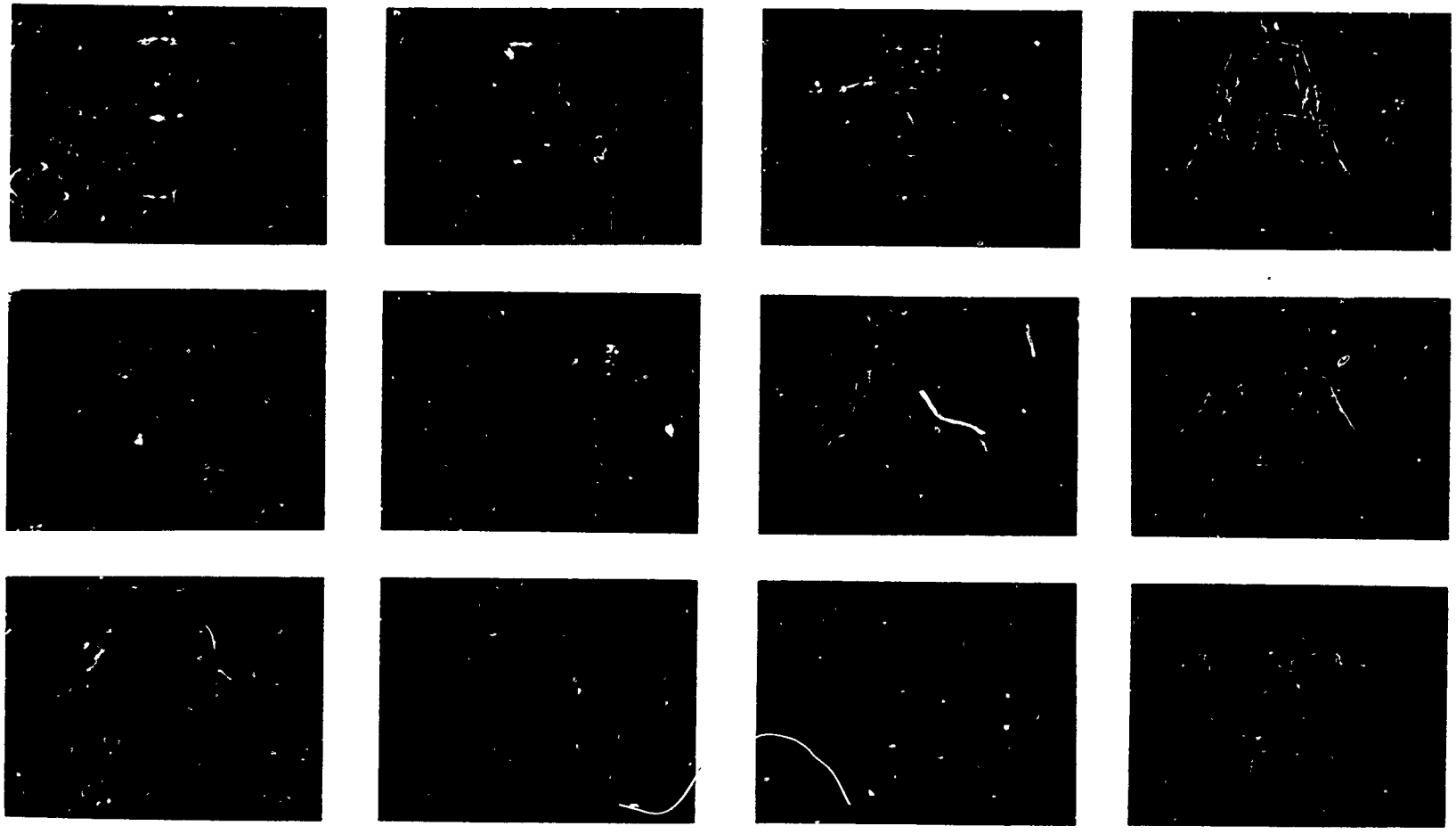

Figure 64. CRT Display of Pure Truss Design.

All three designs were analyzed in stainless steel, titanium, and Borsical® configurations. Borsical® proved to be not only the strongest, but also the lightest of the three materials when incorporated in the housing analysis. Stainless steel was second in both categories, with titanium ranking last. Table XI summarizes the results of the analysis. The stiffnesses shown in this table are for a load applied in the center of the upper main rotor bearing ring.

On the basis of these results, a pure truss configuration was chosen for detail design. Although the analysis showed that Borsical® was the superior material, Custom 455 stainless steel was chosen as the material for the pure truss design. The brazed-bonded Borsical® was eliminated due to its relatively low joint strength.

TABLE XI. SUMMARY OF WEIGHT AND HOUSING STIFFNESS FOR VARIOUS CANDIDATE MATERIALS

Material	Weights, lb		
	"A" Frame Design	Pyramid Design	Pure Truss Design
Stainless Steel Custom 455	327	309	278
Titanium Ti-6Al-4V	330	318	290
Borsical®	290	265	230
	Stiffness, 10^6 pounds per inch		
Stainless Steel Custom 455	11.2	12.0	16.2
Titanium Ti-6Al-4V	10.0	10.4	14.6
Borsical®	12.0	14.0	18.9

DETAIL DESIGN OF THE TRUSS FABRICATED HOUSING

Design Criteria

The final loading diagrams for the fabricated truss-like housing were shown in Figures 23, 24, 31, and 32. Conditions studied were forward crash, side crash, hover, and symmetric dive and pullout. The loads for these four conditions were derived from the weights and CG locations of the components listed in Table III from the aircraft loads report (Reference 2), and from the structural design criteria report (Reference 3).

Description of Truss Geometry

The detail design of the fabricated housing evolved to a symmetrical true truss design, as shown in Figures 65 through 68. The truss-like fabricated housing is shown with skin and access panel details in Figure 67. The housing consists of four support rings, each with constant cross sections. The top ring is used to react loads from the main rotor shaft roller bearing and the bevel gear outer shaft roller bearing. The second ring reacts the loads from the second-stage bevel gear outer shaft tapered roller bearings, and the third ring is used for reacting the ring gear torque and lower housing loads. The lubrication oil transfer glands are located on this ring. The lower cover, which contains the main rotor shaft split-inner-race ball bearings, is the same as the present CH-54B cast housing design. The bottom ring contains the mounting pads to fasten the transmission housing to the airframe support beams.

A left and right side input ring is used to support the second-stage input bevel pinion assembly and is also used to support the first-stage bevel gear input housing assembly and the rear half of the JFT4D engine. These rings are supported by a series of tubes from the main truss structure. An input ring on the left- and right-hand side, also joined through a series of tubes to the main support structure, is used to support the roller bearing of the second-stage input bevel pinion assembly. A ring located in the tail-takeoff section supports the tail-takeoff bevel gear tapered roller bearing attached to the tail-takeoff accessory flange ring. This ring is supported by the main truss structure through a series of tubes. The tail-takeoff accessory flange supports the rear cover, cover-mounted accessories, and oil cooler support structure.

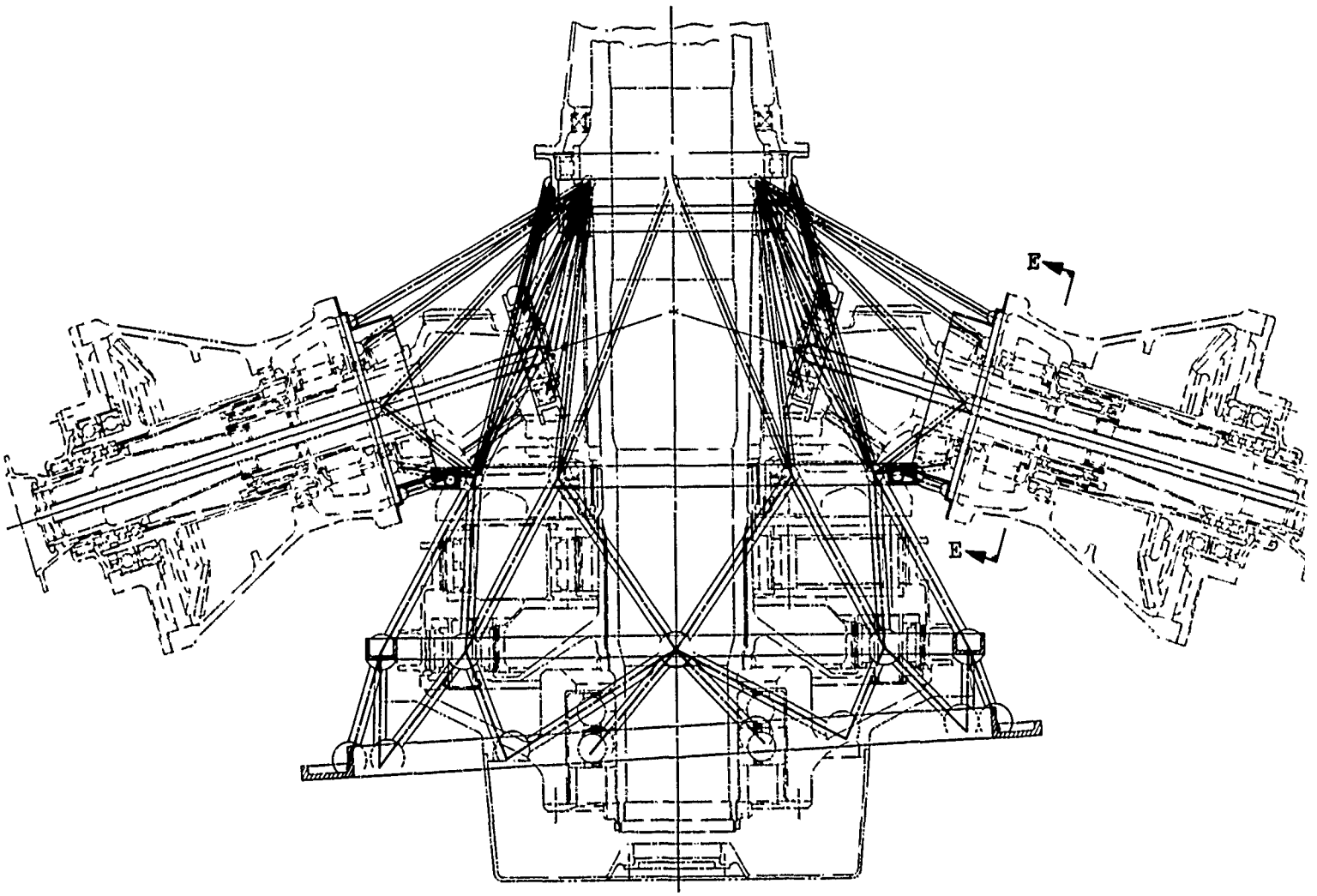

SECT A-A
ROTATED 90° C.C.W.

Figure 65. Detail Design Layout of the Fabricated Transmission Housing (View Looking Aft).

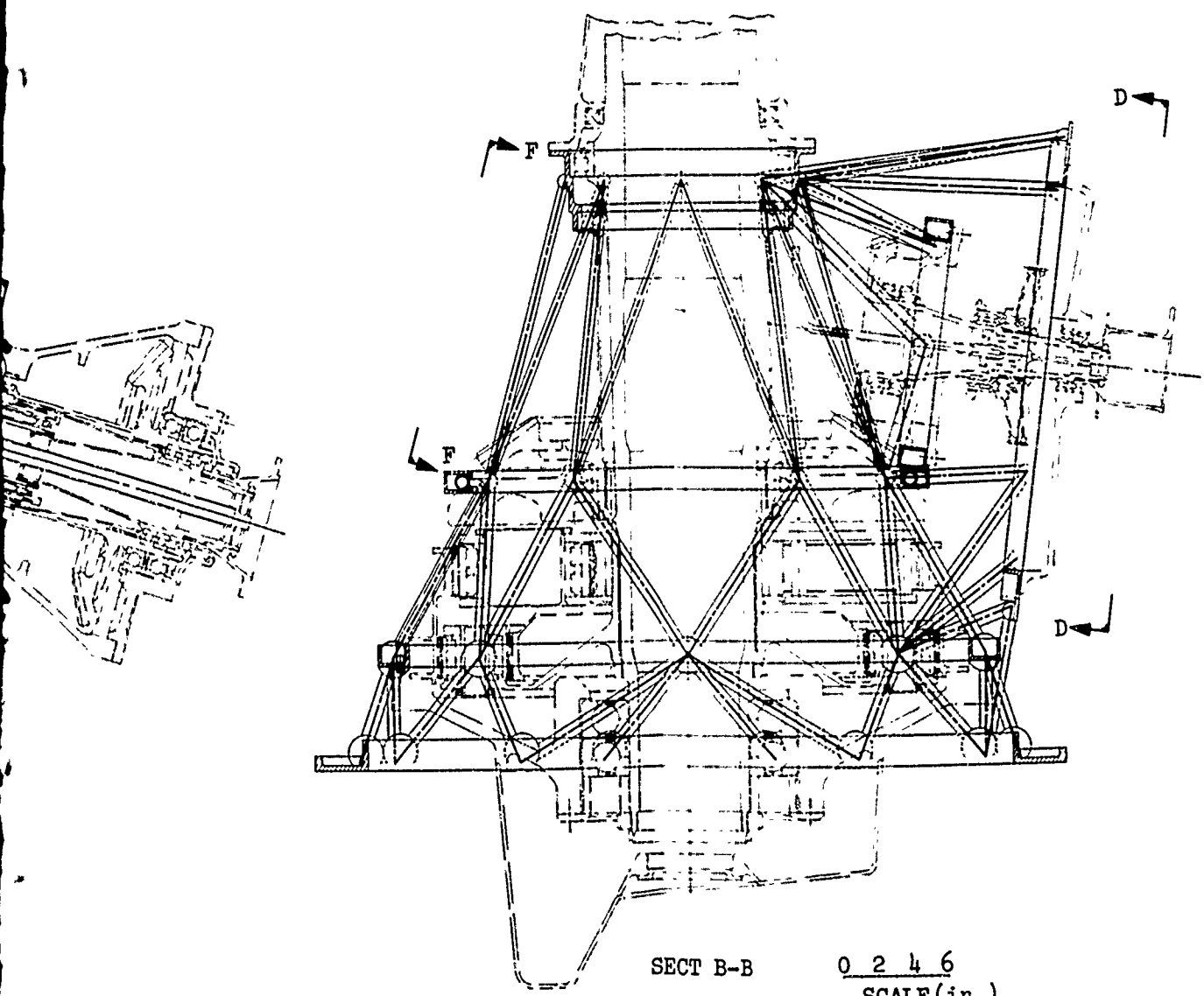

SECT B-B

0 2 4 6
SCALE(in.)

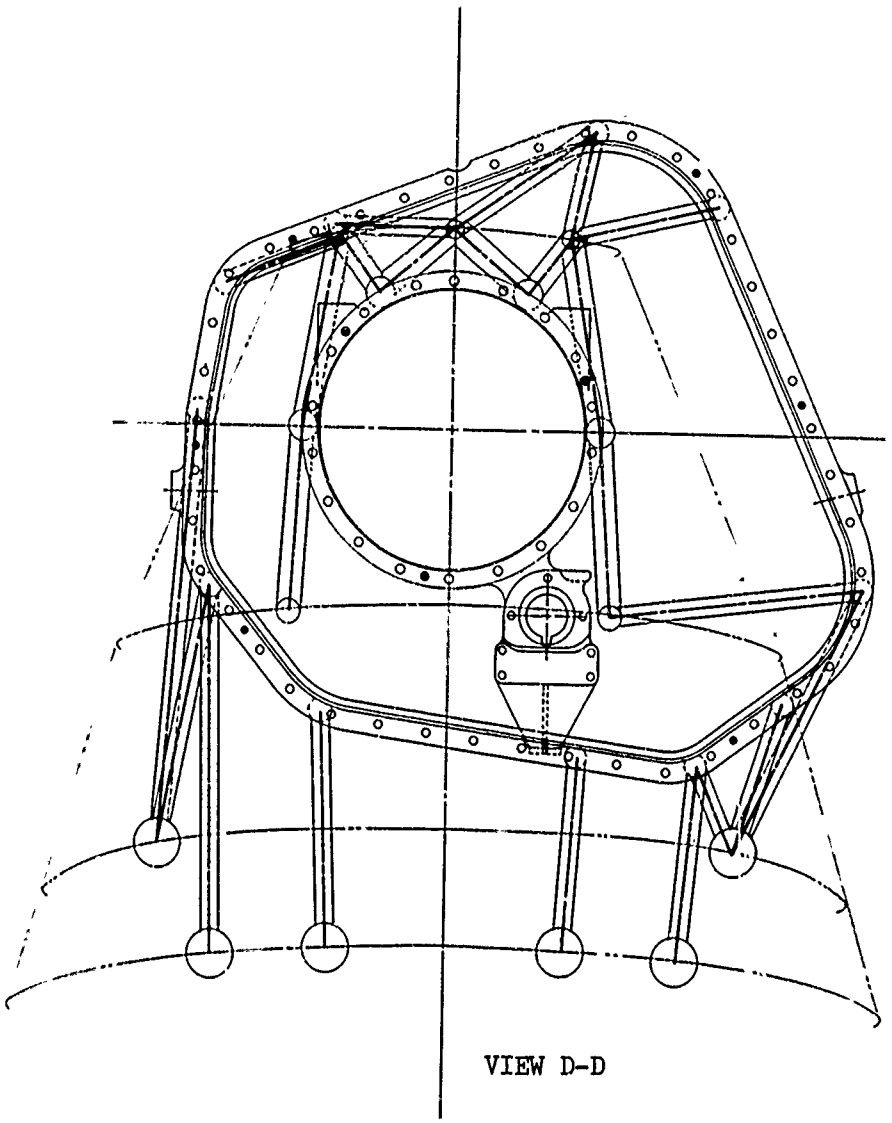

VIEW D-D

0 2 4 6
SCALE (in.)

Figure 66. Detail Design Layout of the Fabricated Transmission Housing (View Looking Forward).

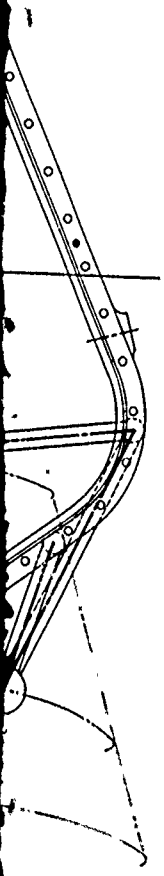

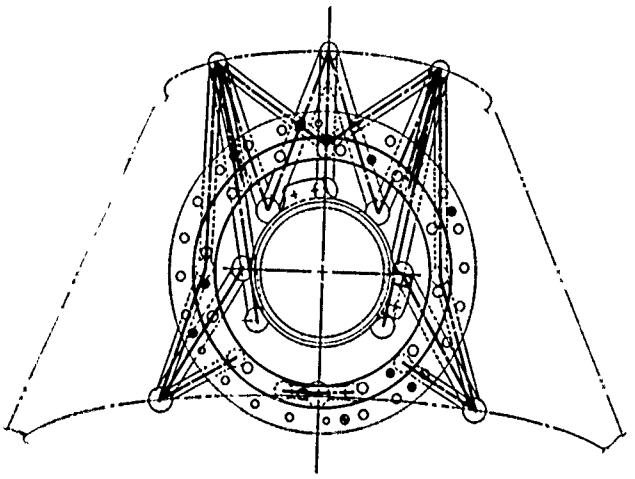

VIEW E-E

0 2 4 6
SCALE (in.)

gn Layout of the Fabricated
n Housing (View Looking

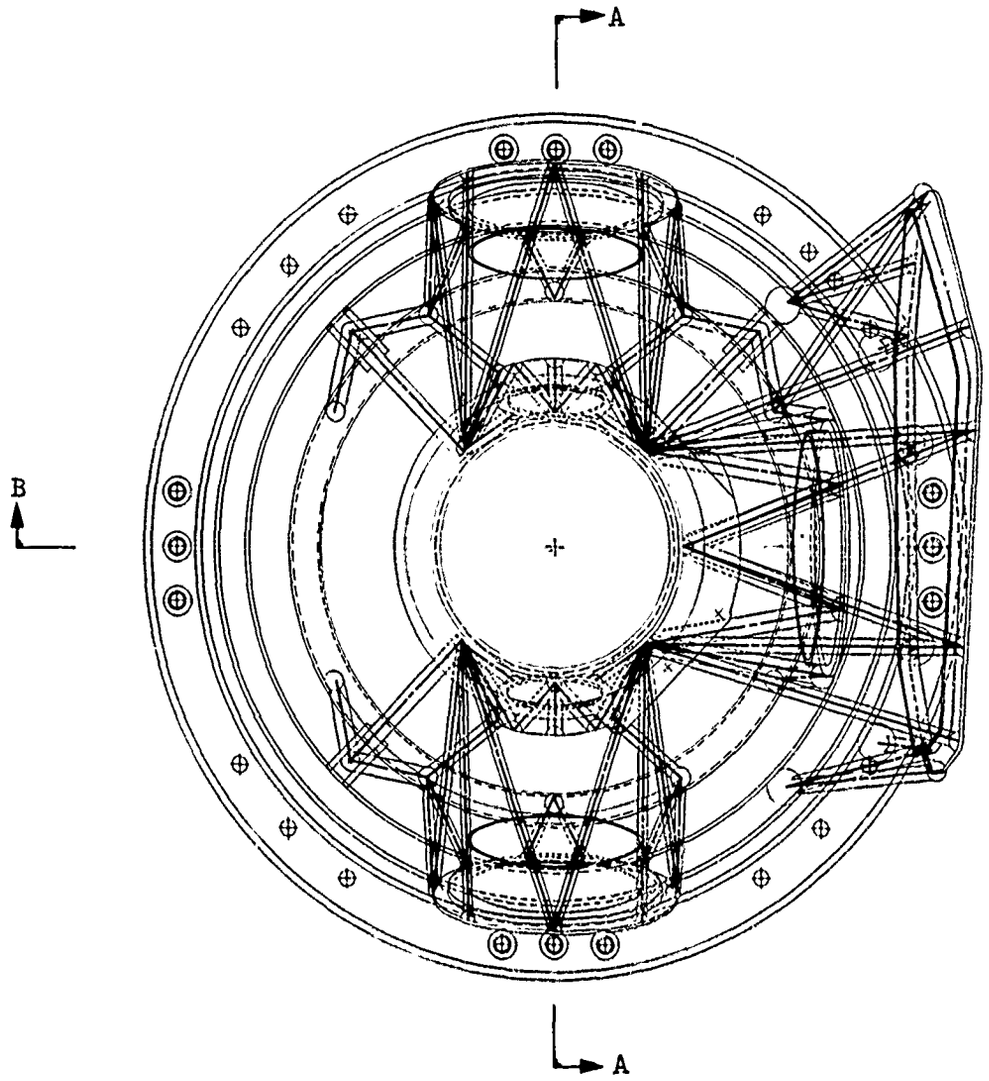

Figure 67. Detail Design Layout of the Fabricated Transmission Housing (Plan View).

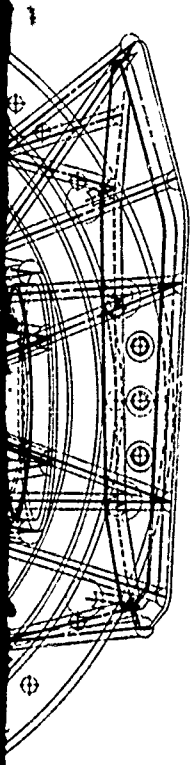

B

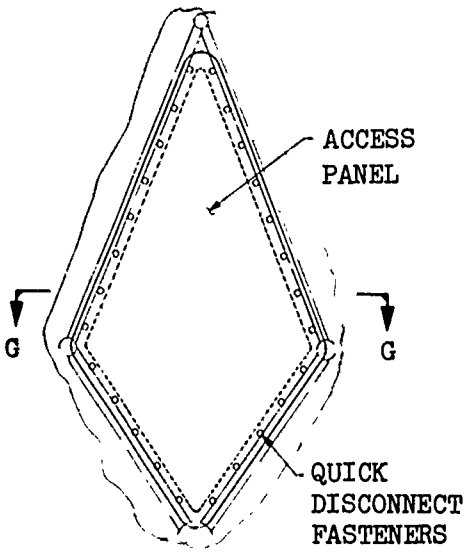

VIEW F-F
ROTATED 15° C.C.W.

SECT G-G

0 2 4 6
SCALE (in.)

yout of the Fabricated
sing (Plan View).

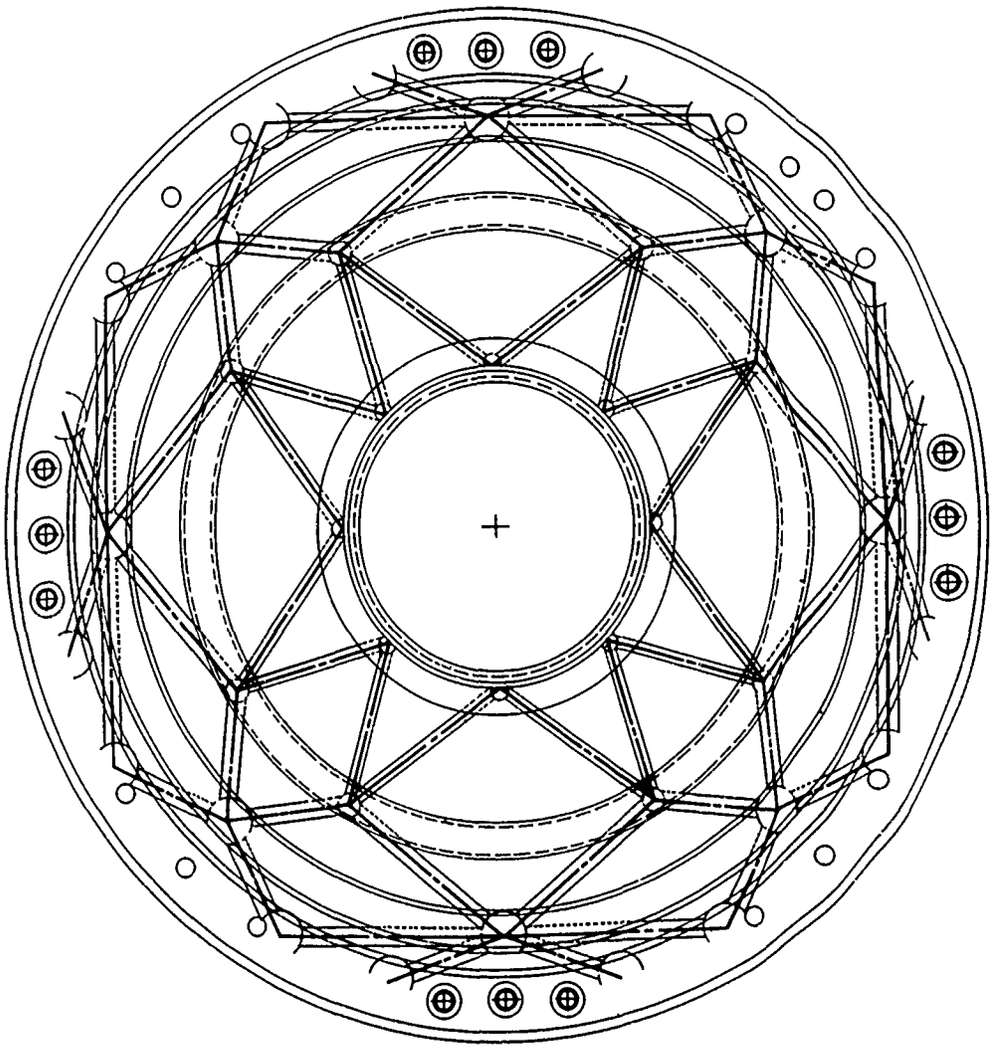

AUXILIARY PLAN VIEW C

0 2 4 6
SCALE(in.)

Figure 68. Detail Design Layout of the Fabricated Transmission Housing (Auxiliary Plan View).

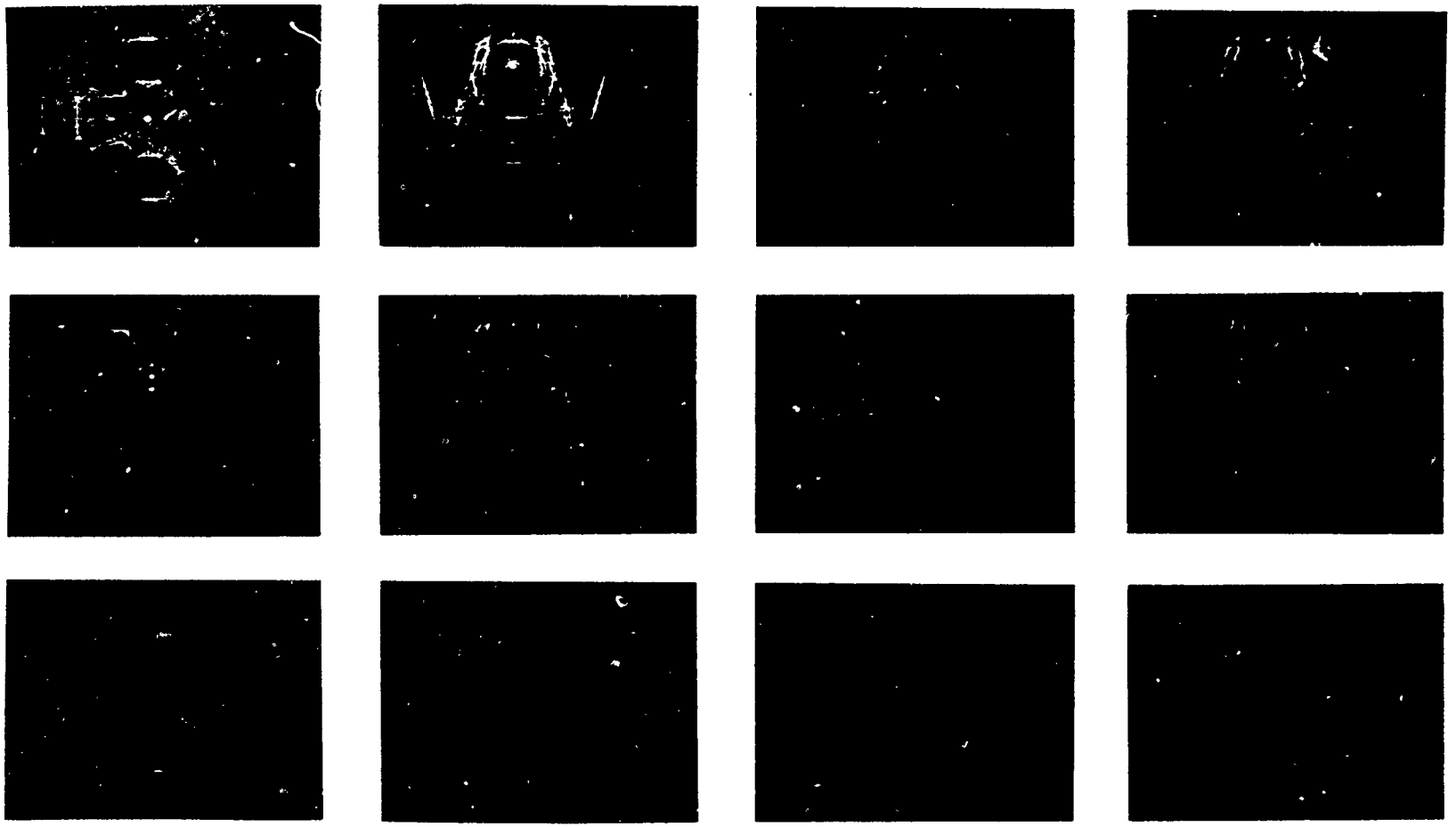

Figure 69. CRT Display of the Final Fabricated Housing Transmission Design.

Analysis

The final truss-like housing design geometry was modeled as a series of thin rings with connecting truss elements. Figure 69 is a series of photographs of the CRT display of the geometry coded for analysis in the NASTRAN program. The inside ring diameter contour is determined by bearing or mounting interface requirements, and the appropriate properties were coded for the analysis. The section properties of each of the rings were kept constant to simplify manufacturing. As a result, the ring is not fully stressed for most of its circumference.

The analytical output from the program gives the internal forces and moments at either end of each structural member and the resulting maximum axial and bending stresses. In addition, displacements at each end of the element are given. The cross-sectional properties and/or the location of the members were modified as necessary to satisfy the overall stiffness requirements and to obtain a minimum margin of safety.

The result of the analysis for the crash design condition is a structure weighing 305 pounds and having a minimum margin of safety for the ultimate strength of Custom 455 stainless steel. Maximum deflection of the upper ring for the crash loading condition is .480 inch.

To determine structural adequacy for normal flight requires the design to be reanalyzed for both the hover and symmetric dive and pullout conditions. Adequacy for these conditions is based on minimum yield margin of safety.

The material properties of Custom 455 are: ultimate allowable tensile strength, 220,000 psi; yield allowable tensile strength, 135,000 psi. The minimum margins of safety for the yield and ultimate allowables were positive for all conditions.

Analysis of buckling for the truss structure members indicated that the critical column length is always greater than the truss member column length for normal flight conditions.

For an analysis of fatigue loading conditions, the ground-air-ground (GAG) cycle column was considered to be critical. The most highly loaded member has the following bending and axial loads:

$M_{xx} = -146$

$M_{yy} = 398$

$F_a = -4456$

The section properties for this structural member are

I_{xx} = .0675

I_{yy} = .0265

A = .4687

The offset to the critical point on this section is x = .4583, y = .6041. The maximum stresses were found to be

f_{xx} = 2530

f_{yy} = 3560

f_a = 9570

The maximum vibratory stress for the GAG cycle was found to be

f_{vib} = 7830 $\pm$ 7830

The margin of safety is

$$M.S. = \frac{1}{\frac{7830}{F_{ty}} + \frac{K_t\ 7830}{(.05\ En)}} - 1 = .16$$

where F_{ty} = Tensile yield strength

En = Endurance limit taken from Table VIII

K_t = Concentration factor

COMPARISON OF THE FABRICATED TRUSS-LIKE HOUSING WITH THE CH-54B CASTING

For a comparison of the fabricated truss-like housing with the conventional casting design, the following were considered: cost, reliability and maintainability, corrosion characteristics, survivability, vulnerability, and manufacturing ease. The cast housing and the fabricated housing were not compared on a structural basis since the casting is less amenable to precise analysis. Characteristics such as weight, cost, stiffness, and corrosion resistance were comparable, however.

The fabricated housing weighed 305 pounds and had a stiffness of 19.2×10^6 pounds per inch. The cast housing weighed 363 pounds and had a stiffness of 12.47×10^6 pounds per inch.

Cost Comparison

Table XII shows comparable costs of the fabricated housing and the cast housing. Materials and labor cost data for order quantities of 5, 10, 25, 50 and up were determined. Tooling estimates of $211,900 for the fabricated housing and $283,500 for the cast housing have been made. The fabricated housing on a unit basis is approximately $11,000 less than the present cast housing.

TABLE XII. COST COMPARISON, CONVENTIONAL CASTING VERSUS FABRICATED HOUSING DESIGN

	Unit Cost	
Quantity	Conventional Housing	Fabricated Housing
5-9	$38,500	$26,600
10-24	$36,280	$24,450
25-49	$32,100	$22,050
50 and up	$28,880	$20,750

The savings reduce to $7,000 with 50 or more units. In addition to being less expensive, the fabricated housing offers a savings in lead time of three months.

Reliability and Maintainability Comparison

The most significant problems common to all CH-54B cast housings in the field are nicks, dents, scattered corrosion, and stress corrosion. Figure 70 is a sketch of the conventional casting arrangement. With the typical casting mounting arrangement, corrosion takes place in fifty percent of the gearboxes at areas C, D, E, F and on the housing and airframe interface surface. Area C corrosion results from the bolt being installed to the airframe without dichromate primer. Area F corrosion is a result of the lack of sealer and the presence of moisture at the mounting interface. The mounting interface, which has the magnesium casting on one side and the aluminum forging on the other, corrodes due to the difference in electrolytic chemical activity. This interface is caulked on the extremity, but there is separation or cracking due to high maneuver vibratory loads. Leaking may also occur near the barrel nut by capillary action, since the barrel nut does not completely fill the hole.

On the fabricated housing, the material and joining methods selected preclude the possibility of these problems. As an example, almost all housings coming to Sikorsky Overhaul and Repair facility exhibit corrosion inside the mounting feet bushings. These bushings are cadmium plated and are used with corrosion-resistant bolts. The corrosion that appears is the result of wearing of the cadmium plating as the bolts are tightened.

Bushings are used on fabricated housings to enable reuse of the component in the event of wear or damage. The bushing flange also provides a large enough area to keep unit stresses low, while the press-fitted bushing body provides a large shear area to react shear loads. Figure 71 is a sketch of the detail of the mounting foot with bolt and bushing installed. Shims are employed as sacrificial elements to prevent water from seeping between the bolt and housing. These shims are approximately 3/16 of an inch thick to prevent splitting under high bearing pressures. The steel bushings are installed in the fabricated housing with wet zinc dichromate primer. The bushings are frozen and then pressed into the housing with an "O" ring under the bushing flange. When the bolt is installed in the bushing to mount the housing to the airframe, the bolt is installed with wet zinc dichromate primer on the bolt with an "O" ring under the bolt head. The "O" ring fits between the chamfer of the bushing and the root radius of the bolt head.

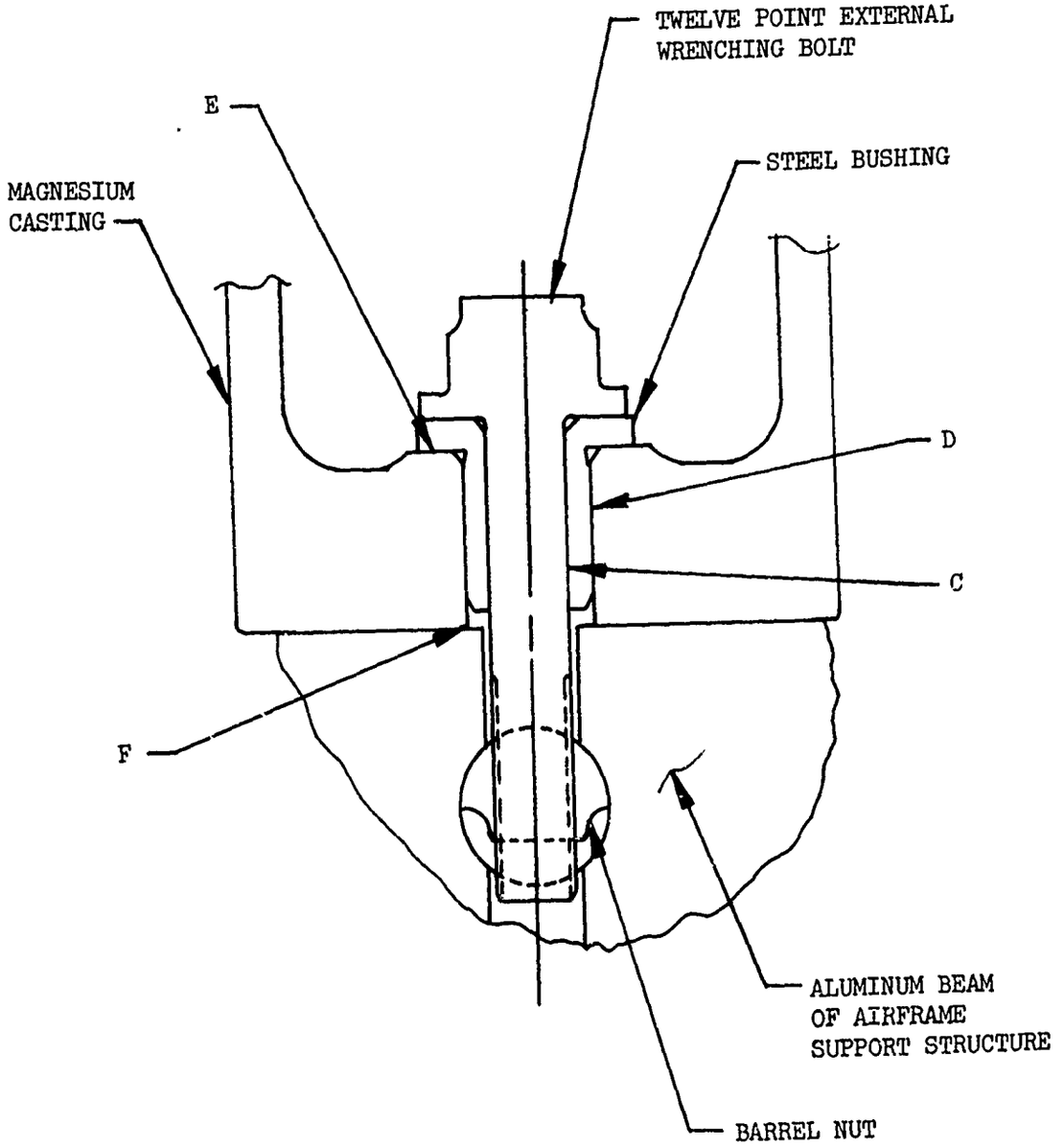

Figure 70. Detail of Typical Casting Mounting Arrangement.

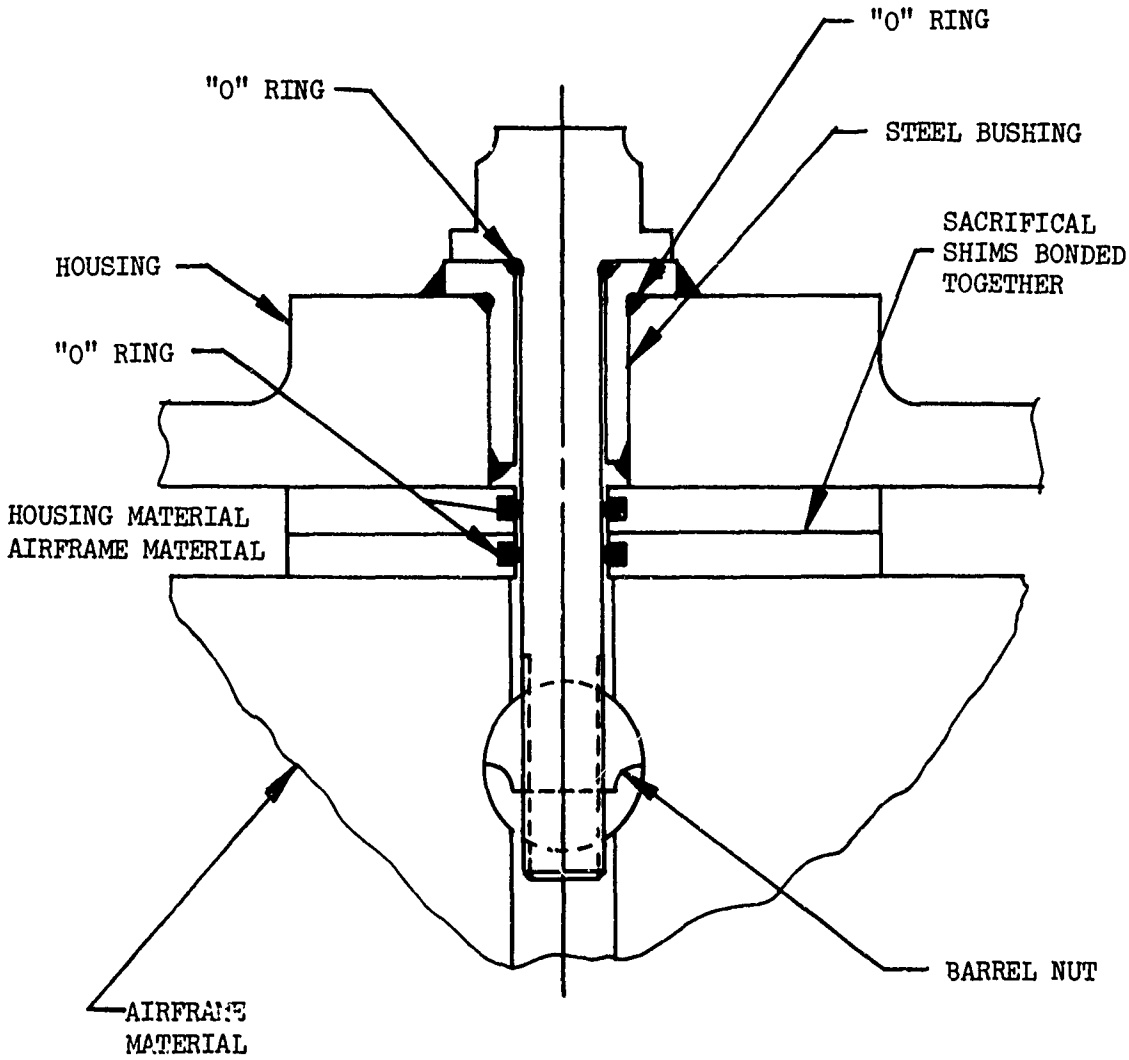

Figure 71. Detail of Typical Fabricated Housing Mounting Arrangement.

The failure modes of a cast magnesium housing in decreasing order of importance include corrosion, creep, fatigue due to GAG cycle, static yield, and stress corrosion cracking due to pressed in bushings and pins. On the fabricated housing the material and joining method selected preclude the possibility of these failure modes with the exception of stress corrosion. The problem of stress corrosion is reduced through the use of Custom 455 which has higher fracture thoughness properties.

The problem of field inspectability of the cast housing has been eliminated with replacement by a fabricated housing. Present castings to be fluorescent inspected require the removal of the protective finish, paint and resin coatings. The fabricated truss housing made of Custom 455 stainless steel has no protective finish on it, since it is self-passivating, and may be inspected on the aircraft through magnetic inspection techniques.

The detectability of cracks on the fabricated housing is simpler through on the aircraft inspection techniques and is not critical to structural integrity of the housing. The fabricated housing is a redundant structure and the loss of any one truss member is easily tolerated.

It is expected that a reduction in housing repair cost will be achieved through the use of a fabricated housing since problems associated with corrosion and creep have been eliminated. Overall reduction of housing failure rates can be expected but are difficult to quantify without test data.

Corrosion Properties Comparison

Custom 455 stainless steel is far superior to cast magnesium with respect to corrosion. The stainless steel, including the welded areas, requires no surface protective film because it is self-passivating. A cast magnesium housing requires a series of protective surface finishes to maintain its corrosion resistance. Even though much work has been done on surface finishes for magnesium and the results are good, self-protecting material was considered a good goal for a fabricated housing design. The scattered corrosion problem would thus be eliminated. Stress corrosion does not exist, since in the weld areas of fabricated housing, the structure is normalized after welding.

Crashworthiness

The work done on crashworthiness indicates that the fabricated housing design would survive for the indicated loading of 20g forward, 18g side and 20g down even though there would be considerable yielding.

Heat Dissipation

A typical main transmission rejects approximately 12-15 percent of the total heat generated through its housing. The rest is rejected through the oil heat exchanger. The actual heat transfer coefficient of a cast housing is unknown, since the cast housing includes dichromate primer and acrylic lacquer on the exterior and a baked resin coating on the interior. The fabricated housing rejects approximately one-third of the heat that a cast housing rejects. This results in a 5-percent degradation in overall heat rejection performance and is a conservative estimate.

Survivability and Vulnerability

The basic study requirements for the fabricated transmission housing omitted a survivability/vulnerability analysis. The redundancy of the multiple-structural-element design makes the improved survivability aspects obvious when compared to the single redundancy of the present monocoque casting construction. With multiple element design, resistance through 23mm HEI is inherent with no weight penalty. The survivability/vulnerability improvements from this design method are several and are listed below:

- The design is multiply redundant compared to the singly redundant approach of castings.
- Ballistic damage or destruction of one or more structural elements removes only those particular load paths and may lead to eventual fatigue crack initiation in other paths as opposed to immediate fatigue initiation and propagation in monocoque structures.
- Gears are already considered survivable against almost all hits from higher threats because of their bulk and hardened steel construction.
- Bearings have remained a problem: additional design freedoms allow alternative solutions to bearing survivability that did not exist before.
- Truss structures may be left open during assembly (and skinned over later), allowing additional stops to be installed on gear shafts to prevent lateral motion of bearings after ballistic damage and to prevent separation of gear mesh.
- Weight savings inherent in multiple element design may be applied to additional passive bearing armor or to multiple redundant bearing installations or emergency lubrication systems, heat pipes, etc.

- Fabricated transmission housing materials have been chosen to operate under emergency conditions (600°F for one-half hour) with minimum deterioration of those portions of the transmission not directly damaged by the projectile(s). Repair of this battle damage has been made far simpler and, with further development, may be reduced to the field or depot level, rather than the present approach of replacing entire transmissions.

It is these gains, more than any others, which make the fabricated transmission housing concept so promising for future incorporation in Army helicopters. At a time when the importance of survivability/vulnerability is becoming recognized in stringent design requirements for future helicopter production, a design technique exists which removes the transmission housing from attrition, forced landing or mission abort and substantially reduces the problem of repair. The technique also saves weight which can be applied to improved survivability of critical high-speed bearings with sufficient amounts of weight reduction left over to improve performance of the vehicle. It is strongly recommended that future fabricated transmission housing requirements include in-depth studies of the survivability/vulnerability aspects outlined above and that design, fabrication and test include definitions of trade-offs (weight, cost, survivability/vulnerability improvements, performance improvements) which should be investigated to meet future Army battle-damage needs.

Manufacturing

The fabricated housing requires considerable labor for jigging and hand welding. The casting requires a lead time of 9 - 10 months for pattern equipment, tooling, and machining. The fabricated housing requires less machining and offers the advantage of easier machining due to increased access (no skin on) areas. The fabricated housing permits repair during manufacture much the same as weld repair procedures are used for cast magnesium. The fabricated housing also has the advantage of permitting manufacture of small subassemblies before joining the main structure.

Summary

A list of parameters for comparison of the cast housing with the fabricated truss housing is shown in Table XIII.

TABLE XIII. SUMMARY OF A CAST MAGNESIUM HOUSING WITH THE FABRICATED TRUSS HOUSING DESIGN

Item	Weight (lb)	Lead Time (mo)
Fabricated Truss Housing	305	6
Cast Housing	363	9

The steel fabricated truss housing has considerable advantage as a replacement for the cast magnesium housing. The fabricated housing offers a saving in weight and lead time and is less expensive.

EFFECT OF SCALING A FABRICATED HOUSING DESIGN

The fabricated housing was additionally analyzed to study the effect on housing size and weight for a ±25 percent change in input torque.

The approach taken in this study consisted of scaling the aircraft size up and down and then identifying the significant parameters that correspond to a ±25 percent change in torque. Since a mathematical model does not exist for the CH-54B aircraft, a utility transport aircraft was modeled and the loads were scaled to the CH-54B. This comparison has inconsequential errors in the estimation of fuselage inertias and weights, since a crane helicopter has almost no cabin area. Figure 72 is a plot of hub moment constant versus design gross weight. Figure 73 gives historical data of hub moment versus design gross weight with aircraft built to date. These figures illustrate the validity of the scaling procedure.

Parametric Scaling of Loads

For the scaling procedure, disc loading and tip speed were kept constant along with number of blades and payload/gross weight ratio. The rotor diameter, gross weight, power required, component weights, and rotor shaft moments were so determined.

Dimensionless plots were developed to provide a basis for determining flight loads and crash loads for ±25 percent change in design input torque. To determine new design gross weights, Figure 74 was used. The design gross weight ratios are 1.15 and .76 for ±25 percent change in design torque ratio. Thus, the gross weights of the sensitivity study aircraft are 54,100 and 37,700 pounds. Figure 75 is a plot of head moment constant ratio versus design torque ratio. For ±25 percent change in design torque ratio, the head moment constant ratios are 1.375 and .875. These ratios correspond to head moment constants for the sensitivity study aircraft of 1020 and 6540 ft-lb/deg. It is assumed that the flight loads vary in direct proportion to the head moment constant. To determine the crash loads, a number of plots of weight group areas were generated (Figures 76 through 79). Plots are included for main rotor group weight ratio versus rotor design torque ratio, and servo group weight ratio versus rotor design torque ratio. Under crash loading conditions, the rotor shaft reactions at the upper roller bearing for ±25 percent change in input torque are 201,660 and 133,450 pounds. For the side load on the lower thrust bearing, the reactions are 98,100 and 64,870 pounds. The flight control weight group ratios indicated that servo crash loads changed with a ±25-percent change in rotor design torque ratio to 793 and 558 pounds.

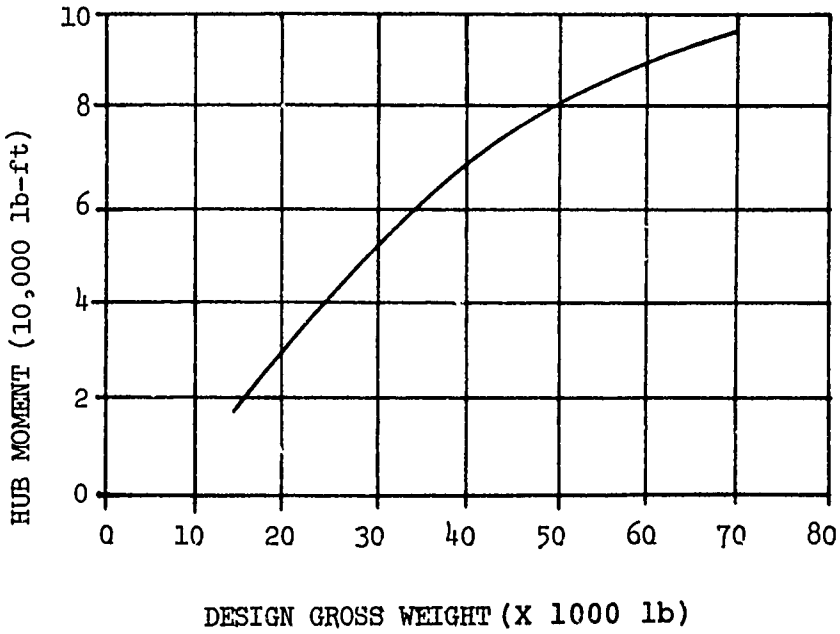

Figure 72. Historical Data - Hub Moment Versus Design Gross Weight.

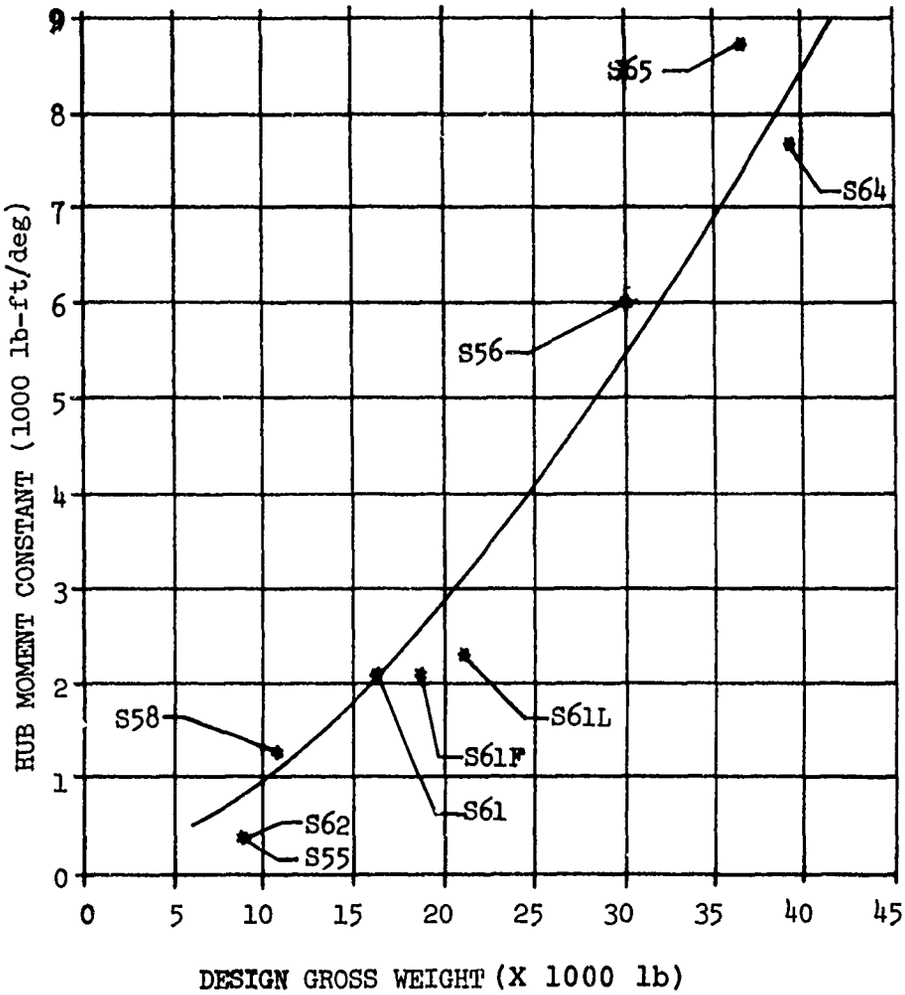

Figure 73. Historical Data - Hub Moment Constant Versus Design Gross Weight.

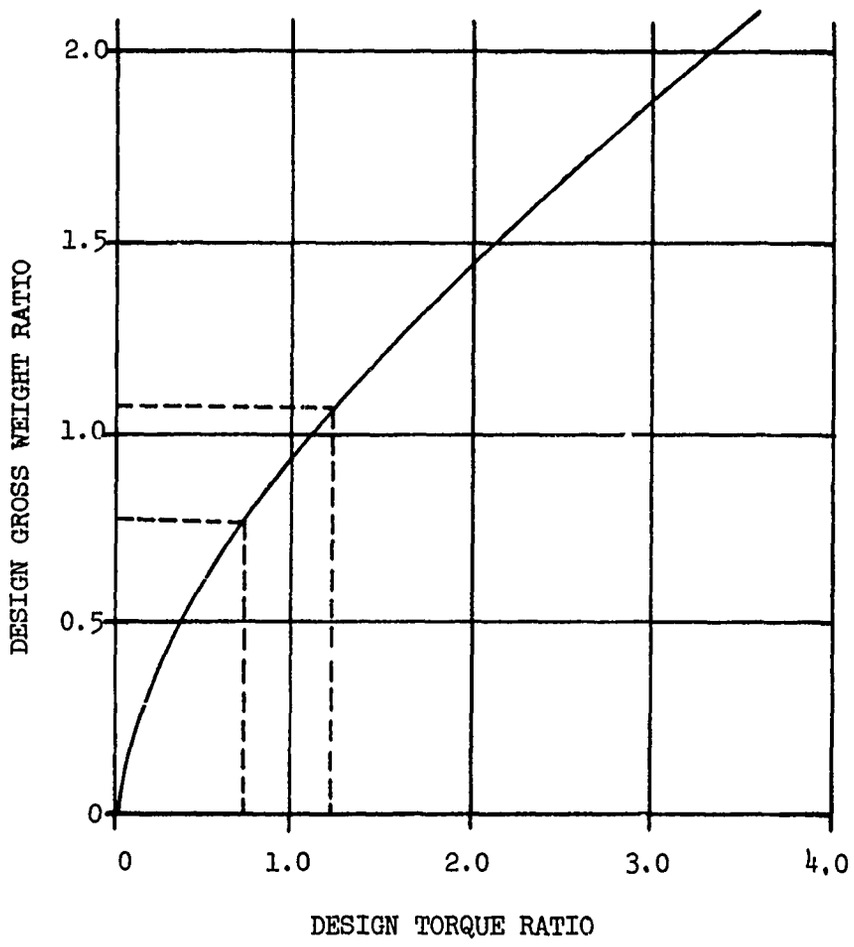

Figure 74. Design Gross Weight Ratio Versus Design Torque Ratio.

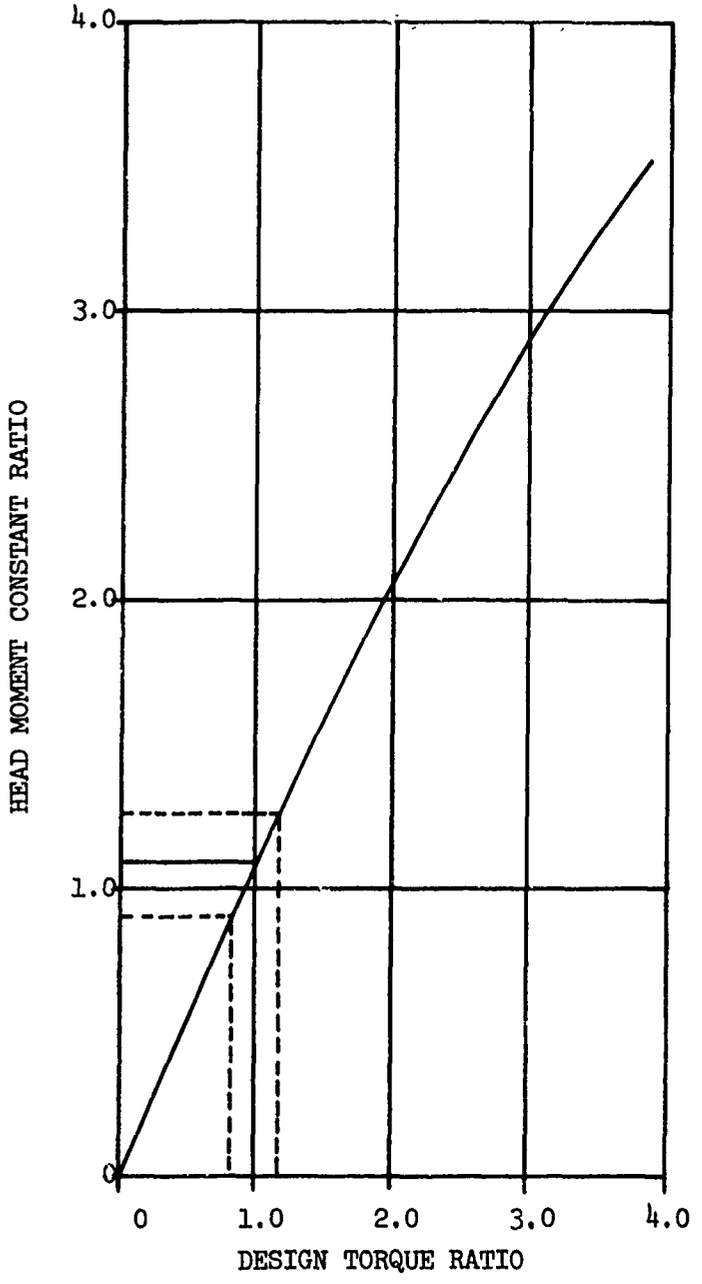

Figure 75. Head Moment Constant Ratio Versus Design Torque Ratio.

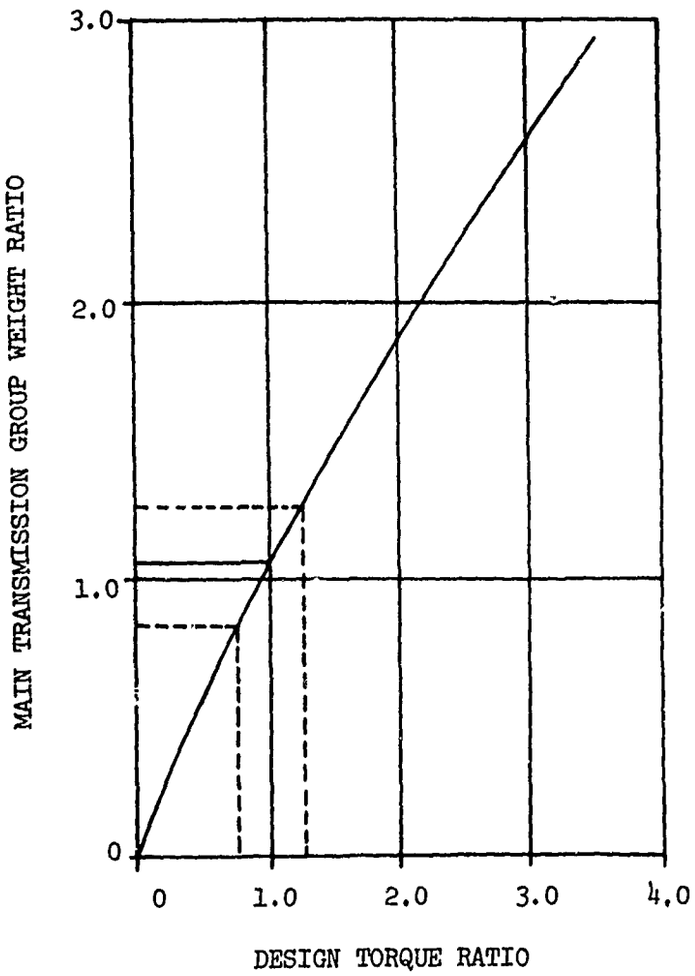

Figure 76. Main Transmission Rotor Group Weight Versus Design Torque Ratio.

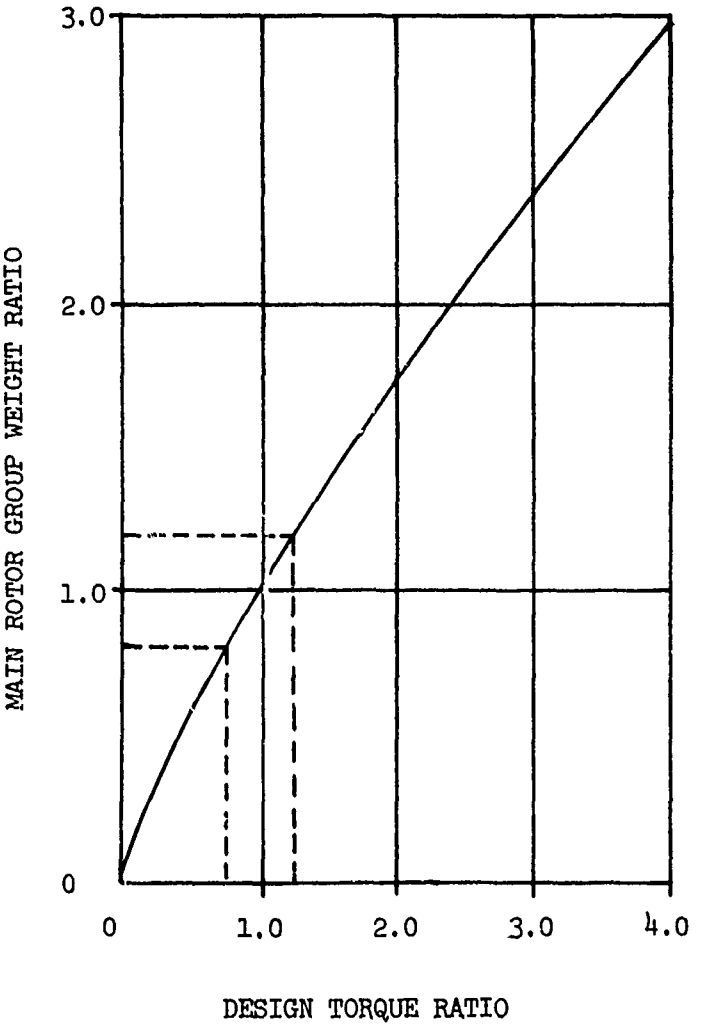

Figure 77. Main Rotor Group Weight Ratio Versus Design Torque Ratio.

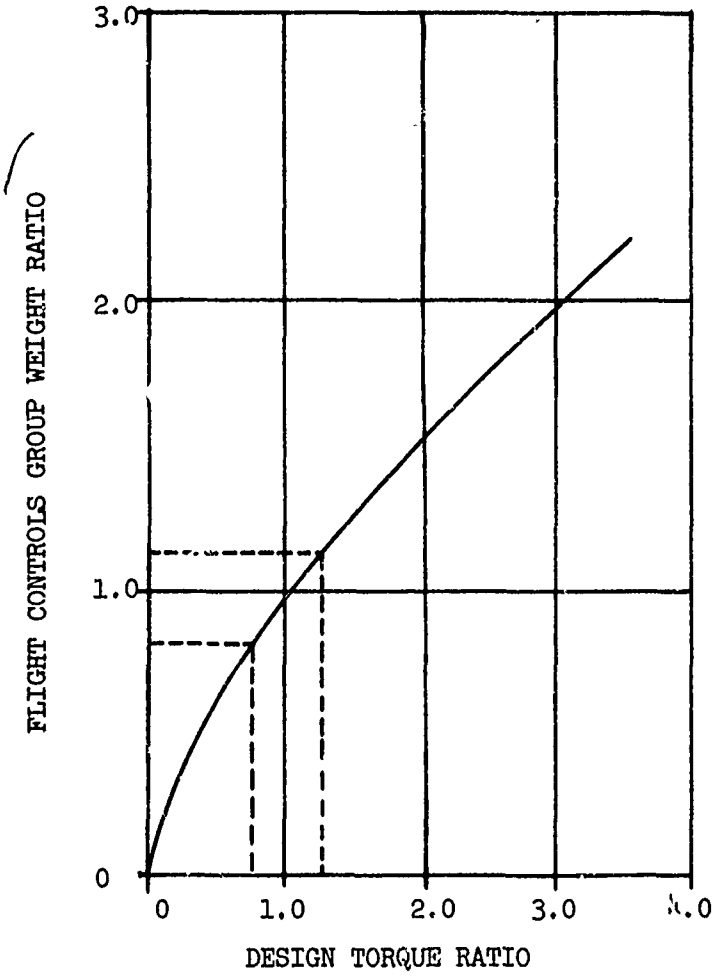

Figure 78. Flight Control Group Weight Ratio Versus Design Torque Ratio.

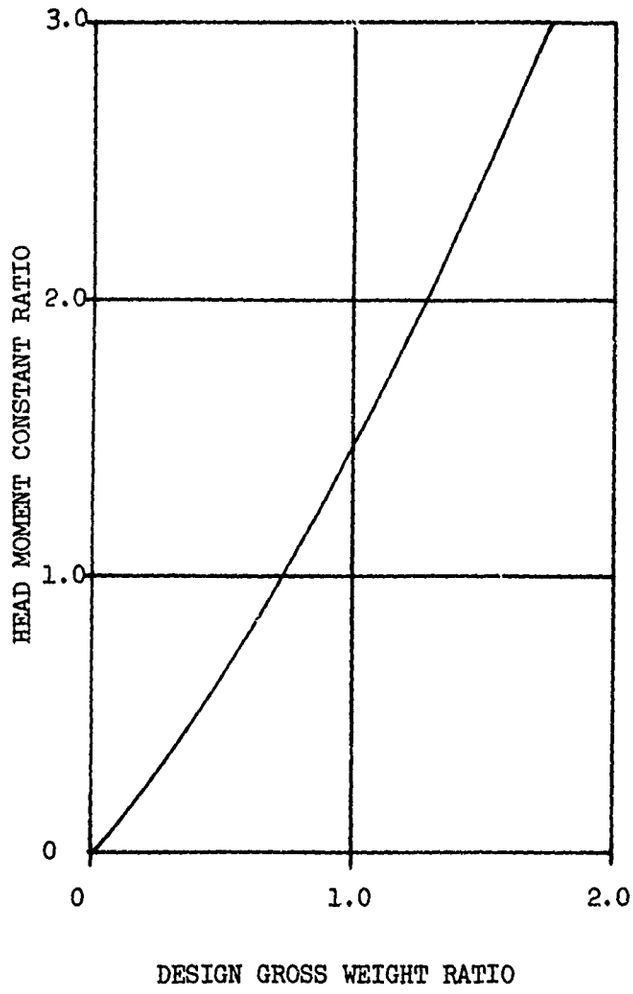

Figure 79. Head Moment Constant Ratio Versus Design Gross Weight Ratio.

For example, Figure 75 shows head moment constant ratio versus design torque ratio. The changes in head moment constant were 1.375 and .875, respectively, for ±25 percent change in input torque. The loads on the upper roller bearing were scaled proportionally with the change in head moment constant. For ±25 percent change in input torque, the upper roller bearing reactions were:

+25 percent	- 25 percent
$R_{ax} = (1.375)(12640) = 17380$	$R_{ay} = (.875)(12640) = 11060$
$R_{ay} = (1.375)(9670) = 13300$	$R_{ay} = (.875)(9670) = 8460$

For the lower thrust bearing horizontal reaction, the scaled loads of ±25 percent in input torque were:

+25 percent	-25 percent
$R_{bx} = (1.375)(-27326) = -37573$	$R_{bx} = (.875)(-27326) = -23910$
$R_{by} = (1.375)(-9676) = -13304$	$R_{by} = (.875)(-9676) = -8466$

Table XIV summarizes the changes in applied loads used in the structural analysis, compared with the fabricated housing design.

Analysis

For a ±25 percent change in input torque, the weights for the final housing design in stainless steel were 362 and 254 pounds.

For the crash conditions, the minimum margin of safety was zero. For flight conditions, the minimum margin of safety that is acceptable was the same as the baseline configuration. For both design criteria, the fabricated housing was adequate.

For a buckling analysis, with the allowable critical buckling stress taken from Table VIII, Fsecant = 156,000 psi at room temperature for Custom 455 stainless steel. For the fabricated housing design with the truss length members selected, the truss member column stress was always less than the critical column stress.

For the low cycle fatigue condition (ground-air-ground cycle), the highest loaded truss member for the -25 percent change in input torque has the following bending and axial stresses:

TABLE XIV. CI
CI

Location	-25% Input Tor		
	Crash		
	x	y	
Rotor Shaft Roller Bearing Reaction	133,444	133,440	-11
Rotor Shaft Lower Thrust Bearing	-64,864	-64,864	23
Left Side Input Ring	3,860	3,860	5
Right Side Input Ring	3,860	3,860	5
Tail-Takeoff Accessory Flange			19
Servo Supports			558
Scissor Bracket			
Combining Bevel Gear Reaction			1
Rotor Shaft Lower Thrust Bearing			
Left Side Input Roller Bearing			1
Right Side Input Roller Bearing			-1
Tail-Takeoff Bevel Pinion			-2

TABLE XIV. CHANGES IN APPLIED HOUSING LOADS FOR A ± 25 PERCENT CHANGE IN INPUT TORQUE

-25% Input Torque					Baseline Configuration				
Crash		Flight			Crash		Flight		
					Forward	Side			
x	y	x	y	z	x	y	x	y	z
133,444	133,440	-11,060	8,467		165,297	165,297	-12,341	9,676	
-64,864	-64,864	23,910	8,466		-81,108	-81,108	27,326	9,676	
3,860	3,860	5,390	7,125	8,040	5,147	5,147	7,120	9,500	10,728
3,860	3,860	5,390	7,125	8,040	5,147	5,147	7,120	9,500	10,728
		19 loads 165 each		-9			19 load 200# each		-12
		558 each	558 each	7,481			690 each	690 each	8,550
		-762	-762	-13			-953	-953	-16
		1,962	-248	-1,692			2,617	-331	-2,256
			37,128	15,408	Thrust & Ring Gear			49,476	94,260
		1,650					2,200		
		-1,650					-2,200		
		-2,755	4,410	9,636			-3,674	5,880	12,840

DS FOR A ± 25 PERCENT

Baseline Configuration					+25% Input Torque				
Crash		Flight			Crash		Flight		
ard	Side				Forward	Side			
	y	x	y	z	x	y	x	y	x
07	165,297	-12,641	9,676		201,860	201,860	-17,381	-13,304	
08	-81,108	27,326	9,676		-98,120	-98,120	37,573	13,304	
47	5,147	7,120	9,500	10,728	6,433	6,433	8,900	11,375	13,404
47	5,147	7,120	9,500	10,728	6,433	6,433	8,900	11,875	13,404
		19 load 200# each		-12			19 load 255 each		-15
		690 each	690 each	8,550			793 each	793 each	11,756
		-953	-953	-16			-1,191	-1,191	20
		2,617	-331	-2,256			3,271	-413	-2,820
t & Ring Gear			49,476	94,260				-61,848	101,328
		2,200					2,750		
		-2,200					-2,750		
		-3,674	5,880	12,840			-4,592	7,350	15,056

f_b = 5959

f_a = 12925

The maximum vibratory stress for the GAG cycle was found to be

$f_{vib} = 9442 \pm 9442$

The highest loaded truss member for the +25 percent change in input torque has the following bending and axial stresses:

f_b = 7135

f_a = 11,427

The maximum vibration stress for the GAG cycle was found to be

$f_{vib} = 9281 \pm 9281$

The allowable material endurance limit for Custom 455 stainless steel to 37,050 psi. The margin of safety for the -25 percent change in input torque is M.S. = 0.72, and the margin of safety for a +25 percent change in input torque is M.S. = 0.75.

DEVELOPMENTAL AREA DEFINITION

Before the fabricated housing concept can be incorporated into actual flight hardware, certain areas will require further development. During this study, these potential problem areas were identified. These areas are associated with the analysis as well as the fabrication and qualification of the housing design.

Analysis

Because of the extreme general nature of the NASTRAN program and its capability of handling very large matrices (orders of 10,000 have already been solved), it is not particularly efficient on small programs, and large expenditures of computer time result. The amount of computer time used increases geometrically with the number of truss members in the structure. For the truss housing of the preliminary design configuration, with approximately 300 elements, about 20 minutes of actual computer program utilization time was required to calculate the stresses, displacements, and margins of safety. For the final housing design configuration, about 60 to 90 minutes of computer time was required for approximately 700 elements in the structure.

The CRT capability permits display of the truss geometry in any orientation. Through use of the Data Editor Program, connectivity changes are permitted, but new element and geometry cannot be added at the tube without going back to the Batch Card Processor (see page 102). Use of this program at the CRT consumes about 20 minutes, during which nothing else can be done at the tube. The handling of more than one deck simultaneously with the Data Editor Program would be desirable. To check load direction, a display capability for the applied loads is needed. To help in understanding the NASTRAN output, a display of normalized deflections relative to the housing geometry display would be extremely useful and permit quick assessment of load path and improvement in structure weight. The analysis of the truss housing with NASTRAN to obtain a minimum weight design was accomplished with a trial-and-error approach. Minimum weight design programs, in conjunction with NASTRAN, would permit a theoretical solution for a minimum weight truss structure. These results would then be changed to limit the number of members of different sizes.

A plastic analysis capability will make possible a lighter structure design for ultimate criteria under crash loading conditions. The bending analysis that was completed assumes a linear, elastic relationship between stress and strain. A plastic analysis program would account for the redistribution in load capability of the structure members as the yield point is exceeded.

A thermal analysis capability will permit the calibration of induced internal stresses as a result of the nonuniform transfer of heat from localized heat sources within the gearbox. Thermal effects at the truss housing interface with the airframe support structure would also be evaluated.

Experimental Verification

The fabricated housing can be substantiated and verified by an endurance test program run at operational loads. Assembly of the gearbox would verify that all of the interface requirements associated with the dynamic components (gears and bearings) as well as peripheral equipment (accessories, input section, etc.) are satisfied. Structural substantiation of the housing structure itself should be shown by a 350-hour endurance test program as outlined below. Also included in the test plan should be a no-load lubrication test and an overtorque test similar or equal to the following:

Test Plan (Suggested)

A proposed test program should consist of a no-load lubrication test and 350 hours of bench testing with simulated loading to represent hub moment and thrust on the housing. The program should be much the same as the program designed to qualify the CH-54B for FAA certification.

Bench testing should be conducted in Sikorsky's CH-54B/S-64 Main Transmission Test Laboratory. The regenerative bench test facility to consist of three closed mechancial loops (two input and one tail-takeoff) in which the required torques are locked in. The required shaft speeds to be provided by a single drive motor and eddy current clutch. The test component experiences the torque equivalent of the rated test power, independently of actual power supplied. The test facility is shown in Figures 80 through 83. A hydraulic load-absorbing system loads the accessory pads of the test transmission right side input. To simulate main rotor shaft moments and thrust, the housing dolly and the fabricated housing upper roller bearing support ring should be arranged to permit loading through hydraulic cylinders, as shown in Figure 83. This would permit the testing of the fabricated housing design under all possible loading conditions prior to a flight test.

Before the 350-hour endurance test, the transmission should be subjected to a production transmission acceptance test.

Thirty-five 10-hour endurance tests should be conducted in accordance with the spectrum presented in Table XV.

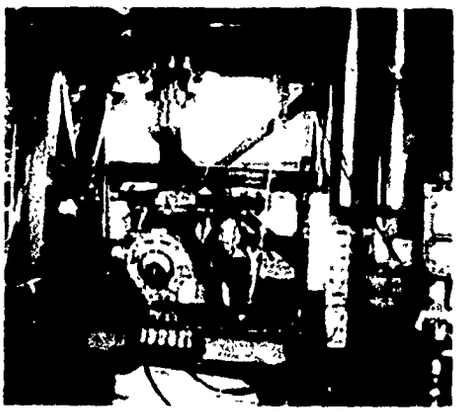

Figure 80. CH-54A/B Regenerative Test Stand - View of Test Stand.

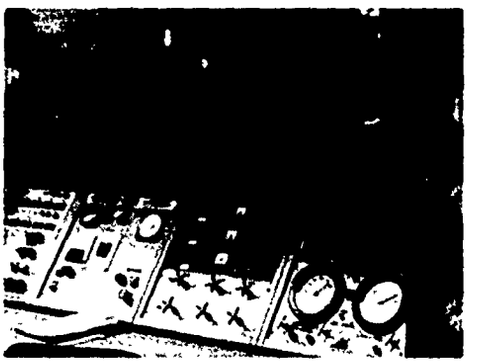

Figure 81. CH-54A/B Regenerative Test Stand Control Room.

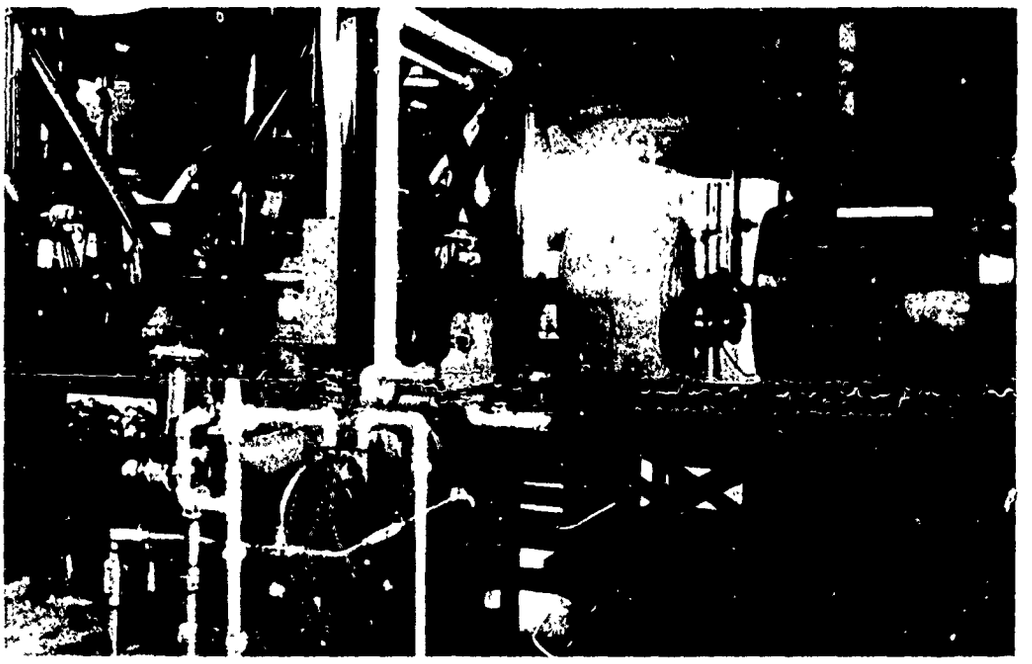

Figure 82. CH-54A/B Regenerative Test Stand - View of Drive.

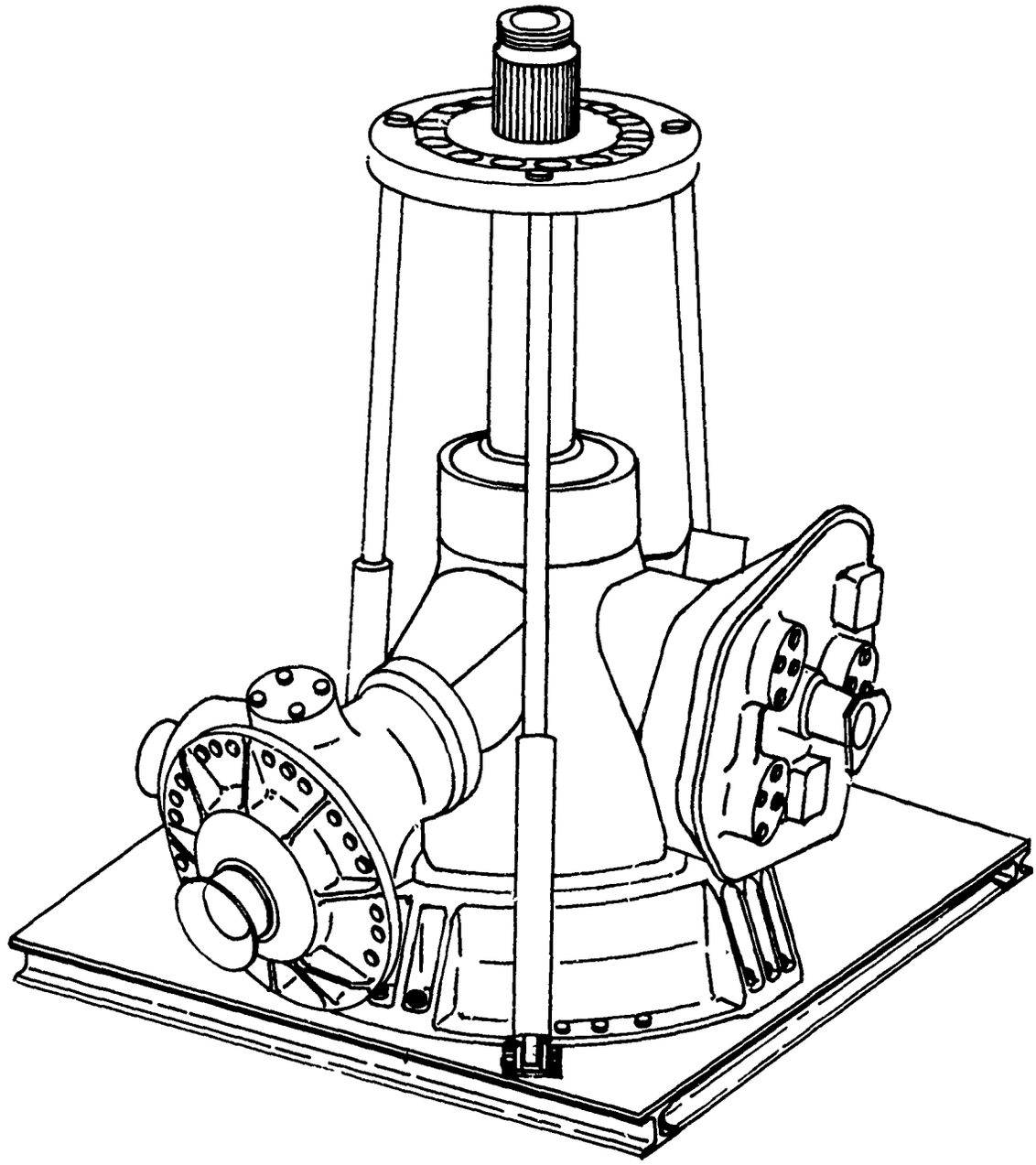

Figure 83. Test Rig To Simulate Main Rotor Shaft Loads.

TABLE XV. 10-HOUR DUAL-ENGINE ENDURANCE TEST CYCLE

Condition	Duration (hr)	L/H Input power (shp)	R/H Input Power (shp)	Total Input Power (shp)	Tail-Takeoff Power (shp)	Thrust (in./lb)	Head Moment (in./lb)	Speed (185 RPM) (%)
Dual Engine	1	3950	3950	7900	1100	52,000	960,000	100
30 Minute	(see note 1)	1000	1000	2000	250	52,000	960,000	100
Rating	1	3950	3950	7900	1100	52,000	960,000	100
	(see note 2)	1980	1980	3960	250	52,000	960,000	100
Max. Cont.	1	3300	3300	6600	400	52,000	960,000	100
Power	1	3300	2800	6600	400	-	-	100
	1	2800	3300	6600	400	-	-	100
90% Max. Cont. Power	1	2970	2970	5940	400	-	-	100
80% Max. Cont. Power	1	2640	2640	5280	400	-	-	100
60% Max. Cont. Power	1	1980	1980	3960	250	-	-	95
30 Min.	1/2	4800	-	4800	250	-	-	100
O.E.I. Power	1/2	-	4800	4800	250	-	-	100
Overspeed	1	3300	3300	6600	450	-	-	104-105

Note 1: Alternate cycles of 5 minutes at 3950 hp and 5 minutes at 1000 hp.
Note 2: One 30-minute cycle at 3950 hp followed by one 30-minute cycle at 1980 hp.

During at least 10 test cycles, the main transmission right-side input hydraulic pumps should be driven and loaded to the maximum rate specified in Table XVI.

TABLE XVI. R/H INPUT ACCESSORY PAD LOADING

Accessory	Operating Pressure (psig)	Flow (gpm)	Speed (rpm)	Horse-power
Second-Stage Servo Pump	3,000	14	4584	30
Hoist Pump	4,000	30	3796	80

To demonstrate main transmission housing overtorque capability, the main transmission should be subjected to twenty-two 10-second cycles at 8700 total input shaft horsepower and 1100 horsepower at the tail-takeoff. A complete dual-engine overtorque cycle is described in Table XVII.

The following data should be obtained during the tests:

1. strain gage measurement of the fabricated housing for all loading conditions,

2. spectographic analysis of lubricating oil samples at 25-hour intervals during the bench test,

3. transmission oil pressures, temperatures, and flow at all test conditions during the bench test, and

4. housing surface temperatures.

At the end of 200 hours of endurance testing, the fabricated housing transmission should be condition inspected. A spectrographic oil analysis, chip detector inspection, and strainer inspection should also be conducted. The fabricated housing transmission used for the bench test should be completely disassembled on completion of the 350-hour test. The transmission components, truss housing, and skin covering should be subjected to a condition inspection including zyglo/magnaflux and a conformity inspection. The test report should include the following items.

1. 200-hour and 350-hour inspections performed during program.

2. Spectographic oil analysis performed during test program.

3. Applied housing loads and strain gage measurements.

4. Conclusion and recommendations.

Design Guidelines

1. Use a structural design of many lightweight truss members for redundancy, rather than a fewer number of large-size members.

2. Assume that the skin covering does not contribute to structural stiffness and carries no load.

3. Assume the bearing loads to be sinusoidal and to lie in the same plane.

4. Make use of a rigid, weightless loading spoke to input sinusoidal bearing loads.

5. Assume each connection to have the same properties as the structure it connects.

6. Use welding for joint fabrication. Welding offers simple joint design, lighter weight joints, and high static joint efficiency.

7. Provide access for machining joints after welding to eliminate stress risers.

8. Locate truss members so that their line of action passes through the centroid of the ring cross section or truss member it joins.

9. Initially size structure for crash loads.

10. Use symmetrical cross sections for truss members. They are easier to code and use in the analysis.

11. Minimize the number of different size sections for the truss members to simplify manufacture and analysis.

12. Use constant cross sections for reaction rings to simplify manufacture and analysis.

13. Use of a redundant structure computer program, such as NASTRAN, is mandatory.

TABLE XVII. DUAL ENGINE OVERTORQUE TEST CYCLE (110% OF DUAL-ENGINE 30-MINUTE RATING)

Duration (sec)	L/H Input Power (shp)	R/H Input Power (shp)	Total Input Power (shp)	Tail-Takeoff Power (shp)	Thrust (in./lb)	Head Moment (in./lb)	Main Rotor Speed (%)
10 (see Note)	4350	4350	8700	1100	98,000	1,470,000	100
10 Minimum	1000	1000	2000	150	98,000	1,470,000	100

Note: Repeat 20-sec cycle 22 times. R/2

AREAS FOR FUTURE STUDY

Areas requiring additional development effort before the fabricated housing concept can become operational include a welding development program and improved analytical methods. The welding development program is necessary to improve joint integrity through better quality control of welded joints. Improved analytical methods should include determination of skin covering strength effects, a method for plastic and thermal stress analysis, development of a preprocessor to reduce coding of input data, and development of a specific program to handle the required structural analysis.

A fabricated housing should be built and tested as outlined in the program to verify cost analysis, fabrication techniques, and weight savings. In conjunction with an endurance test program, a thermal mapping study should be made to determine the heat dissipation characteristics of the fabricated housing design.

To reduce the risk and cost of building a full-scale CH-54B fabricated main transmission housing, a CH-54B tail gearbox should be considered. The CH-54B tail gearbox was previously described in Description of Drive Train.

This housing considered for a truss-like fabricated housing replacement has the advantages of simulating all the loadings experienced in a main transmission housing and is smaller in size, easier to test, and less costly to fabricate.

The loading on the tail gearbox housing consists of the internal bevel gear reaction load supported in two different housings, tail rotor servo support mounting load to simulate various accessories, and tail rotor shaft loading to simulate the main rotor loading.

Figure 84 is an isometric of a tail gearbox housing in a truss-like configuration. The gearbox consists of three housings jointed at the ring interfaces for assembly and disassembly of the gearbox. The bottom housing contains the airframe interface mounting ring and a series of rings to support the bevel pinion. The center housing is a truncated conical structure that supports the bevel gear and tail rotor shaft and reacts tail rotor thrust loads. The third housing is a cylindrical structure that supports the outboard end of the tail rotor shaft.

A tail gearbox fabricated truss-like housing offers potentially a lighter weight design, simulates the loading of a main transmission, is smaller in size, can be tested in the tail-takeoff test loop shown in Figure 80, and is less costly to fabricate.

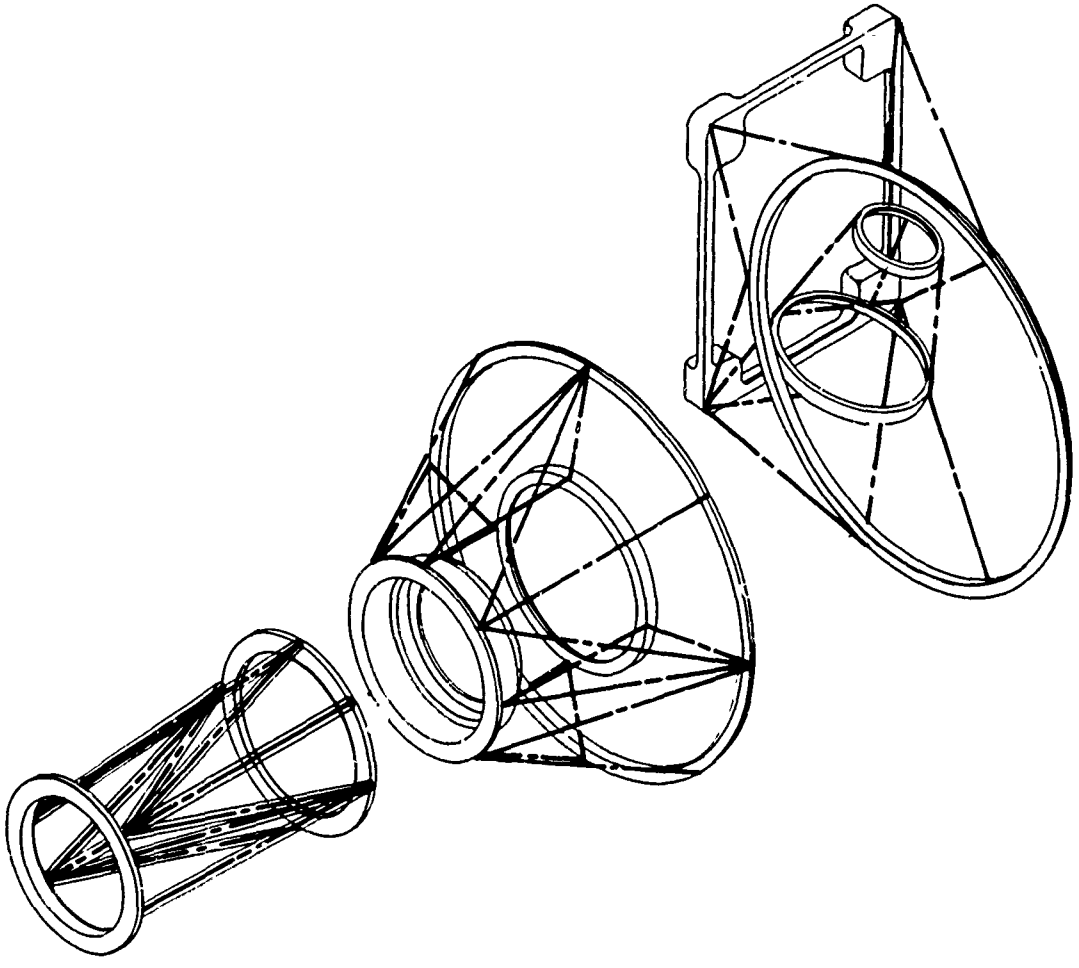

Figure 84. Isometric of a Tail Gearbox Housing as a Truss-Like Structure.

SUMMARY

A fabricated truss-like transmission housing was designed which could replace the conventional cast magnesium main housing on the U. S. Army CH-54B helicopter.

The fabricated housing replaces the upper main casting and lower support forged housing. This design enables use of the present input housing assemblies, rear cover assembly, all internal gearing and bearings, and the swashplate guide. Design criteria for flight and crash conditions, including loads and stiffness requirements, were developed to allow comparison with the existing casting design.

A material and joining method study, which included sixteen materials with various joining processes, indicated that welded Custom 455 stainless steel should be used for the fabricated truss-like housing. Thin sheet covers of the same material, mechanically fastened to the truss, with gasket material for sealing, are used to retain oil and have only a negligible weight penalty.

A number of fundamentally different truss housing geometries with different materials were coded, checked through the use of a CRT, and analyzed in NASTRAN. A final design configuration evolved, which consisted of many structural members joining the rings of a welded stainless steel truss. The weight of the final design configuration was 305 pounds as compared to 363 pounds for magnesium casting.

A $\pm$25 percent change in input torque results in a truss structure weight in stainless steel of 362 and 254 pounds.

Before a fabricated housing can become operational, the analysis must be correlated with experimental test data to verify the analytical model. A test plan is included for testing a CH-54B housing design.

To reduce the risk and cost of building a fabricated truss-like main transmission housing, preliminary design and testing should be conducted on a CH-54B tail gearbox. This gearbox has loading characteristics similar to the main housing but on a much smaller scale.

CONCLUSIONS

The fabricated truss-like housing is feasible using today's materials, analytical methods, and fabrication techniques and represents low technical risk. A fabricated housing should be built to verify cost, analysis, fabrication method, and weight savings.

The selected material for the fabricated housing is Custom 455 stainless steel for both the structural members and the non-structural skin covering.

The fabricated truss-like housing is 15 percent lighter than the present cast magnesium housing.

In quantities up to ten housings, the fabricated housing unit cost is approximately 30 percent less than the cast magnesium

Design and manufacture of a fabricated housing is expected to offer a shorter lead time of approximately three months.

The fabricated housing was designed to operate at gearbox temperatures up to 600°F, and its fatigue, ultimate, yield and creep properties are superior to those of the present cast magnesium housing.

A large number of redundant structural truss members improves fail-safe characteristics. A simplified, conservative analysis indicates improved survivability with ballistic damage and greater credibility for survival against ballistic threats such as 23 mm API and HEI hits.

Verification of the fabricated housing design is necessary before it can be considered as flight hardware. Preliminary testing should be conducted on a fabricated housing designed for a production gearbox such as the CH-54B tail gearbox. This gearbox, although smaller than the main gearbox, has similar loading characteristics and complexity. Test results would be indicative of the practicality of a fabricated housing design.

LITERATURE CITED

1. Caseria, P. T., ACTUAL WEIGHT AND BALANCE REPORT, Sikorsky Aircraft; SER-64316, Sikorsky Aircraft, November 1970.

2. Mongillo, A. L., FLIGHT LOADS AND CONDITIONS, CH-54B, Sikorsky Aircraft; SER-64442, Sikorsky Aircraft, August 1969.

3. Frye, R., STRUCTURAL DESIGN CRITERIA REPORT, MODEL CH-54B HELICOPTER, Sikorsky Aircraft; SER-62386, Sikorsky Aircraft, August 1969.

4. Stiegler, D., THE SHALLOW CONICAL SHELL, Sikorsky Aircraft; SER-50361, Sikorsky Aircraft, November 1963.

5. Sanders, W. W., FATIGUE BEHAVIOR OF ALUMINUM ALLOY WELDMENTS, Engineering Research Institute, Iowa State University, Ames Iowa, No. ISU-AMES-7.031, October 1971.

6. Jones R. E., FRACTURE TOUGHNESS AND FATIGUE CRACK GROWTH PROPERTIES OF 7175-T736 ALUMINUM ALLOY FORGING AT SEVERAL TEMPERATURES, AFML-TR-72-1, February 1972.

7. Peshak, C. M., THE INFLUENCE OF WELD DEFECTS ON PERFORMANCE, Welding Research Supplement (to the Welding Journal), February 1969, pp 45S-56S.

8. Lobb, A. E., et al., TITANIUM ALLOY WELDING, SST Technology Follow-on Program - Phase I, The Boeing Company, Commercial Airplane Group, P. O. Box 3707, Seattle, Washington, D6-6029, July 1972.

9. Anon., ARMCO 17-4PH STAINLESS STEEL BAR AND WIRE, Armco Steel Corp., Middletown, Ohio. 1968.

10. Dunsley, J. A., and Walker, A. C., THE FATIGUE STRENGTH OF BUTT-WELDED AND PLAIN SPECIMENS OF 18 (250) MARAGING STEEL PLATE, National Research Council of Canada, MS-122, May 1969.

11. Anon., CARPENTER CUSTOM 455 HIGH-STRENGTH STAINLESS STEEL, Carpenter Technology, 1971.

12. Degnan, W. G., Sikorsky Aircraft Engineering Materials Manual, Sikorsky Aircraft.

13. SD-24 Vol. II General Spec for Design and Construction of Aircraft Weapon Systems (Rotor Aircraft).

NOTE: If references are not expressly given, the data source was one of the standard handbooks, such as MIL-HDBK-5b or Aerospace Structural Metals Handbook.

APPENDIX I

CH-54B DIMENSIONS AND PERFORMANCE DATA

The aircraft chosen for study in this program is the U. S. Army CH-54B TARHE helicopter. Overall dimensions are contained in Table XVIII.

TABLE XVIII. GENERAL DIMENSIONS, CH-54B

Overall Length	88 ft 6.0 in.
Overall Width	21 ft 10.0 in.
Overall Height	25 ft 4.0 in.
Weight (Empty)	19,700 lb

The CH-54B is powered by twin JFTD 12A-5A Pratt & Whitney engines with a takeoff rating of 4,800 horsepower. These engines feature isochronous steady state governing, transient rotor droop of less than 4%, and rapid recovery to low power/high-rate descents (see Figure 85). Engine output power is monitored within 2% accuracy by phase displacement torquemeters. With their low vibration environment, these engines have a TBO of approximately 1,000 hours. The main transmission of the CH-54B is rated at 7,900 horsepower for 30 minutes.

The main and tail rotors dimensions of the CH-54B are contained in Table XIX.

The tail rotor incorporates a viscous damped tail drive shaft support which reduces high frequency vibrations, increases misalignment allowances and reduces stress on contingent support structures. It also uses self-centering pitch control links which contain low-friction Teflon bearings. In addition, both tail and main rotors have completely independent, self-contained, continuous lubrication systems.

The fuselage and landing gear (see Table XX) have been specifically designed for the CH-54B's cargo handling duties.

Minimum fuselage bulk provides maximum visibility of cargo and cargo handling plus a large open space for the cargo itself. The wide-stance gantry type landing gear enables the aircraft to straddle close-in loads. The cargo handling system in single and four-point configurations features a 25,000-pound powered winch with 100 feet of usable cable, a 25,000-pound four-point suspension system for pods or pallets, normal operation control

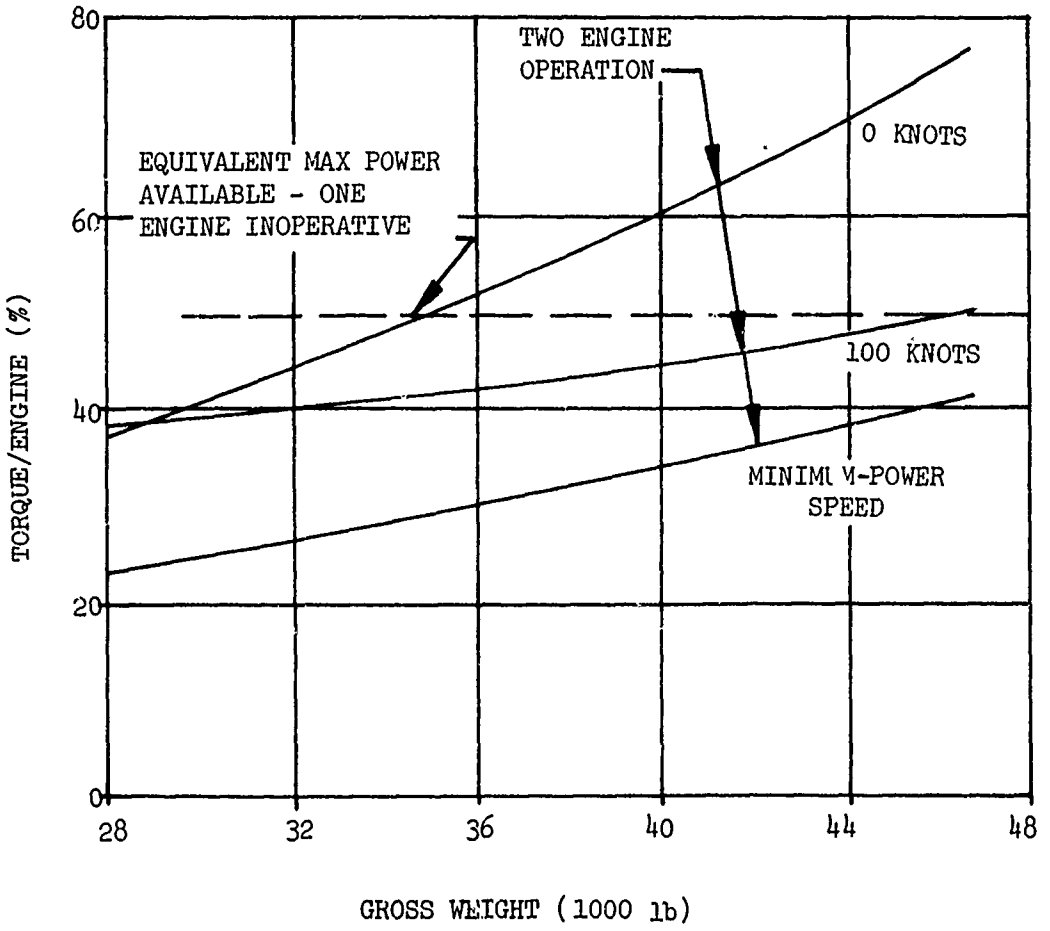

Figure 85. Forward-Flight Performance, Sea Level Standard.

TABLE XIX. ROTOR DIMENSIONS, CH-54B

Main Rotor Disc Area	4072.0	square feet
Main Rotor Blade Area (6 at 62.87 sq ft)	377.22	square feet
Antitorque (Tail) Rotor Disc Area	201.1	square feet
Antitorque (Tail) Rotor Blade Area (4 at 8.15 sq ft)	32.6	square feet
Tail Area (Horizontal)	40.00	square feet
Main Rotor (Blades) True Diameter	72.236	feet
Main Rotor Blade Chord:		
At Root	26.0	inches
At Tip	26.0	inches
Antitorque (Tail) Rotor Diameter	16.0	feet
Antitorque (Tail) Rotor Blade Chord:		
At Root	15.4	inches
At Tip	15.4	inches
Main Rotor Blade Thickness (% Chord)	11	percent
Airfoil Section	NACA 0011 (MOD)	
Antitorque (Tail) Rotor Blade Thickness (% Chord)	12	percent
At Root	1.850	inches
At Tip	1.850	inches
Airfoil Section	NACA 0012	
Main Rotor Solidity Ratio Effective	0.115	
Main Rotor Blade Twist (Nonlinear)	10.65	degrees
Distance Between Rotors	44 feet 5 inches	
Static Ground Clearance of Main Rotor Blades (Static Droop)	13 feet 6 inches	
Span, Maximum - Main Rotor Blades Positioned	62 feet 4 inches	
Horizontal Tail (Stabilizer):		
Span (Right Hand)	8 feet 7 inches	
Chord (Construction): At root and tip	56.00	inches
Section: At root and tip	NACA 0012	
Thickness (% Chord): At root and tip	12	percent
Aspect Ratio	1.75	

TABLE XX. FUSELAGE/LANDING GEAR DATA, CH-54B

Wheel Base	24 feet 5 inches	
Vertical Travel of Axles:		
Main wheels	20 inches	
Nose wheel	12 inches	
Areas of Vision (minimum):		
Pilot and copilot with eye position fixed (Reference Station 96, W.L. 164.5, B.L. ±21)	Pilot	Copilot
Vision downward (Pilot C.L.)	21°	21°
Vision upward (Pilot C.L.)	35°	35°
Vision horizontal - left	8 °	125°
Vision horizontal - right	125°	80°
Angle between lines joining center of gravity with points of ground contact of main wheel tires, static deflection of 1W (Front elevation) degrees	75°	36'
Angle of line through center of gravity and ground contact point of main wheel tire to vertical line, reference line level, static deflection of 1W (side elevation) degrees	21°	6'
Maximum slope helicopter can be parked upon without overturning, nose uphill	21°	6'
Critical turnover angle about line between main and nose wheel	30°	6"

Note (1): Rearward vision is available to pilot through aft-facing position enclosure.

(2): The above angles based on weight of aircraft without payload.

from all pilot stations, and multiple hard points with universal attachments for any type of load. Added precision and safety in cargo handling are insured by the rear-facing operator position, which has full authority in all control axes and positive control priority over the forward-facing operator position.

These design features all contribute to the overall performance of the aircraft. With a large useful load to gross weight ratio, the CH-54B has the ability to pickup, transport, and place heavy external loads with precision. Although the empty weight of this aircraft is 19,700 lb, it is certified to operate at sea level with a gross weight of 47,000 lb to a temperature of 118°F. On a standard day (temperature 58.7°F), this gross weight drops only slightly to 43,000 lb (see Figure 86). Mission productivities, up to 480 Ton-Knots at 40 nautical miles radius (see Figure 87), are calculated assuming:

(1) Warm-up and takeoff - 5 min at transmission rating

(2) Cruise outbound with max payload at 80 knots

(3) Hover out of ground effect and drop payload - 2 min

(4) Cruise inbound at 130 knots

(5) Land with 10% reserve fuel

For missions that include a ferry leg, climb capability exceeds 3,500 ft/min at sea level standard (see Figure 88).

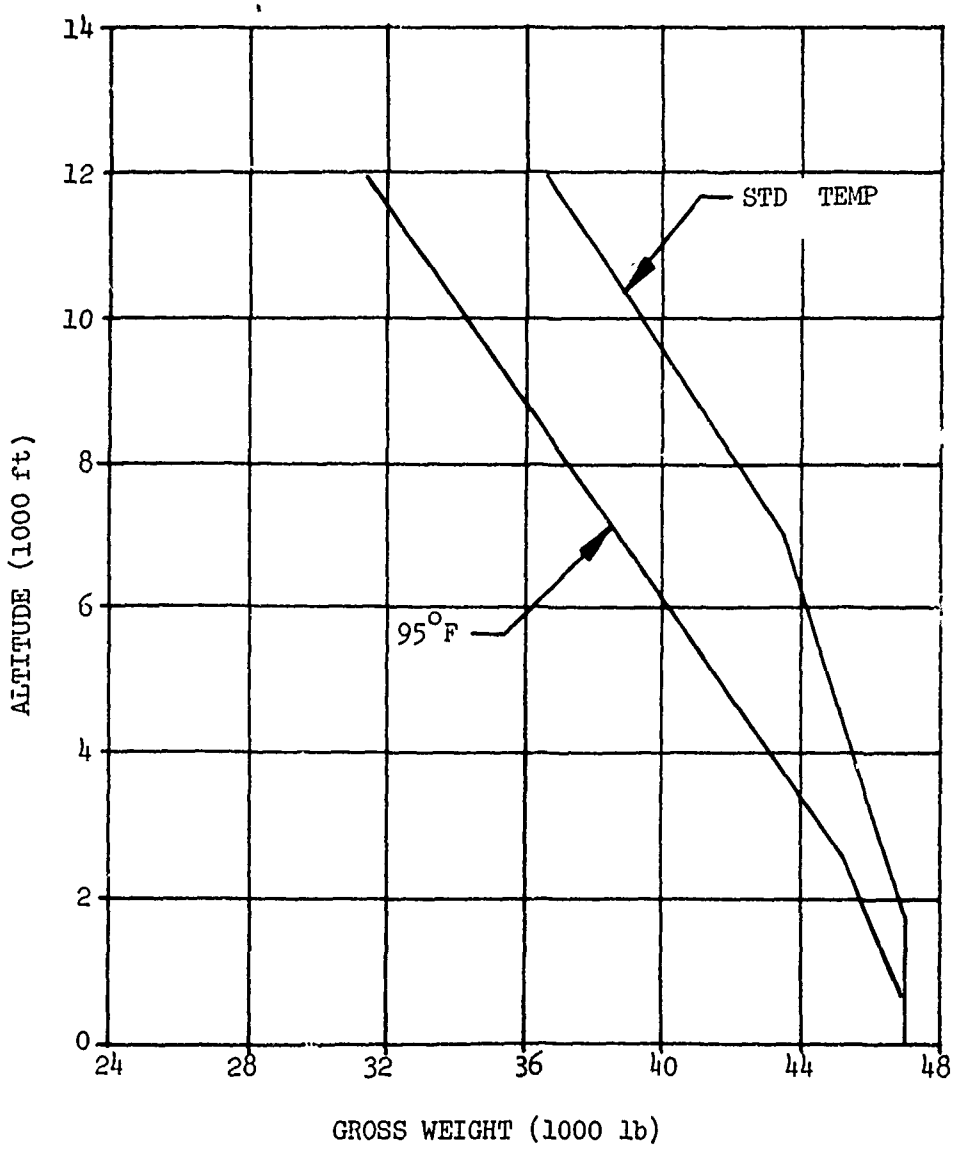

Figure 86. Hover Ceiling, Two-Engine CH-54B.

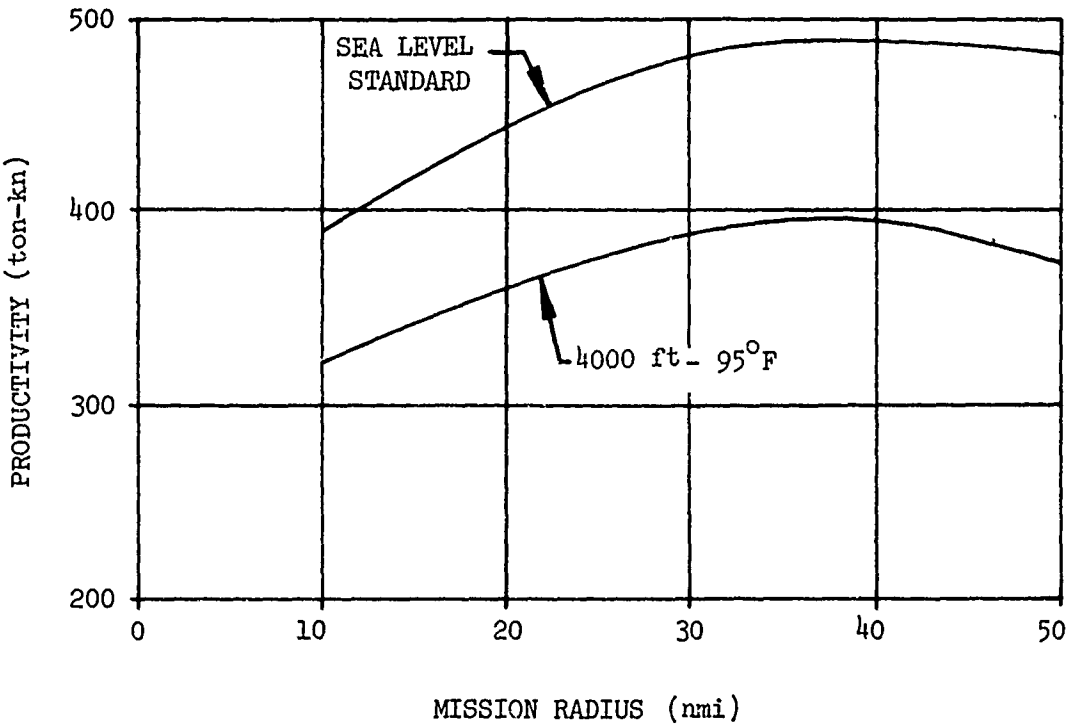

Figure 87. Productivity Versus Mission Radius, CH-54B.

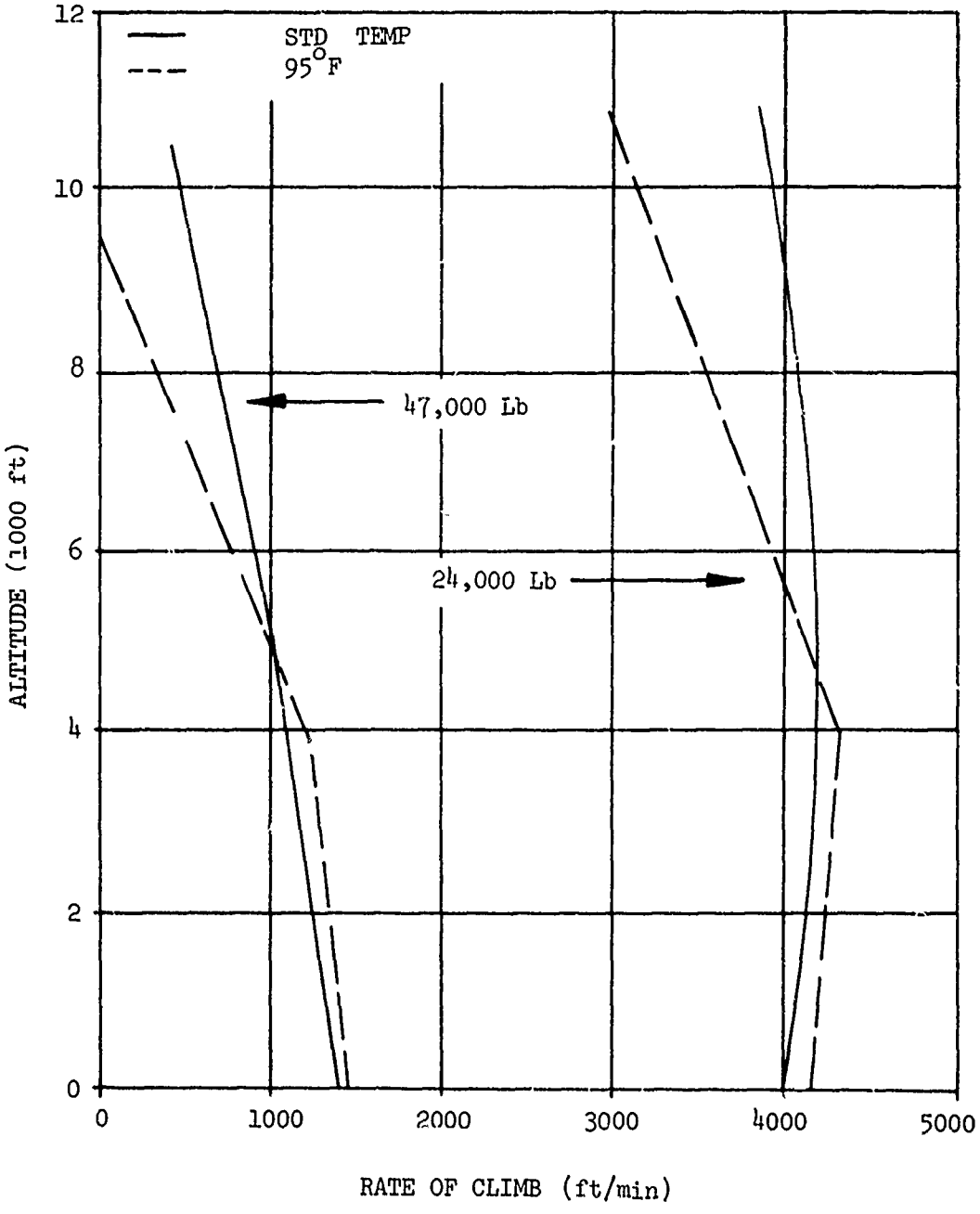

Figure 88. Forward Climb Performance, CH-54B.

APPENDIX II

MATERIAL CHARACTERISTICS

The material properties for the sixteen candidate materials considered in the material and joining method study are included in the following pages. Included are static, fatigue, and creep characteristics of the following materials:

Magnesium Alloys
- AZ91C
- ZE41A

Aluminum Alloys
- 6061-T6
- 7175-T736

Titanium Alloys
- Ti-6Al-4V Alpha-Beta Processed
- Ti-6Al-4V Beta Processed
  (Beta Forging, Beta-STOA, and Beta Extrusion)
- Ti-8Mo-8V-2Fe-3Al

Steel Alloys
- 17-4Ph
- 16% Ni 250 Grade Maraging
- 4130/4340
- Carpenter Custom 455

Composite
- Glass "E" Type
- Glass "S" Type
- Graphite High Modulus
- Graphite High Strength
- Borsical

ALLOY: AZ91C

General Description

AZ91C is a heat-treatable magnesium-aluminum-zinc alloy most often used for sand and permanent mold castings. The alloy combines good ductility with good strength up to 300°F and good pressure tightness with good welding properties (important in the weld repair of castings).

Physical Properties

Density	.0652 lb/in.^{3}
Melting Temperature Range	785° - 1105°F
Coefficient of Thermal Expansion	14.5 x 10^{-6} in./in./°F
Specific Heat	.25 Btu/lb°F
Thermal Conductivity	32.4 Btu/ft/hr ft^2°F

Fabricability

Castings

Castings require generous fillets and uniformity of wall thickness. Minimum wall thickness on sand and permanent mold castings is .125 inch. Casting temperature range is 1150° to 1250°F.

Welding

Welding of AZ91C is done in accordance with an in-house standard. Weld properties after heat treatment to -T6 are as good as the parent material. Castings are welded in the -T4 temper and then re-solution heat treated and aged to the -T6 temper. Buildup of AZ91C components by welding is acceptable as long as heat treatment after welding can be accomplished.

Brazing and Soldering

Brazing and soldering of magnesium alloys is not recommended.

Adhesive Bonding

Adhesive bonding of structural components is not usually done, but can be carried out in accordance with an in-house standard.

Mechanical Fastening

Care must be taken in mechanical fastening to avoid bridging and galvanic corrosion.

Corrosion Resistance

This alloy is slightly inferior in general corrosion resistance to wrought alloys, and to casting alloys not alloyed with zinc or aluminum. Care should be taken to avoid galvanic corrosion. Anodic Dow 17 or equivalent treatment is strongly recommended.

TABLE XXI. MECHANICAL PROPERTIES OF AZ91C-T6

Property	Specified Locations Class 1	Class 2	Class 3	Unspecified Locations
F_{tu}, ksi	35	29	27	17
F_{ty}, ksi	18	16	14	12
F_{cy}, ksi	18	16	14	12
F_{su}, ksi	-	-	-	-
F_{bru}, ksi	-	-	-	-
e percent in 2 inches	4	3	2	.75
E, 10^6 psi	-	6.5	-	-
E_c, 10^6 psi	-	6.5	-	-
G, 10^6 psi	-	2.4	-	-
Poisson's Ratio	-	.35	-	-

ALLOY: ZE41A

General Description

ZE41A is a heat-treatable magnesium-zinc-zirconium rare earth (cerium) alloy used for sand castings. This alloy combines good castability and weldability, high strength at ambient and moderate elevated temperatures, and pressure tightness. The alloy is considered to be as castable as AZ91C and, combined with higher mechanical properties, better creep resistance, and good weldability, may be considered as a replacement for AZ91C.

Physical Properties

Density	.066 lb/in.^{3}
Melting Temperature Range	990° - 1180°F
Coefficient of Thermal Expansion	15.1 x 10^{-6} in./in./°F
Specific Heat	.230 Btu/lb/°F
Thermal Conductivity	61.8 Btu ft/hr ft^2°F

Fabricability

Castings

Castings are designed much the same as for AZ91C. Tendency to microporosity is low, and the alloy solidifies in fine equiaxed grains. Tendency toward alloy constituent segregation is low.

Welding

Welding is currently done in the as-cast condition, only in areas demonstrated free of microporosity, and the welded assembly is aged to the -T5 temper (no intermediate stress relief required). Welded ZE41A-T5 promises to have the same properties as the base metal both statically and in fatigue. It is easier to weld than AZ91C-T6 and shows no decrease in properties when the ground weld is compared to the as-cast surface.

Brazing and Soldering

Brazing and soldering of magnesium alloys is not recommended.

Adhesive Bonding

Ahesive bonding of structural components is not usually done, but can be carried out in accordance with an in-house standard.

Mechanical Fastening

Mechanical fastening requires the usual care with magnesium alloys to avoid bridging and galvanic corrosion.

Corrosion Resistance

No specific data is available in house, but reports from England and the Continent indicate that ZE41A has the same resistance to corrosion as AZ91C Anodic treatment with Dow 17, and a good paint system is strongly recommended.

TABLE XXII. MECHANICAL PROPERTIES OF ZE41A-T5

	Specified Locations		Unspecified Locations	
Property	50-Lb Casting Weight	50-Lb Casting Weight	50-Lb Casting Weight	50-Lb Casting Weight
F_{tu}, ksi	26	26	25.5	23.5
F_{ty}, ksi	17.5	17	17	16.5
F_{cy}, ksi	17.5	17	17	16.5
F_{su}, ksi	17.5	17.5	17	15.5
F_{bru}, ksi	56	56	55	50
F_{bry}, ksi	41	40	40	39
e percent in 2 inches	2.0	2.0	1.0	1.0
E, 10^6 psi	-	6.5	-	-
E_c, 10^6 psi	-	6.5	-	-
G, 10^6 psi	-	2.4	-	-
Poisson's Ratio	-	.35	-	-

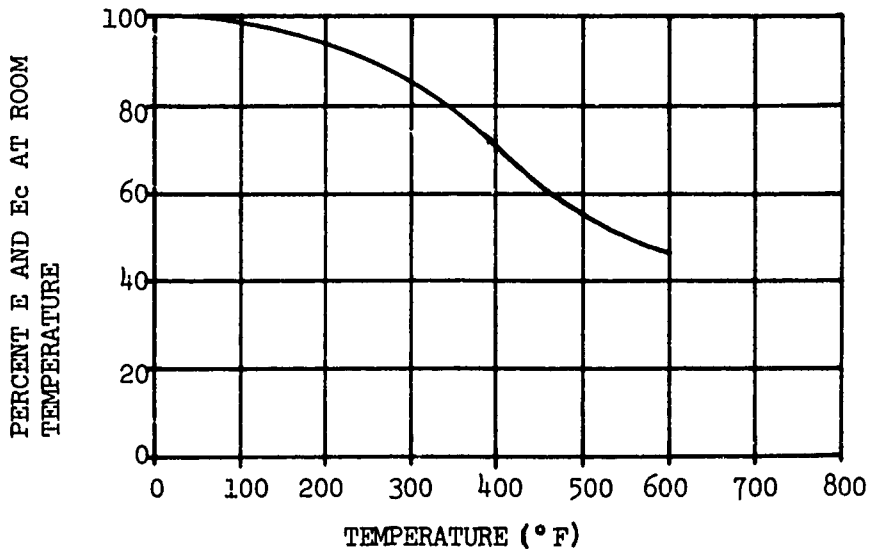

Figure 89. Effect of Temperature on the Tensile and Compressive Moduli (E and E_c) of Cast AZ91C-T6.

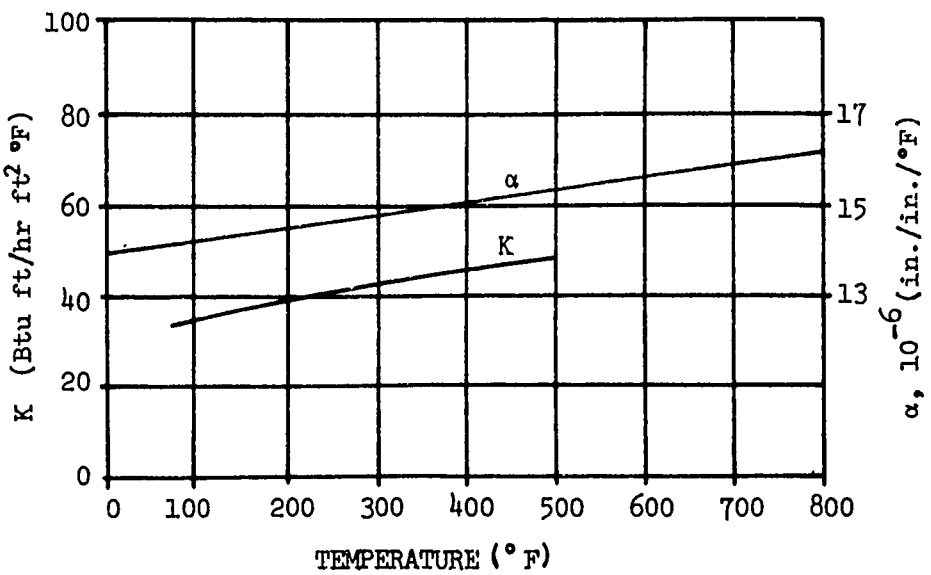

Figure 90. Effect of Temperature on the Physical Properties of Cast AZ91C-T6.

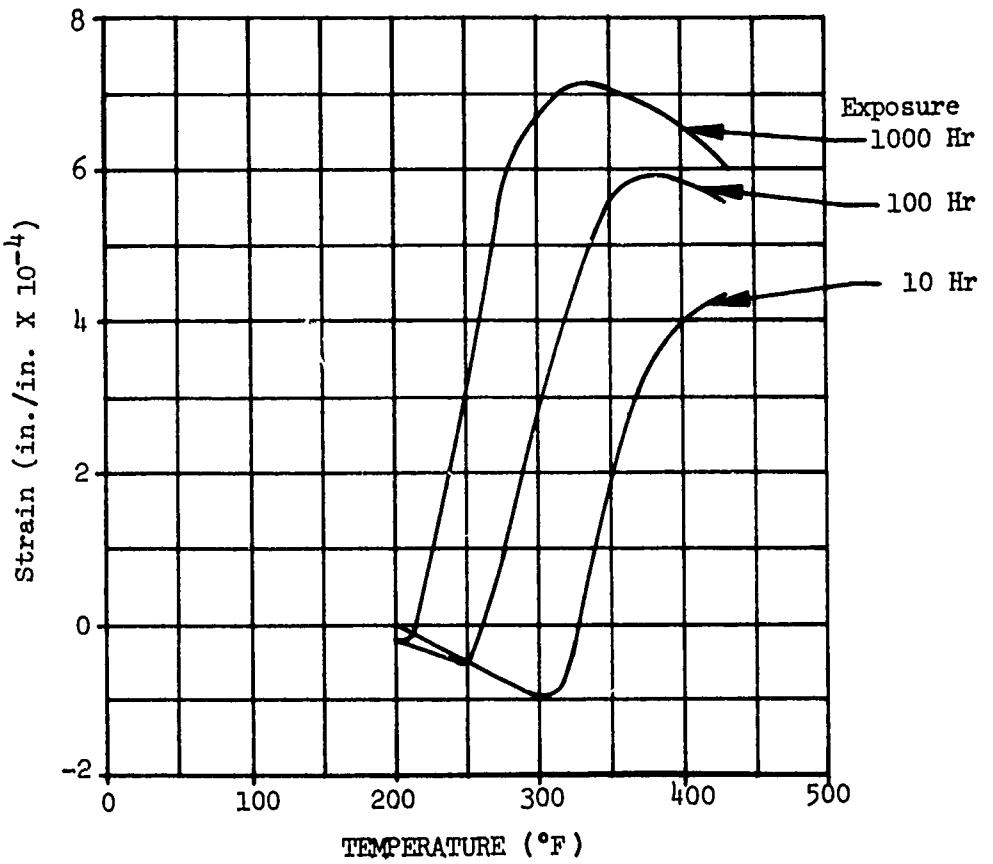

Figure 91. Dimensional Changes of AZ91C-T4 Sand Castings at 200° to 400°F.

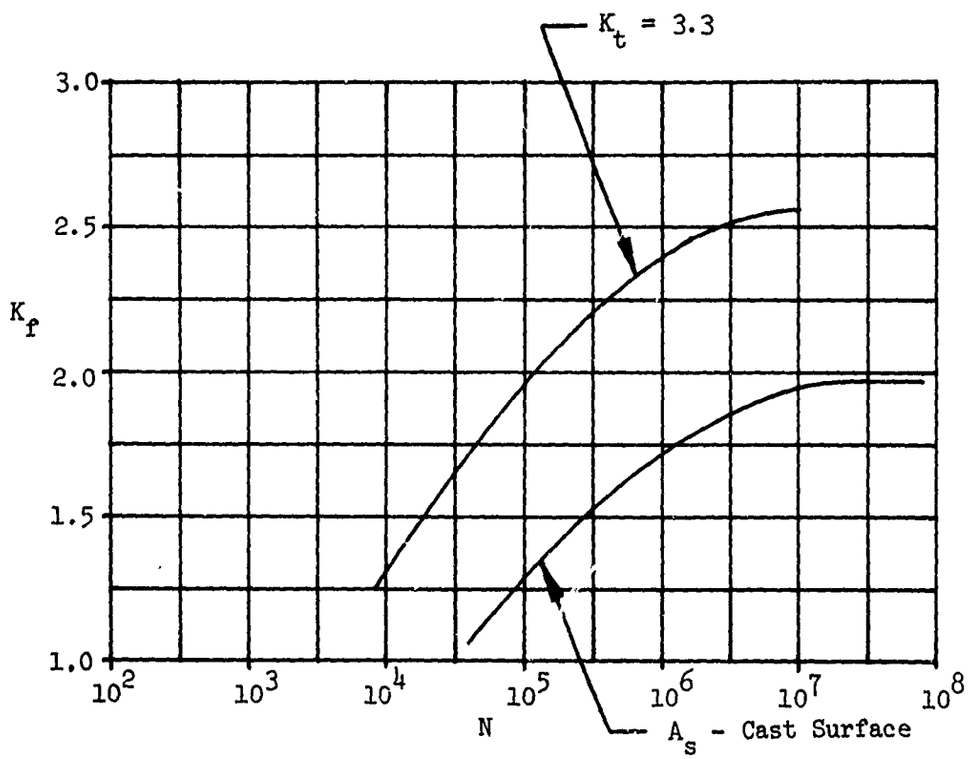

Figure 92. Effect of Cycles on K_T, S_M = 0, + 10 KSI, K_T = 3.3, AZ91C-T6 Magnesium Alloy.

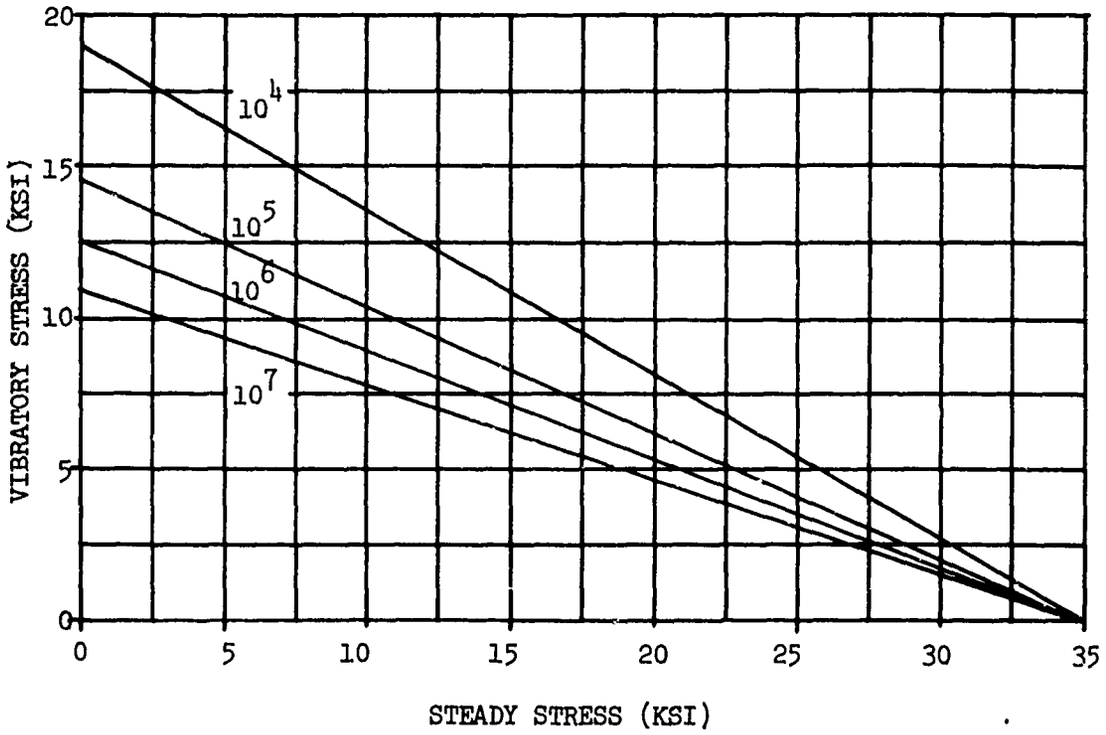

Figure 93. Constant-Life Fatigue Diagram, AZ91C-T6 Magnesium Alloy, K_T = 1.0.

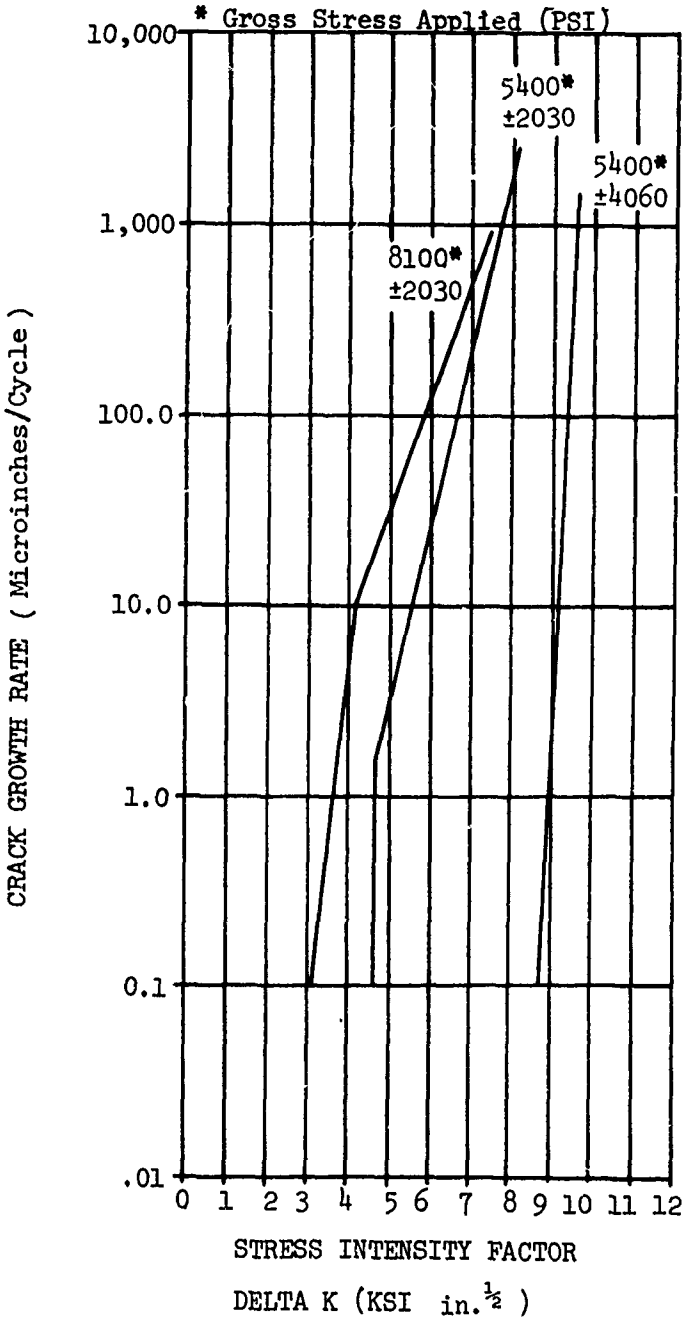

Figure 94. Crack Growth Rate Versus Stress Intensity Factor, AZ91C-T6 With As-Cast Surface in Laboratory Environment.

ALLOY: 6061-T6

General Description

6061 is the most versatile of the wrought, heat-treatable aluminum alloys. It is available in all wrought forms. However, this aluminum-magnesium-silicon alloy is not as strong as most other heat-treatable aluminum alloys. Good corrosion resistance is present and not significantly affected by variations in heat treatment. This alloy possesses excellent formability in the annealed and solution treated conditions, and is readily welded by all methods. It is the only heat-treatable alloy commonly fusion welded.

Physical Properties

Density	.098 lb/in.^{3}
Melting Temperature Range	1080° - 1200°F
Coefficient of Thermal Expansion	13 x 10^{-6} in./in./°F
Specific Heat	.23 Btu/lb/°F
Thermal Conductivity	96 Btu ft/hr ft^2°F

Fabricability

Forming

This alloy has excellent formability in the annealed condition. It can also be formed in the T4 condition and aged to the T6 condition.

Welding

Welding of 6061 may be accomplished by TIG, MIG and spot welding with two limitations: In T6, heavy sections have a tendency to crack, and in the annealed condition, spot welds present some production problems. If the configuration allows, reheat treating restores parent metal static properties; if not reheat treated, 6061-T6 welded has approximately the strength of the T4 temper. Fusion welding is covered in MIL-W-8604 and spot welds per MIL-W-6858.

Fatigue strength of welds has been well documented and a constant-life fatigue diagram is included as Figure 95. Figure 96 is a constant-life fatigue diagram at 200°F. A synergistic interaction between creep and fatigue that occurs near aging temperatures is discussed in Appendix III.

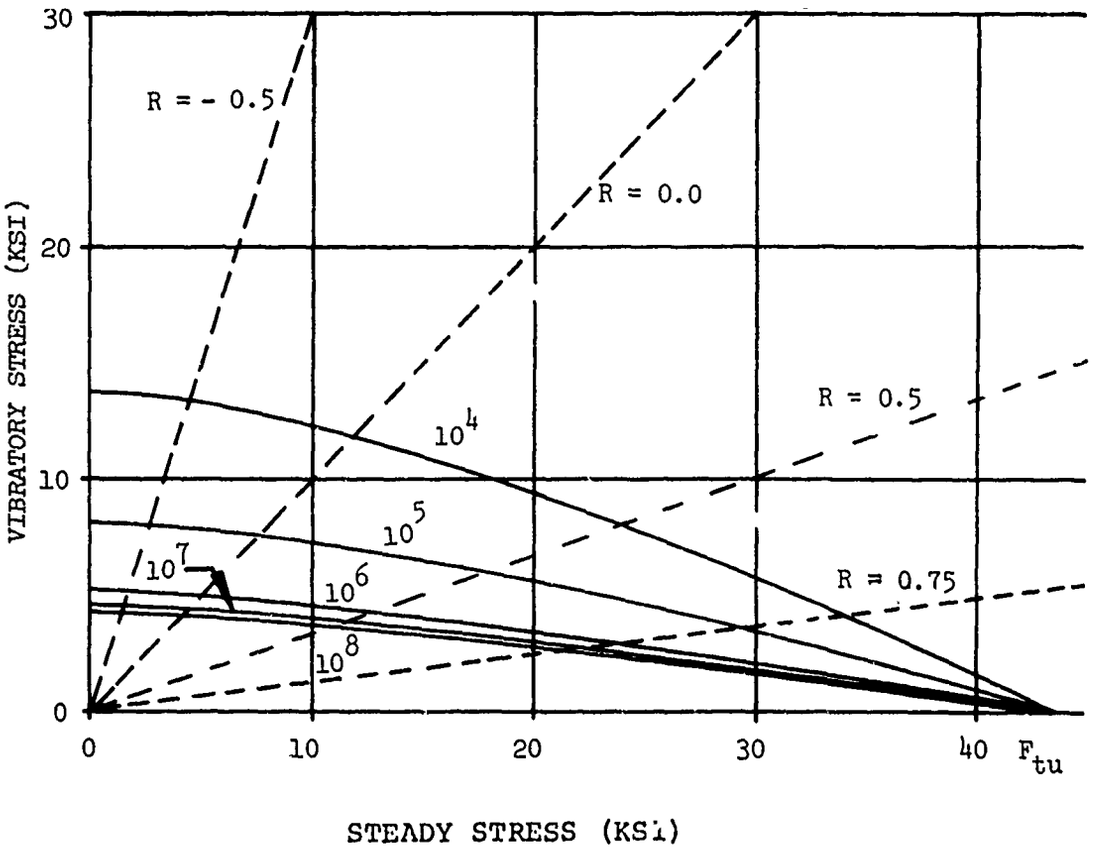

Figure 95. Constant-Life Fatigue Diagram For Welded and Heat-Treated 6061-T6 (Reference 5).

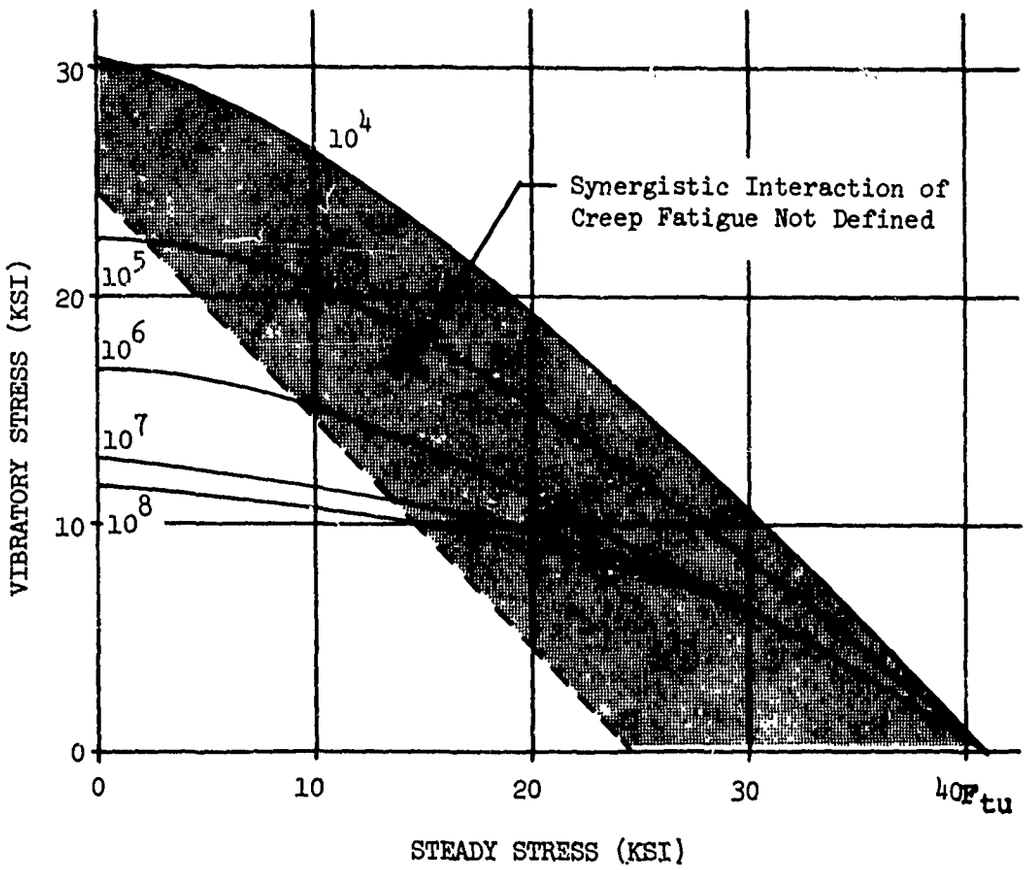

Figure 96. Constant-Life Fatigue Diagram For 6061-T6 Wrought Products at 200°F.

Brazing

The alloy 6061 has excellent brazing characteristics with all methods, resulting in annealed properties of the assemblies.

Mechanical Fastening

This alloy is readily joined with most conventional fasteners. Attention should be directed to prevention of galvanic corrosion.

Corrosion Resistance

The corrosion and stress corrosion resistance of the -T6 temper is the best of the heat-treatable alloys. In general, resistance to corrosion is not significantly affected by variations in heat treatment.

TABLE XXIII. MECHANICAL PROPERTIES OF 6061-T6

Property	Bar & Rod QQ-A-225/6	Extruded Shapes QQ-A-200/8	Welded Joints	
			T6 As Welded	Welded HT to T6
F_{tu}, ksi	42	36	22	40
F_{ty}, ksi	35	33	15	34
F_{cy}, ksi	34	34	-	-
F_{su}, ksi	27	24	19	26
F_{bru}, ksi				
e/D = 1.5	67	61	-	-
e/D = 2.0	88	80	-	-
F_{bry}, ksi				
e/D = 1.5	49	49	-	-
e/D = 2.0	56	56	-	-
e percent	10	-	-	-
E, 10^6 psi	-	9.9	-	-
E_c, 10^6 psi	-	10.1	-	-
G, 10^6 psi	-	3.8	-	-
Poisson's Ratio	-	.32	-	-

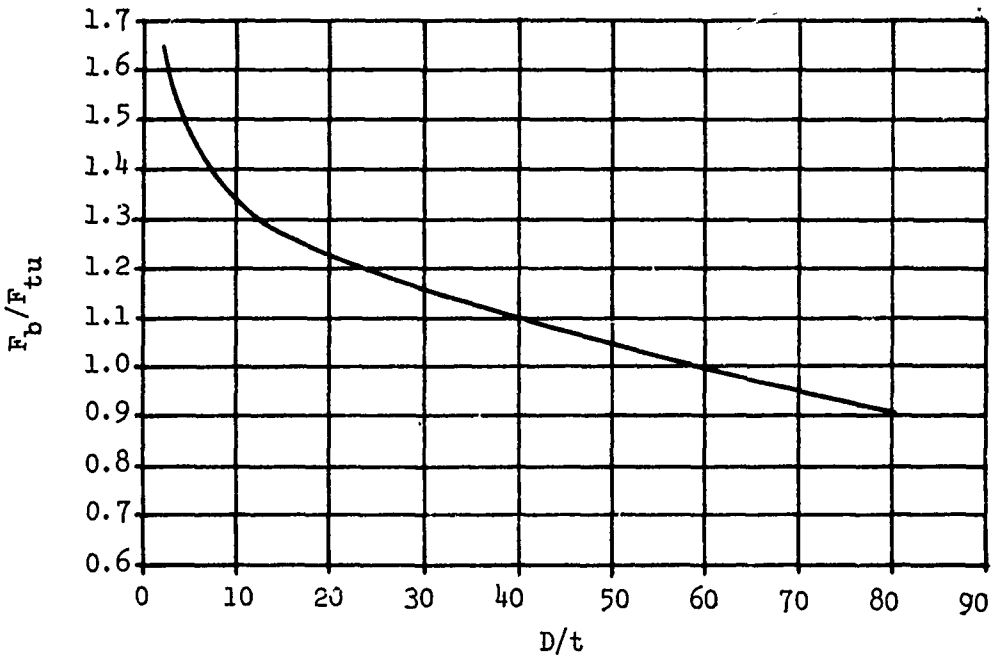

Figure 97. Bending Modulus of Rupture For 6061-T6 Round Tubing.

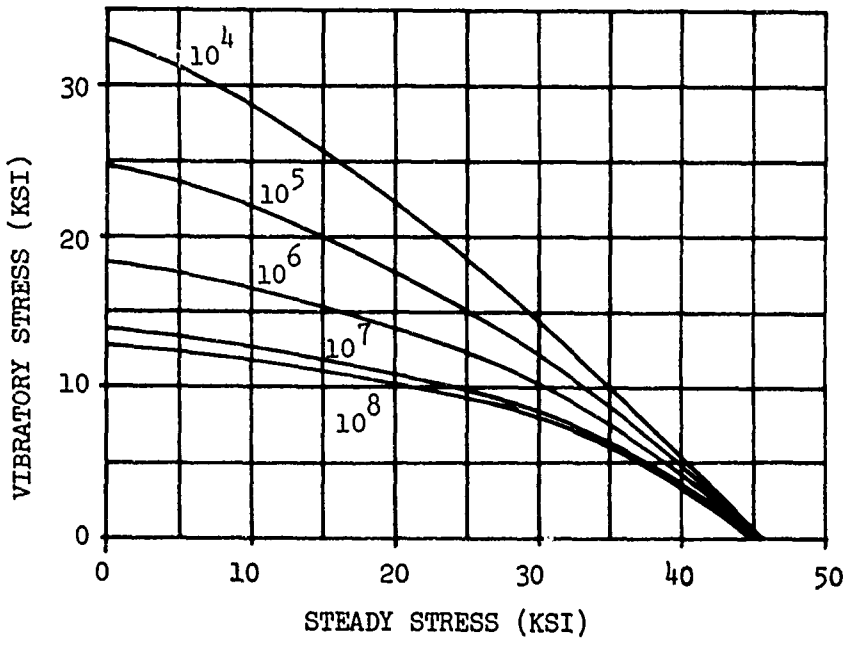

Figure 98. Constant-Life Fatigue Diagram For 6061-T6 Wrought Products, K_t = 1.0.

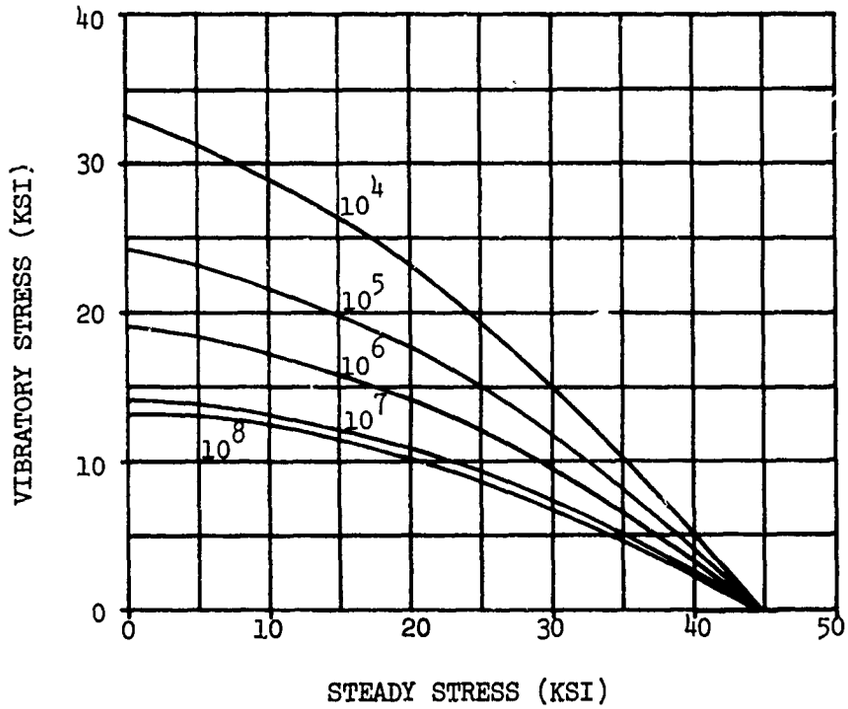

Figure 99. Constant-Life Fatigue Diagram for 6061-T6 Extrusions.

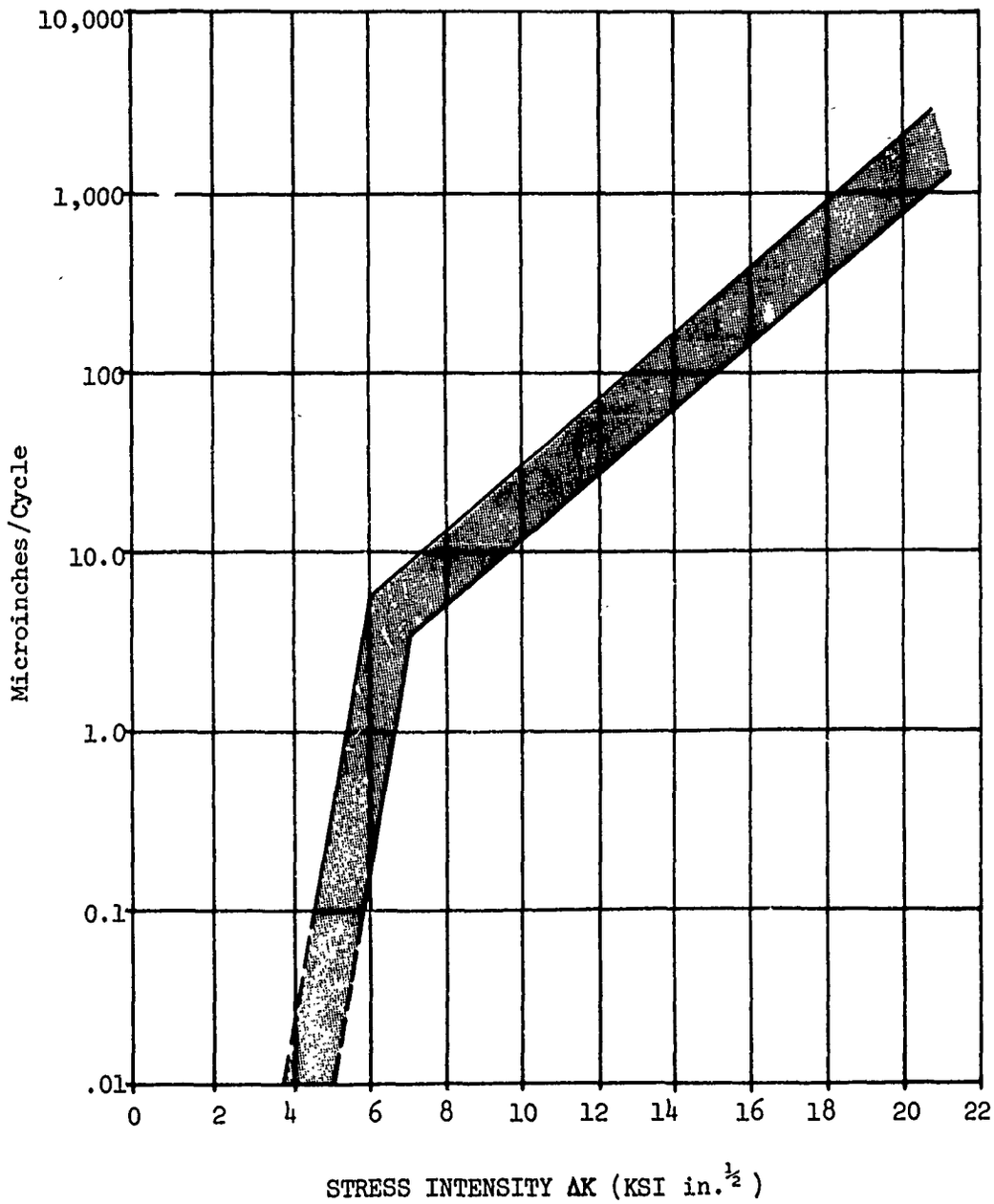

Figure 100. Crack Growth Rate Versus Stress Intensity Factor, 6061-T6 Extrusions.

ALLOY: 7175-T736

General Description

7175, a heat-treatable aluminum alloy, is a special, high-purity, premium-strength forging grade of 7075. 7175 has a chemistry within the specification limits of 7075 and has many of the same characteristics. 7175 has been applied only to forgings. Although elevated temperature properties have not been defined, there is no reason to expect different percentage reductions than 7075.

The elevated temperature strength, however, is inferior to that of 2024. It is available in all wrought forms and is readily formable in the annealed and unstable solution treated tempers. This alloy can be resistance welded, while fusion welding of this alloy is avoided. Its corrosion resistance is slightly superior to 2024 and may be further improved by cladding. 7075 is subject to stress corrosion cracking in the -T6 temper, particularly in the short transverse direction in thick sections (forgings), and has largely been replaced by the -T73 temper for forgings.

Physical Properties

Density	.101 lb/in.^{3}
Melting Temperature Range	890° - 1130°F
Coefficient of Thermal Expansion	(Reference 12)
Specific Heat	(Reference 12)
Thermal Conductivity	70 Btu ft/hr ft^2°F

Fabricability

Forming

The annealed condition has forming properties inferior to those of 2024-0. In the unstable solution treated condition, 7075-W possesses the same formability as 2024-W. For maximum formability, the total time at room temperature between quenching and forming should not exceed 30 minutes. The T6 condition has limited formability at room temperature.

Welding

This alloy is not normally fusion welded. In resistance welding, the performance of this alloy is inferior to 2024. For the transmission structure this alloy is not weldable,

and hence mechanical fastening must be considered.

Brazing and Soldering

Brazing and soldering of this alloy is not recommended.

Mechanical Fastening

This alloy is readily joined with most conventional fasteners. Attention should be directed to preventing galvanic corrosion.

Corrosion Resistance

General corrosion resistance is similar to that of 2024. Resistance to stress corrosion cracking of 7075-T6 type tempers is only moderate, as with the 2024-T4 type tempers. 7075-T73 has a high resistance to stress corrosion cracking.

TABLE XXIV. MECHANICAL PROPERTIES OF 7075-T736

Property	Value
F_{ty}, ksi	
L	76
ST	71
F_{ty}, ksi	
L	66
ST	62
F_{cy}, ksi	
L	66
ST	75
F_{su}, ksi	42
F_{bru}, ksi	
e/D = 1.5	110
e/D = 2.0	141
F_{bry}, ksi	
e/D = 1.5	89
e/D = 2.0	99
e, percent	
L	7
ST	4
E, 10^6 psi	10.3
E_c, 10^6 psi	10.5
G, 10^6 psi	3.9
Poisson's Ratio	.33

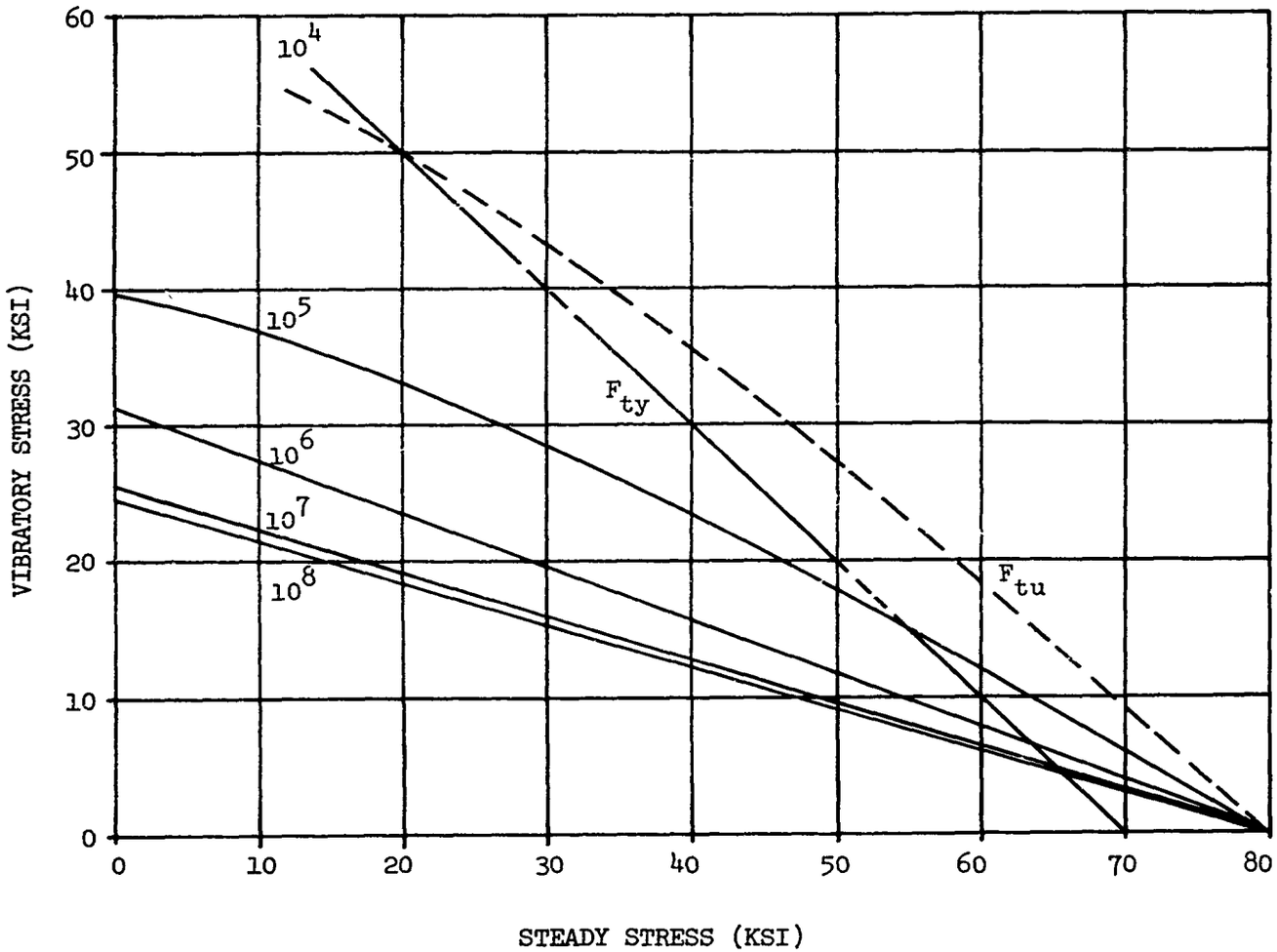

Figure 101. Constant-Life Fatigue Diagram 7175-T736 Aluminum Alloy, K_T = 1.0.

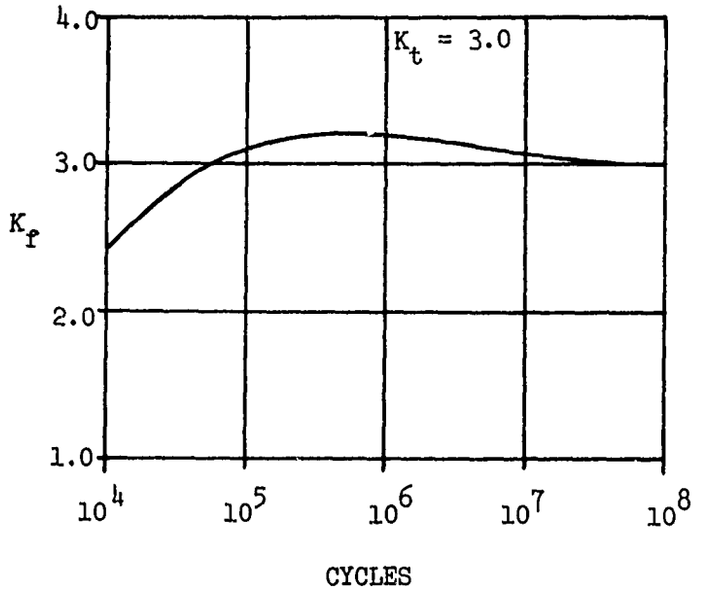

Figure 102. Effect of Cycles on K_T, R = 0.00, 7175-T736 Aluminum Alloy.

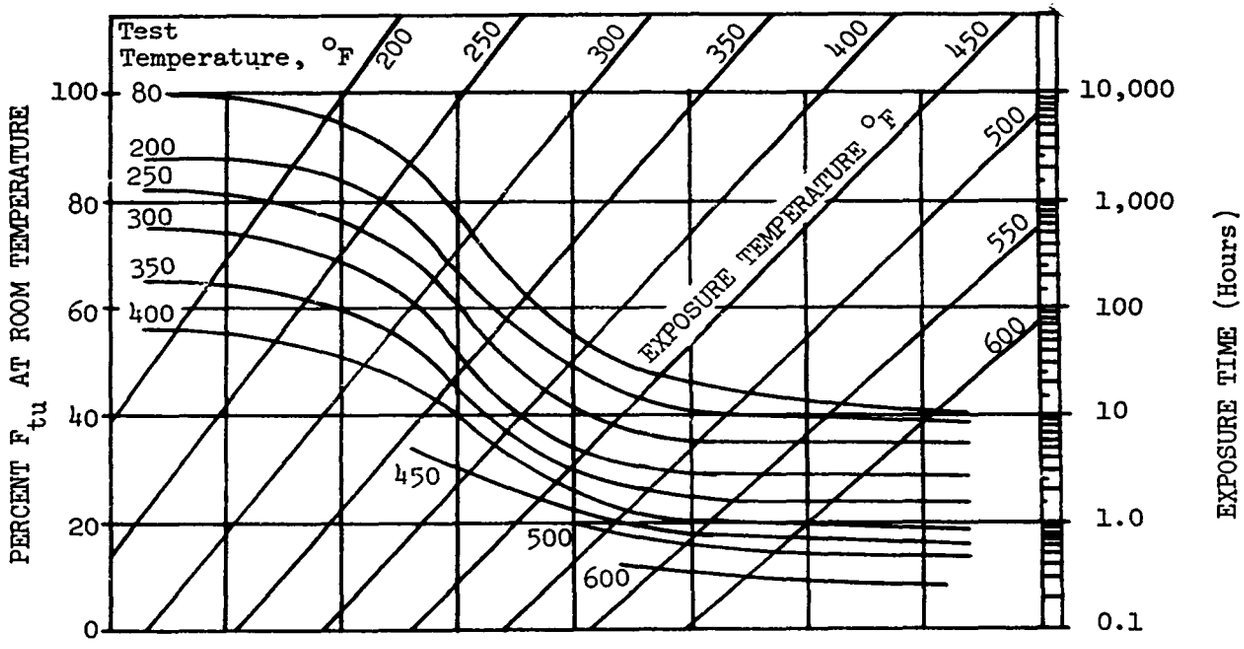

Figure 103. Effect of Temperature on the Ultimate Tensile Strength (F_{tu}) of 7075-T651 Aluminum Alloy.

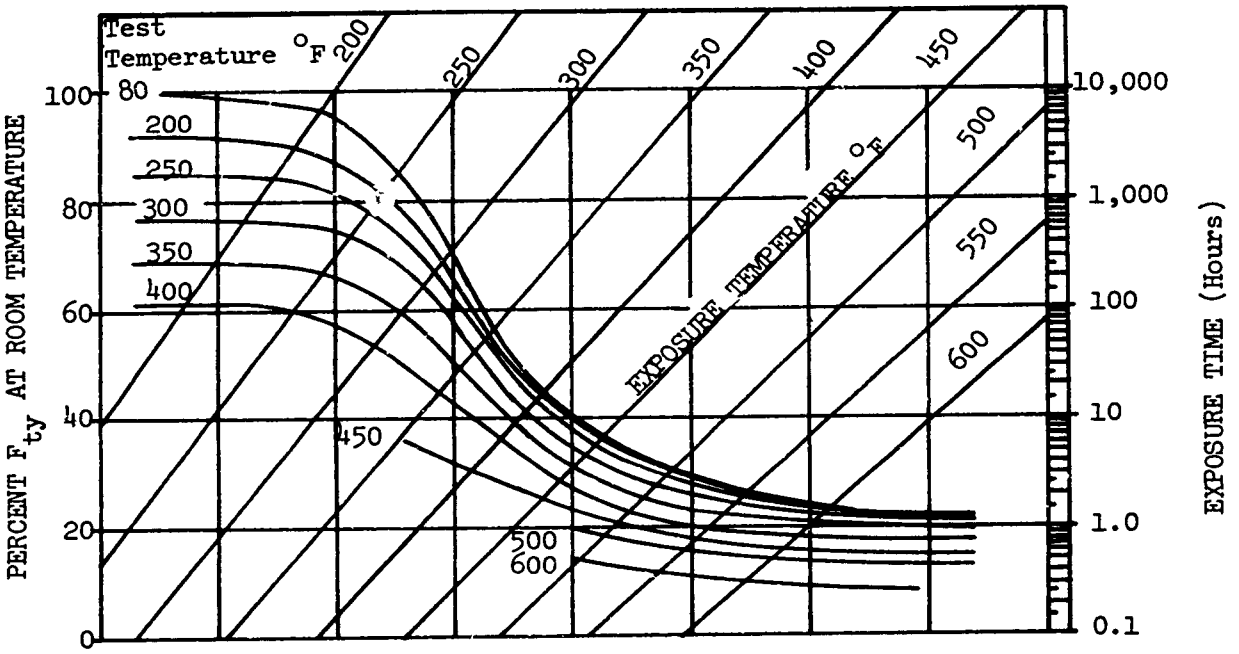

Figure 104. Effect of Temperature on the Tensile Yield Strength (F_{ty}) of 7075-T651 Aluminum Alloy.

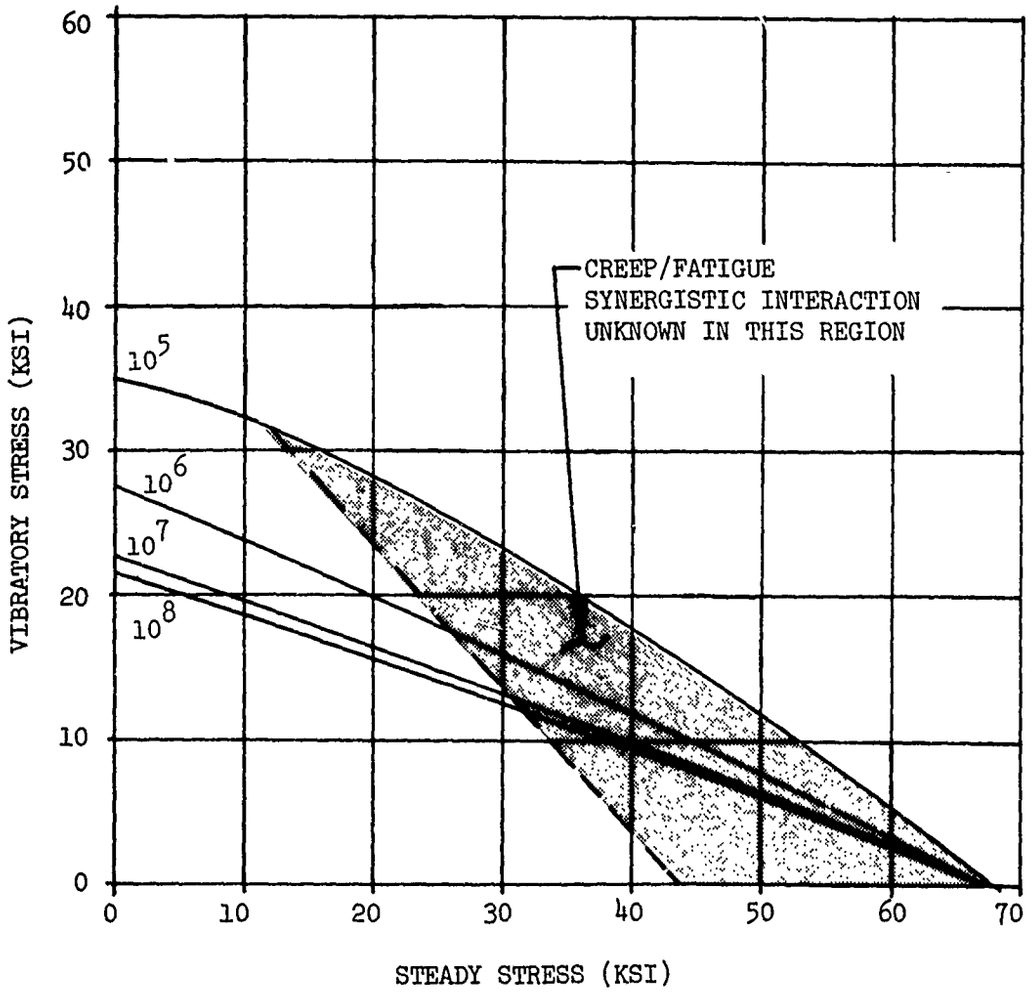

Figure 105. Constant-Life Fatigue Diagram for 7075-T736 Wrought Products at 200°F.

TABLE XXV. FRACTURE TOUGHNESS PROPERTIES OF 7175-T736 ALUMINUM ALLOY FORGING (REFERENCE 6)

Temperature		
Room	Transverse (WL)	22.7 23.4* 23.8*
Room	Short Transverse (TW)	33.1 29.1 33.5 31.9 Avg.
200°F	Short Transverse	33.0 35.0 34.4 34.1 Avg.
0°F	Short Transverse	26.4 27.1 26.3 26.6 Avg.
-65°F	Short Transverse (TW)	26.0 26.7 26.1 26.3 Avg.

* Invalid test; crack length does not meet ASTM standards.

TABLE XXVI. TYPICAL ROOM TEMPERATURE FRACTURE TOUGHNESS PROPERTIES FOR SEVERAL HIGH-STRENGTH ALUMINUM ALLOYS (REFERENCE 6)

Alloy and Temper	Configuration	Cross-Sectional Configuration (in. x in.)	Direction: Longitudinal YS (ksi)	Longitudinal K_{IC} (1/2) (ksi)	Transverse YS (ksi)	Transverse K_{IC} (1/2) (ksi)	Sh. Transverse YS (ksi)	Sh. Transverse K_{IC} (1/2) (ksi)
7075-T7352	Hand Forging	2 x 8	65.8	31.4	65.3	24.0	-	-
7075-T7352	Hand Forging	6 x 24	50.7	39.5	48.9	27.7	47.2	25.6
7075-T651	Plate	1 x 20	78.0	30.6	75.0	27.8	-	-
7075-T7351	Plate	1 x 20	62.0	35.3	59.0	31.1	-	-
7075-T6511	Extrusion	3 - 1/2 x 7 - 1/2	74.7	30.9	67.2	20.8	-	19.0
7175-T73	Die Forging	2 - 1/2 x 2 - 1/2	74.6	-	66.3	22.7	64.9	31.9

ALLOY: Ti-6Al-4V Beta Processed (Beta-Forging, Beta-STOA & Beta Extrusion)

General Description

Ti-6Al-4V is a heat-treatable sheet and bar alloy possessing excellent elevated temperature strength up to 750°F, good notch toughness, and fair to good weldability. This is normally used in the annealed condition.

Physical Properties

Density	.163 lb/in.^{3}
Melting Temperature Range	3000° - 3040°F
Coefficient of Thermal Expansion	(Reference 12)
Specific Heat	(Reference 12)
Thermal Conductivity	(Reference 12)

Fabricability

Forming

Limited forming is possible at room temperature, with heating to 400° - 1200°F required for many forming operations. It is readily creep formed.

Machining

Machining characteristics are similar to those for austenitic stainless steels. Required are sharp tools, rigid setups, heavy feeds, slow speeds, no dwell in cutting, and soluble oil coolant in quantity. Sawing is best performed with high-speed friction saws in the range of 4000 to 4500 ft/min. Grinding can be performed as a finishing operation in accordance with an in-house developed procedure. Unlike heat-treated steels, there is no warpage associated with deep machining cuts.

Chem Milling

Chem milling has been applied to titanium on a limited basis to remove alpha case and to achieve specific dimensions.

Welding

Titanium may be fusion welded under an inert gas atmosphere and then must be treated with proper post-weld annealing to obtain high static joint efficiencies. Spot welding is done in accordance with MIL-W-6858. While electron-beam welding can be done, it is usually not applied to the generic structures made from the alloy.

Brazing and Soldering

Brazing and soldering are not recommended, but it is possible to braze with proper protection. Latest developments in low-temperature brazes appear to give adequate strengths with minimum erosion.

Adhesive Bonding

Good bonding characteristics are obtained from all titanium bonds when attention is paid to surface preparation and design technique.

Mechanical Fastening

Titanium alloys are readily joined with conventional fasteners, including both aluminum and Monel.

Corrosion Resistance

Corrosion resistance of titanium alloys is excellent. The high resistance of this material to attack by harsh chemicals has led to broad applications in the chemical industry. Most other metals except Monel and stainless steels will sacrifice to titanium under galvanic attack. The only basic problem which can be generated by a titanium application is the galvanic attack of adjacent, less corrosion resistant materials.

Note on Fatigue of Titanium Welds

As a direct result of Sikorsky research on welded metal titanium main rotor blades, welding technology has and is under continuing development to achieve the highest fatigue crack initiation resistance in welded titanium structures. Both Sikorsky research and other research have determined that the source of fatigue strength reduction in welds is small, including the hydrogen-filled voids distributed throughout the weld structure. The source of these voids is water vapor, and the solution is to keep the water vapor out of the weld area. Water vapor will probably never be eliminated but can be reduced by the methods currently in use and outlined below:

1. Avoid the use of filler metal in all welds. For plasma arc welding, this limits the weld thickness to .50 inch.

2. If filler metal is used, only well finished, vacuum-annealed (degassed) ELI grade rod, protected against moisture pickup in the welding process, should be used.

3. Use low-moisture argon blankets, taking care that moisture pickup does not occur in transit from storage tanks to weld chamber.

4. Use automatic welding equipment to avoid the human variable.

5. Establish and control precleaning procedures.

6. Use good machined surfaces on faces to be welded and adjacent areas. Never weld sheared surfaces or surfaces with flowed metal.

The notch sensitivity of Ti-6Al-4V weldments has been documented in References 7 and 8. Figure 106 is a plot of K_f vs. K_t for welded titanium. The notch sensitivity data shown in based on room temperature data. It can be expected that at 600°F the reduction in notch sensitivity will be 73% at 10^4 cycles and 53% at 10^7 cycles. For material in the 200°F operating environment, the reduction in notch sensitivity will be 9% at 10^4 cycles and 12% at 10^7 cycles.

For the stress concentration factor of voids in weld, Figure 107 from Reference 7 gives the theoretical relationship between void parameters and stress concentration factor. Only the ratio of void radius to depth below the surface controls the magnitude of the stress concentration factor. For the problems of voids close to the surface, the solution is to shot peen the weld. With this approach, a stress concentration of 2.6 would allow anything up to a .008-inch-diameter void .015 inch below the surface.

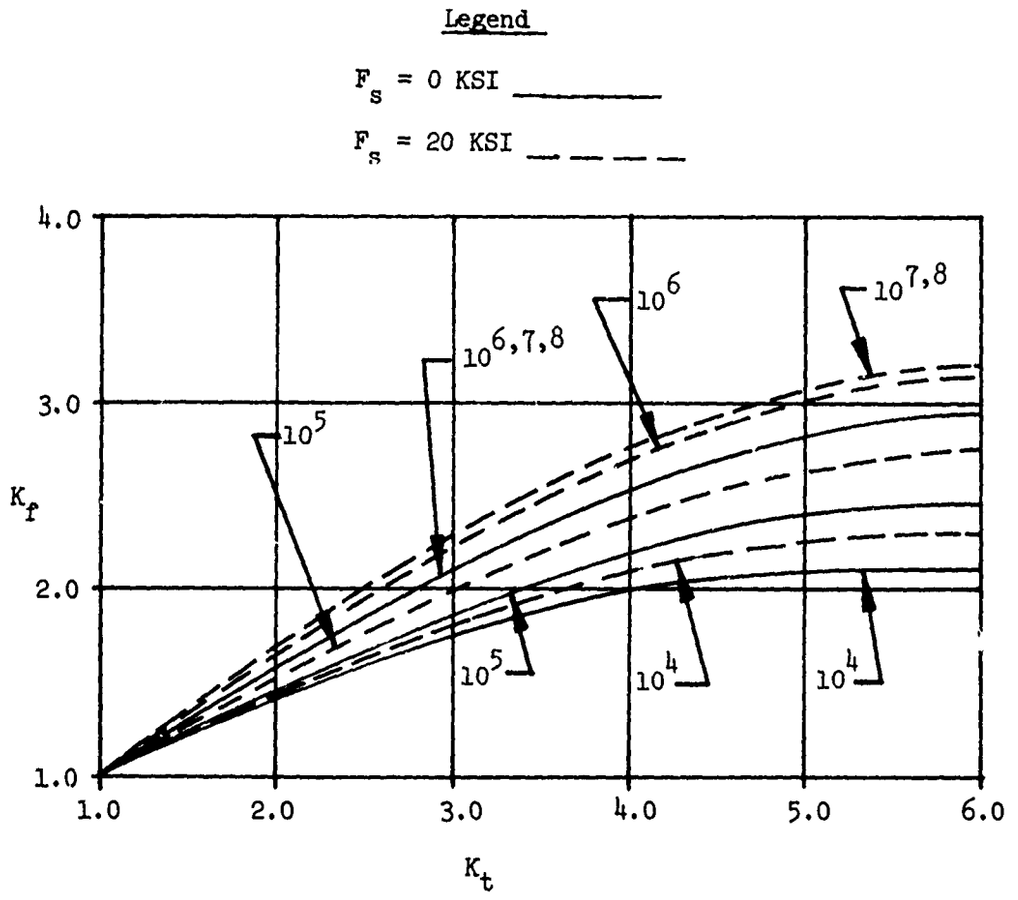

Figure 106. Notch Sensitivity of Ti-6Al-4V Weld Metal (K_f Versus K_t) at Two Steady Stresses.

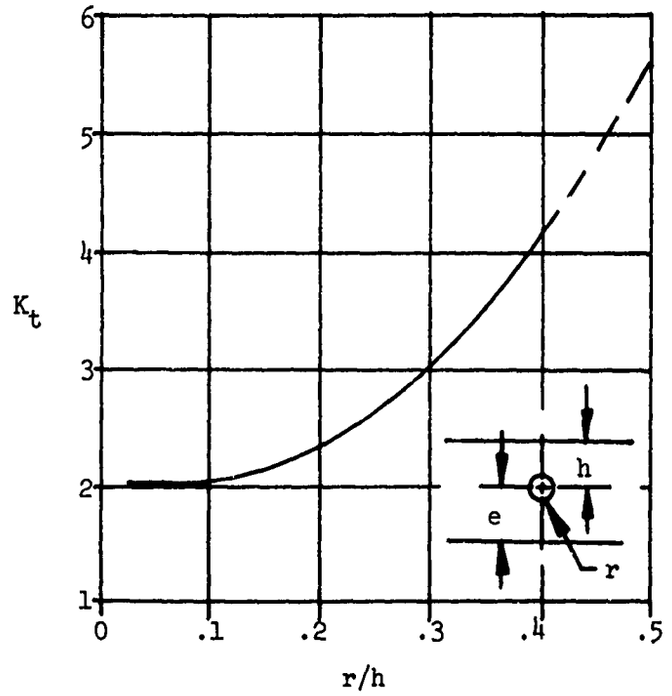

Figure 107. K_t as a Function of Defect Geometry.

TABLE XXVII. MECHANICAL PROPERTIES OF TITANIUM BETA FORGING STOA MIL-T-9097 TYPE III, COMPOSITION A

Thickness or Diameter	0-0.2 in.	0.2-1½ in.	1½-2 in.	2-4 in.	4 in.
Basis		S	S	S	S
Mechanical Properties					
F_{tu}, ksi	154	140	140	135	130
F_{ty}, ksi	145	130	130	125	120
F_{cy}, ksi	(150)	(136)	(136)	(130)	(125)
F_{su}, ksi	(94)	(86)	(86)	(82)	(80)
F_{bru}, ksi					
(e/D = 1.5)	(230)	(211)	(211)	(205)	(195)
(e/D = 2.0)	(290)	(267)	(267)	(255)	(245)
F_{bry}, ksi					
(e/D = 1.5)	(210)	(188)	(188)	(180)	(174)
(e/D = 2.0)	(245)	(222)	(222)	(214)	(205)
e.% in 2 in.	5.0	7.0	7.0	9.0	10.0
E, 10^6 psi	16.0	16.0	16.0	16.0	16.0
E_c, 10^6 psi	16.4	16.4	16.4	16.4	16.4
G, 10^6 psi	6.1	6.1	6.1	6.1	6.1
Poisson's Ratio	0.32	0.32	0.32	0.32	0.32
Density, Lb/in.^{3}	0.16	0.16	0.16	0.16	0.16

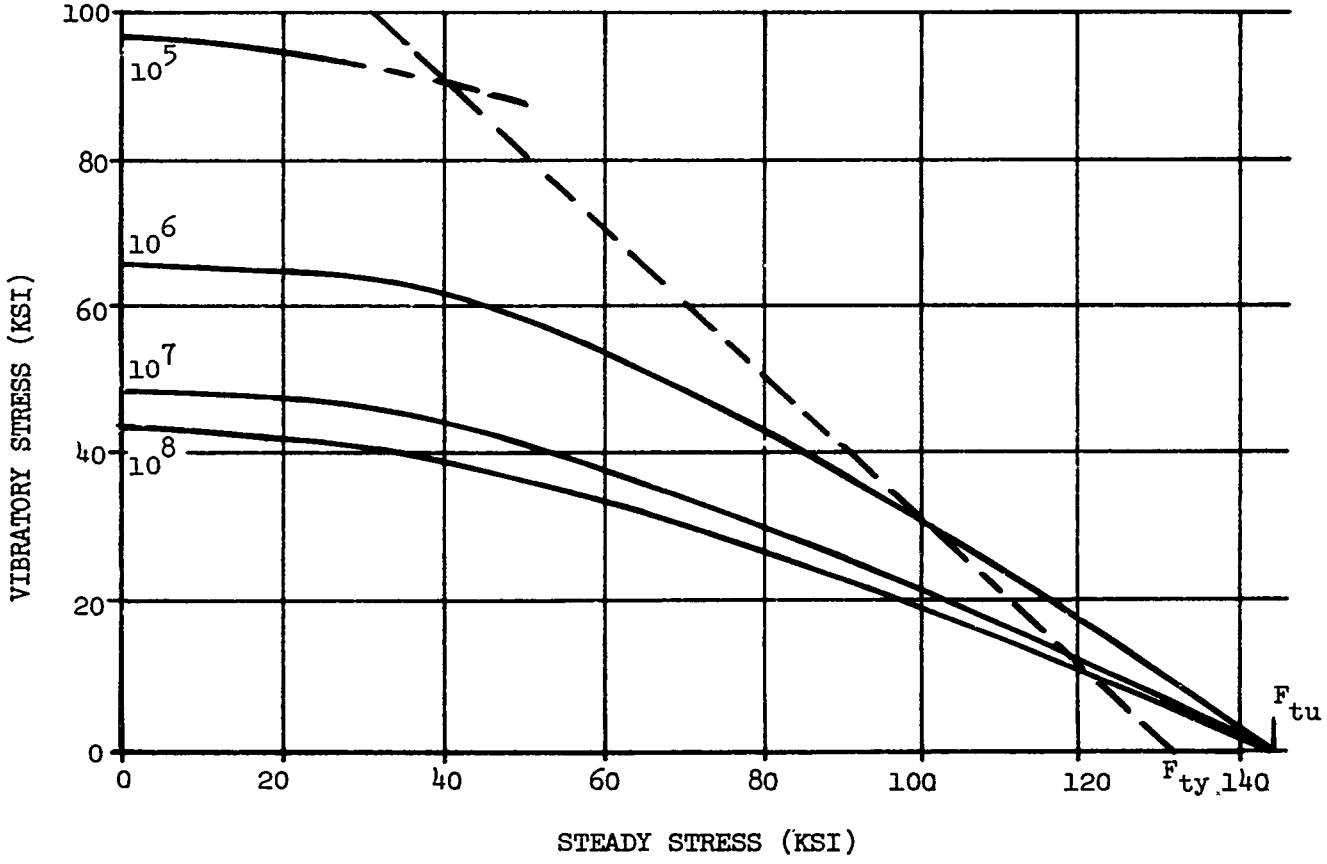

NOTE: Shot-Peened, S-70 Shot, 0.006-0.008N Intensity.

Figure 108. Constant-Life Diagram for Shot-Peened Ti-6Al-4V.

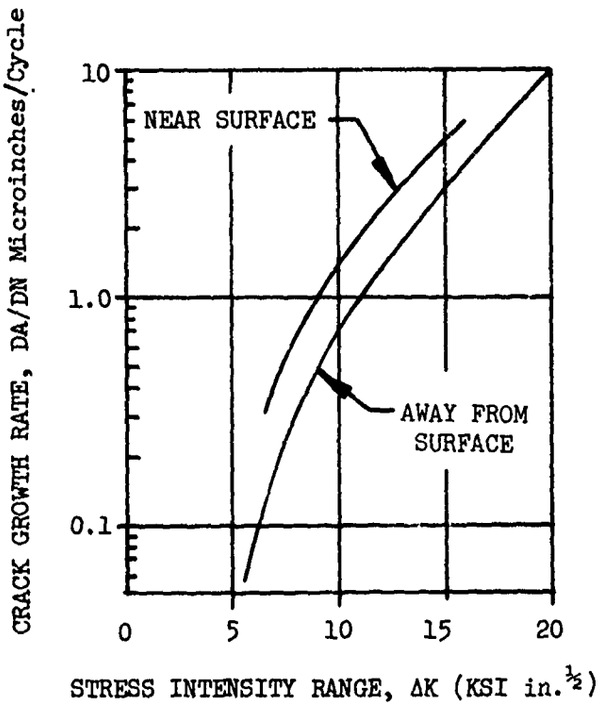

Figure 109. Fatigue Crack Propagation Superior in Ti-6Al-4V, BETA-STOA.

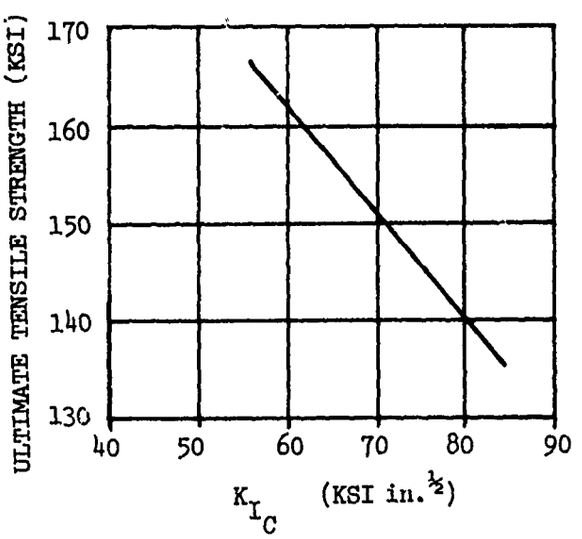

Figure 110. Fracture Toughness of Beta-Processed Titanium Ti-6Al-4V.

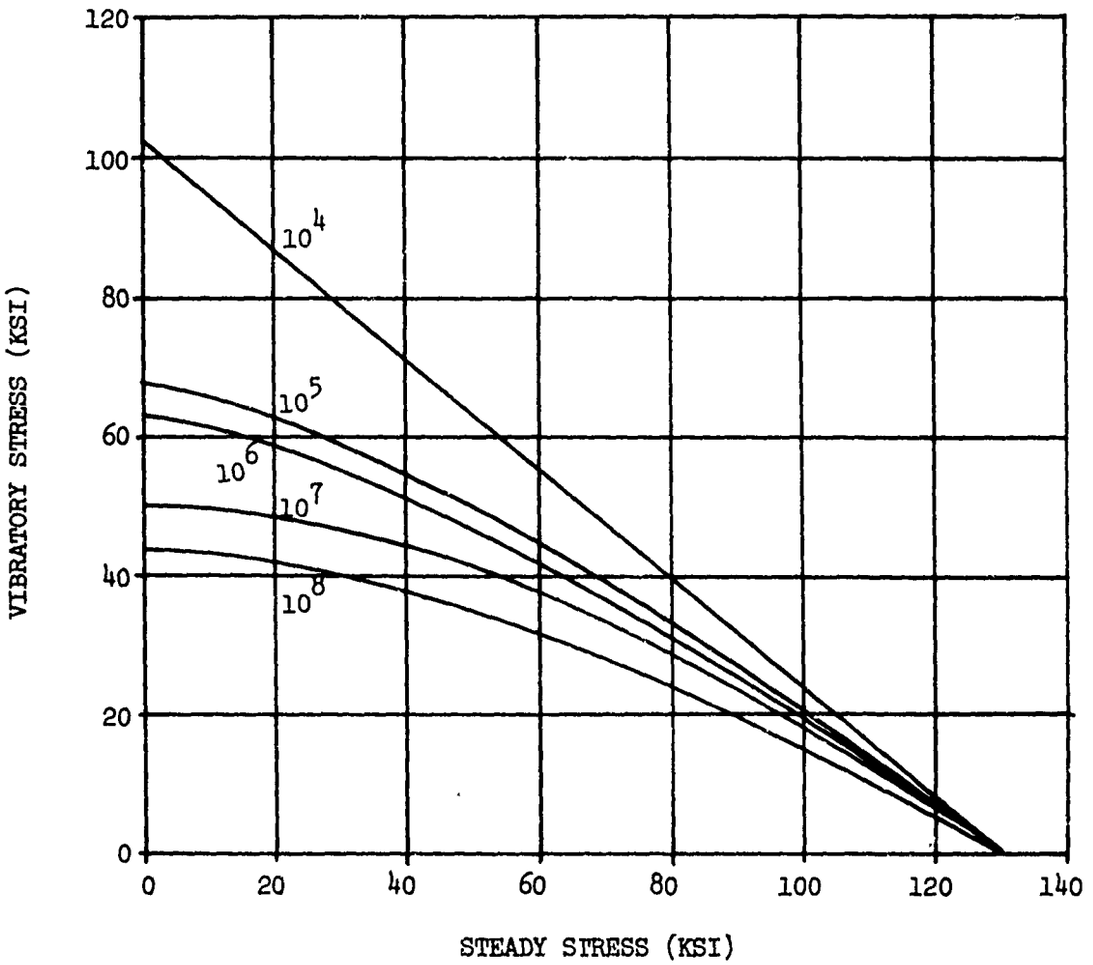

Figure 111. Constant-Life Diagram, Ti-6Al-4V Annealed Sheet, Room Temperature, K_t = 1.0 (Reference 8).

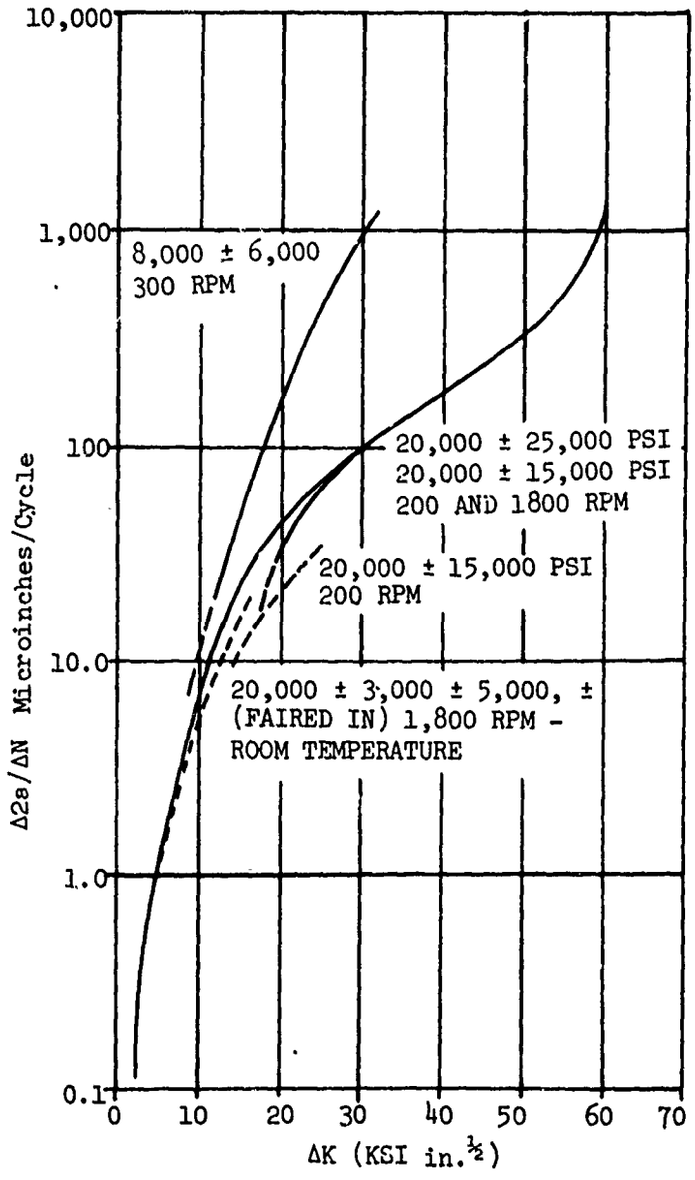

Figure 112. Crack Growth Rate Versus Stress Intensity Factor, Mill Annealed Ti-6Al-4V Titanium Sheet.

TABLE XXVIII. MECHANICAL PROPERTIES OF TITANIUM 6Al-4V EXTRUSIONS, BETA EXTRUDED MIL-T-81556, TYPE III, COMPOSITION A (a)

Form	Extruded Bars, Rods, and Special Shaped Sections					
Condition	Annealed					
Thickness or Diameter, in.	4.00	0.50	0.51-0.75	0.76-1.00	1.01-2.00	2.01-4.00
Basis	S	S	S	S	S	S
Mechanical Properties						
F_{tu}, ksi L	130	160	155	150	140	130
F_{ty}, ksi L	120	150	145	140	130	120
F_{cy}, ksi L	126	-	-	-	-	-
F_{su}, ksi L	80	-	-	-	-	-
F_{bru}, ksi (e/D = 1.5)	196	-	-	-	-	-
F_{bru}, ksi (e/D = 2.0)	248	-	-	-	-	-
F_{bry}, ksi (e/D = 1.5)	174	-	-	-	-	-
F_{bry}, ksi (e/D = 2.0)	205	-	-	-	-	-
e, percent in 2 inches	-	6	-	-	-	-
e, percent in 4D	10	-	6	6	6	6
E, 10^6 psi	-	-	16.0	-	-	-
E_c, 10^6 psi	-	-	16.4	-	-	-
G, 10^6 psi	-	-	6.1	-	-	-
Poisson's Ratio	-	-	0.32	-	-	-

TABLE XXVIII - Continued

(a) Static properties are the same for both MIL-T-81556 and AMS 4935B, but neither specification satisfactorily completes all Sikorsky (internal) requirements concerning removal of alpha-case.

(b) Properties of extrusions are applicable in the longitudinal (extrusion) direction only. Not included are the room-temperature notched stress-rupture requirements of AMS 4935B (not required by MIL-T-81556).

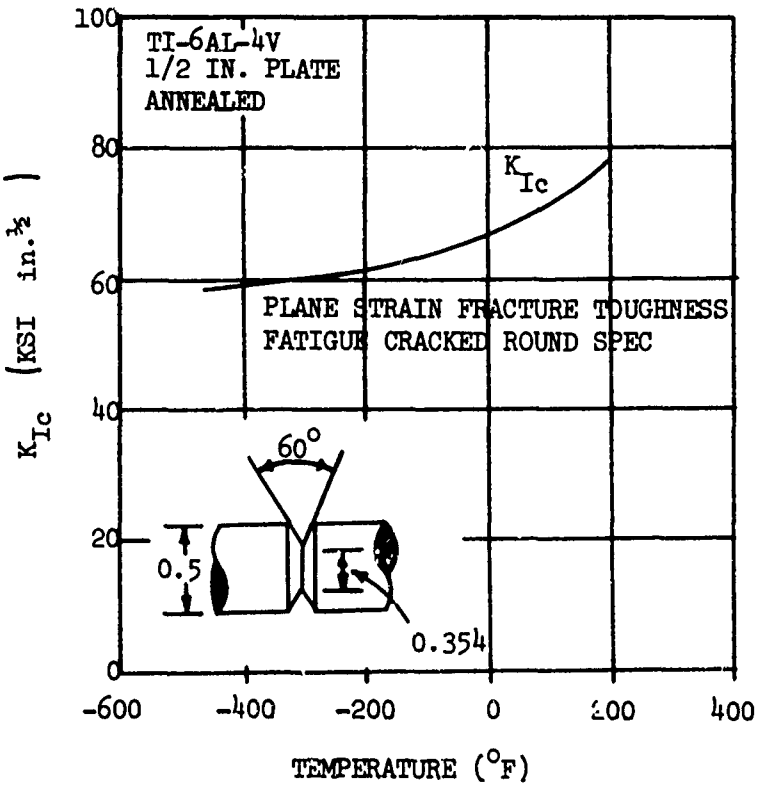

Figure 113. Plane Strain Fracture Toughness of Ti-6Al-4V.

Note: Considerable scatter exists in this parameter both as a function of testing methods and between-lot variation. Additional data on Ti-6Al-4V Forgings (typical data) are as follows:

Conventionally forged and annealed	40 - 50 ksi $(in.)^{\frac{1}{2}}$
Conventionally forged and heat treated	30 - 45 ksi $(in.)^{\frac{1}{2}}$
Beta forged and annealed	57 - 70 ksi $(in.)^{\frac{1}{2}}$

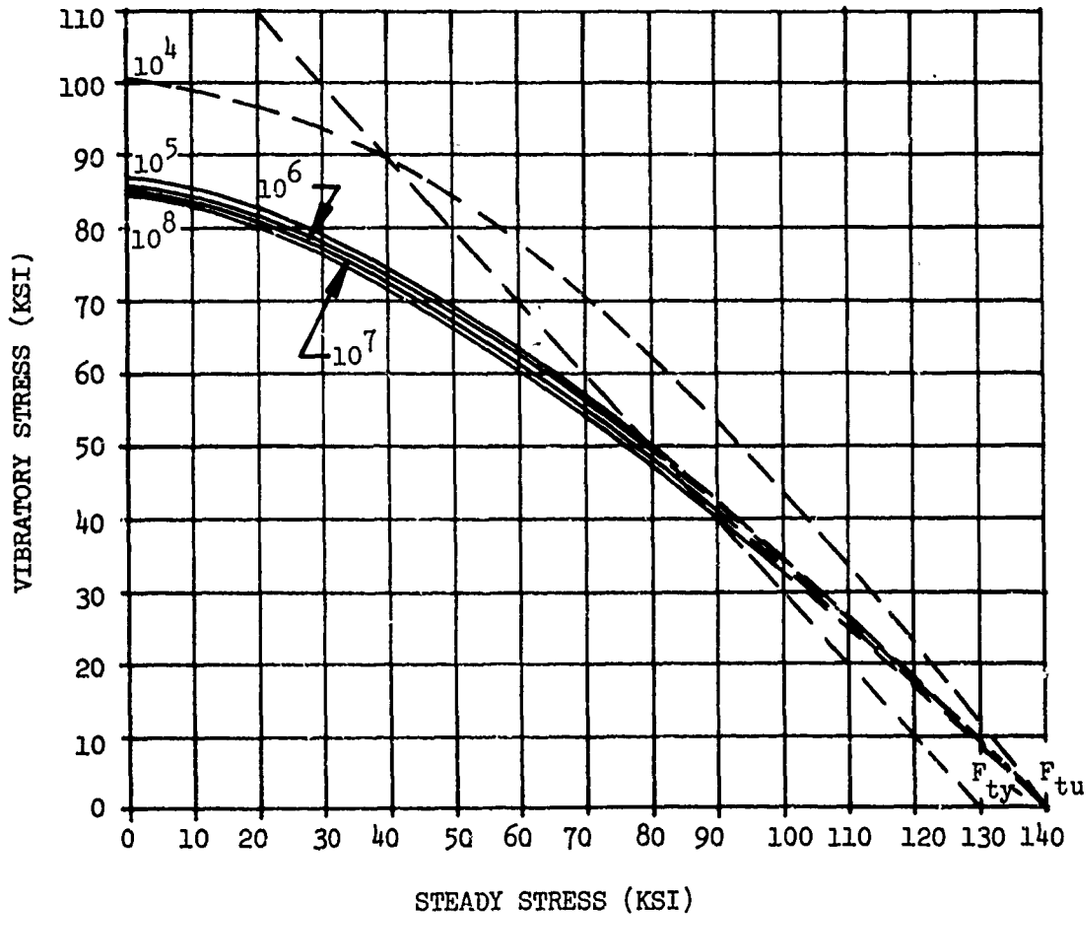

Figure 114. Constant-Life Diagram of Titanium Ti-6Al-4V BETA-STOA 0.5 Inch From As-Quenched Surface, Polished Specimens.

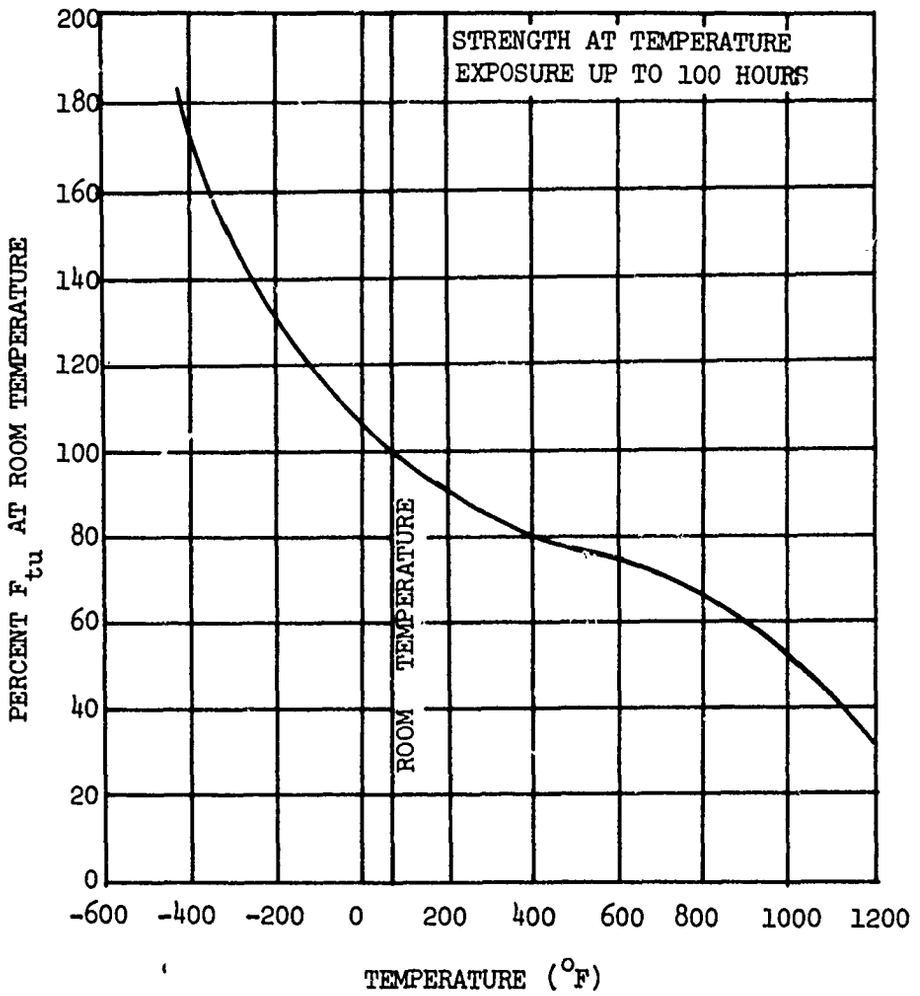

Figure 115. Effect of Temperature on the Ultimate Tensile Strength of Annealed Ti-6Al-4V Sheet and Bar.

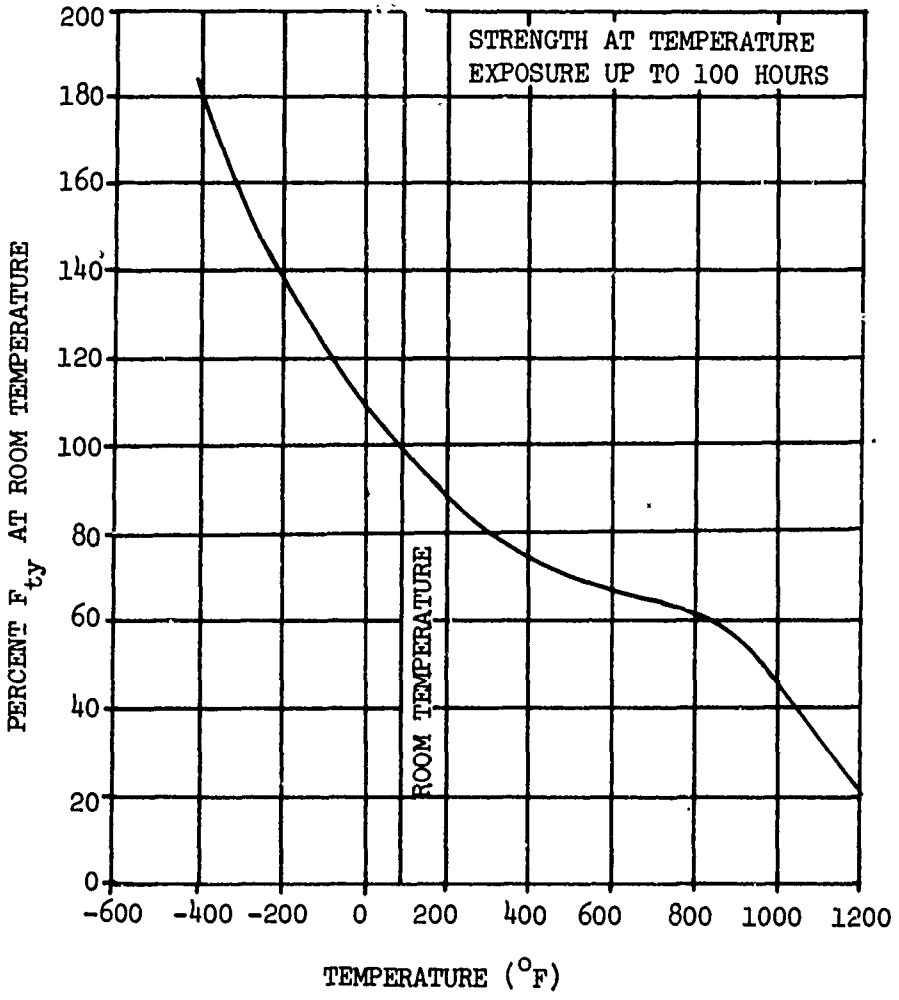

Figure 116. Effect of Temperature on the Compressive Yield Strength of Annealed Ti-6Al-4V Sheet and Bar.

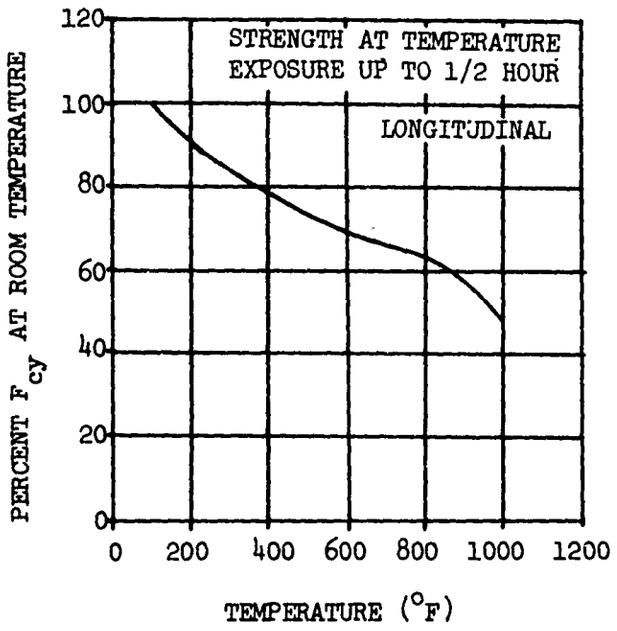

Figure 117. Effect of Temperature on the Compressive Yield Strength of Annealed Ti-6Al-4V Sheet and Bar.

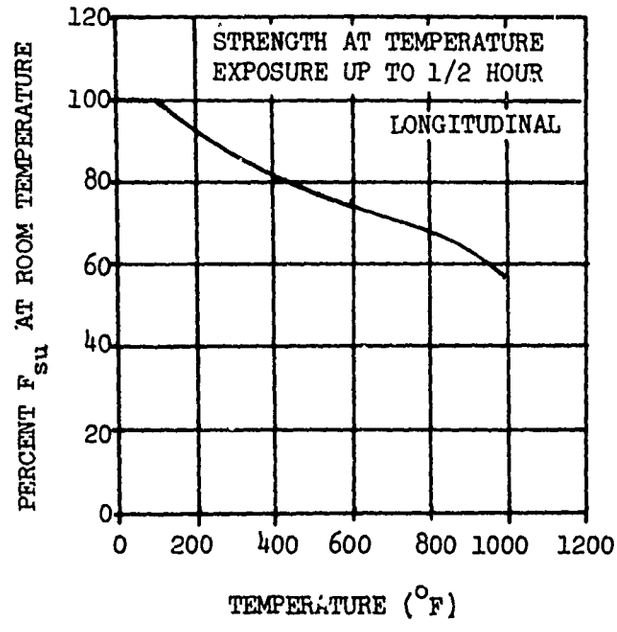

Figure 118. Effect of Temperature on the Ultimate Tensile Shear Strength of Annealed Ti-6Al-4V Sheet and Bar.

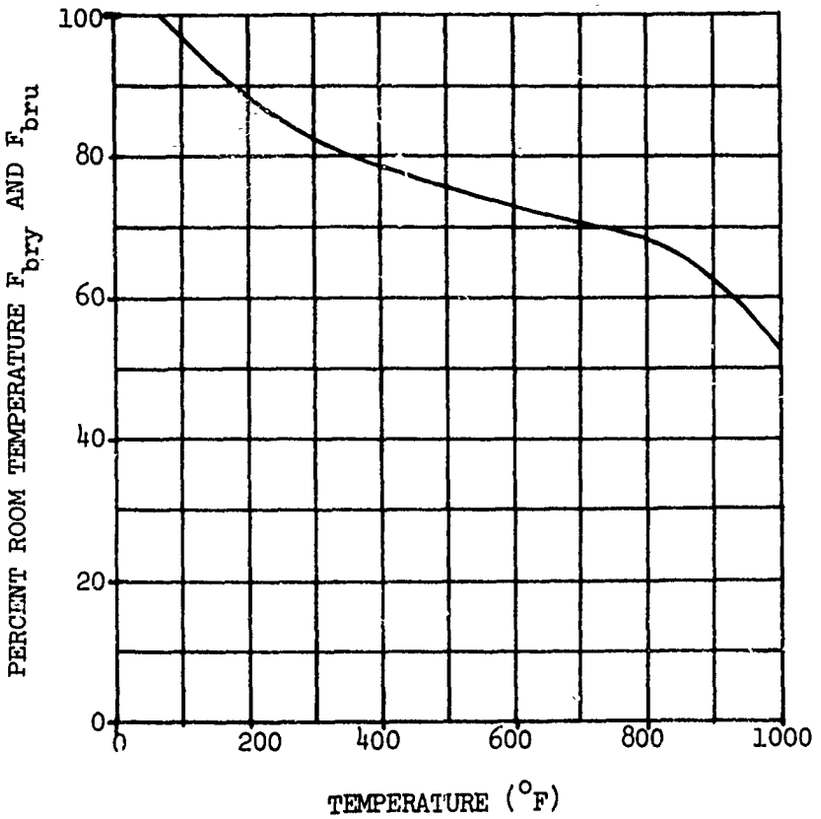

Figure 119. Effect of Temperature on the Ultimate Bearing Strength and Bearing Yield Strength of Annealed Ti-6Al-4V Sheet and Bar.

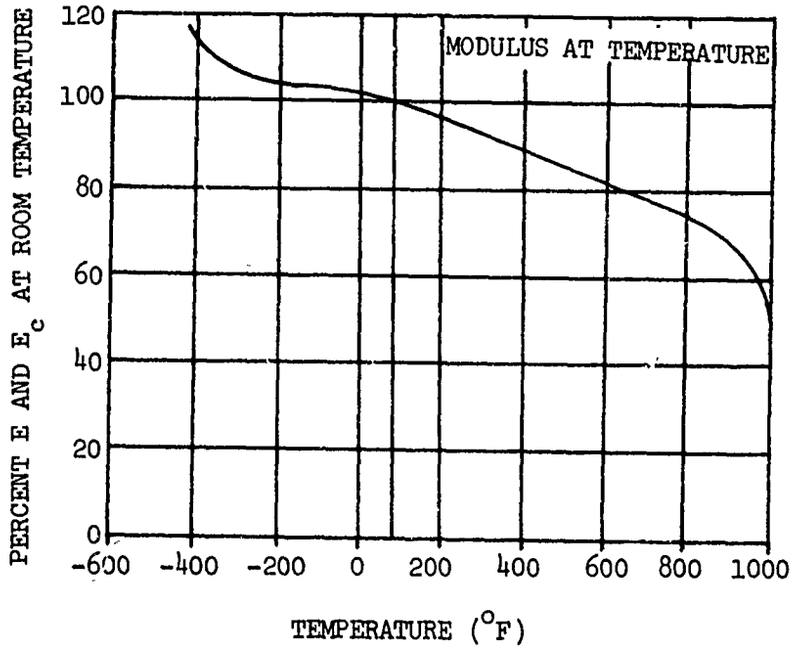

Figure 120. Effect of Temperature on the Tensile and Compressive Moduli of Annealed Ti-6Al-4V Sheet and Bar.

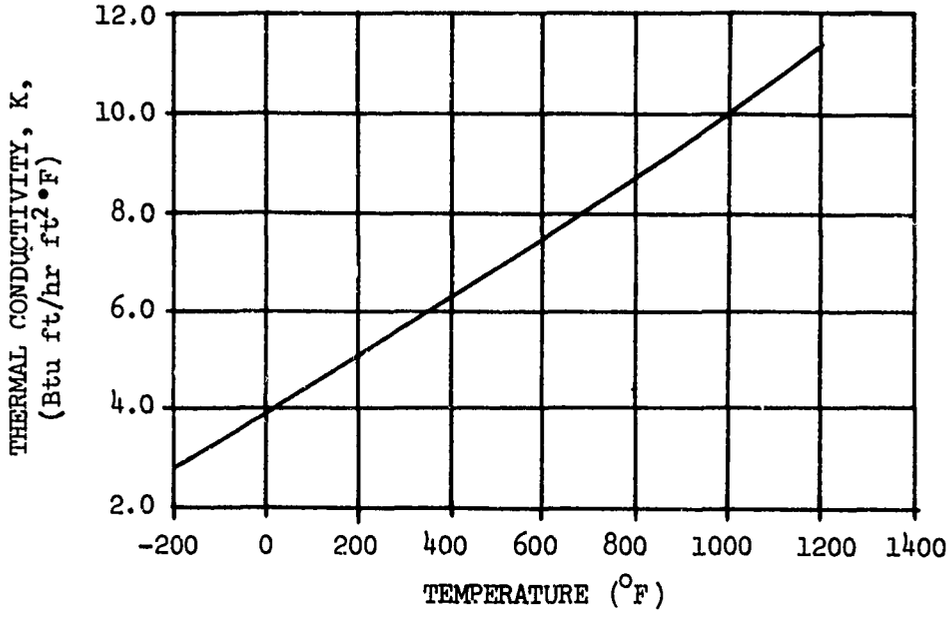

Figure 121. Effect of Temperature on the Thermal Conductivity of Ti-6Al-4V (Annealed or Solution Heat-Treated and Aged).

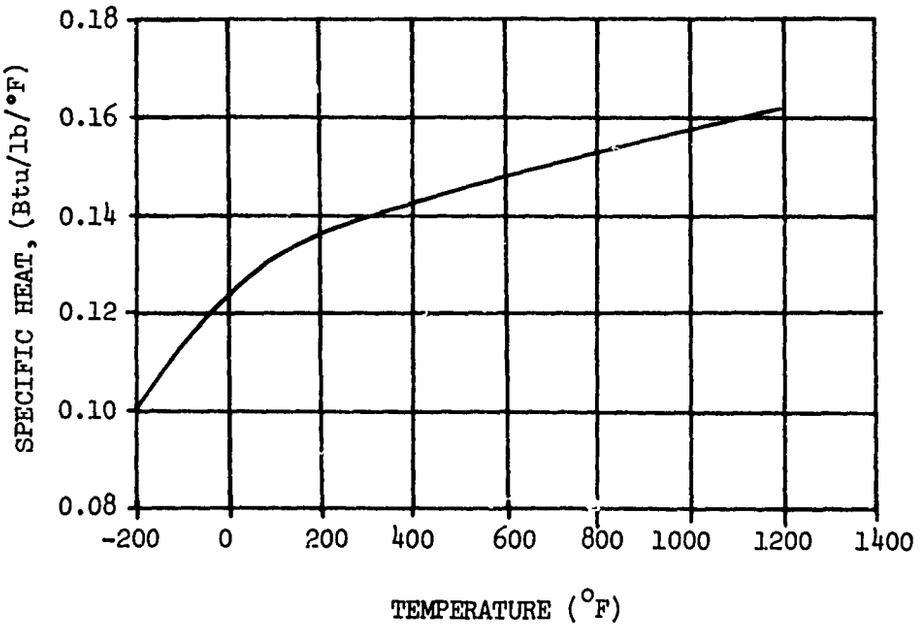

Figure 122. Effect of Temperature on the Specific Heat of Ti-6Al-4V (Annealed or Solution Heat-Treated and Aged).

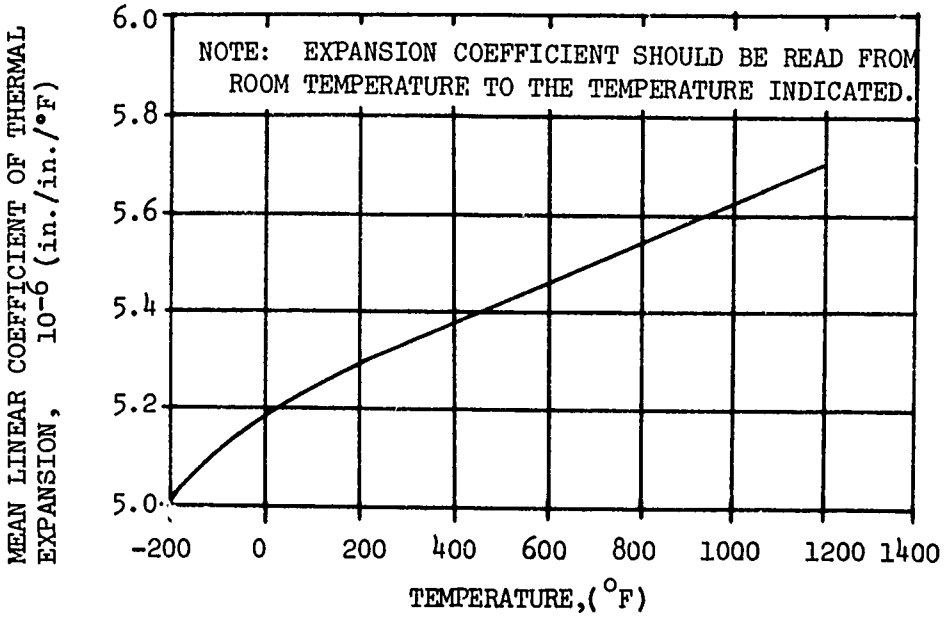

Figure 123. Effect of Temperature on the (Mean) Linear Coefficient of Thermal Expansion of Ti-6Al-4V.

TABLE XXIX. TYPICAL ELEVATED TEMPERATURE DEFORMATION AND RUPTURE PROPERTIES OF MILL ANNEALED Ti-6Al-4V SHEET

Temperature (°F)	Time (hr)	Stress, 1000 psi, To Produce Indicated Percentage Deformation or Rupture												
		0.1%		0.2%		0.5%		1.0%		2.0%		5.0%		
		C	TD	C	TD	C	TD	C	TD	C	TD	C	TD	Rupture
700	1	86	-	106	-	113	-	120	-	-	-	-	-	-
	10	73	-	83	-	100	-	105	-	-	-	-	-	-
	100	49	-	58	-	78	-	87	-	-	-	-	-	-
	1000	40	-	48	-	57	-	73	-	-	-	-	-	-
800	1	69	-	80	-	88	-	94	-	-	-	-	-	-
	10	49	33	56	44	67	61	75	-	-	-	95	-	100
	100	24	13	32	29	47	39	48	47	68	57	80	-	86
	1000	-	-	-	21	46	26	43	32	-	38	70	47	75
900	1	45	-	52	-	62	-	72	-	-	-	-	-	-
	10	24	15	30	20	38	31	43	36	-	-	68	-	74
	100	11	5	14	13	25	20	30	25	33	-	42	-	50
	1000	-	-	-	-	11	11	15	13	-	-	-	-	-
1000	1	15	-	18	-	-	-	-	-	-	-	-	-	-
	10	8	7	12	9	15	15	18	18	-	-	-	-	-
	100	1	1	4	3	7	7	10	10	12	-	15	-	-
	1000	-	-	-	-	2	2	3	3	-	-	-	-	-

C = Creep (Strain); TD = Total Deformation (Strain)

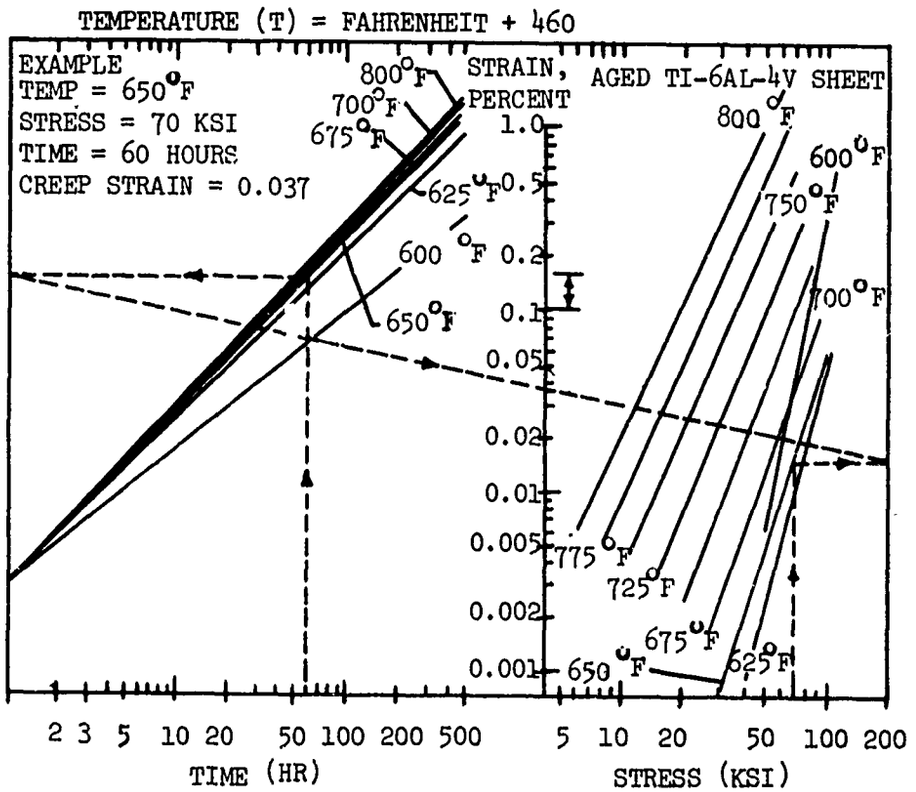

Figure 124. Creep Properties of Solution Heat-Treated and Aged Ti-6Al-4V Sheet.

ALLOY: 17-4PH Stainless Steel

General Description

The 17-4PH alloy steel is a martensitic, precipitation hardening alloy which exhibits good corrosion resistance and ductility and strength to 600°F.

Physical Properties

Density	.283 lb/in.^{3}
Melting Temperature Range	2560° - 2626°F
Coefficient of Thermal Expansion	Figure 125
Specific Heat	Figure 125
Thermal Conductivity	Figure 125

Fabricability

The alloy 17-4PH is readily forged, investment cast welded, and brazed. Machining requires the same precautions as with the austenitic stainless steels except that work-hardening is not a problem. When heavy sections are to be welded under conditions of high restraint, prior stress relief obtained by four hours heating at 1100° or 1150°F is advisable to maximize fracture toughness properties and to preclude cracking in planes normal to the thickness direction.

Corrosion Resistance

The resistance of 17-4PH to stress corrosion cracking in chloride environments has been found to be superior to the alloy steels and the hardenable chromium stainless steels.

TABLE XXX. MECHANICAL PROPERTIES OF 17-4PH STAINLESS STEEL H1025*

Property	Value
F_{tu}, ksi	155
F_{ty}, ksi	145
F_{cy}, ksi	(145)
F_{su}, ksi	(100)
F_{bru}, ksi	
(e/D = 1.5)	(245)
(e/D = 2.)	(300)
F_{bry}, ksi	
(e/D = 1.5)	(216)
(e/D = 2.0)	(238)
e, in two inches	12
E, 10^6 psi	28.5
E_c, 10^6 psi	30.0
G, 10^6 psi	11.2
Poisson's Ratio	.272

* H900 temper used as basis of properties in parentheses ( ) but avoided due to stress corrosion problems with this temper.

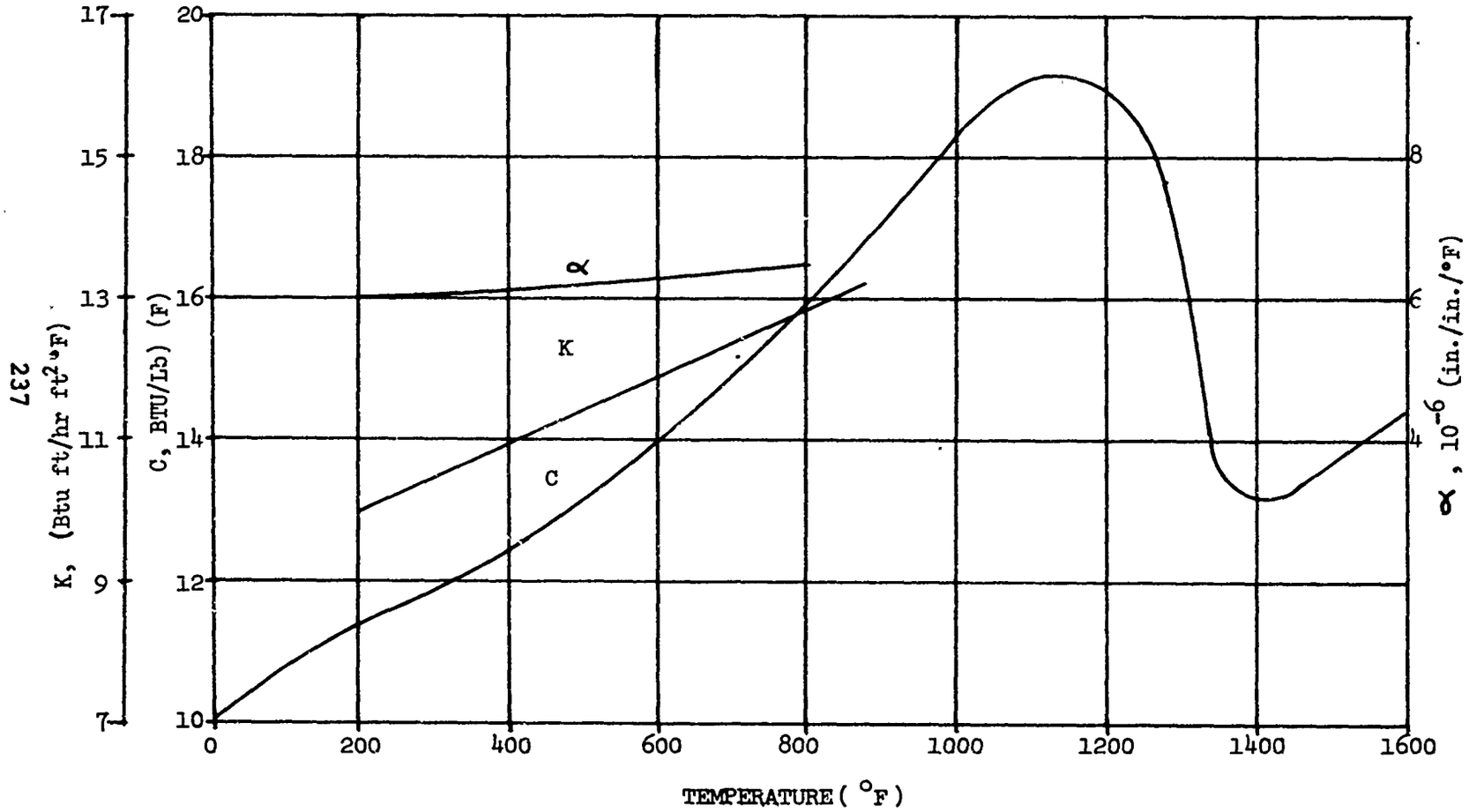

Figure 125. Effect of Temperature on the Physical Properties of 17-4PH Stainless Steel.

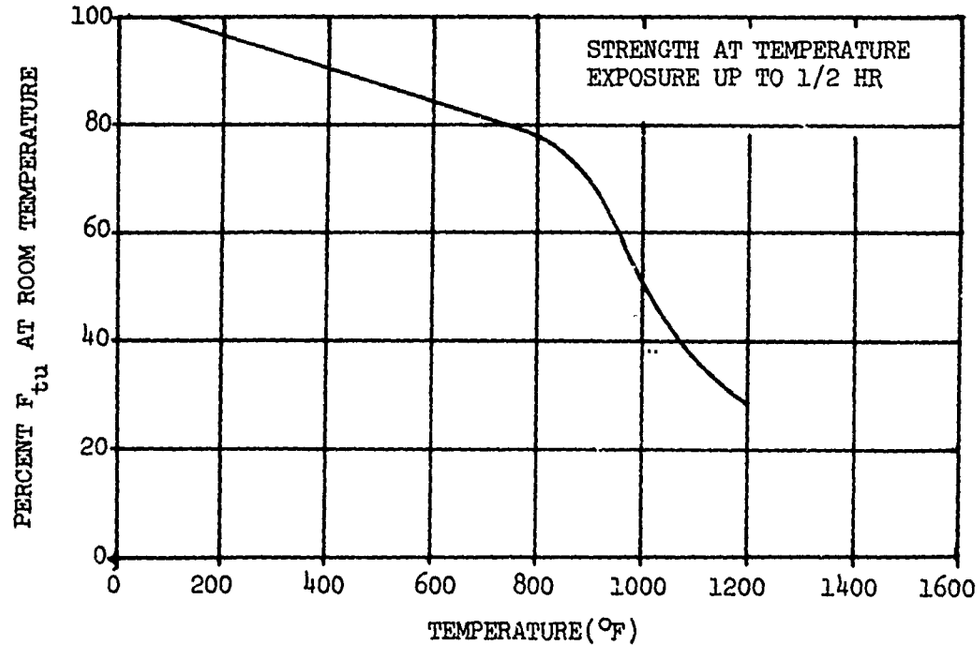

Figure 126. Effect of Temperature on the Ultimate Tensile Strength (F_{tu}) of 17-4PH Stainless Steel (Bar and Forgings).

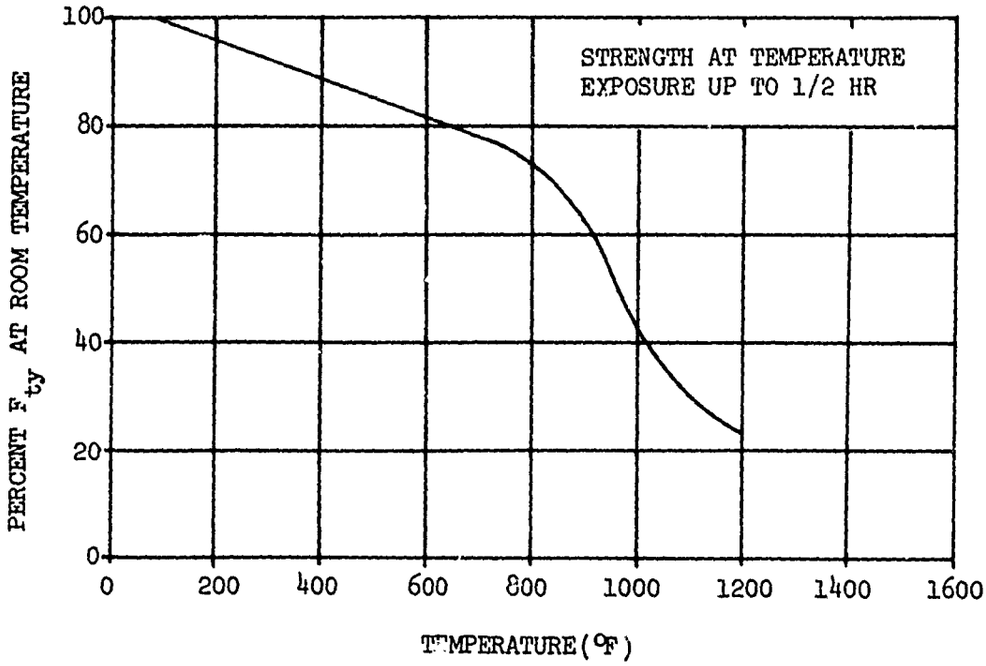

Figure 127. Effect of Temperature on the Tensile Yield Strength (F_{ty}) of 17-4PH Stainless Steel (Bar and Forgings).

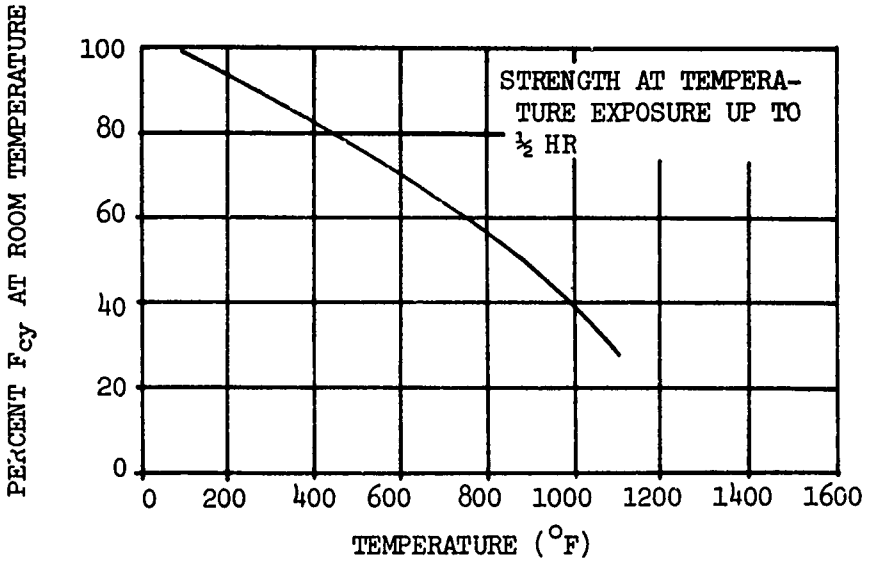

Figure 128. Effect of Temperature on the Compressive Yield Strength (F_{cy}) of 17-4PH Stainless Steel (Bar and Forgings).

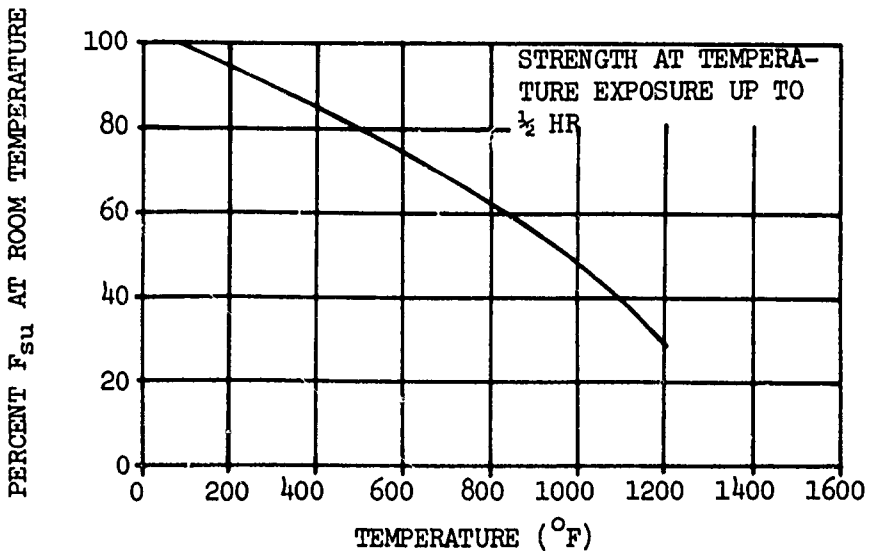

Figure 129. Effect of Temperature on the Ultimate Shear Strength (F_{su}) of 17-4PH Stainless Steel (Bar and Forgings).

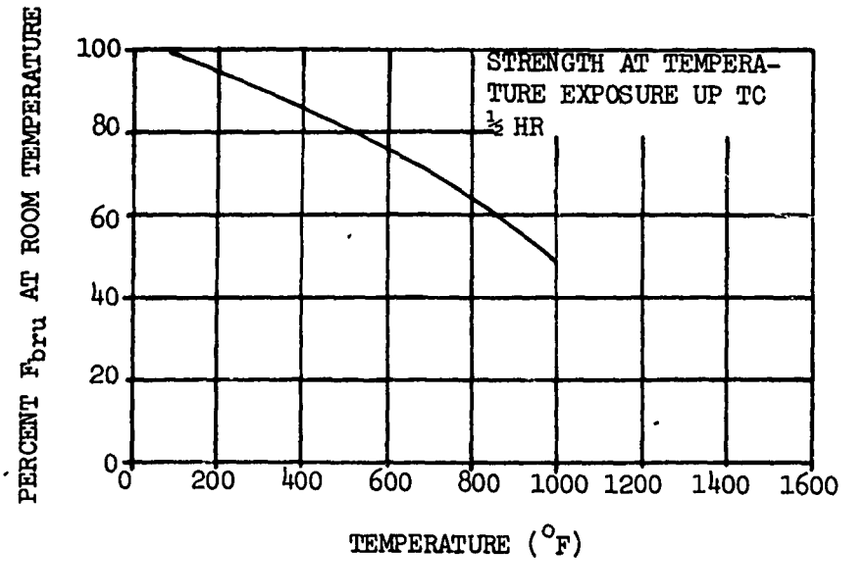

Figure 130. Effect of Temperature on the Ultimate Strength (F_{bru}) of 17-4PH Stainless Steel (Bar and Forgings).

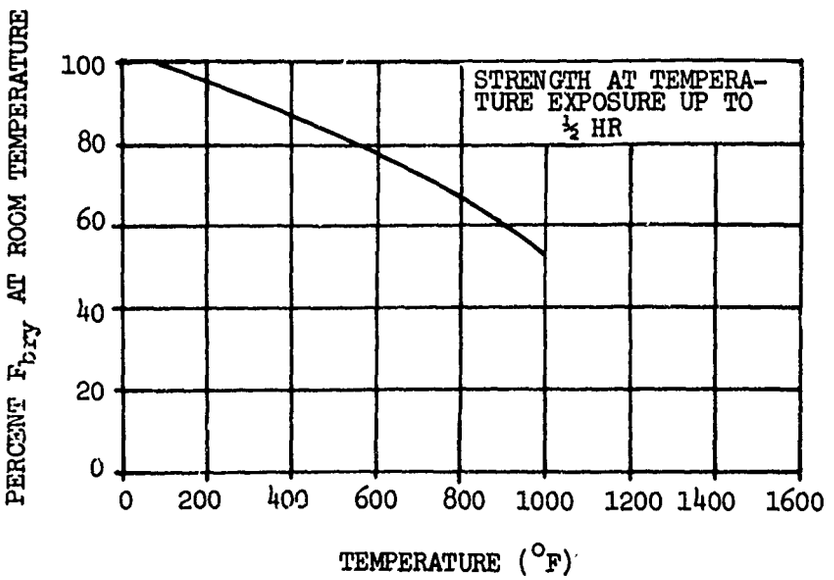

Figure 131. Effect of Temperature on the Bearing Yield Strength (F_{bry}) of 17-4PH Stainless Steel (Bar and Forgings).

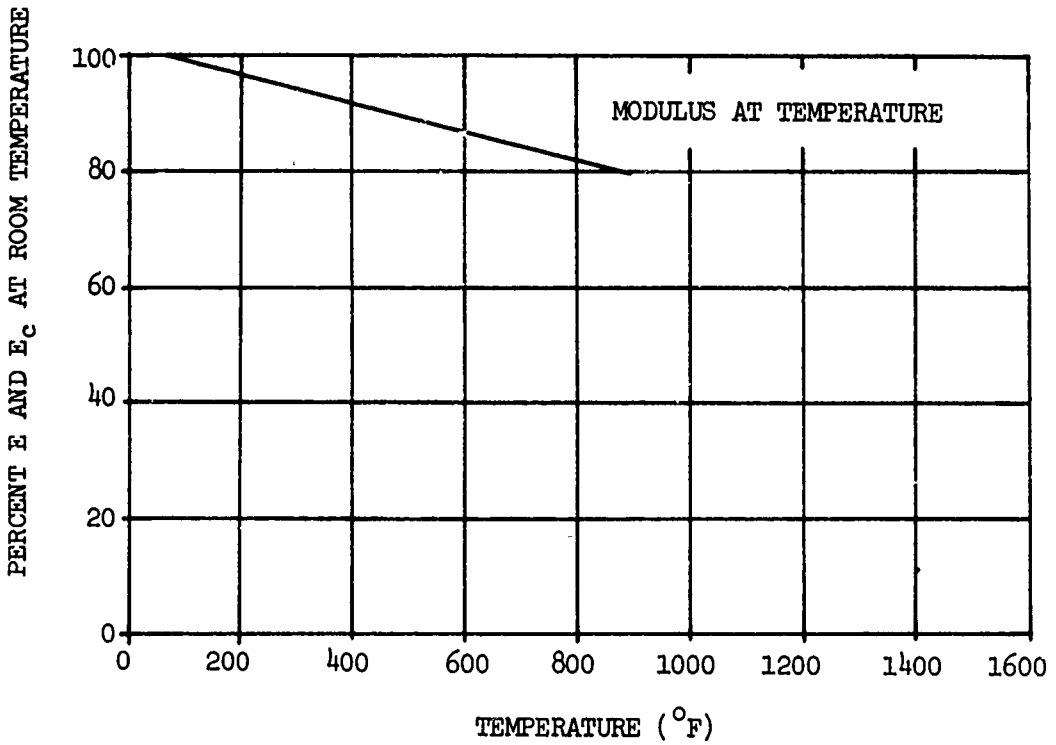

Figure 132. Effect of Temperature on the Tensile and Compressive Modulus (E and E_c) of 17-4PH Stainless Steel (Bar and Forgings).

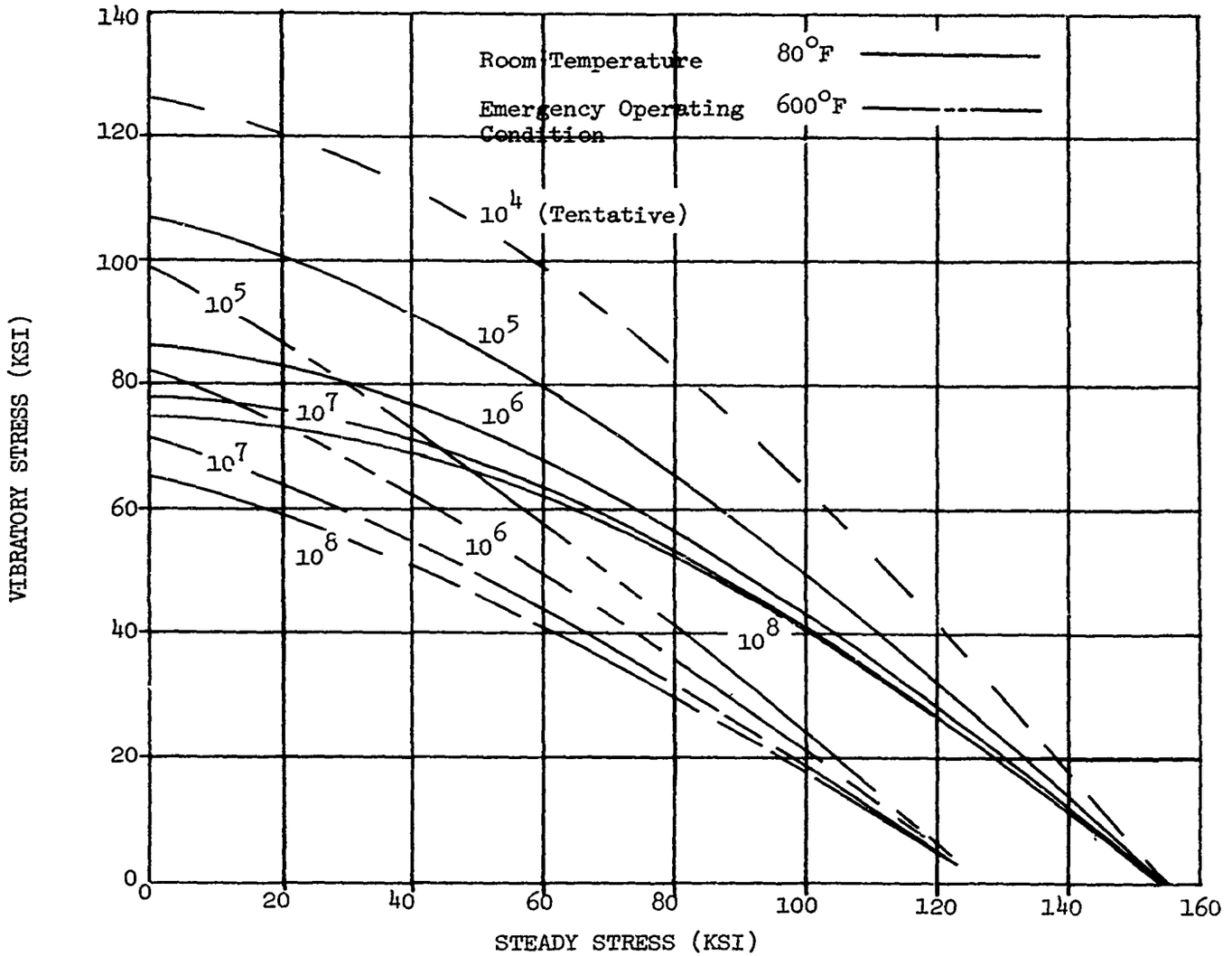

Figure 133. Constant-Life Diagram, 17-4PH Bar and Wire (Reference 9).

ALLOY: 18% Ni 250 Grade Maraging Steel

General Description

The 18% Ni 250 Grade 250 alloy is one of a class of maraging types which develops its strength primarily as a result of a complex precipitation reaction in a low carbon Fe-Ni martensite. Fracture properties of heavy section can be directional and are lowest in the short transverse direction. Corrosion and oxidation resistance are somewhat better than 4340.

Physical Properties

Density	.289 lb/in.^{3}
Melting Temperature Range	2600° - 2650°F
Coefficient of Thermal Expansion	5.6 x 10^{-6} in./in./°F (70° - 900°F)
Specific Heat	.11 Btu/lb/°F (200°F)
Thermal Conductivity	17 Btu ft/hr ft^2 °F (200°F) 19 Btu ft/hr ft^2 °F (600°F)

Fabricability

Forming

Formability is excellent in the annealed condition, and machining offers no special problems.

Brazing and Soldering

Brazing and soldering of 250 Grade Maraging steel is not usually done.

Welding

Welding requires special precautions; the toughness of the weld is generally about one-half of that of the parent material. Welding is normally done in the annealed condition and is subjected to a full re-annealing and aging prior to final machining.

Corrosion Resistance

Corrosion resistance of 250 Grade Maraging steel is superior to that of 4340. Banding has been experienced in and adjacent to welds as a result of alloy segregation in the welding process.

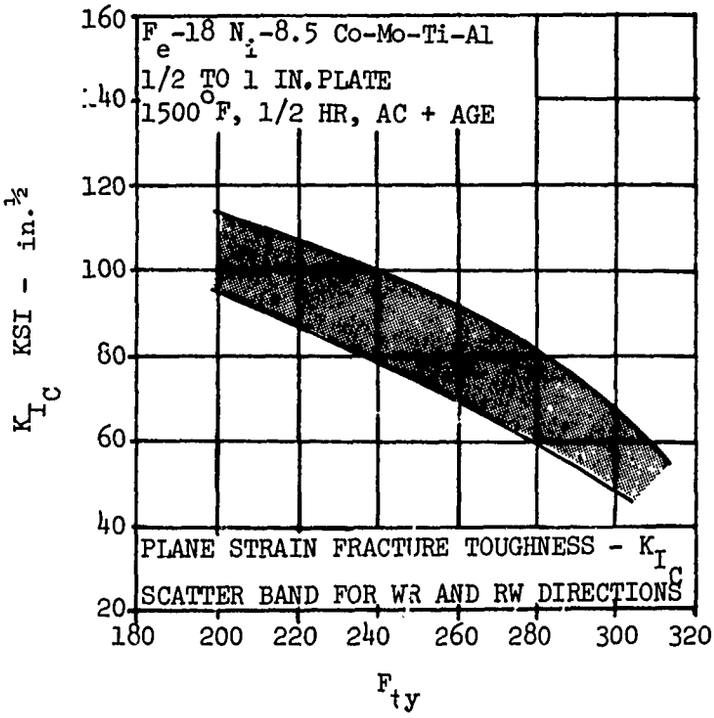

Figure 134. Plane Strain Fracture Toughness of Ten Heats of Annelaed and Aged Plate as a Function of Yield Strength.

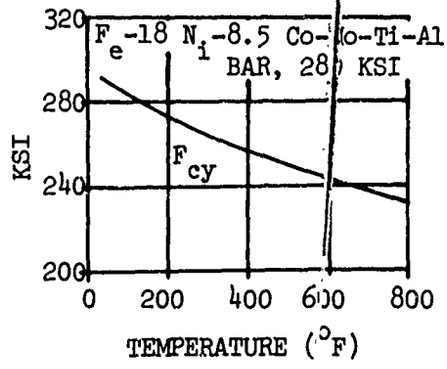

Figure 135. Effect of Temperature on Compressive Yield Strength of 280-KSI Bar.

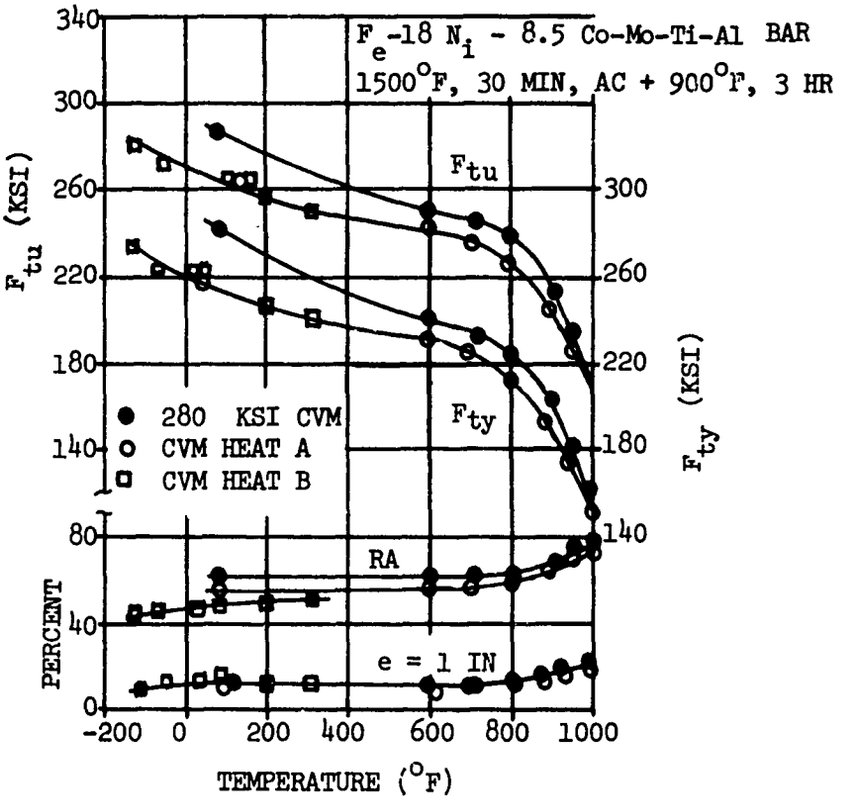

Figure 136. Effect of Test Temperature on Tensile Properties of Annealed and Aged Bar.

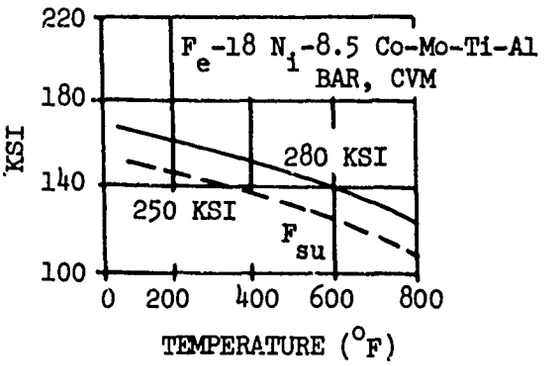

Figure 137. Effect of Test Temperature on Shear Ultimate Strength of 250- and 280-KSI Bar.

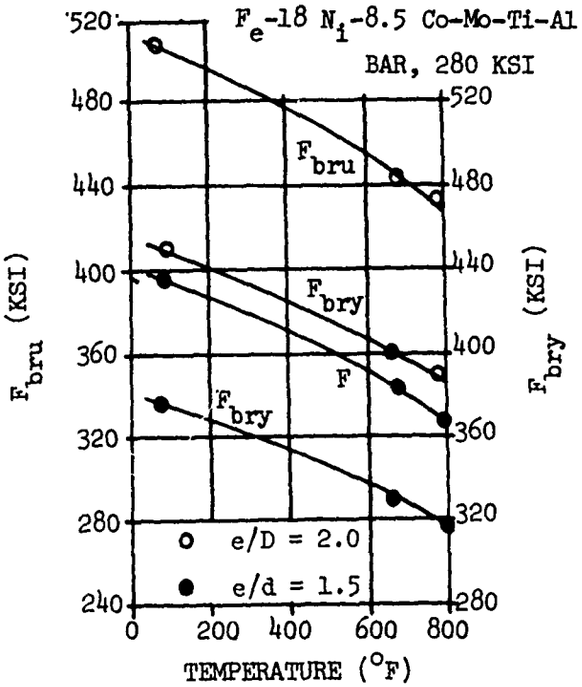

Figure 138. Effect of Test Temperature on Bearing Strength of 280-KSI Bar (Reduce Proportionally for lower UTS).

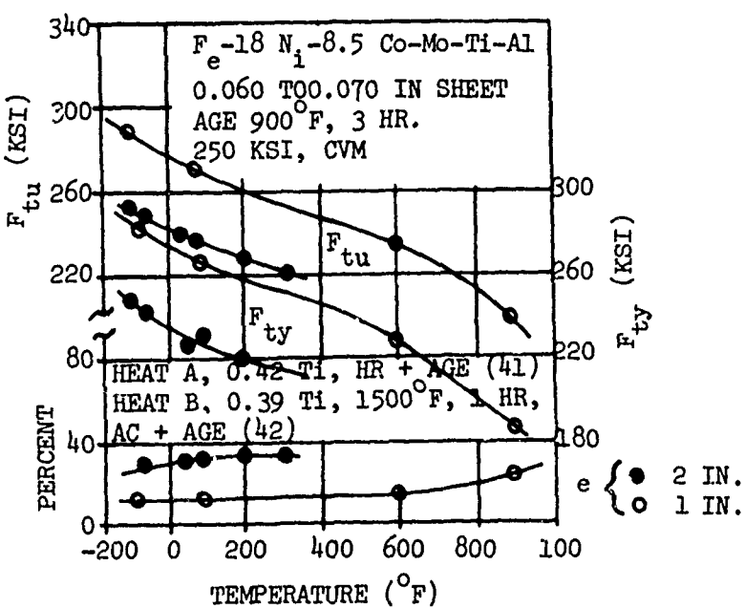

Figure 139. Effect of Test Temperature on the Tensile Properties of Two Heats of 280-KSI CVM Sheet.

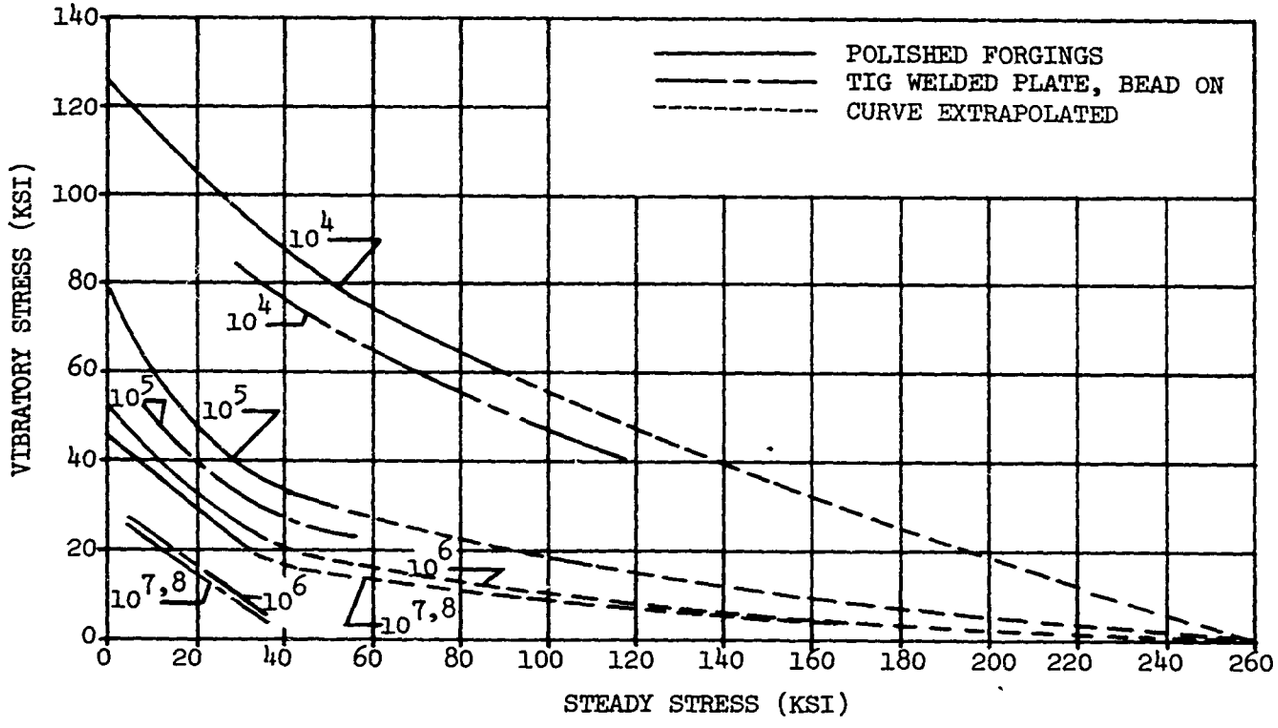

Figure 140. Constant-Life Fatigue Diagram for 18 Ni (250 Grade) Maraging Steel; Room Temperature, K_t = 1.0, Smooth, Polished (Reference 10).

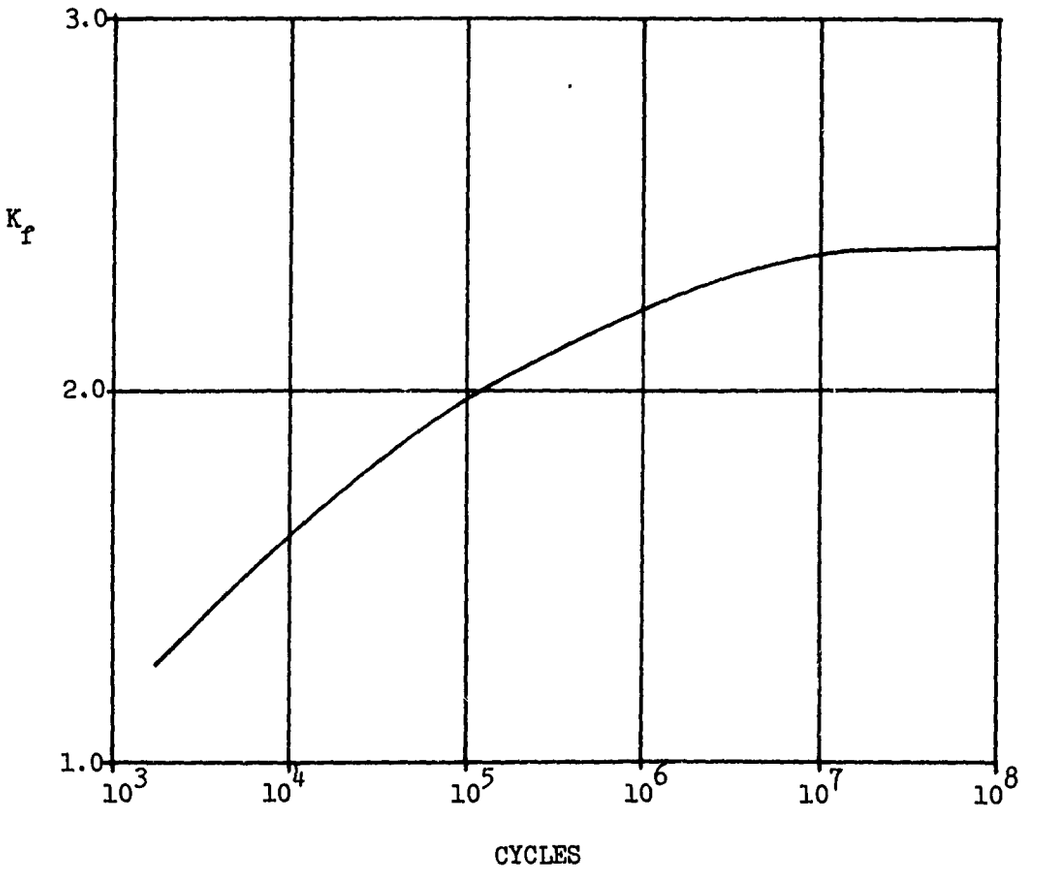

Figure 141. K_f Versus Cycles, Welded 250 Grade Maraging Steel, R = 0.1 (Reference 10).

ALLOY: 4130/4340 Steel

General Description

The 4130/4340 alloy steels contain carbon by the last two digits in hundredths and various alloying elements to improve their strength, depth of hardening, toughness or other properties of interest. These steels are available in a variety of finishes ranging from hot or cold rolled to quenched and tempered. They are generally heat treated before use to develop the desired properties. They may be carburized and then heat treated to produce a combination of high surface hardness and good core toughness.

Physical Properties

Density	.283 lb/in.^{3}
Melting Temperature	approximately 2740°F
Coefficient of Thermal Expansion	Figure 142
Specific Heat	Figure 142
Thermal Conductivity	Figure 142

Fabricability

The alloy steels are only slightly more difficult to forge than carbon steels. For cold forming, alloy steels are usually formed in the annealed condition. The machining of alloy steels is generally more difficult than unalloyed steels of the same carbon content. The low carbon grades are readily welded or brazed by all techniques. Alloy steels can be welded without loss of strength in the heat-affected zone provided that the welding heat input is carefully controlled. 4340 steel is normally welded to an in-house standard.

Corrosion Resistance

The corrosion properties of AISI alloy steels are comparable to those of plain carbon steels. Alloy steels containing chromium or high percentages of silicon have somewhat better oxidation resistance than carbon or other alloy steels.

TABLE XXXI. MECHANICAL PROPERTIES OF 4130/4340 STEEL

Form	4130 Sheet Strip Plate			4340, 4130 All Wrought Form		
Condition	N			Quenched and tempered		
Property				Value		
F_{tu}, ksi	95	90	125	150	180	200
F_{ty}, ksi	75	70	103	132	163	176
F_{cy}, ksi	75	70	113	145	173	181
F_{su}, ksi	57	54	75	90	108	120
F_{bru}, ksi (e/D = 1.5)	-	-	194	219	250	272
F_{bru}, ksi (e/D = 2.0)	200	190	251	287	326	355
F_{bry}, ksi (e/D = 1.5)	-	-	151	189	230	255
F_{bry}, ksi (e/D = 2.0)	129	120	180	218	256	280
E, 10^3 ksi	-	29.0	-	29.0	-	-
E_c, 10^3 ksi	-	29.0	-	29.0	-	-
G, 10^3 ksi	-	11.0	-	11.0	-	-
Poisson's Ratio	-	.32	-	0.32	-	-

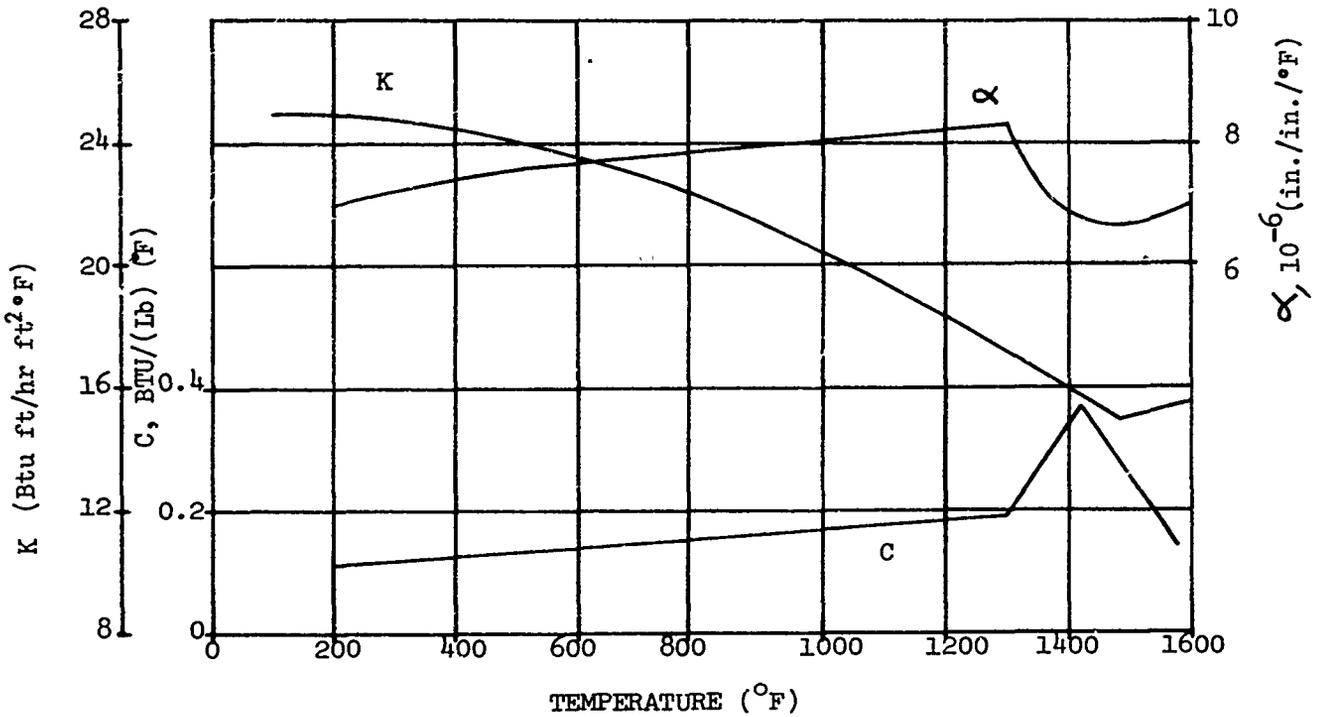

Figure 142. Effect of Temperature on the Physical Properties of AISI 413C.

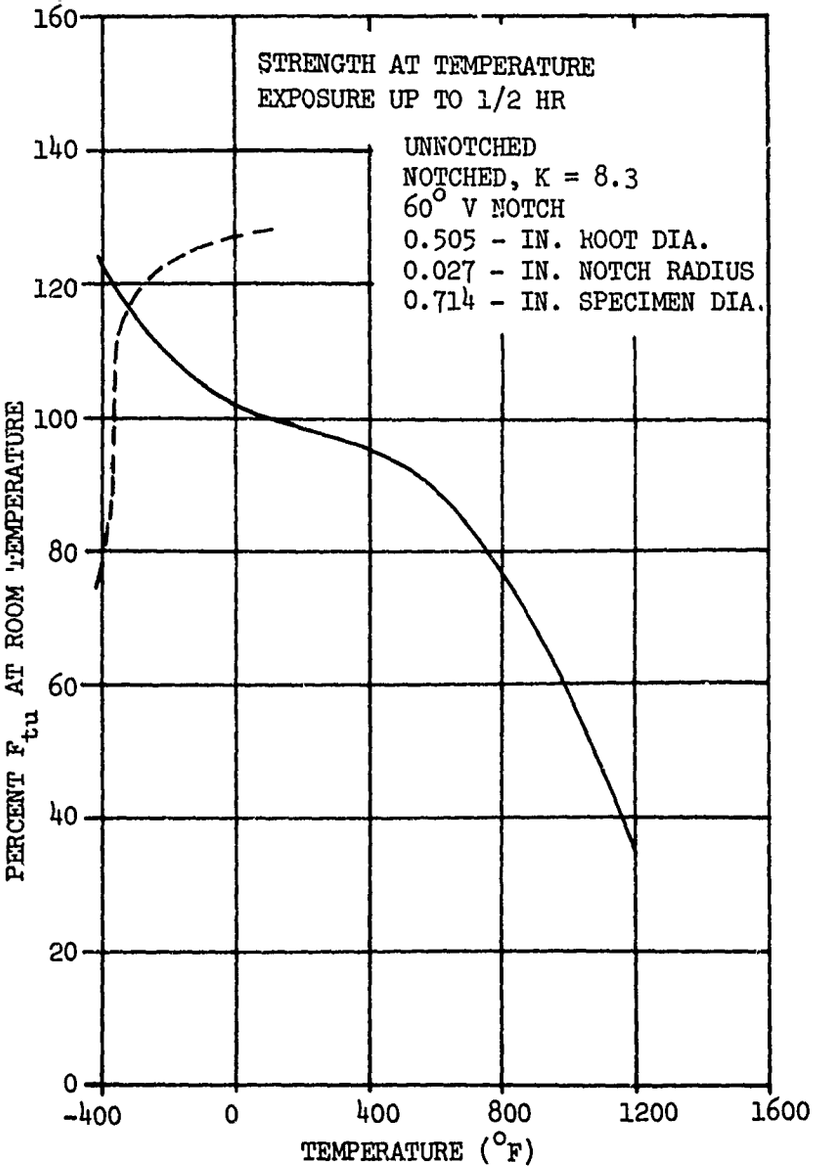

Figure 143. Effect of Temperature on the Ultimate Strength (F_{tu}) of AISI Alloy Steels.

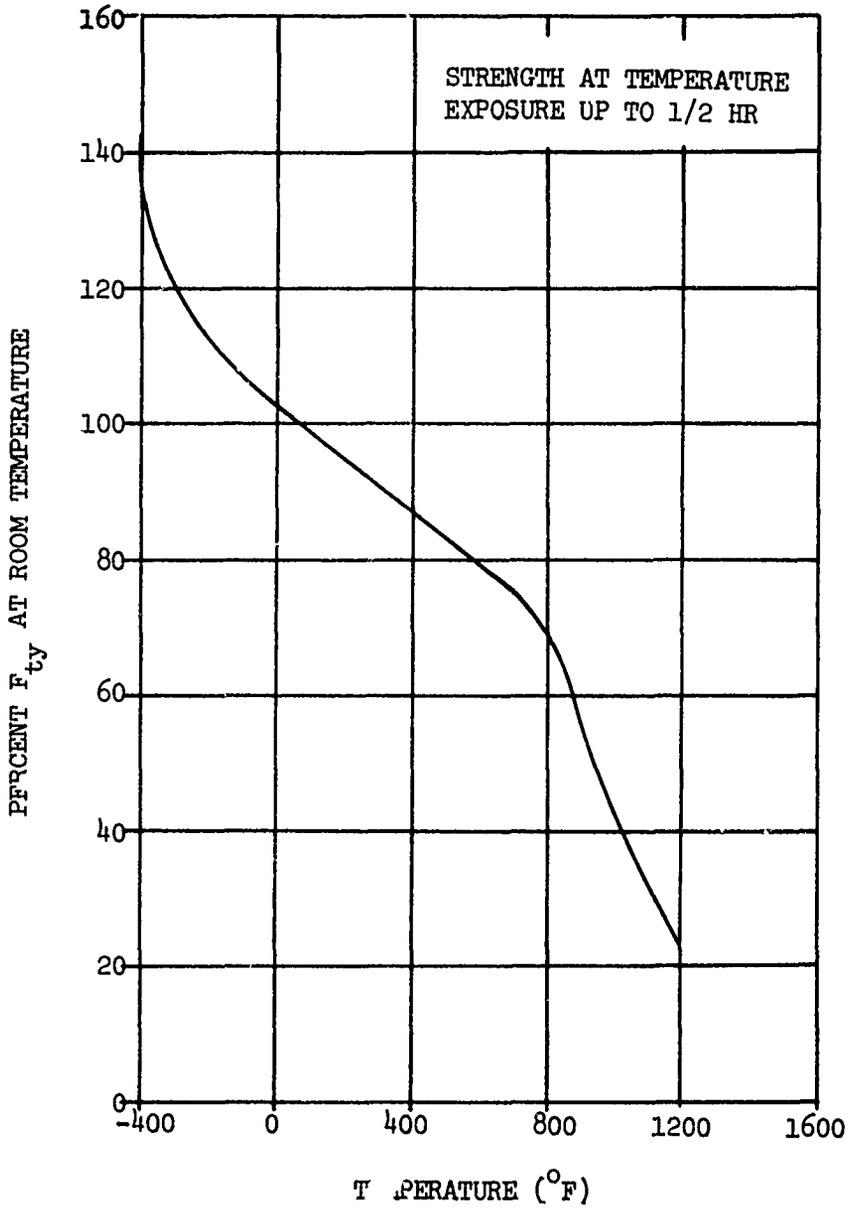

Figure 144. Effect of Temperature on the Tensile Yield Strength (F_{ty}) of AISI Alloy Steels.

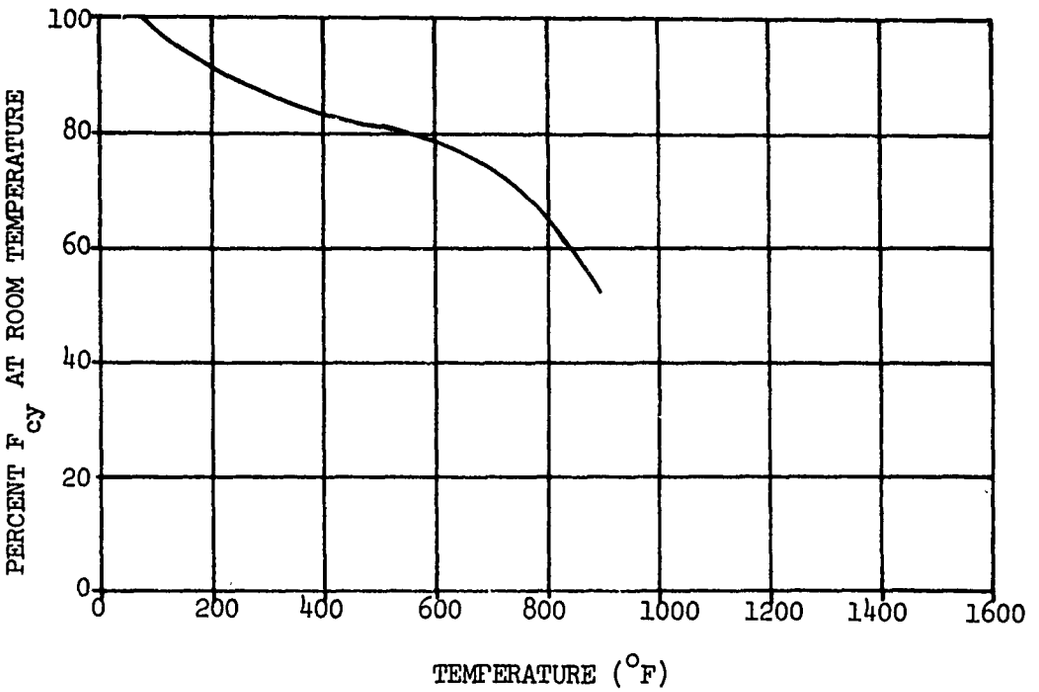

Figure 145. Effect of Temperature on the Compressive Yield Strength (F_{cy}) of Heat-Treated AISI Alloy Steels.

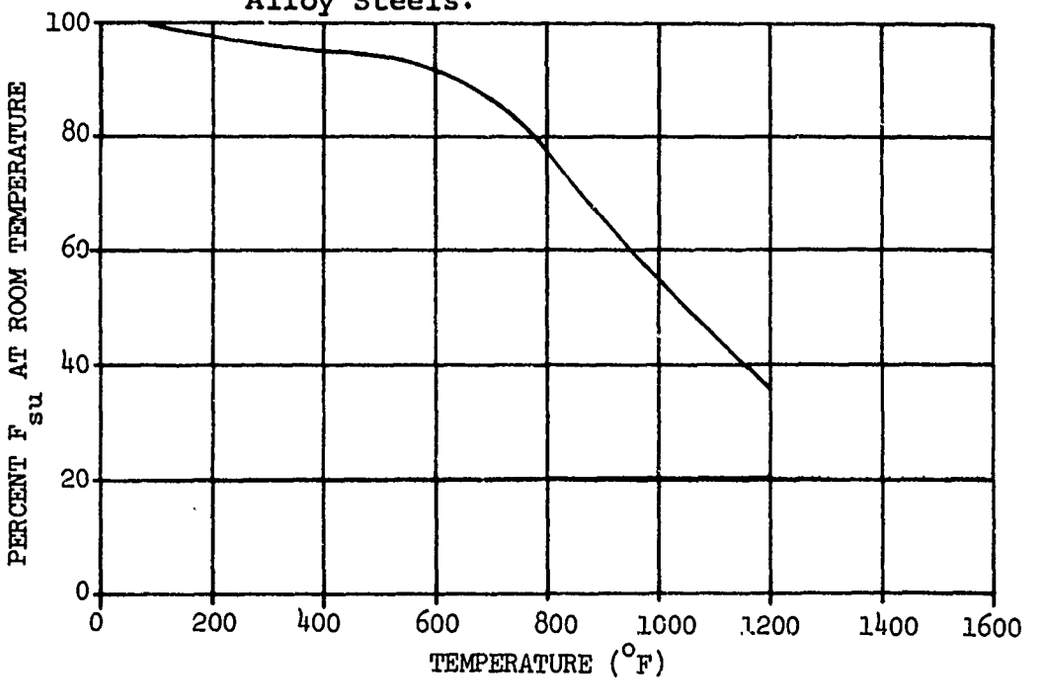

Figure 146. Effect of Temperature on Shear Ultimate Strength (F_{su}) of Heat-Treated AISI Alloy Steels.

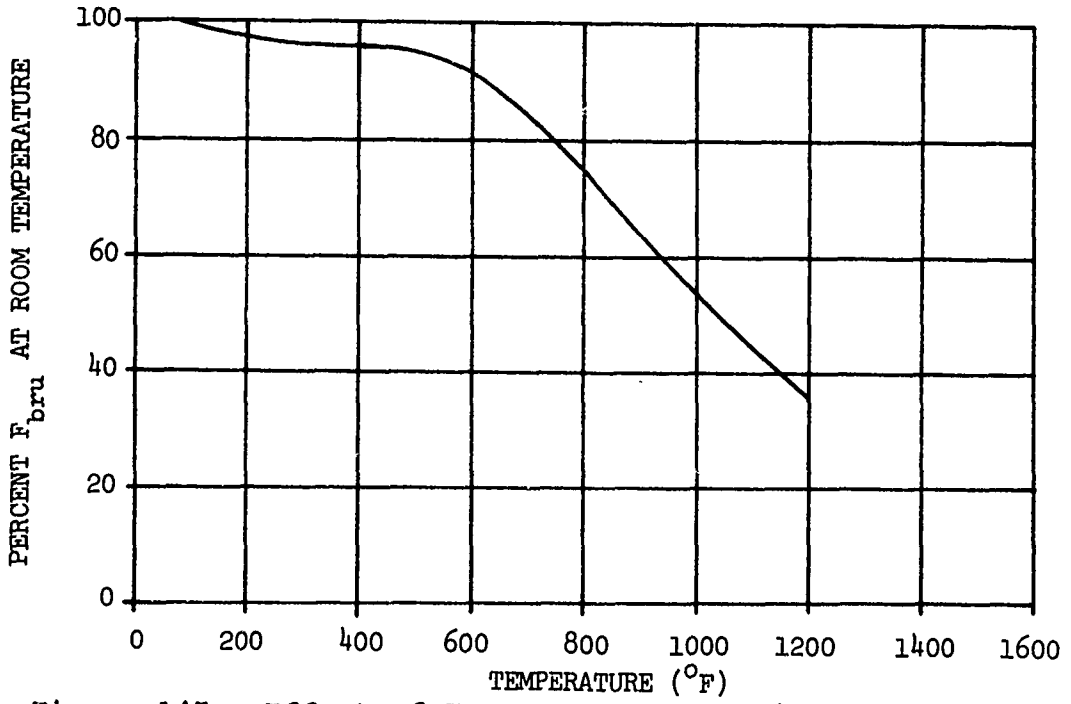

Figure 147. Effect of Temperature on Ultimate Bearing Strength (F_{bru}) of Heat-Treated AISI Alloy Steels.

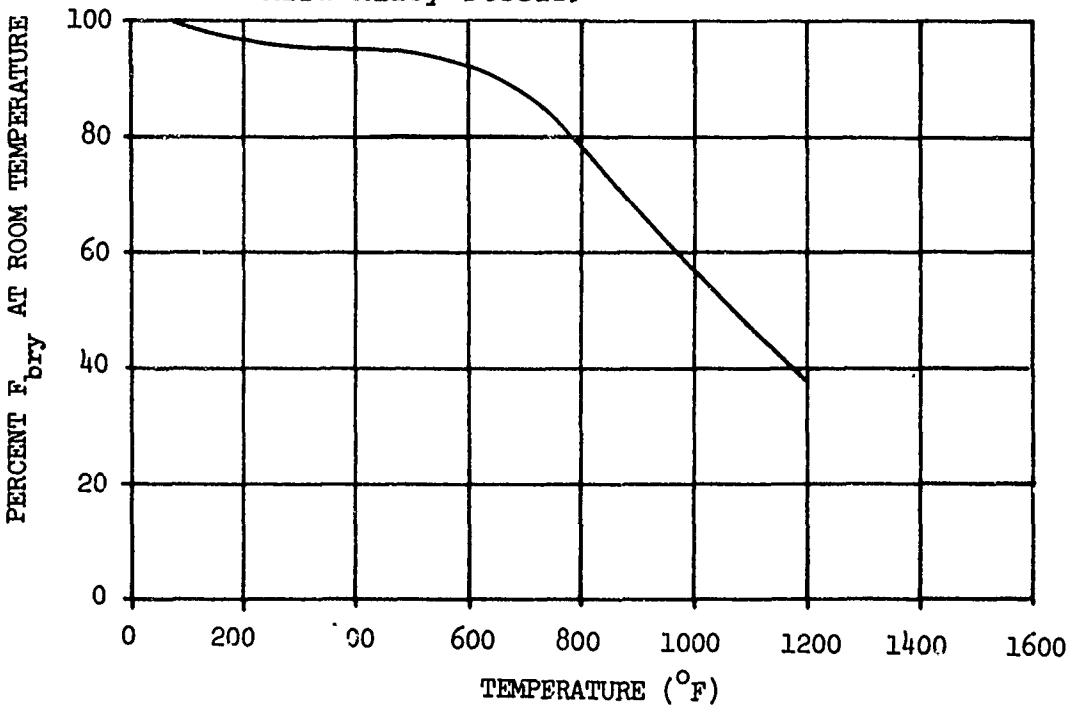

Figure 148. Effect of Temperature on the Bearing Yield Strength (F_{bry}) of Heat-Treated AISI Alloy Steels.

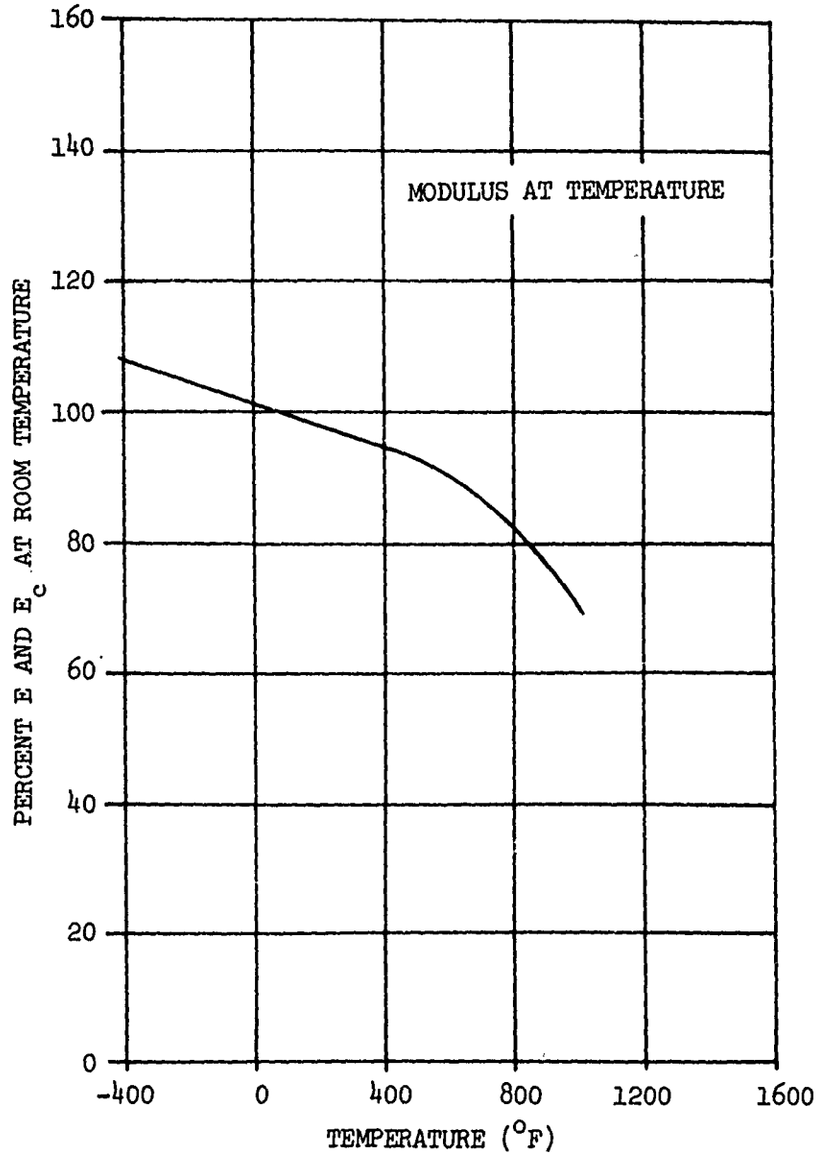

Figure 149. Effect of Temperature on Tensile and Compressive Modulus (E and E_c) of AISI Alloy Steel.

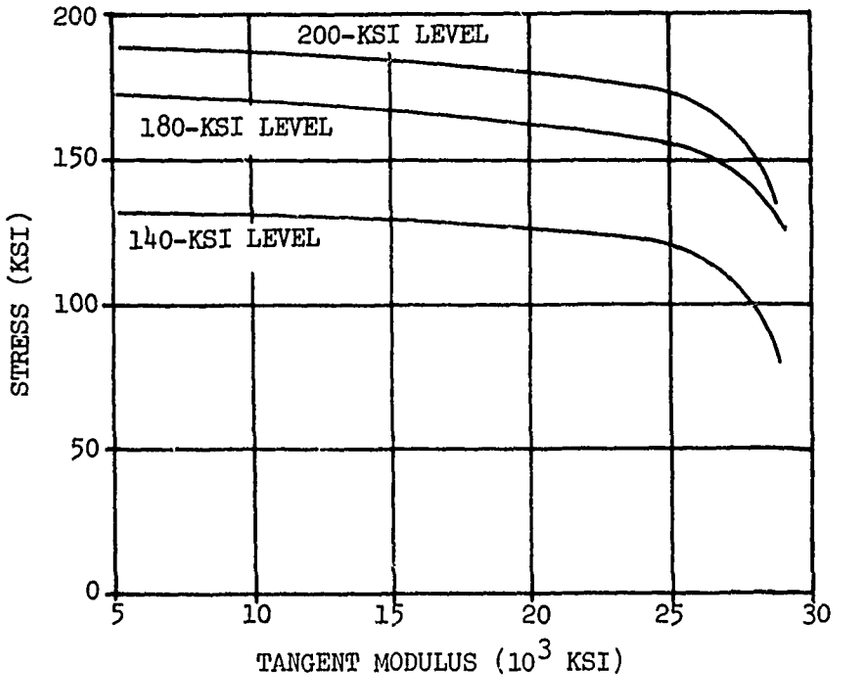

Figure 150. Typical Tensile Tangent-Modulus Curves at Room Temperature for Heat-Treated AISI 4340 Alloy Steel.

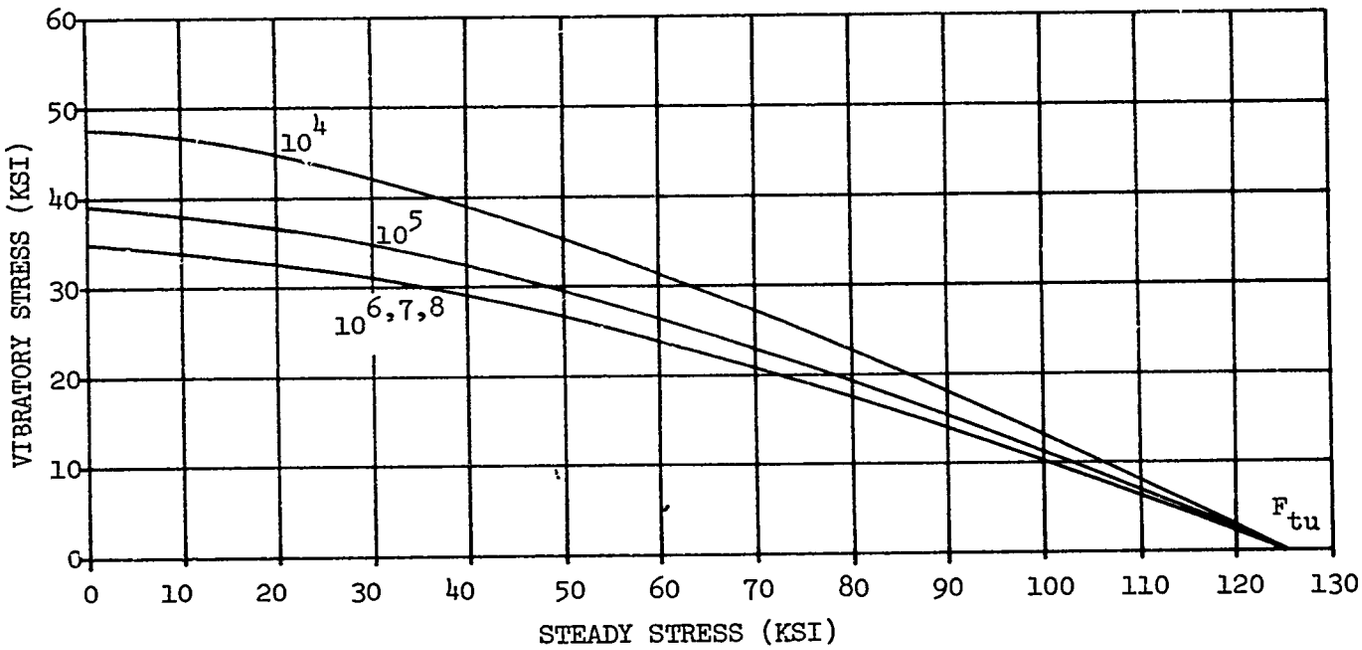

Figure 151. Constant-Life Fatigue Diagram for 4130/4340 Steel Weldments, Heat Treated to 150-KSI Ultimate Tensile Strength.

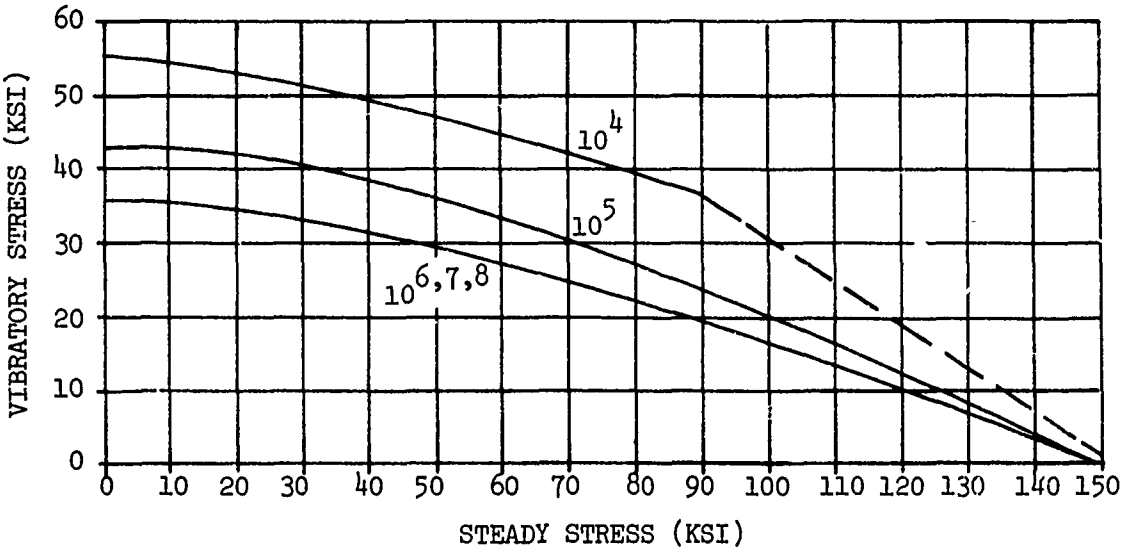

Figure 152. Constant-Life Fatigue Diagram for 4340 Steel Weldments, Heat Treated to 180-KSI.

ALLOY: Carpenter Custom 455 (Stainless Steel)

General Description

Carpenter Custom 455 is an improved chemistry 17-4PH which is a precipitation-hardening, martensitic stainless steel used for parts requiring high strength and good corrosion and oxidation resistance up to 600°F.

Physical Properties

Density	.283 lb/in.^{3}
Melting Temperature	Approximately 2640°F
Coefficient of Thermal Expansion	5.90×10^{-6} in./in./°F (72° - 200°F)
Specific Heat	Approximately 0.11 Btu/lb/°F
Thermal Conductivity	10.4 Btu ft/hr ft^2 °F (to 212°F)

Fabricability

The alloy Carpenter Custom 455 can be readily forged, welded and brazed. Machining requires the same precautions as the austenitic stainless steels except that work hardening is not a problem. The alloy can be worked in the annealed condition, welded, re-annealed and aged to high strengths. Welded strengths are good. Static joint efficiency with the joint welded, annealed and aged is in excess of 95%. Welded fatigue properties show a 75% to 80% joint efficiency at 10^7 cycles with bead ground off. The following heat treatment is recommended for maximum toughness in the weld and adjacent area: weld in the annealed condition, re-anneal at 1525°F for 1 hour, and fan-air cool; then age at 975°F for 4 hours and air cool (cooling rate not sensitive).

TABLE XXXII. MECHANICAL PROPERTIES OF CARPENTER CUSTOM 455

Property	Annealed	Aged 900°F/4 hr	Aged and 200°F	Aged and at 600°F
F_{ty}, ksi	140	220	214	187
F_{by}, .2%, ksi	115	205	200	172
e %	12	10	10	12
R.A. %	50	40	40	50
K_{IC}, ksi (in)1/2	-	73	125	-
K_{ISCC}, ksi (in)1/2	-	58	(117)	-

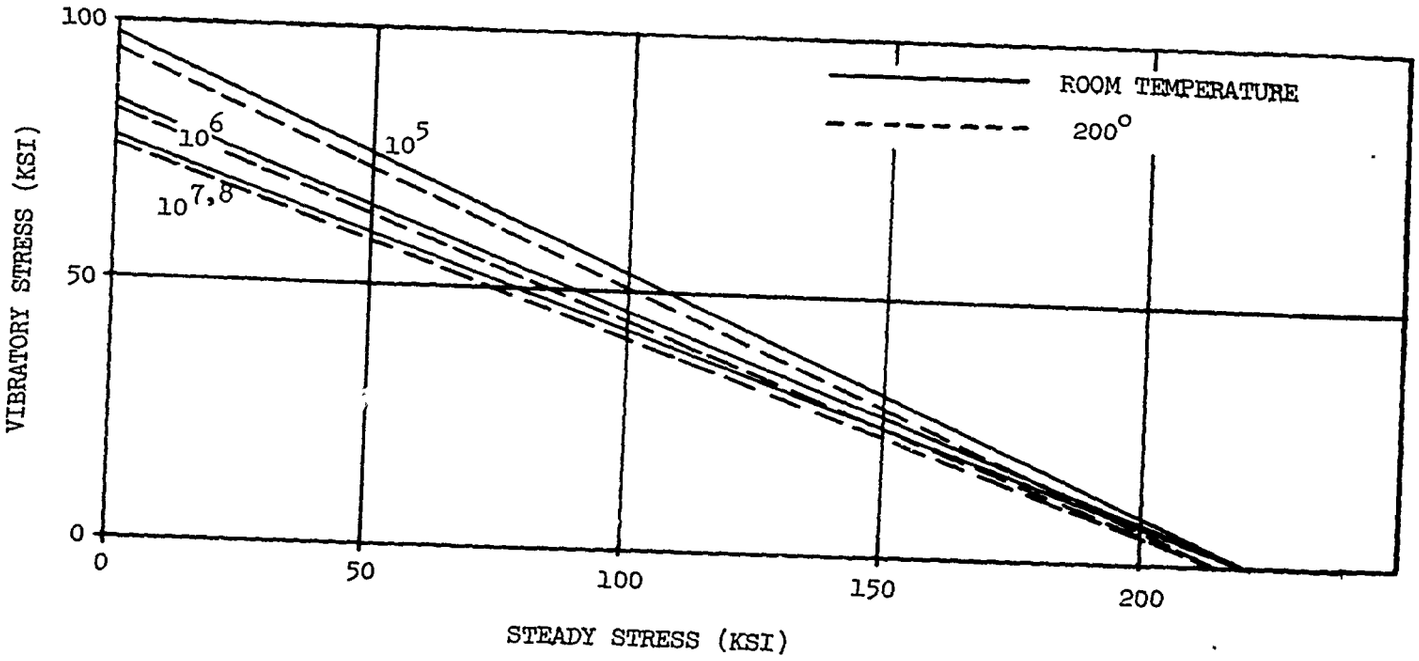

Figure 153. Constant-Life Fatigue Diagram for Carpenter Custom 455 at Room Temperature and 200°F (Reference 11).

COMPOSITES: Glass, Graphite, PRD

The tables and graphs included in the following pages characterize boron filament, glass filament and graphite filament reinforced polymer matrix composites. Included are elastic and strength properties of unidirectional, cross-ply and angle-ply composite, and physical properties of composites, filaments and resin matrices.

Orthotropic elastic properties for unidirectional composites fabricated from SP272-3M and Narmco 5505 prepreg boron-epoxy tapes are given in Table XXXV.

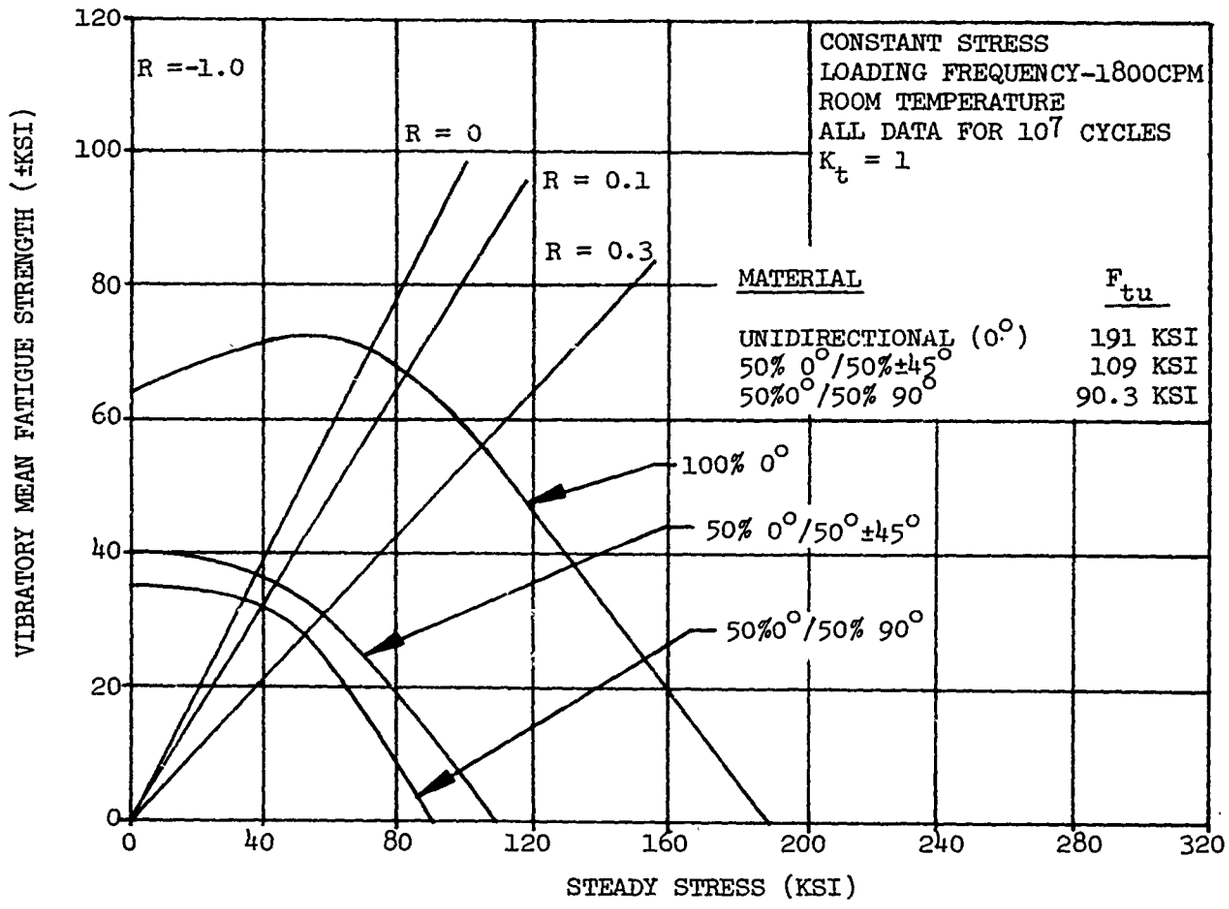

Figure 154. Boron Epoxy Characterization - Goodman Diagram.

TABLE XXXIII. PHYSICAL PROPERTIES OF BORON

PROPERTIES	Units	SP272- Composite	Ref.*	Resin Matrix	Ref.*	Compos
Fiber Volume Fraction	%	54 Nom.	M	-		53 Nom
Coefficient of Thermal Expansion	in/in/°F	-		21.8×10^{-6}	M	2.5x10 13.1x10
Density	lb/in^3	.075	M	.0443	M	.074
Specific Gravity (water disp)	-	2.07	M			2.03
Resin Content	% by wt.	28.4	C			28.9
Resin Flow	%	10 Nom.	M			14 Nom
Volatile Content	%	2	M			10 Max
Barcol Hardness	-	85 - 95	M			85 - 9
Thickness per Ply	in.	.0051	M			.0052

*M = experimentally measured values

C = calculated values

E XXXIII. PHYSICAL PROPERTIES OF BORON EPOXY, BORON FILAMENT AND RESIN MATRICES

P272-			Narmco 5505				Fibe
ef.*	Resin Matrix	Ref.*	Composite	Ref.*	Resin Matrix	Ref.*	Boron
M	-		53 Nom.	M			
	21.8×10^{-6}	M	2.5×10^{-6} @ 0° 13.1×10^{-6} @90°	M	24.5×10^{-6}	M	2.7×10^{-6}
M	.0443	M	.074	M	.043	M	.095
M			2.03	M			
C			28.9	C			N/A
M			14 Nom.	M			N/A
M			10 Max.	M			N/A
M			85 - 95	M			N/A
M			.0052	M			.004 dia.

N EPOXY, BORON FILAMENT AND RESIN MATRICES

	Narmco 5505			Fiber	
osite	Ref.*	Resin Matrix	Ref.*	Boron	Ref.*
Nom.	M				
10^{-6} @ 0°	M				
$x10^{-6}$ @90°		$24.5x10^{-6}$	M	$2.7x10^{-6}$	M
4	M	.043	M	.095	M
8	M				
9	C			N/A	
Nom.	M			N/A	
Max.	M			N/A	
- 95	M			N/A	
052	M			.004 dia. Nom.	M

TABLE XXXIV. ELASTIC CONSTANTS OF BORON EPOXY COMPOSITES

Elastic Constants**	Boron-Epoxy Mean Values SP272-3M	Ref.*	Narmco 5505	Ref.*
E_{11}	33.1×10^6 psi	M	31.7×10^6 psi	M
E_{22}	3.1×10^6 psi	M	3.0×10^6 psi	M
E_{33}	3.1×10^6 psi	C	3.0×10^6 psi	C
$G_{12} = G_{13}$	1.2×10^6 psi	M	1.1×10^6 psi	M
G_{23}	1.1×10^6 psi	C	1.0×10^6 psi	C
$\mu_{21} = \mu_{31}$ (Major Poisson's Ratio)	.22	M	.21	M
$\mu_{12} = \mu_{13}$ (Minor Poisson's Ratio)	.0206	C	.0199	C
23 = 32	.32	C	.38	C

* C = calculated values
* M = experimentally measured values
** definitions of elastic constants

E_{ii} = elastic modulus defined by the ratio of the stress in the i^{th} direction to the strain produced in the i^{th} direction

G_{ij} = the shear modulus defined by the ratio of the shear stress τ_{ij} to shear strain γ_{ij} in the ij^{th} plane

μ_{ij} = Poisson's ratio which indicates the ratio of the induced strain in the i^{th} direction to the strain due to an applied load in the j^{th} direction

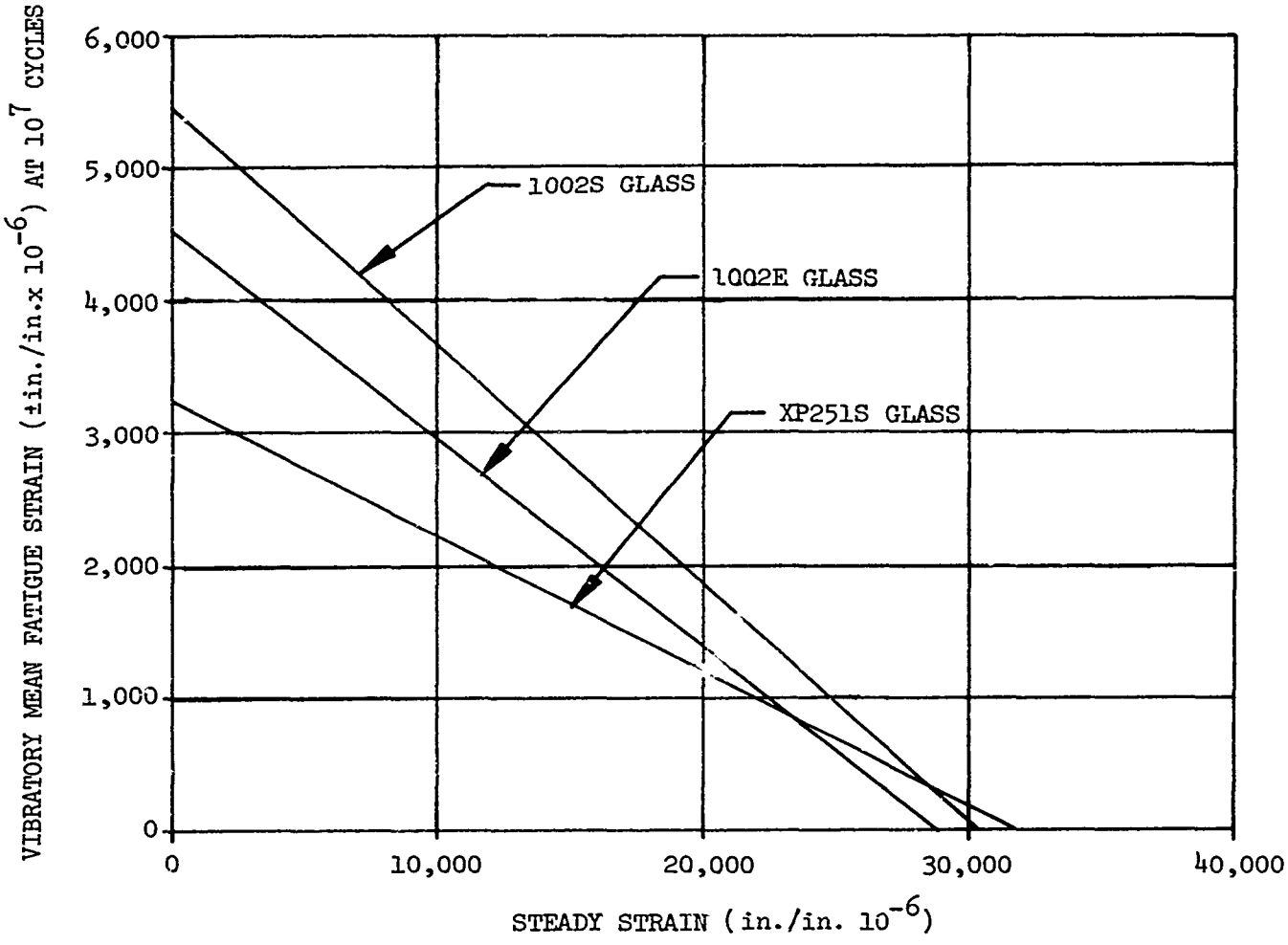

Figure 155. Goodman Strain Diagram at 10^7 Cycles for E and S Glass Epoxy Unidirectional Laminates.

TABLE XXXV. STRENGTH AND PROPOR

Material		Boron-Epoxy			
Fiber Orientation		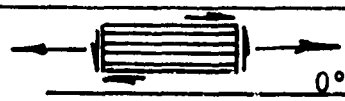 0°		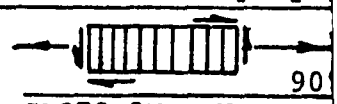 90	
		SP272-3M	Narmco 5505	SP272-3M	Narmco
Fiber Volume Fraction	(%)*	54 Nom.	53 Nom.	54 Nom.	53 Nom
Density	(lb/in^3)	.075	.074	.075	.074
Ultimate Strength	(psi)	212,000	208,300	11,700	9,590
"A" Allowables	(psi)	(18,400)	(159,400)	--	--
"B" Allowables	(psi)	(204,300)	(177,300)	--	--
Tensile - Proportional Limit	(psi)	136,000	120,000	6,700	5,200
Data Modulus	(psi)	$33.1x10^6$	$31.7x10^6$	$3.1x10^6$	$3.0x10^6$
"A" Allowables	(psi)	$(30.96x10^6)$	--	--	--
"B" Allowables	(psi)	$(32.065x10^6)$	--	--	--
Ultimate Strength	(psi)	250,000	262,000	38,000	41,000
Compression-Proportional Limit	(psi)	190,000	196,000	16,600	16,000
Data Modulus	(psi)	$33.1x10^6$	$31.7x10^6$	$3.6x10^6$	
Shear Data -Ultimate Strength	(psi)	18,700	17,300	18,700	17,300
Inplane Proportional Limit	(psi)	7,000	6,500	7,000	6,500
Modulus	(psi)	$1.2x10^6$	$1.1x10^6$	$1.2x10^6$	$1.1x10^6$
Poisson's Ratio		$\mu_{21}=\mu_{31}=$ .22	$\mu_{21}=\mu_{31}$	$\mu_{12}=\mu_{13}$.-2-6	$\mu_{12}=\mu_{13}$ .0198

"B" Allowables - 90% Probability with 95% Confidence
"A" Allowables - 99% Probability with 95% Confidence
(-) - Statistical values obtained from experimental data.

* These are experimentally determined values and not to be used in computer pr

** These data are derived from narrow specimens and are probably not representa
Preliminary wide specimen data are almost twice as high.

TABLE XXXV. STRENGTH AND PROPORTIONAL LIMIT OF BORON EPOXY COMPOSITES

Boron-Epoxy							
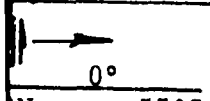 0°	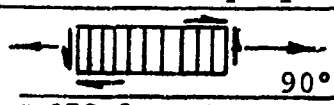 90°		 ± 45°		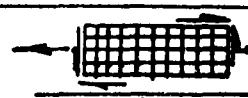 50%/50% 0°/90°		
Narmco 5505	SP272-3M	Narmco 5505	SP272-3M	Narmco 5505	SP272-3M	Narmco 5505	SP272
53 Nom.	54 Nom.	53 Nom.	54 Nom	53 Nom	54 Nom.	53 Nom.	54 No
.074	.075	.074	.075	.074	.075	.074	.075
208,300	11,700	9,590	22,200**	17,800**	108,000	103,400	--
(159,400)	--	--	--	--	--	(65,600)	--
(177,300)	--	--	--	--	--	(73,000)	--
120,000	6,700	5,200	11,900**	10,700	33,600	35,000	--
31.7×10^6	3.1×10^6	3.0×10^6	3.9×10^6	3.6×10^6	17.2×10^6	18.0×10^6	--
--	--	--	--	--	--	--	--
--	--	--	--	--	--	--	--
262,000	38,000	41,000	30,000	29,000	225,000	245,000	--
196,000	16,600	16,000	12,600	12,000	147,000	--	--
31.7×10^6	3.6×10^6		3.7×10^6	3.5×10^6	17.8×10^6	17.6×10^6	--
17,300	18,700	17,300	65,700	63,200	29,000	27,700	--
6,500	7,000	6,500	37,900	37,000	3,800	--	--
1.1×10^6	1.2×10^6	1.1×10^6	8.75×10^6	8.7×10^6	1.08×10^6	1.0×10^6	--
$\mu_{21}=\mu_{31}$	$\mu_{12}=\mu_{13}$.-2-6	$\mu_{12}=\mu_{13}=$ .0198	$\mu_{21}=\mu_{12}=$ .78	$\mu_{21}=\mu_{12}=$ .80	$\mu=.065$	$\mu=.073$	--

dence
dence
ntal data.

and not to be used in computer programs.

s and are probably not representative.
vice as high.

IT OF BORON EPOXY COMPOSITES

	 ± 45°		 50%/50% 0°/90°		 50%/50% 0°/±45°	
	2-3M	Narmco 5505	SP272-3M	Narmco 5505	SP272-3M	Narmco 5505
	om	53 Nom .074	54 Nom. .075	53 Nom. .074	54 Nom. .075	53 Nom. .074
	00**	17,800**	108,000	103,400	--	112,300
		--	--	(65,600)	--	(89,900)
		--	--	(73,000)	--	(100,000)
	00**	10,700	33,600	35,000	--	38,000
	10^6	3.6×10^6	17.2×10^6	18.0×10^6	--	17.2×10^6
		--	--	--	--	--
		--	--	--	--	--
	0	29,000	225,000	245,000	--	208,000
	0	12,000	147,000	--	--	--
	0^6	3.5×10^6	17.8×10^6	17.6×10^6	--	13.0×10^6
	0	63,200	29,000	27,700	--	50,000
	0	37,000	3,800	--	--	--
	$\times10^6$	8.7×10^6	1.08×10^6	1.0×10^6	--	5.75×10^6
	$\mu_{12}=$	$\mu_{21}=\mu_{12}=$ .80	$\mu=.065$	$\mu=.073$	--	$\mu=.743$

TABLE XXXVI. PHYSICAL PROPERTIES OF GLASS FILAMENT AND EPOX

Physical Properties	Units	Composites 1002 E-Glass	1002 S-Glass	XP 251 S-Glass
Filament Volume Fraction	%	48	48	59
Coefficient of Thermal Expansion	in./in. °F	4.8×10^{-6} uni at 0°	3.5×10^{-6} uni at 0°	-
Density	lb/in^3	0.067	0.067	0.071
Specific Gravity	-	1.90	1.90	2.0
Resin Content	% by wgt.	34 nom.	34 nom.	22 nom.
Resin Flow	%	10	10	10
Volatile Content	%	2 max.	2 max.	2 max.
Barcol Hardness	-	70	70	75
Thickness per Ply	in.	.010	.010	.0075
Filament Diameter	in.	-	-	-

VI. PHYSICAL PROPERTIES OF GLASS EPOXY COMPOSITES, GLASS FILAMENT AND EPOXY RESIN MATRICES

	Composites		Filaments		Matrices	
ss	1002 S-Glass	XP 251 S-Glass	E-Glass	S-Glass	Scotchply X1002	Scotchply XP 251
	48	59	-	-	-	-
10^{-6} 0°	3.5×10^{-6} uni at 0°	-	2.8×10^{-6}	1.6×10^{-6}	-	3.78×10^{-5}
	0.067	0.071	0.092	0.089	0.043	0.0439
	1.90	2.0	2.54	2.49	1.19	1.216
	34 nom.	22 nom.	-	-	-	-
	10	10	-	-	-	-
	2 max.	2 max.	-	-	-	-
	70	75	-	-	-	-
	.010	.0075	-	-	-	-
	-	-	.00039	.00039	-	-

TABLE XXXVII. ULTIMATE STRENGTH, PROPORTIONAL LIM

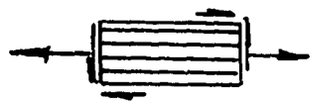

		Uni - 0°			
		Scotchply 1002E-Glass	Scotchply 1002S-Glass	Scotchply XP251S-Glass	Scotchply 1002E-Glass
Fiber Volume Fraction (%)		48 Nom.	48 Nom.	59 Nom.	48 Nom.
Density (lb/in.^{3})		.067	.067	.071	.067
Tensile Data	Ultimate Strength (psi)	160,000	195,000	270,000	4,800
	Proportional Limit (psi)	100,600	129,000[C]	188,000	2,400[C]
	Modulus (psi)	5.5×10^6	6.4×10^6	8.4×10^6	1.5×10^6
Compressive Data	Ultimate Strength	90,000	110,000	120,000	20,000
	Proportional Limit	45,200	67,300	105,200	-
	Modulus	4.70×10^6	5.8×10^6	7.3×10^6	1.2×10^6
Shear Data	Ultimate Strength	5,200	5,400	9,940	5,200
	Modulus (In-Plane Shear)	.47	$.90\times10^6$	1.0×10^6	$.47\times10^6$
Poisson's Ratio		$\mu_{21}=0.26$	$\mu_{21}=0.26$	$\mu_{21}=0.26$	$\mu_{12}=0.064$

TABLE XXXVII. ULTIMATE STRENGTH, PROPORTIONAL LIMIT AND ELASTIC CONTENTS

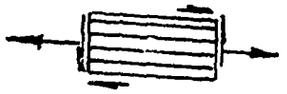

	Uni - 0°					Uni -
	Scotchply 1002E-Glass	Scotchply 1002S-Glass	Scotchply XP251S-Glass	Scotchply 1002E-Glass	Scotchply 1002S-Glass	Scotchp XP215S-
	48 Nom.	48 Nom.	59 Nom.	48 Nom.	48 Nom.	59 Nom.
	.067	.067	.071	.067	.067	.071
i)	160,000	195,000	270,000	4,800	6,700	11,900
i)	109,600	129,000[C]	188,000	2,400[C]	3,900	4,500
i)	5.5×10^6	6.4×10^6	8.4×10^6	1.5×10^6	2.1×10^6	2.40x1
	90,000	110,000	120,000	20,000	-	26,500
	45,200	67,300	105,200	-	-	14,300
	4.70×10^6	5.8×10^6	7.3×10^6	1.2×10^6	-	2.3×10^6
	5,200	5,400	9,940	5,200	5,400	9,940
r)	.47	$.90\times10^6$	1.0×10^6	$.47\times10^6$	$.90\times10^6$	1.0×10^6
	$\mu_{21}=0.26$	$\mu_{21}=0.26$	$\mu_{21}=0.26$	$\mu_{12}=0.064$	$\mu_{12}=0.089$	$\mu_{12}=0.$

ENTS FOR GLASS EPOXY

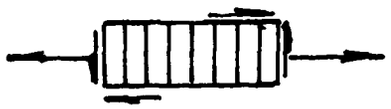

hi - 90°	± 45°			50%/50% 0°/90°		
otchply 215S-Glass	Scotchply 1002E-Glass	Scotchply 1002S-Glass	Scotchply XP251S-Glass	Scotchply 1002E-Glass	Scotchply 1002E-Glass	Scotchply XP251S-Gla
Nom.	48 Nom.	48 Nom.	59 Nom.	48 Nom.	48 Nom.	59 Nom.
1	.067	.067	.071	.067	.067	.071
,900	22,200	28,900	30,300	75,000	105,000	130,000
,500	-	-	-	-	25,600	24,000
$40x10^6$	$1.50x10^6$	$2.2x10^{6C}$	$2.8x10^{6C}$	$3.5x10^6$	$4.0x10^6$	$5.2x10^6$
,500	23,000	-	-	76,400	88,000	100,000
,300	-	-	-	43,000	43,000	43,700
$3x10^6$	-	-	-	$2.80x10^6$	$3.60x10^6$	$4.40x10^6$
940	-	42,000	43,600	5,200	5,400	9,940
$0x10^6$	$1.5x10^6$	$1.9x10^{6C}$	$2.5x10^{6C}$	$.47x10^{6C}$	$.90x10^{6C}$	$1.0x10^{6C}$
2=0.076	μ=0.63	μ=0.46^C	μ=0.51^C	μ=0.11^C	μ=0.12^C	μ=.13

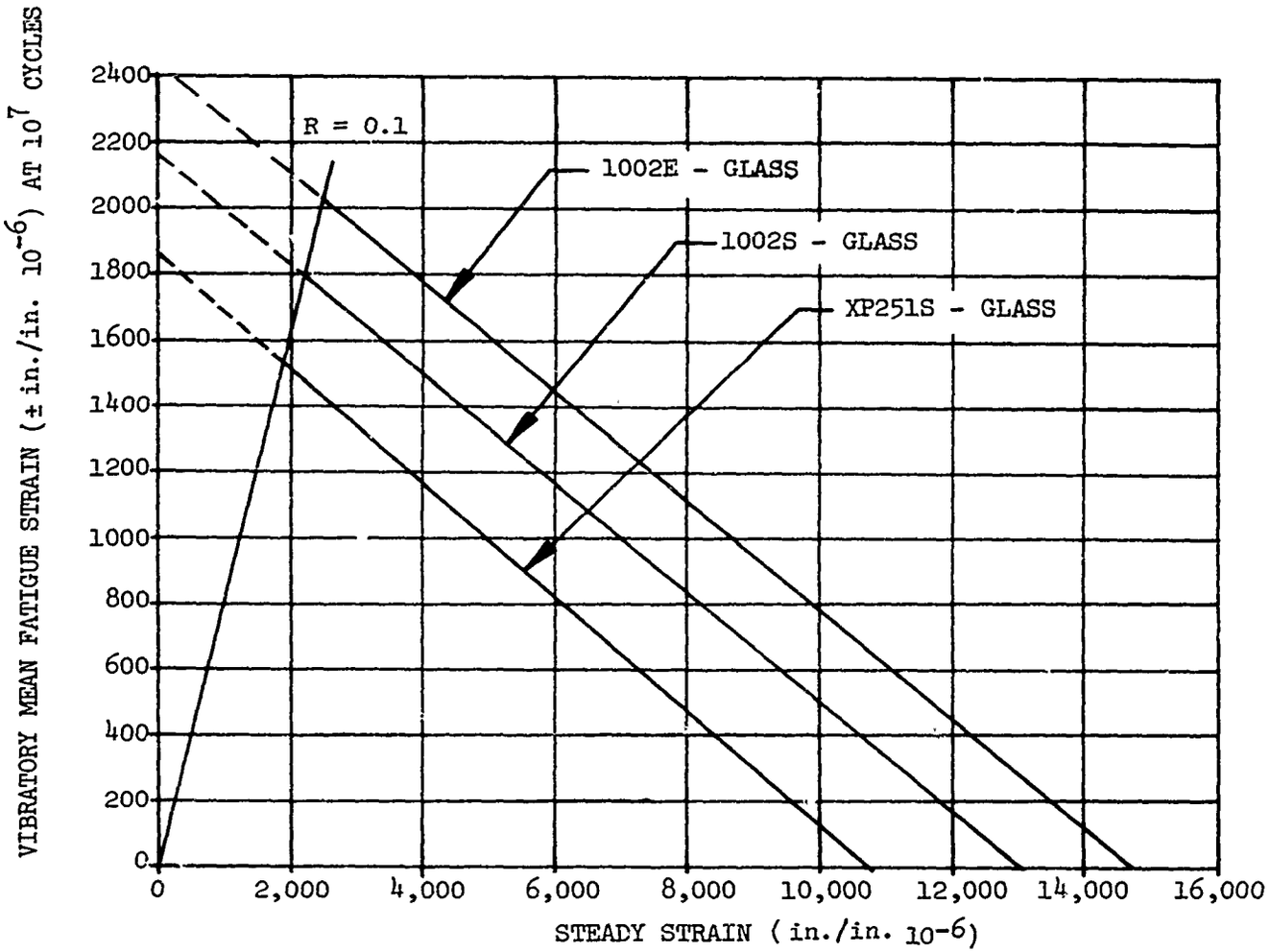

Figure 156. Goodman Strain Diagram at 10^7 Cycles for E and S Glass - Epoxy ±45° Laminates.

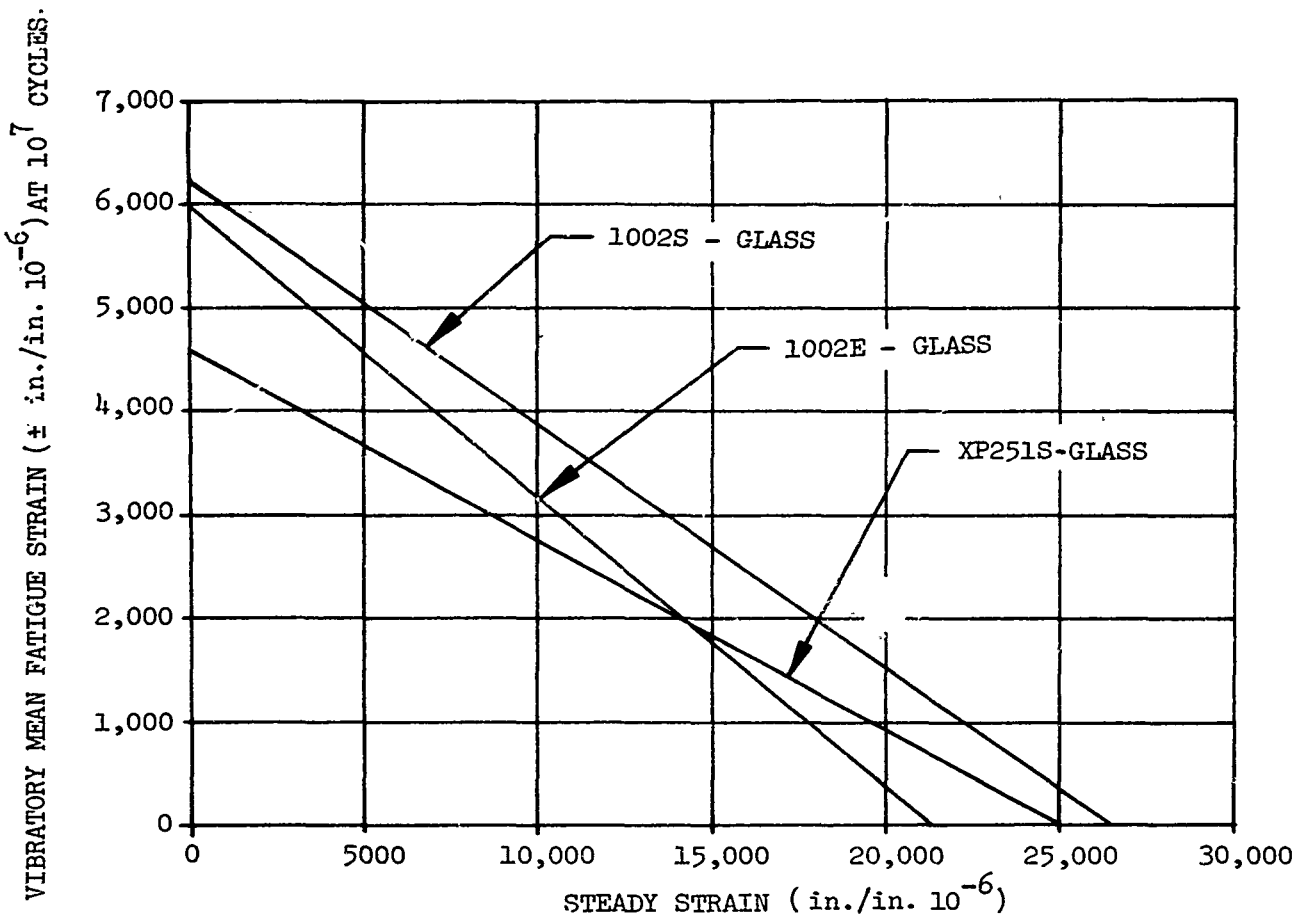

Figure 157. Goodman Strain Diagram at 10^7 Cycles for E and S Glass - Epoxy 50%-0°/50%-90° Laminates.

The orthotropic elastic constants for Scotchply SP286 and Fiberite E1305 graphite epoxy unidirectional laminates are given in Table XXXVIII.

TABLE XXXVIII. ELASTIC CONSTANTS FOR GRAPHITE EPOXY COMPOSITES

Elastic Constants	Scotchply SP286 & Fiberite E1305	
Unidirectional Configuration	High Modulus	High Strength
E_{11} Modulus-Longitudinal psi	26×10^6	20×10^6
E_{22} Modulus-Transverse psi	1.6×10^6	1.5×10^6
G_{12} Shear Modulus psi	0.57×10^6	0.61×10^6
μ_{12} Poisson's Ratio	0.300	0.300
V_f Filament Volume Fraction %	55	55

TABLE XXXIX. PHYSICAL PROPERTIES OF GRAPHITE EPOXY GRAPHITE FILAMENTS AND RESIN MATRICES

Properties	Scotchply SP-286		Fiberite HyE-1305		Filament		Resin Matrix	
	High Modulus	High Strength	High Modulus	High Strength	High Modulus	High Strength	SP-286	HyE-1305
Fiber Volume Fraction (%)	58%	55%	52.5%	51.2	-	-	-	-
Coef. - Thermal Expansion (in./in.°F x 10^{-6})	-0.25	-0.25	-0.40	-.40	-0.55	-0.55	40 Approx.	40 Approx.
Density #in.^{3}	0.053	0.057	0.057	0.054	0.070	0.065	0.045	N/A
Specific Gravity	1.50	1.60	1.61	1.52	1.96	1.70	1.27	N/A
Resin Content (% wgt.)	-	-	34.8	37.7	-	-	-	-
Thickness per Ply (in.)	.0075	.0075	.008	.008	-	-	-	-
Mean Filament Diameter in. x 10^{-3}	-	-	-	-	0.30	0.33	-	-

TABLE XXXX. STRENGTH AND ELASTIC CONSTANTS FOR GRAPHITE EPOXY COMPOSITES

Fiber & Load Orientation	Uni - 0°		Uni - 90°		+45°		50% - 0°/50%-90°	
Material	H. MOD.	H. STRG.	H. MOD.	H. STRG.	H. MOD.	H. STRG.	H. MOD.	H. STRG.
Fiber Volume Fraction %	55	55	55	55	53	60	42	62
Tensile Ultimate Strength Psi	100,000	134,000	7,000	8,000	18,400	30,600	61,500	69,000
Tensile Modulus Psi	26×10^6	20×10^6	1.6×10^6	1.5×10^6	2.8×10^6	2.5×10^6	12.2×10^6	10×10^6
Compressive Ultimate Strength Psi	85,000	115,000	22,000	30,000	23,000	37,800	51.1×10^6	80,000
Compressive Modulus Psi	26×10^6	20×10^6	1.6×10^6	1.5×10^6	2.9×10^6	2.35×10^6	11.4×10^6	10.4×10^6
Shear Ultimate Strength Psi	8,000	16,000	8,000	16,000	24,200	37,700		15,100
Shear Modulus Psi	0.57×10^6	0.61×10^6	0.57×10^6	0.61×10^6	6.2×10^6	4.3×10^6		0.65×10^6
Poisson's Ratio	0.300					.818		

APPENDIX III

DISCUSSION OF SYNERGISTIC INTERACTION BETWEEN CREEP AND FATIGUE PROPERTIES

Synergistic interaction of two variables is the nonlinear addition of the effects of two variables in which the sum may be significantly greater than the individual parts. Applying a synergism to creep and fatigue is difficult without test data applicable to the specific design stresses.

Most of the research to date has been in characterizing the synergistic interaction of creep and fatigue on high-temperature steels. In the case of aluminum, 6061-T6, the interaction problem is compounded by the fact that cyclic stresses at temperature will affect the overaging characteristics of the aluminum. This overaging will occur faster or at a lower temperature than the static test data reported in MIL-HDBK-5A.

The nature of synergism with respect to creep is that low cyclic stresses have a tendency to cause creep rates to increase markedly. Under certain circumstances, materials can change creep rates by an order of magnitude. Total creep elongation at failure can also be reduced.

With respect to fatigue, creep stresses and creep (permanent strains) have a tendency to break up dislocation networks which are a contributing cause of fatigue crack initiation. The net result is an apparent increase in fatigue strength particularly at appreciable steady stresses. Some of the steel constant life fatigue diagrams for elevated temperatures in MIL-HDBK-5 show a marked improvement in fatigue strength at combined elevated temperatures and steady stresses.

In some cases, the fatigue strength of the material at steady stress and elevated temperature is higher than the fatigue strength at zero steady stress and the same temperature. The test conditions (material, temperature, cyclic stress ratio, steady and vibratory stress) must duplicate the design application. Significant errors can result without well-matched test condtions.

Test data to assess the synergistic creep/fatigue effects on notch sensitivity has resulted in mixed and conflicting interpretations. Apparently, if compressive residual stresses are inherent in the machining and the machined stress concentration relieved by synergism, then the notch effect becomes more severe. If the stress concentration becomes blunted by creep, then the notch effect becomes less severe.

LIST OF SYMBOLS

A	area, square inches
a	characteristic radial dimension
C_u^p	stiffness coefficient
C_u^v	stiffness coefficient
C_w^p	stiffness coefficient
C_w^v	stiffness coefficient
D	pitch diameter, inches
D_R	rotor force - aft, pounds
d_m	bevel gear mean pitch diameter, inches
d_p	pinion pitch diameter, inches
E	modulus of elasticity, pounds per square inch
e	elongation, percent
E_c	modulus of elasticity in compression, pounds per square inch
F	face width, inches
F_a	force at a, pounds
F_{bru}	ultimate bearing strength, pounds per square inch
F_{bry}	yield bearing strength, pounds per square inch
F_{rib}	force on rib, pounds
F_{su}	ultimate strength in shear, pounds per square inch
F_{tu}	ultimate strength in tension, pounds per square inch
F_{ty}	yield stress, pounds per square inch

f_a	axial stress, pounds per square inch
f_b	bending stress, pounds per square inch
f_{rib}	stress in rib, pounds per square inch
f_{vib}	maximum vibratory stress, pounds per square inch
f_{xx}	maximum stress in x direction, pounds per square inch
f_{yy}	maximum stress in y direction, pounds per square inch
G	modulus of elasticity in shear, pounds per square inch
g	acceleration of gravity, feet per second^2
h	thickness, inches
I_{xx}	moment of inertia about x axis, inches^4
I_{yy}	moment of inertia about y axis, inches^4
K	geometry factor, inches^4
K_f	notch sensitivity factor
K_{IC}	fracture toughness, pounds per square inch (inches$^{1/2}$)
K_t	stress concentration factor
$K_{Lateral}$	lateral spring rate, pounds per inch
$K_{Vertical}$	vertical spring rate, pounds per inch
M_A	moment about bearing A, inch-pounds
M_B	moment about bearing B, inch-pounds
M_{xR}	rotor moment about x axis, inch-pounds
M_{xx}	moment about x axis, inch-pounds
M_{yR}	rotor moment about y axis, inch-pounds
M_{yy}	moment about y axis, inch-pounds
M_{ZR}	rotor moment about x axis, inch-pounds
N	speed, revolutions per minute
n	pinion speed, revolutions per minute

P	radial shear, pounds
$R_{A_{bl}}$	bearing reaction in butt line plane, pounds
R_{A_h}	horizontal bearing reaction at bearing A, pounds
$R_{A_{Sta}}$	bearing reaction in station plane, pounds
R_{A_t}	horizontal bearing reaction at A, pounds
R_{A_v}	vertical bearing reaction at A, pounds
R_{A_x}	bearing reaction - main rotor, pounds
R_{A_y}	bearing reaction - main rotor, pounds
$R_{B_{bl}}$	bearing reaction in butt line plane, pounds
R_{B_H}	horizontal bearing reaction at B, pounds
$R_{B_{Sta}}$	bearing reaction in station plane, pounds
R_{B_t}	horizontal bearing reaction at B, pounds
R_{B_v}	vertical bearing reaction at B, pounds
R_{B_x}	bearing reaction - main rotor, pounds
R_{B_y}	bearing reaction - main rotor, pounds
R_{a_x}	bearing reaction at a, pounds
R_{a_y}	bearing reaction at a, pounds
R_{b_x}	bearing reaction at b, pounds

R_{b_y}	bearing reaction at b, pounds
R_{A_x}	axial load on thrust bearing, pounds
r_1	radius at top of conical section, inches
r_2	radius at bottom of conical section, inches
S_R	rotor force, pounds
T	gear torque, inch-pounds
T_{R_1}	torque on first-stage ring gear, inch-pounds
T_{R_2}	torque on second-stage ring gear, inch-pounds
u	lateral deflection, inches
V	vertical shear, pounds
V_R	vertical rotor force, pounds
V_f	filament volume fraction, percent
W_H	horizontal gear load component, pounds
W_r	radial component of gear tooth load, pounds
$W_{r_{in}}$	radial gear tooth load in, pounds
W_t	tangential tooth load, pounds
$W_{t_{in}}$	tangential tooth load in, pounds
$W_{t_{out}}$	tangential tooth load out, pounds
W_v	vertical gear load, pounds
W_x	axial component of gear tooth load, pounds
$W_{x_{in}}$	axial gear tooth load in, pounds
w	vertical deflection, inches

YS	yield strength, pounds per square inch
Z	elevation of shell above base plane, inches
α	cone angle, degrees
ψ	spiral angle, degrees
γ	pitch angle, degrees
Φ	pressure angle, degrees
ν	Poisson's ratio